CUCUMBER GREEN MOTTLE MOSAIC VIRUS AS A NANOPARTICLE: BIODISTRIBUTION, IMMUNOSTIMULATION AND EXPRESSION

LEE WEI WEI

FACULTY OF SCIENCE

UNIVERSITI MALAYA

KUALA LUMPUR

2022

CUCUMBER GREEN MOTTLE MOSAIC VIRUS AS A NANOPARTICLE: BIODISTRIBUTION, IMMUNOSTIMULATION AND EXPRESSION

LEE WEI WEI

THESIS SUBMITTED IN FULFILMENT OF THE REQUIREMENTS FOR THE DEGREE OF DOCTOR OF PHILOSOPHY

INSTITUTE OF BIOLOGICAL SCIENCES

FACULTY OF SCIENCE

UNIVERSITI MALAYA

KUALA LUMPUR

2022

UNIVERSITI MALAYA

ORIGINAL LITERARY WORK DECLARATION

Name of Candidate: **LEE WEI WEI**

Matric No: **17016390/3**

Name of Degree: **DOCTOR OF PHILOSOPHY**

Title of Thesis ("this Work"):
CUCUMBER GREEN MOTTLE MOSAIC VIRUS AS A NANOPARTICLE: BIODISTRIBUTION, IMMUNOSTIMULATION AND EXPRESSION

Field of Study:

PLANT BIOTECHNOLOGY

I do solemnly and sincerely declare that:

(1) I am the sole author/writer of this Work;
(2) This Work is original;
(3) Any use of any work in which copyright exists was done by way of fair dealing and for permitted purposes and any excerpt or extract from, or reference to or reproduction of any copyright work has been disclosed expressly and sufficiently and the title of the Work and its authorship have been acknowledged in this Work;
(4) I do not have any actual knowledge nor do I ought reasonably to know that the making of this work constitutes an infringement of any copyright work;
(5) I hereby assign all and every rights in the copyright to this Work to the University of Malaya ("UM"), who henceforth shall be owner of the copyright in this Work and that any reproduction or use in any form or by any means whatsoever is prohibited without the written consent of UM having been first had and obtained;
(6) I am fully aware that if in the course of making this Work I have infringed any copyright whether intentionally or otherwise, I may be subject to legal action or any other action as may be determined by UM.

Candidate's Signature Date: 20/7/2022

Subscribed and solemnly declared before,

Witness's Signature Date: 20/07/2022

Name:

Designation:

CUCUMBER GREEN MOTTLE MOSAIC VIRUS NANOPARTICLE: BIODISTRIBUTION, IMMUNOSTIMULATION AND EXPRESSION

ABSTRACT

Viral nanoparticles (VNPs) derived from plant viruses have many advantages due to their bio-compatibility and bio-degradability *in vivo*, ability to self-assemble in 3 dimensions and capacity for large scale production. Compared to the animal VNPs, plant VNPs are likely to be less or non-pathogenic to human. *Cucumber Green Mottle Mosaic Virus* (CGMMV) is a single stranded, positive sense RNA virus from the family of *Tobamovirus* that has the potential to be developed as a nanoparticle for vaccine and adjuvant applications. In this study, CGMMV nanoparticles were found to be produced more efficiently in its native host *Cucumis melo* var Earl favorite compared to the other alternative local varieties. *In vivo* study of subcutaneously injected CGMMV nanoparticles in a mouse model demonstrated that it is distributed in a wide range of tissues without causing any toxicity and inflammation. It is also able to induce high level of antibody production without the need of adjuvants. Infectivity of CGMMV nanoparticles extracted from the mouse tissues however is greatly reduced. Moreover, CGMMV nanoparticles can act as immunostimulator *in vitro* by stimulating the innate immune response and confer protection against *Vesicular stomatitis virus* (VSV) and *Sendai virus* (SeV) infection in RAW246.7 cells. Lastly, chimeric CGMMV vectors were engineered to express selected M1 influenza epitopes at the 3' terminal of coat protein. The epitopes can be co-expressed at the surface of the viral coat protein during replication in plants. However, no significant difference in immune response was observed between the chimeric and wild-type CGMMV nanoparticles upon testing in mice. Taken together, the results suggest that CGMMV nanoparticle is a potential vaccine carrier and adjuvant candidate. Further study is needed to tease out the underlying factor required for CGMMV chimeric nanoparticles to induce immune response against influenza epitopes.

Keywords: Virus nanoparticles, CGMMV, biodistribution, immunostimulator, epitopes

NANOPARTIKEL VIRUS CUCUMBER GREEN MOTTLE MOSAIC: BIODISTRIBUSI, PERANGSANG IMUN DAN EKSPRESI

ABSTRACK

Nanopartikel-nanopartikel virus (NPVs) berdasarkan virus tumbuhan mempunyai banyak kelebihan berbanding dengan nanopartikel sintetik kerana keserasian dan mampu diurai secara *in vivo*, kemampuan untuk memasang sendiri kebentuk struktur 3 dimensi dan dapat dihasilkan dalam skala besar dengan kos yang lebih rendah. Berbanding dengan NPV haiwan, VNP tumbuhan kurang atau tidak patogenik kepada manusia. *Cucumber Green Mottle Mosaic Virus* (CGMMV) adalah virus RNA positif bebenang tunggal dari keluarga *Tobamovirus* yang berpotensi dikembangkan sebagai nanopartikel untuk aplikasi vaksin dan adjuvan. Dalam kajian ini, nanopartikel CGMMV didapati dihasilkan dengan lebih cekap dalam perumah asalnya *Cucumis melo* var Earl favorite berbanding dengan varieti tempatan alternatif lain. Dalam kajian *in vivo* nanopartikel CGMMV yang disuntik secara subkutaneus pada model tikus menunjukkan bahawa ia diedarkan dalam pelbagai tisu tanpa menyebabkan keracunan dan keradangan. Ia juga dapat mendorong pengeluaran antibodi tahap tinggi tanpa bantuan adjuvan. Infektiviti nanopartikel-nanopartikel CGMMV yang diekstrak dari tisu bagaimanapun didapati berkurangan. Tambahan lagi, ia juga bertindak sebagai perangsang imun dengan merangsang tindak balas imun semulajadi dan dalam model *in vitro* dapat menghalang replikasi *Virus Vesikular Stomatitis* (VSV) dan *Virus Sendai* (SeV) dalam sel RAW246.7. Terakhir, kimera vektor CGMMV dibina untuk mengekspresikan M1 epitop influenza terpilih dalam protein kot di terminal 3'. Epitop boleh ditunjukan pada permukaan protein lapisan virus semasa replikasi pada tumbuhan. Walau bagaimanapun, tidak terdapat perbezaan yang ketara dalam tindak balas imun antara nanopartikel CGMMV jenis kimera dan liar semasa ujian pada tikus. Secara keseluruhan, hasilnya menunjukkan bahawa nanopartikel CGMMV adalah pembawa vaksin dan adjuvant yang berpotensi. Kajian lebih lanjut

diperlukan untuk mengetahui factor yang diperlukan untuk mendorong tindak balas imun nanopartikel kimera CGMMV terhadap epitop influenza.

Kata Kunci: Nanopartikels virus, CGMMV, biodistribusi, perangsang imun, epitope

ACKNOWLEDGEMENTS

Firstly, I would like to express my sincere gratitude to my advisor Prof. Dr. Rofina Yasmin for the continuous support of my Ph.D study, for her great patience, motivation, and immense knowledge. Her guidance helped me in all the time of research and writing of this thesis. I would also like to thank my late co-supervisor, Prof. Dr. Noor Hasima Nagoor for her insightful comments and hard question which inspired me to widen my research from various perspectives. Their professionalism and commitment have given me the pleasure to work with them, and I have learned a lot from their deepest knowledge.

I would like to express my appreciation to Dr. Eddie Lim Yat Yuen and Dr. Afiq Aziz who helped me in my final stage of thesis correction and papers submission. My gratitude also goes to my lab-members, Dr. Jameel, Dr. Teo Chee How, Dr. Tey Ser Huy, Dr. Ili, Ms Jacinth Poon, Mr Taufiq and others for the stimulating discussions, kindness, help, knowledge, and assistance in one way or another to the completion of my project. Furthermore, I would like to thank Centre for Research in Biotechnology for Agriculture (CEBAR) and High Impact Research (HIR) central facility for lending me their equipment to complete my work.

My sincere thanks also go to Dr. Ea Chee Kwee and Dr. Eddie Lim Yat Yuen who provided me an opportunity to join their team and gave me access to the laboratory and research facilities. Many thanks to epigenetics members, Dr. Yeoh Kok Siong, Dr. Ng Wei Lun, Dr Taznim, Mr Tan Ming Cheang, Ms Wong Wan Ying and Ms Tan Ke En for giving me the space to work and valuable assistance. Without they precious support it would not be possible to conduct this research.

Last but not the least, I would like to thank my family: my parents and to my brothers and sister for supporting me spiritually throughout writing this thesis and my life in general.

TABLE OF CONTENTS

LIST OF FIGURES

LIST OF TABLES

LIST OF SYMBOLS AND ABBREVIATIONS

x g	:	Acceleration of gravity
ºC	:	Degree Celsius
µ	:	Micro
m	:	Milli
n	:	Nano
%	:	Percentage
3D	:	3 dimensions
AMV	:	*Alfafa mosaic virus*
APCs	:	Antigen presenting cells
BHV-1	:	*Bovine herpesvirus* type 1
BMV	:	*Brome Mosaic virus*
BRV	:	*Bovine rotavirus*
CCMV	:	*Cucumber chlorotic mosaic virus*
CGMMV	:	*Cucumber green mottle mosaic virus*
CNS	:	Central nervous system
CP	:	Coat protein
CPMV	:	*Cowpea mosaic virus*
CPV	:	*Canine parvovirus*
CTB	:	Cholera toxin B subunit
CTL	:	Cytotoxic T lymphocyte

DC	:	Dendritic cell
Der p 5	:	Dermatophagoides pteronyssinus group 5 allergen
DNA	:	Deoxyribonucleic acid
EVs	:	Epitope-based vaccines
FMDV	:	*Foot and mouth disease virus*
FnBP	:	Fibronectin-binding protein B
GAP31	:	*Gelonium* anti-HIV protein
GFP	:	Green fluorescent protein
HA	:	Hemagglutinin
HBsAg	:	Hepatitis B surface antigen
HCRSV	:	*Hibiscus chlorotic ringspot virus*
HCV	:	*Hepatitis C virus*
HIV	:	*Human immunodeficiency virus*
IEDB	:	Immune Epitope Database and Analysis Resources
IFN- γ	:	Interferon gamma
IgG	:	Immunoglobulin G
IL	:	Interleukin
pI	:	Isoelectric point
I-TASSER	:	Iterative threading assembly refinement
KLH	:	Keyhole limpet hemocyanin
L	:	Liter

LTB	:	Labile toxin B subunit
M	:	Matrix
M2e	:	M2 ectodomain
MAb	:	Monoclonal antibody
MAP30	:	*Momordica* anti-HIV protein
ME	:	Minimum energy
MEV	:	*Mink enteritis virus*
MHC	:	Major histocompatible complex
MHV	:	*Murine hepatitis virus*
MP	:	Movement protein
MRFV	:	*Maize rayado fino virus*
MRI	:	Magnetic resonance imaging
mRNA	:	Messenger RNA
NA	:	Neuramiridase
NDV	:	*Newcastle disease virus*
NEP	:	Nuclear export protein
NHS	:	N-hydroxysuccinimide
NP	:	Nucleoprotein
NS1	:	Non-structural protein 1
NS2	:	Non-structural protein 2
ORFs	:	Open reading frames

PA	:	Polymerase acidic protein
PB1	:	Polymerase basic protein 1
PB2	:	Polymerase basic protein 2
PDB	:	Protein database
PPV	:	*Plum pox potyvirus*
pVNPs	:	Plant virus nanoparticles
PVX	:	*Potato virus X*
QIV	:	Quadrivalent influenza vaccine
RCNMV	:	*Red clover necrotic mosaic virus*
RdRp	:	RNA-dependent RNA polymerase
RGD	:	Arginylglycylaspartic acid
RHDV	:	*Rabbit hemorrhagic disease virus*
RNA	:	Ribonucleic acid
RNP	:	Ribonucleoprotein
RSV	:	*Respiratory syncytial virus*
SAG1	:	Surface antigen 1
SV	:	*Sendai virus*
TBSV	:	*Tomato bushy stunt virus*
Th	:	T-Helper
TIV	:	Trivalent influenza vaccines
TMV	:	*Tobacco mosaic virus*

VEGFR-1	:	Vascular endothelial growth factor receptor-1
VLP	:	Virus like particles
VNP	:	Virus nanoparticles
vRNA	:	Viral RNA
VSV	:	*Vesicular stomatitis virus*
vvIBDV	:	Very virulent Infectious bursal disease virus
WHO	:	World Health Organization
ZGMV	:	*Zucchini yellow mosaic virus*

LIST OF APPENDIXES

CHAPTER 1: INTRODUCTION

1.1 Introduction

Nanotechnology has emerged as a rapidly evolving field that involves formulation, fabrication and innovation of nanomaterials with dimensions in a range of 1-100 nm (Ahmed et al., 2017). This idea was first presented in 1959 at the annual meeting of the American Physical Society (APS) by Richard Feynman (published in "There's Plenty of Room at the Bottom: An Invitation to Enter a New Field of Physics" (Feynman, 1961). The term "nanotechnology" was further shaped by Professor Norio Taniguchi of Tokyo Science University to describe the manufacture process these of materials (Taniguchi, 1974). The unique characteristics of nanoparticles include its size, shape, structure as well as high purity and surface area to volume ratio that enables them to be used in diverse fields including biomedicine (Khan et al., 2019).

A total of 23 nanoparticles have been approved by FDA for therapeutic purposes while 45 nanoparticles are currently under investigation. Among the 45 nanoparticles, 38 are for therapeutic applications while are for diagnostic applications (Mitchell et al., 2021). To combat the recent Covid-19 pandemic, new anti-viral drugs and vaccines are also under development using nanotechnology-based platforms (Tang et al., 2021; Weiss et al., 2020).

There are several methods to produce nanoparticles. Biological synthesis has taken over physical and chemical synthesis due to the latter two having disadvantages which include high production cost, release of toxic by-products, time and energy consuming (Kumari et al., 2019). Nanoparticles derived from organic materials are known as biogenic nanoparticles or nanobioparticles (Cachau et al., 2007; Rana et al., 2020). One emerging biological synthesis platform are viruses. In material science term, viruses can be defined as a supramolecules surrounded by multiple copies of coat proteins that differ

in shapes and sizes ranging from ten to hundreds nm (Liu et al., 2012). The coat proteins provide protection to the genomic material inside especially under extreme conditions (Pokorski & Steinmetz, 2011). Besides its robustness, the homogeneity in size, highly symmetrical structure and larger surface to volume ratio have enable viruses to be used as nanoparticles (Wen & Steinmetz, 2016).

The ability to package material (or 'cargo'), penetrate, target and deliver the cargo to specific tissue makes viruses a potential and attractive "smart" vehicle in nanomedicine. Those cargos include contrast agents or therapeutics for imaging or treatment purposes (Chariou et al., 2020). Adeno-based virus, a mammalian viral vector has been established to treat several medical conditions for example, lipoprotein lipase deficiency, RPE65 mutation-associated retinal dystrophy and spinal muscular atrophy. Due to the immunogenicity, cytotoxicity and inflammatory reactions in human cells to mammalian viral vectors, researchers have shifted their interest to plant viruses as they are generally safer to human, easy to manipulate and have a low cost of production (Jeevanandam et al., 2019; Nikitin et al., 2016).

Plant viruses have also been investigated for development as vaccines, drug delivery and imaging tools (Balke & Zeltins, 2020; Dang & Guan, 2020; Shahgolzari & Pazhouhandeh, 2020; Vankayala et al., 2020). The highly symmetrical and well-organized structure can be recognized by the immune system and thus, has indicated the potential of plant viruses as immunostimulators that are able to induce both innate and adaptive immune responses in human and animals (Evtushenko et al., 2020a; Zhuang et al., 2019). They can also be genetically and chemically modified as expression vectors to display the epitopes of pathogens on the surface of their coat protein (Balke and Zeltins, 2020; Kirtane et al., 2021). The application of recombinant plant virus nanoparticles as candidate vaccines have been increasingly studied (Santoni et al., 2020; Wen et al., 2020).

Many plant viruses including *Tobacco mosaic virus* (TMV), *Cowpea mosaic virus* (CPMV), *Potato virus X* (PVX) and *Papaya mosaic virus* (PapMV) have been intensively studied *in vivo* as adjuvants and expression vectors (Abrahamian et al., 2020; Evtushenko et al., 2020; Hefferon, 2017). The monopartite, positive single stranded RNA genome of *Cucumber green mottle mosaic virus* (CGMMV) is relatively easy to manipulate. It is a rod shape *Tobamovirus* with a dimension of 18 nm x 300 nm (Okada, 1986; Wang a Stubbs, 1994). Although CGMMV-SH strain has been previously reported as an expression vector to express *Hepatitis B virus* surface antigen and dengue epitopes in our laboratory (Ooi et al., 2006; Teoh et al., 2009), the potential studies of CGMMV as an expression vector to express other epitopes has not been fully explored while its *in vivo* characteristics and its function as an adjuvant have not been studied.

1.2 Objectives

In this work, the characteristics of CGMMV nanoparticles, its potential to function as an adjuvant and as an expression vector for influenza epitopes in both *in vitro* and *in vivo* settings is studied. In addition, this study will also attempt to identify alternative propagation host from local cucumber plants which is easier to obtain to replace its original temperate host, *Cucumis melo* var Earl favorite that need to import from Japan, to improve its efficiency of production within a tropical environment. Thus, the objectives of the study are:

1. To identify potential new local propagation hosts for CGMMV.
2. To determine the *in vivo* behavior of CGMMV nanoparticles in mice.
3. To investigate the function of CGMMV nanoparticles as an immunostimulator.
4. To construct CGMMV chimeric expression vector to express influenza epitopes and to study the immune response against the chimeric vectors in mice.

CHAPTER 2: LITERATURE REVIEW

2.1 Nanotechnology and nanoparticles in biomedicine

Nanotechnology is a combination of science and engineering of submicroscopic particles ranging between 1 to 100 nm in at least one dimension. Fabrication and manipulation of newly designed or improved nanoparticles of different sizes, chemical characteristics and structures are broadly applied in material sciences, electrical, energy, agriculture, foods and medical applications (Ahmad et al., 2019; Ahmadi et al., 2019; Amudhavalli & Ravi, 2019; Contreras et al., 2017; Jain et al., 2020; Kumar et al., 2020; Shang et al., 2019).

In the field of biomedical sciences, nanoparticles have been developed to become "smart" targeted formulations which have been linked to targeting molecules for therapeutic and diagnostic purposes. Applications include drug and gene delivery (Dang & Guan, 2020; Ding et al., 2020; Kim et al., 2011; Yao et al., 2020; Yuan et al., 2011; Zelepukin et al., 2019; Zhu et al., 2012), anti-bacterial and anti-viral (Akhtar et al., 2019; Hajipour et al., 2012; Karagoz et al., 2021; Khandelwal et al., 2014; Salleh et al., 2020; Shao, 2014), modulation of immune responses (Ben-Akiva et al., 2019; Fromen et al., 2015; Liu et al., 2017b; Saeed et al., 2019), as antioxidants (Omidi & Kakanejadifard, 2019; Park et al., 2008; Rajoka et al., 2020; Xia et al., 2008), neuroprotective substances (Amato et al., 2018; Dudhipala & Gorre, 2020; Schubert et al., 2006; Xue et al., 2020), promotion of bone formation (Lee et al., 2018; Moore et al., 2013; Shuai et al., 2020; Wu et al., 2019), virus detection (Chou et al., 2011; Draz & Shafiee, 2018; Medhi et al., 2020; Saylan et al., 2019) and imaging tools (Ehlerding et al., 2018; Kalyane et al., 2019; Portney & Ozkan, 2006; Spicer et al., 2018).

Metallic nanoparticles, ceramic nanoparticles, quantum dots, dendrimers, liposomes, polymeric vesicles, polymeric micelles, albumin-based nanoparticles, polysaccharide-

based nanoparticles and engineered viral nanoparticles are common nanoparticle platforms today and are either approved or have entered clinical trials (Autio et al., 2018; Everts et al., 2006; Hyung et al., 2006; Jordan et al., 2006; La-Beck & Gabizon, 2017; Lux et al., 2019; Roy et al., 2003; Soussan et al., 2009; Torchilin, 2007; Torchilin, 2005; Xie et al., 2006; Xing & Rao, 2008; Zhang et al., 2008).

2.2 Plant viruses as nanoparticles

With the advancement in synthetic biology and chemistry, various nanoscale tools can be synthesized for different purposes. The biggest challenge in manufacturing is to produce homogenous nanoparticles in a large scale (Desai, 2012; França et al., 2013). The ability to assemble millions of identical nanoparticles based on virus templates presents a viable option and solution for this problem. Virus nanoparticles (VNPs) consist of nucleic acid (RNA or DNA) encapsidated within a protein coat (CP) while virus like particles (VLPs) are genome-free. The nucleic acid encodes the genetic information for reproduction while the coat protein function to protect the nucleic acid. Viruses are very efficient in infecting its hosts and delivering its genetic material. When inside the host, viruses can hijack the host machinery to produce its progeny, producing virions that can self-assemble and form highly symmetrical structures using self-encoded protein subunits. Importantly, VNPs can be genetically engineered to replace the internal cavity with therapeutic molecules, imaging matters or other substances (Beatty & Lewis, 2019; Niehl, et al., 2016a; Vardhan et al., 2018) whereas the external surface can be conjugated with targeting ligands to allow for cell-specific delivery (Aljabali et al., 2019; Cho et al., 2017).

VNPs are biodegradable and inexpensive to produce as it can replicate continuously inside the living cell. Hence, they are amenable and favourable for industrial manufacturing. Among the reported applications of these modified viruses are to act as

diagnostic tools, for imaging and for treatment of human diseases and disorders (Look et al., 2010; Singh et al., 2006; Steinmetz, 2010). Other reports have included the use as biosensors for virus detection, imaging devices, targeted and drug delivery system as well as a chimeric vaccine for infectious diseases and cancers (Alemzadeh et al., 2018; Balke & Zeltins, 2020; Beatty & Lewis, 2019; Cho et al., 2017; Dang & Guan, 2020; Esfandiari et al., 2015; Hu et al., 2019; Le et al., 2017; Madden et al., 2017; Niehl, et al., 2016a; Sokullu et al., 2019; Steinmetz, 2011; Steinmetz & Evans, 2007).

Plant viruses are safe to handle as they lack the ability to infect human cells making them good candidates as VNPs. The production of plant viruses is relatively simple and cheap; by simply inoculating a leaf with the virus or its genetic material. High yield and easy to scale up of virus production can be achieved via their autonomous replication and *in vivo* assembly abilities within a short time (Brumfield et al., 2004; Peyret & Lomonossoff, 2015; Sainsbury & Lomonossoff, 2014; Wellink, 1998). As a result, plant viruses can be obtained in gram scales from 1 kg of infected leaf material within just 2–4 weeks (Evans, 2008; Werner et al., 2006).

The genetics and physical structure of plant viruses have been well studied. Plant viruses can self-regulate and self-assemble into highly symmetrical and polyvalent three-dimension (3D) structures with distinct shape and size in its natural hosts. The shape of plant viruses has a few varieties ranging from icosahedral (*Cucumber chlorotic mosaic virus*, CCMV, *Cowpea mosaic virus*, CPMV), *Brome mosaic virus* (BMV), *Cucumber mosaic virus* (CMV), *Hibiscus chlorotic ringspot virus* (HCRSV), *Red clover necrotic mosaic virus* (RCNMV), rods (*Tobacco mosaic virus*, TMV) to filamentous (*Potato virus X*, PVX) (Descriptions of plant viruses, 2020) (Figure 2.1).

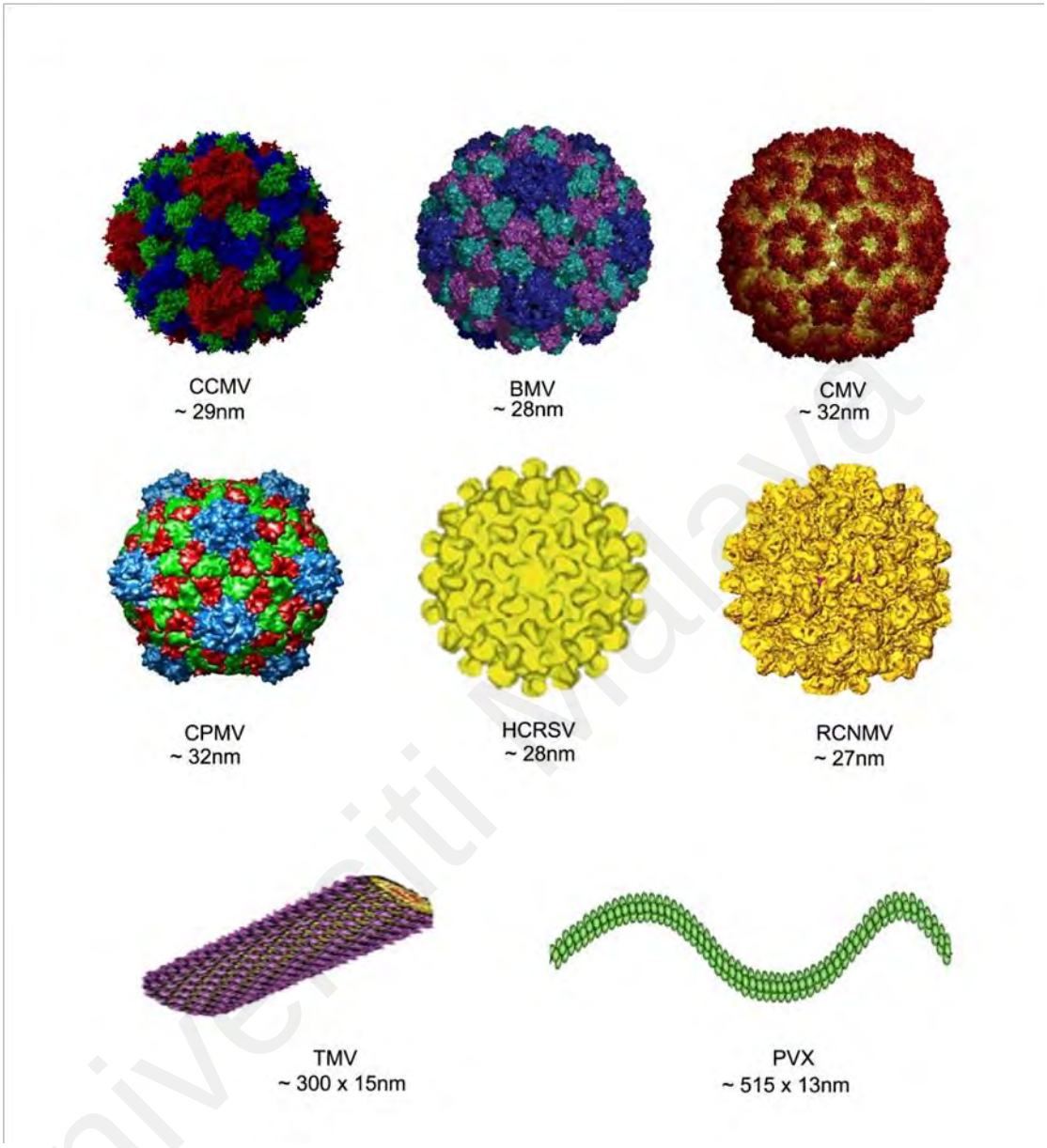

Figure 2.1: Structures of plant viruses that have been used as virus-based nanoparticles. *Cowpea chlorotic mottle virus* (CCMV), *Brome Mosaic virus* (BMV), *Cucumber mosaic virus* (CMV), *Cowpea Mosaic virus* (CPMV), *Hibiscus chlorotic ringspot virus* (HCRSV), *Red clover necrotic mosaic virus* (RCNMV), *Potato virus X* (PVX) and *Tobacco mosaic virus* (TMV) (Photo sourced from Virus World, http://www.virology.wisc.edu/virusworld/viruslist.php 2017).

The extremely robust and rigid plant viruses can tolerate harsh environments and remain intact and stable. CPMV, PVX, HCRSC and TMV are stable at 60°C, 68°C, 80°C and 90°C respectively (King et al., 2011; Lin & Johnson, 2003). They can also remain robust at extreme pH. It was reported that CPMV is stable pH ranging from 3.5 to 9.0 (Lin & Johnson, 2003); TMV is stable at pH ranging from 2 to 10 (King et al., 2011) while HCRSC is stable at acidic pH (King et al., 2011). On the other hand, plant viruses also can withstand detergent, organic solvents and high salt condition. Examples include BMV which is stable at low detergent and high salt concentrations (Yildiz et al., 2012) while HCRSV which is insensitive to organic solvents and non-ionic detergents (King et al., 2011). Last but not least, TMV can survive and remain infectious in sap for number of years (King et al., 2011).

Capsids of plant viruses consists of identical subunits, non-covalently bound with one another and are flexible to dis-assemble/re-assemble into a discrete structure with specific dimensions (Bennett et al., 2018; Daniel et al., 2010; Sikkema et al., 2007; Wong & Ren, 2018). Under different conditions of aqueous medium or by removal of certain metal ions (Liu et al., 2003; Oda et al., 2000), different morphologies of viruses can be obtained in addition to its original structure (Nguyen et al., 2009; Nguyen & Iii, 2008). TMV and PVX rods can be thermally re-shaped into spherical nanoparticles (SNPs) (Atabekov et al., 2011; Bruckman et al., 2016; Nikitin et al., 2016) while icosahedral structure of the CCMV and CPMV can be turned into multi-walled shells and tubular structures (Lavelle et al., 2009; Narayanan & Han, 2017). Under specific conditions, virus nucleic acids can be dissociated from its capsid to form empty VLPs (Villagrana-Escareño et al., 2019) with identical dimensions as the native viruses. These empty VLPs act like nano-scale protein cages which enables encapsulation of specific molecules inside. For examples CCMV was reported to carry mRNA-EGFP as a cargo and reporter gene (Villagrana-

Escareño et al., 2019) while HCRSV was loaded with polystyrenesulfonic acid and polyacrylic acid (Ren et al., 2006; Wong & Ren, 2018).

The side-chain groups of plant viruses are composed of carboxylic acids, amines and different hydroxyl-groups, including a phenolic group which can be changed from charged to neutral or vice versa. Generally, the chargeable groups in the side-chain are more accessible for common organic reactions. This gives the possibility to add non-natural components with specific properties like fluorescence dyes for tracking or imaging purposes (Shukla et al., 2018; van Rijn & Böker, 2011; Vankayala et al., 2020; Yildiz et al., 2013). In addition, native and mutant virions displayed different reactive groups on the exterior and interior surfaces which included amine containing residues (lysine) and thiols containing residues (cysteine) as well as carboxylates derived from glutamic acid and aspartic acid residues. In general, it allows the attachment of selective molecules on these residues via standard bio-conjugation techniques. For example, N-hydroxysuccinimide (NHS) activated molecules was used to decorate lysines and maleimide reactive moieties was used to decorate cysteines (Bruckman & Steinmetz, 2014; Lee et al., 2014; Steinmetz, 2011; Wege & Geiger, 2018; Young et al., 2008). Other techniques using SpyTag (ST)/SpyCatcher (SC) systems have been reported to enable specific binding to Trichoderma reesei endoglucanase Cel12A enzyme to PVX (Roeder et al., 2017).

2.3 *In vivo* characteristics of plant virus nanoparticles (pVNPs)

Before applying any pVNPs in biomedicine, it is crucial to understand their *in vivo* characteristics using animal models. Several pathways have been identified on pVNPs uptake including microtubules transport, micropinocytosis and endocytosis that is mediated by caveolar, clathrin or integrin receptors (Rajendran et al., 2010). CPMV nanoparticles entered murine RAW264.7 macrophages and human epithelial cells

through caveolar endocytosis and micropinocytosis pathways (Plummer & Manchester, 2013) while TMV nanoparticles taken up by human epithelial cells through caveolar endocytosis and micropinocytosis pathways (Tian et al., 2016). It was also observed that same pVNPs with different aspect ratio were taken up through different routes of specific cell lines. TMV nanoparticles with aspect ratios of 4 and 8 (SNPs) are taken up by HeLa cells via microtubules transport, while these nanoparticles entered HUVEC cells through clathrin endocytosis (Liu et al., 2016). On the other hand, entry of wild-type rod shape TMV nanoparticles (aspect ratio of 17) in HeLa and HUVEC cells were mediated by caveolar endocytosis and microtubules transport respectively (Liu et al., 2016).

Upon cell entry, pVNPs undergo intracellular trafficking through various compartments and located in organelles (Nkanga & Steinmetz, 2021). Genetic material or cargo carried by the pVNPs were released due to the proteolytic activity within the acidic endolysosomes as shown by CPMV and TMV nanoparticles (Gulati et al., 2018; Wen et al., 2015). Alternate pathways through lipofectamine or cell penetrating peptides have also been reported in delivery of therapeutic nucleic acids as shown in CCMV nanoparticles delivering mRNA (Azizgolshani et al., 2013), CCMV nanoparticles and TMV nanoparticles delivering siRNA (Lam & Steinmetz, 2019; Tian et al., 2018).

Studies have shown that native pVNPs are non-toxic and cause no clinical symptoms when administered *in vivo* however toxicity might occur through the cargo carried with the VNPs (Nkanga & Steinmetz, 2021). Except of CCMV which is not detected in brain, pVNPs are widely distribute in a variety of tissues including liver, spleen, kidney, lung, brain, pancreas and duodenum regardless of the routes of administration (Blandino et al., 2015; Kaiser et al., 2007; Nikitin et al., 2018; Rae et al., 2005; Shukla et al., 2014a; Singh et al., 2007). The shape of pVNPs affect the biodistribution profile *in vivo*. Filamentous pVNPs, PVX was found most abundant in the spleen compared to the icosahedral pVNPs, CPMV which accumulated most in the liver (Shukla et al., 2013). Modification of TMV

and PVX nanoparticles by PEGylation increased circulation time in blood stream and delayed clearance from the body tissues from hours to days (Bruckman et al., 2014; Lee et al., 2015). Longer circulation time increases the concentration of nanoparticles in target tissues, but it also prolongs the risk of toxicity and background noise in imaging (Thurber et al., 2010).

In term of pVNPs clearance, liver and spleen are the two main organs of the reticuloendothelial system which are responsible for eliminating pVNPs from the blood stream. Macrophages, for example Kupffer cells in liver and B cells in white pulp of spleen are the main responsible cells (Kaiser et al., 2007; Le et al., 2019; Lico et al., 2016; Rae et al., 2005; Shukla, et al., 2014a; Singh et al., 2007; Wu et al., 2013). On the other hand, degraded pVNPs are extracted through urine and faeces as seem in CCMM and PVX (Kaiser et al., 2007; Shukla et al., 2014a).

2.4 Plant virus nanoparticles as immunostimulatory

Adjuvants are added to boost the effectiveness when vaccine alone is not enough to generate protective immunity (Pasquale et al., 2015). Instead of using traditional adjuvant such as alum that mainly induces the humoral responses, researchers are beginning to add various pathogen-associated molecular patterns (PAMPs) into the formulation of candidate vaccines to boost the cellular responses through activation of the Toll-like receptor (TLR) pathway (Gupta et al., 2020; Tizard, 2021; Yan et al., 2021). There are 10 and 12 TLRs members in human and mouse respectively which recognized PAMPs from viruses, bacteria and fungi (Akira & Takeda, 2004; Kawasaki & Kawai, 2014). Most of the TLRs that recognized bacterial products are expressed at the cell surface while those recognized self and foreign genetic material (DNA and RNA) are located at endosomal compartment (Barbalat et al., 2011).

Majority of pVNPs can penetrate through the lymph vessel pores, travel into the lymph node and stimulate the antigen-presenting cells (APCs) (Shukla et al., 2017). The highly organized and repetitive nature of VNPs and VLPs mimics the PAMPs which can be recognized by diverse pattern recognition receptors (PPRs) of APCs and facilitates internalization by APCs (Gallucci & Matzinger, 2001; Irvine et al., 2013; Matzinger, 1994). Due to the DNA or RNA that encapsulated inside the coat protein of pVNPs, pVNPs are more immunogenic than VLPs and disassembled coat protein (Lebel et al., 2014; Wang et al., 2019a). Thus, make them an attractive adjuvant candidate. DNA was recognized by TLR9; double stranded RNA (dsRNA) was recognized by TLR3 while ssRNA was recognized by TLR7 and 8 (Barbalat et al., 2011).

Plant VNPs have been proven as an effective immunostimulatory. PapMV as a ssRNA pVNP can induce the expression of CD86, CD69, or H-2Kb on splenic DCs, B cells, or $CD8^+$ T cells while it's CP alone did not. This finding suggests that the ssRNA molecule within the pVNPs is responsible for its immunomodulatory properties and was further confirmed through TLR7 pathways (Lebel et al., 2014). High amount of inflammation cytokines (IFN-α and IL-6) were also detected in dendritic cells (DCs) treated with PapMV nanoparticles (Lebel et al., 2014). Similarly, CPMV, another ssRNA pVNPs stimulated proinflammation cytokines (IL-6, IL-1β, IL-12, interferon beta (IFN-β), and granulocyte-macrophage colony-stimulating factor (GM-CSF) stronger than its VLP in tumor cells through the TLR pathways (Wang et al., 2019b). The expression of CD40, CD54, CD86, and MHC I and II in mice post treatment with TMV (ssRNA) nanoparticles showed that pVNPs also can activate $CD4^+$ and $CD8^+$ subtype T-cells (Ole Kemnade et al., 2014).

The proof of concept that pVNPs could act as immunostimulator was clearly demonstrated in experiments on their anti-tumor properties. *In situ* vaccination of CPMV nanoparticles in a tumor microenviroment activated and recruited innate immune cells

with cytotoxic effects such as monocytes, tumor infiltrating neutrophils and natural killer cells to the cancer cells (Kerstetter-Fogle et al., 2019; Wang et al., 2019b). The increasing number of APCs subsequently lead to the adaptive anti-tumor immunity against metastases through $CD4^+/CD8^+$ cells (Lizotte et al., 2015). It was also noticed that the survival rate of mice bearing ovarian tumor was higher when treated with CPMV nanoparticles compared its VLPs (Lebel et al., 2014; Wang et al., 2019b). This further proved the important interaction between the viral RNA and TLR-7/8 stimulated APCs to boost and produce cytokines to initiate the anti-tumor responses (Albakri et al., 2020). On the other hand, TMV nanoparticles of different aspect ratio (300 × 18 nm of native TMV and 50 × 18 nm of sphere-like TMV particles) also showed a potent antitumor immunity against dermal melanoma (Murray et al., 2018).

Comparison among the different pVNPs suggested that the immune activation mechanisms, particularly the pro-inflammatory cyto/chemokine profiling are different. CPMV and PVX nanoparticles induced high level of IFN-γ while TMV nanoparticles activated IL-6 cytokines production (Lee et al., 2017; Murray et al., 2018). Although PapMv nanoparticles also induced the TLR-7/8 signalling as an *in-situ* adjuvant during cancer immunotherapy which is consistent with CPMV nanoparticles, it mainly acts through *IFN-α* secretion (Carignan et al., 2018; Lebel et al., 2016). In sum, the pVNPs possessed immunostimulatory properties which make them good adjuvant candidates of vaccines.

2.5 Plant virus nanoparticles as expression vectors

Plant virus-based vectors were first initiated with the genetic fusion of antigenic sequences (epitopes) to the viral CP. Viral CP can be altered by inserting, deleting or replacing of specific epitopes or amino acids residues at the N terminus, C terminus or in between the loop of the coat protein (Klem et al., 2003; Miller et al., 2007; Peabody,

2003; Plummer & Manchester, 2011; Taylor et al., 2000; Wang et al., 2002). By using this approach, the structural integrity of viral carriers can be maintained. Generally, relatively short antigenic sequences can be accommodated in most cases. Chemical coupling or physical binding of the antigen to the VLP surface using binding partner molecules were developed as an alternative to adapt whole antigens (Pomwised et al., 2016). Both genetically fused and chemical conjugate vaccines can induce the production of neutralizing antibodies and provide protection against the corresponding pathogen in animal models (Table 2.1)

Several plant virus-based vaccines have proceeded to clinical trials in humans to test their tolerability, safety and efficacy. The first such vaccine was an edible rabies vaccine expressed in spinach leaves using a TMV virus vector. Ingestion of raw spinach leaves containing these chimeric virus particles induced antibody responses to rabies virus in volunteers (Kushnir et al., 2012; Yusibov et al., 2002).

Malaria transmission-blocking vaccine based on a recombinant fusion of the *Plasmodium. falciparum* antigen, Pfs25 is the first vaccine produced under cGMP (compliance of good manufacturing production) conditions using AMV (*Alfafa mosaic virus*) virus vector. A phase I study suggested that the vaccine candidate is safe and induce antibodies against Pfs25. However, the formulation needed to be improved as the antibody level did not significantly reduce the *P. falciparum* transmission from mosquitoes to human host cells (Chichester et al., 2018). Cabral and colleagues (2017) chemically conjugated another malaria antigen, the thrombospondin-related adhesive protein (TRAP) to CMV with microcrystalline tyrosine (MCT) as an adjuvant. This formulation stimulated significant protection in the challenge with recombinant *P. berghei* (Cabral-Miranda et al., 2017).

Table 2.1: Plant virus vectors used for vaccine development against infectious disease and cancer.

Plant virus vectors	Antigen/antigens	Immune responses	References
***Alfafa mosaic virus* (AMV)**	15 amino acids domain-4 of the *Bacillus anthracis* protective antigen (PA-D4s)	Intraperitoneal injections of mice with recombinant plant virus particles harboring the PA-D4s epitope elicited both native PA antigen and the AMV CP.	(Brodzik et al., 2005)
	Peptides of rabies glycoprotein (G5-24) and rabies nucleoprotein (31D)	Elicited specific virus-neutralizing antibodies in immunized mice. Mice were protected against challenge infection with a lethal dose of rabies virus after 3rd doses delivered intraperitoneally. Oral administration of the antigen stimulated serum IgG and IgA and reduced the clinical signs caused by intranasal infection with an attenuated rabies virus strain.	(Modelska et al., 1998; Yusibov et al., 1997)
	Rabies virus glycoprotein (G protein) (amino acids 253–275) and nucleoprotein (N protein) (amino acids 404–418)	Parenteral immunization of mice was protected against challenge infection. Orally administered showed detectable levels of rabies virus-neutralizing antibodies in human.	(Yusibov et al., 2002)
	G-protein of the human *Respiratory syncytial virus*, RSV A2 strain (NF1-RSV/172–187 and NF2-RSV/170–191)	Balb/c mice immunized intraperitoneally with three doses of the purified recombinant viruses showed high levels of serum antibody specific for RSV G-protein and were protected against infection with RSV Long strain.	(Belanger et al., 2000)
	21-mer peptide (170–190) of *Respiratory syncytial virus* (RSV) G protein	Generated strong T cells responses in human DCs and both T and B cells responses in non-human primates.	(Yusibov et al., 2005)
	Amino acids 23–193 of Pfs25 of *Plasmodium falciparum*	Immunization of mice with one or two doses of Pfs25-CP VLPs plus Alhydroge induced serum antibodies with complete transmission blocking activity through the 6 months study period.	(Chichester et al., 2018; Jones et al., 2013)

Table 2.1, continued

		Phase I human study showed the vaccine was safe in healthy volunteer.	
***Bamboo mosaic virus* (BaMV)**	*very virulent Infectious bursal disease virus* (vvIBDV) VP2 protein	Immunized chicken produced antibodies against IBDV and protected from vvIBDV (V263/TW strain) challenges.	(Chen et al., 2012)
	37 amino acid residues (T128-N164) of *Foot and mouth disease virus* (FMDV) VP1	Induced anti-VP1 neutralizing antibodies and *IFN-γ* production in swine. Immunized swine were protected against FMDV challenge.	(Yang et al., 2007)
	2A peptide (LLNFDLLKLAGDVESNPGP) of *Foot and mouth disease virus* (FMDV)	Stimulated effective neutralizing antibodies against FMDV infection in mice.	(Chen et al., 2017)
***Cowpea Chlorotic Mottle Virus* (CCMV)**	Chemically conjugate of S9 peptide (a mimic of the group B streptococcal type III capsular Polysaccharide)	Chemically conjugate vaccine elicited a Th1 response in mice.	(Pomwised et al., 2016)
***Cowpea mosaic virus* (CPMV)**	Outer membrane protein F peptide 18 linked to OM protein F peptide 10 of *Pseudomonas aeruginosa*	Generated high titres of *P. aeruginosa*-specific IgG that opsonized the bacteria for phagocytosis by human neutrophils and afforded protection upon challenge with two different immunotypes of *P. aeruginosa* in mice. Protection against challenge with *P. aeruginosa* in the mouse model of chronic pulmonary infection.	(Brennan et al., 1999; Gilleland Jr. et al., 2000)
	17-mer peptide sequence from *Canine parvovirus* (CPV) VP2 protein	Developed IgG2a isotype peptide-specific antibody response and the released of *IFN- γ*. Serum antibody from both subcutaneously vaccinated and intranasally-vaccinated mice showed neutralizing activity against CPV *in vitro*. Protected dogs from lethal challenge from CPV.	(Langeveld, et al., 2001; Nicholas et al., 2002)
	D2 peptide of fibronectin-binding protein B (FnBP) of *Staphylococcus aureus*	Intranasal immunization of mice primed CPMV-specific T cells and generated high titers FnBP-specific immunoglobulin G (IgG) in sera. Oral immunization also	(Brennan et al., 1999)

Table 2.1, continued

		generated CPMV- and FnBP-specific serum IgG at lower titers.	
	19 amino acids of B cells epitope from the merozoite surface antigen-1 of the malaria parasite *Plasmodium falciparum*	Induced *P. flaciparum specific* antibody in rabbit.	(Yasawardene et al., 2003)
	22 amino acids of the transmembrane gp41 protein of HIV-1 IIIB	Immunized intranasally produced both HIV-1-specific IgA in feaces and IgG2a, serum antibody in mice.	(Durrani et al., 1998)
	VP2 capsid protein of *Mink enteritis virus* (MEV)	Protect mink from lethal challenge from MEV.	(Dalsgaard et al., 1997)
	Human "consensus" M2e peptide (SLLTEVETPIRNEWGCRCNDSS DP, M2eh) and the M2e peptide of avian influenza virus strain A/Chicken/Kurgan/05/2005 (SLLTEVETPTRNEWEC RCSDSSD, M2ek).	Intranasal immunization of mice with purified Flg-4M protein induced high levels of M2e-specific serum antibodies and provided protection against lethal challenge with influenza virus.	(Mardanova et al., 2015)
	Chemically conjugate of S9 peptide (a mimic of the group B streptococcal type III capsular Polysaccharide)	Chemically conjugated vaccine elicited a Th1 response (IgG2a, IFN-) in mice.	(Pomwised et al., 2016)
	Human epidermal growth factor receptor 2 (HER2) peptides CH401 (AA 163-182), P4 (AA 378-394)	Peptide-VLPs elicit the production of HER2-specific antibodies in mice.	(Shukla et al., 2017)
	Human epidermal growth factor receptor 2 (HER2) CH401 epitope (AA 163-182)	*In vivo* tumor challenge of pre-immunized mice reduces tumor growth and improved survival.	(Cai et al., 2019)
***Cucumber green mottle mosaic virus* (CGMMV)**	41 amino acids *Hepatitis B virus* surface antigen (HBsAg).	Stimulated approximately three-fold of anti-HBsAg immunoglobulin production by cultured peripheral blood mononuclear cells (PBMC).	(Ooi et al., 2006)
	R9 mimotope of *Hepatitis C virus* (HCV) envelope protein E2	Elicited a R9-specific humoral response in rabbits. Displayed a significant immunoreactivity in patient	(Natilla et al., 2004; Piazzolla et al., 2005)

Table 2.1, continued

***Cucumber mosaic virus* (CMV)**		serum. Down-modulated the lymphocyte surface density of CD3 and CD8 in patients with chronic HCV infection and induced a significant release of IFN-γ, IL-12 p70 and IL-15 by lymphomonocyte cultures.	
	Chemically coupled *Plasmodium vivax* thrombospondin-related adhesive protein fused to a universal T-cell epitope of the tetanus toxin (CMVtt), formulated with Microcrystalline tyrosine	Induced the strong T cells response and conferred protection against challenge with recombinant *P. berghei*.	(Cabral-Miranda et al., 2017)
***Papaya mosaic virus* (PapMV)**	23 amino acids of M2e protein of influenza virus	Induced production of anti-M2e antibody and led to 100% protection against a challenge of 4LD50 with the WSN/33 strain.	(Denis et al., 2008)
	Hepatitis C virus (HCV) E2 epitope	Internalized *in vitro* by bone-marrow-derived antigen presenting cells (APCs) and induced anti-E2 specific antibody in C3H/HeJ mice.	(Denis et al., 2007)
	Influenza virus M1 epitope gp100 protein epitope	Mediate MHC class I cross-presentation and generate avid T antigen-specific cells in human cells.	(Leclerc et al., 2007)
	Chemically couple of influenza nucleoprotein (NP)	Combination of the NP nanoparticles with the PapMV-M2e nanoparticles protects mice from infectious challenges by influenza strains H1N1 and H3N2.	(Bolduc et al., 2018)
	Chemically conjugate influenza nucleoprotein with Sortase A (adjuvant)	Significantly improved the humoral and CTL immune response in mice.	(Laliberté-Gagné et al., 2019)
***Plum pox potyvirus* (PPV)**	VP60 structural protein of *Rabbit hemorrhagic disease virus* (RHDV)	Protected rabbit against a lethal challenge with RHDV when delivered subcutaneously.	(Fernández et al., 2001)
	VP2 capsid protein of *Canine parvovirus* (CPV)	Developed CPV-specific neutralizing antibodies in immunized mice and rabbits.	(Fernández et al., 1998)

Table 2.1, continued

***Tomato bushy stunt virus* (TBSV)**	13-amino-acid of HIV-1 p24 nucleocapsid protein derived from the V3 loop of *Human immunodeficiency virus* (HIV-1) glycoprotein 120 (gp120)	Reacted with p24-specific antibodies. Recognized by V3-specific monoclonal antibody and by human sera from HIV-1-positive patients.	(Joelson et al., 1997; Zhang et al., 2000)
	Ricine toxin chain A peptide (16 AA)	Antibodies from immunized mice recognized ricin toxin.	(Kumar et al., 2009)
***Potato virus X* (PVX)**	Highly conserved ELDKWA epitope from glycoprotein (gp) 41	Elicited high levels of HIV-1-specific immunoglobulin G (IgG) and IgA antibodies in intraperitoneally or intranasally immunized mice.	(Marusic et al., 2001)
	Peptides of the classical swine fever E2 Glycoprotein	Partially purified virions were able to induce an immune response in rabbits.	(Marconi et al., 2006)
	Human papillomavirus- E7 fusion oncoprotein	Immunized C57BL/6 mice developed both humoral and cell-mediated immune responses and were protected from tumor development after challenge with the E7-expressing C3 tumoral cell line.	(Franconi et al., 2002)
	Surface antigen 1 (SAG1) of *Toxoplasma gondii.*	C3H mice vaccinated with SAG1 showed significantly lower brain cyst burdens. Immunization with SAG1-expressing leaves elicited a specific humoral response with predominant participation of type IgG2a.	(Clemente et al., 2005)
	R9 peptide from the *Hepatitis C virus* (HCV) envelope protein E2	35% of sera from patients infected chronically with HCV were found to react specifically with PVXR9-2ACP particles.	(Uhde-holzem et al., 2010)
	C-terminal fused *Hepatitis C virus* (HCV) E2 epitope	Pro-long humoral response (more than 4 months) against both the CP and the fused HCV E2 epitope.	(Denis et al., 2007)
	Human "consensus" M2e peptide (SLLTEVETPIRNEWGCRCNDSS DP, M2eh), and the M2e peptide of avian influenza virus strain A/Chicken/Kurgan/05/2005 (SLLTEVETPTRNEWEC RCSDSSD, M2ek).	Intranasal immunization of mice with purified Flg-4M protein induced high levels of M2e-specific serum antibodies and provided protection against lethal challenge with influenza virus.	(Mardanova et al., 2015)

Table 2.1, continued

	B-cell epitope from the extracellular domain of Human epidermal growth factor receptor 2 (HER2)	Immunizations of FVB/N mice resulted in the production of HER2-specific antibodies, as shown by ELISA and confocal microscopy using HER2-positive human cancer cell lines.	(Shukla et al., 2014b)
	Human epidermal growth factor receptor 2 (HER2) peptides CH401 (AA 163-182), P4 (AA 378-394)	Peptide-VLPs elicit the production of HER2-specific antibodies in mice.	(Shukla et al., 2017)
PVX/ CMV CP	36–51 amino acids of the *New Castle disease virus* (NDV) F protein epitope	Purified VLPs were immunoreactive with CMV antibodies as well as with epitope-specific antibodies to NDV. Chickens immunized with purified VLPs developed antigen-specific response.	(Natilla et al., 2006; Natilla & Nemchinov, 2008)
***Tobacco mosaic virus* (TMV)**	VP1 protein from *Foot and mouth disease virus* (FMDV) epitope	Protective against challenge of FMDV in guinea pig and swine through parenterally administration. Protective against challenge of FMDV in guinea pig through oral administration.	(Jiang et al., 2006; Wu et al., 2003)
	Bovine herpesvirus type 1 (BHV-1) protein glycoprotein D (gDc) epitope	Vaccinated cattle developed specific humoral and cellular immune responses directed against both the viral gD and BHV-1 particles. Induced protection after challenge with the virulent BHV-1.	(Filgueira et al., 2003)
	Neutralizing epitope of *Hepatitis C virus* (HCV) fused to the C-terminal of the B subunit of cholera toxin (CTB).	Intranasal immunization of mice elicited both anti-CTB serum antibody and anti-HVR1 serum antibody which specifically bound to HCV virus-like particles.	(Nemchinov et al., 2000)
	Nontoxic B subunit of heat-labile toxin (LTB) of *Escherichia coli*	Intranasal delivery of recombinant LTB TMV induced LTB-specific IgG1 antibodies in mice.	(Wagner et al., 2004)
	Peptide of outer membrane protein F of *Pseudomonas aeruginosa*	Developed protection against challenge with wild-type *P. aeruginosa* in a mouse model of chronic pulmonary infection.	(Gilleland Jr. et al., 2000; Staczek et al., 2000)

Table 2.1, continued

	15 amino acids of the poliovirus type 1 Sabin viral capsid proteins (VP3 and VP1)	Induced antibodies against VP1 and VP3 as well as TMV CP in mice after intraperitoneal immunization.	(Fujiyama et al., 2006)
	VP8 fragment of the VP4 protein from *Bovine rotavirus* (BRV) strain C-486	Intraperitoneal immunization of mice developed specific antibody against VP8 and protected against challenge of BRV.	(Filgueira et al., 2004b)
	Human immunodeficiency virus type 1 (HIV-1) Tat protein epitope	Oral immunization of mice developed specific antibody against HIV-1 Tat protein.	(Karasev et al., 2005)
	Epitope of ore protein, p24, from a clade C *Human immunodeficiency virus type 1* (HIV-1)	Immunization of rabbit developed strong and specific humoral response.	(Filgueira et al., 2004a)
	Domain III of the dengue 2 envelope protein (D2EIII, amino acids 298–400)	Intramuscular immunization of mice developed neutralization antibody against dengue type 2 virus.	(Saejung et al., 2007)
	F1 and V antigens of *Yersinia pestis*	Subcutaneously immunization of guinea pigs generated systemic immune responses and provided protection against an aerosol challenge of virulent *Y. pestis.*	(Santi et al., 2006)
	5B19 epitope from the spike protein of *Murine hepatitis virus* (MHV)	Induced parenteral and mucosal immunization in mice and protection from challenge with MHV strain JHM.	(Koo et al., 1999)
	OmpA-like protein, chaperone protein DnaK and lipoprotein Tul4 of highly virulent *F. tularensis* SchuS4 strain.	Induced a strong humoral immune response and protected mice against respiratory challenge.	(Banik et al., 2015)
	Pfs25 protein of *Plasmodium falciparum*	Induced transmission blocking antibodies that persisted for up to 6 months post immunization in mice and rabbits.	(Jones et al., 2015)
	RhoA protein of *Respiratory syncytial virus* (RSV)	Inhibition of RSV growth in cell culture.	(Konstantin et al., 2015)
	Chemically conjugate of Virulence factors F1 (17.6 kDa) and LcrV (37 kDa) of *Yersinia pestis*	Conjugated F1 and LcrV viral particles protected mice against lethal challenge of *Y. pestis*.	(Arnaboldi et al., 2016)

Table 2.1, continued

	Tetra-antigen vaccine of *Francisella tularensisis* with CpG as adjuvant	Two vaccine doses protected 80% of mice from lethal pathogen challenge.	(Mansour et al., 2018)
***Zucchini yellow mosaic virus* (ZYMV)**	Dermatophagoides pteronyssinus group 5 allergen (Der p 5)	Squash extract containing vDer p 5 inhibited Der p 5-specific IgE synthesis and airway inflammation in mice.	(Hsu et al., 2004)
	MAP30 (Momordica anti-HIV protein, 30 kDa) and GAP31 (Gelonium anti-HIV protein 31 kDa)	Exhibit comparable anti-viral, anti-tumor, and anti-microbial activities in cell cultures.	(Arazi et al., 2002)

Several plant virus-based peptide vaccines are also being evaluated in veterinary trials. Among them are vaccine against parvovirus designed using CPMV vector proved can protect dogs against lethal challenge with canine parvovirus (Langeveld et al., 2001); *Foot and mouth disease virus* (FMDV) vaccine constructed using a *Bamboo mosaic virus* (BaMV) vector protected swine against FMDV challenge (Yang et al., 2007) while vaccine against *Porcine circovirus* (PCV) integrated on CMV nanoparticles protected pigs against PCV (Gellért et al., 2012).

Cancer is one of the leading causes of death globally. A melanoma-specific peptide was fused onto TMV coat protein via chemical coupling. The modified TMV nanoparticles showed better protection in the tested animals than the peptide alone in tumor challenge (McCormick et al., 2006b). The p33 peptide derived from *Lymphocytic choriomeningitis virus* (LCMV) chemically conjugated onto CMV coat protein together with microcrystalline tyrosine effectively slowed the development of mouse melanoma (Mohsen et al., 2019). Besides, three icosahedral plant viruses (CCMV, CPMV and *Sesbania mosaic virus* (SeMV)) were chemically coupled with HER2 CH401 epitope, a breast cancer epitope. Although all 3 chimeric vaccines can induce T-cell-mediated immune responses, reduced tumor development and enhanced the survival rate in a mouse tumor model, CPMV-based vaccine shown better immunotherapeutic than CCMV and SeMV (Cai et al., 2019). The studies above showed that plant viruses can be genetically modified to express epitopes or cancer peptides and induced stronger immunity as well as protection compared to epitopes or peptide alone.

2.6 Plant VNPs as expression vector of influenza

2.6.1 Influenza -Taxonomy, transmission and epidemiology

Influenza or also known as the flu in general, is an extremely contagious disease that repeatedly infects respiratory system of human and animals. It is cause by the pathogen known as influenza virus, a respiratory virus from the family "*Orthomyxoviridae*" (Shaw & Palese, 2013). Up to date, there are six genera of *Orthomyxoviridae* reported. They are *Influenza viruses A*, *B*, *C*, *D*, *Thogotoviruses* and *Isavirus* (Collin et al., 2015; Hause et al., 2014; Palese & Shaw, 2007; Sugawara et al., 1991). Influenza A, B and C are closely related but serological and immunological distinctive by their internal nucleoprotein and matrix proteins (Palese & Young, 1981; Sugawara et al., 1991; Usha et al., 1993; Yamashita et al., 1988; Palese & Shaw, 2007). Type A is broadly found in warm-blooded animals for example mammals, birds and bats whereas types B and C are dominant in humans (Brunotte et al., 2016; Ma et al., 2015; Lamb and Krug, 1996). *Influenza A viruses* (IAV) are divided into subtypes based on the surface antigens, hemagglutinin (HA) and neuramiridase (NA). Up to date, there are 18 subtypes HA (H1-H18) and 11 subtypes NA (N1-N11) of influenza A (Brunotte et al., 2016; Ma et al., 2015; Tong et al., 2013). H1N1 and H3N2 are the 2 known IAV subtypes currently circulating among humans (Centers of Disease Control and Prevention, 2021).

Influenza viruses spread in human population via air droplets, direct skin to skin contact or indirect contact with respiratory secretion (Kamps and Reyes-Terán, 2006). Common symptoms are sudden onset of high fever, aching muscles, headache and severe malaise, non-productive cough, sore throat and rhinitis. Duration of symptoms is longer in the elderly compared to young adults (Metlay et al., 1998). Most infected people can self-recover within one to two weeks without medication. However, complication including pneumonia, myocarditis, sinusitis, encephalitis, myositis, Reye's syndrome might occur in young children, the elderly and immunocompromised patients and cause

fatalities (Zimmerman, 2007). Acute respiratory distress syndrome was the main death cause of adults in 1918 due to a cytokine storm (Osterholm & Ph, 2005).

Every year, there is 3-5 million severe influenza diseases reported worldwide accompanied by 250,000-500,000 deaths (World Health Organization (WHO), 2021). The people who are in the high-risk group are elderly aged more than 65 and children less than 2 years old as well as those with medical conditions Centers of Disease Control and Prevention, 2021). In Malaysia, influenza virus is also detected throughout the year (Sam et al., 2013) and contributed about 2-3.2% of total respiratory virus detected in children (Khor et al., 2012; Rahman et al., 2014; Zamberi et al., 2003) where influenza A is more dominant than influenza B (Sam, 2015) (22.3% for seasonal H1N1 and 14.7% for seasonal H3N2).

When a strain of influenza virus mutates due to antigenic shift, there will be an influenza pandemic and spreads globally. The 1918-1919 Spanish pandemic was one of the most devastating disease outbreaks in human history. It was caused by the H1N1strain (Reid et al., 1999; Taubenberger et al., 1997) and resulted in about 20-50 million deaths globally (Taubenberger et al., 2001). Re-emergence of H1N1 influenza at 2009 was designated by the WHO as a pandemic 2009 virus. It was first reported in Mexico in April 2009 and estimated to have caused more than 200,000 deaths during the first 12 months of its circulation (Dawood et al., 2012). In Malaysia, the virus was first identified on 15th May 2009 and reached the peak of the outbreak between August to September with 12,307 cases reported and 77 deaths. Sam and colleagues showed that the seroprevalence of A(H1N1)pdm09 increased from 3.7% pre-pandemic to 21.9% post-pandemic, which is about 18.1% of cumulative incidence, mostly in people aged <30 years old (Sam et al., 2013).

2.6.2 Structures and genomics of influenza virus

Influenza viruses are complex enveloped viruses with pleomorphic structure (Figure 2.2). The lipid envelope of the virus is originated from the host cell membrane, covered by three protruded proteins, the hemagglutinin (HA) and neuraminidase (NA) and matrix 2 (M2). The ratio of HA:NA varies from 4:1 to 5:1 with a small proportion of M2 (Goraya et al., 2015; Palese & Shaw, 2007). Underneath the envelope and three integral membrane proteins is a layer of matrix (M1) protein which surrounds the virion core in helix order (Calder et al., 2010). Inside the virion core are eight copies of rod-like of ribonucleoprotein (RNP) with different length (Noda et al., 2006). The negative sense, single stranded viral RNAs (vRNAs) are surrounded by nucleoprotein (NP) and the RNA-dependent RNA polymerase (RdRp) complexes (polymerase basic protein 1 (PB1), polymerase basic protein 2 (PB2) and polymerase acidic protein (PA). These vRNAs encode 11 types of proteins namely PB1, PB2, PA, NP, HA, NA, M1, NS1, NEP, M2, and PB1-F2. The nuclear export protein (NEP, previously known as non-structural protein 2, NS2) is also present in the virion core and associated with the M1 protein (Richardson et al., 1991; Yasuda et al., 1993) (Figure 2.3). Table 2.2 is summary of influenza A protein's functions.

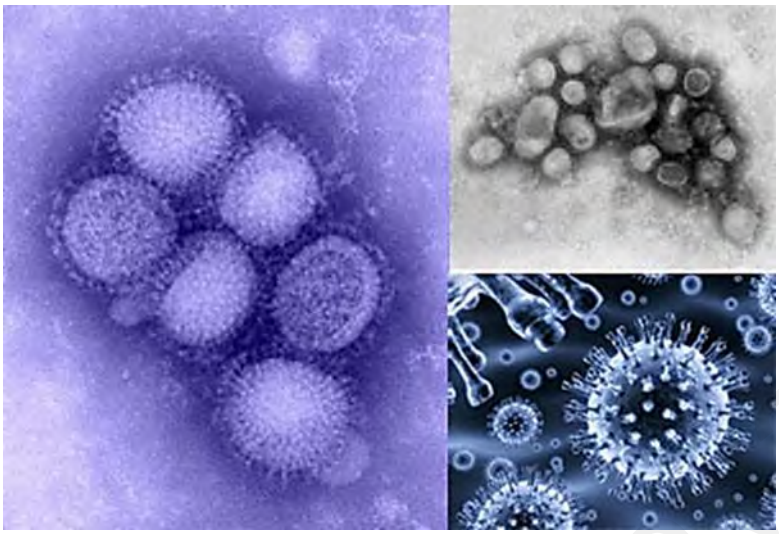

Figure 2.2: Electron micrographs of H1N1 Virus - Center for Disease Control. It has a pleomorphic structure with spherical, filamentous, elliptical or occasionally irregular shape (Noda, 2012) (Photo sourced from Center for Disease Control and Prevention (https://www.cdc.gov/h1n1flu/images.htm?s_cid=cs_001).

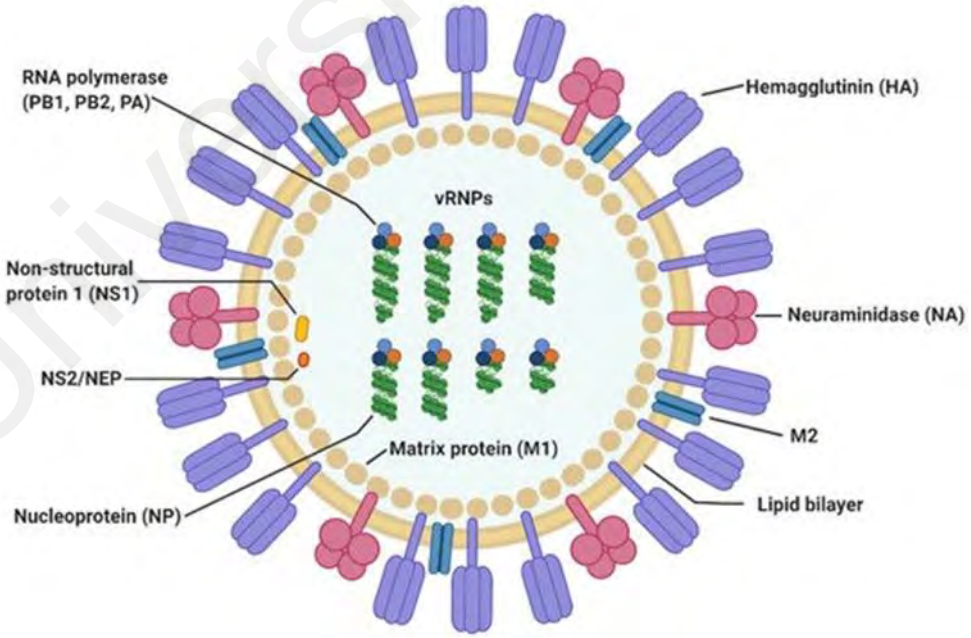

Figure 2.3: Structure of an *Influenza A virus* (Photo sourced from Jung & Lee, 2020).

Table 2.2: Influenza virus proteins and their functions.

Proteins	Functions	References
Polymerase Protein complexes (PB1, PB2, PA)	Templates for transcriptional and replication activity; virus pathogenesis (induce apoptosis); host range determination	(Chen et al., 2001; Eisfeld et al., 2015; Maier et al., 2008)
Hemagglutinin (HA)	Antigenic sites recognize by the host immune system; cleavage sites by host proteases; receptor binding sites attaching to sialic receptors on the target cell; fusion peptides mediating membrane fusion	(Riwilaijaroen & Uzuki, 2012)
Neuraminidase (NA)	Responsible for virus approach to the target cells by cleavage of sialic acids from respiratory tract mucins; fusion of viral and cell membranes; facilitates budding of new virions; induce apoptosis	(Matrosovich et al., 2004; Shtyrya et al., 2009; Wagner et al., 2000)
Nucleoprotein (NP)	Trafficking of RNPs in nuclear and cytoplasmic; mediating viral mRNA transcriptional and vRNA replication	(Portela & Digard, 2002; Turrell et al., 2013)
Matrix protein (M1)	Virus budding and assemblies; virions morphology determinant; nuclear export of viral nucleoproteins (with vRNP and NEP/NES)	(Burleigh et al., 2005; Calder et al., 2010; Gomez-Puertas et al., 2000)
Membrane protein (M2)	Ion channel; inducing apoptosis and blocking macroautophagy; uncoating of the viral RNA from the matrix protein M1; filamentous virion formation; budding of virions	(Gannagé et al., 2009; Rossman et al., 2010a; Rossman et al., 2010b; Schnell & Chou, 2008; Wang et al., 2011)
Nuclear export protein, NEP (NS2)	Export of newly synthesis RNPs to cytoplasm; regulating viral genomic vRNA, cRNA and viral mRNA synthesis; host range adaptation; aid in release of budding virions	(Paterson & Fodor, 2012)
Multi-functional protein (NS1)	Inhibition of host immune responses (interferon α/β production); modulate virus replication cycle (vRNA replication, viral protein synthesis and general host-cell physiology)	(Hale et al., 2008; Jia et al., 2010)

2.6.3 Current treatments for influenza

Currently, there are 4 classes of anti-influenza drugs available in the market. The neuraminidase inhibitors (Oseltamivir, oral; Zanamivir, inhalational; Peramivir, intravenous/intramuscular; and Laninamivir, inhalational), M2 inhibitors (Adamantanes, Rmantadine and rimantadine), viral RNA synthesis inhibitor (Ribavirin) and polymerase inhibitor (Favipiravir) (Dunning et al., 2014; Lee & Ison, 2012). A new class of antiviral drug for influenza, Baloxavir Marboxil (trade name, Xofluza) was approved recently. It targets the viral PA polymerase subunit and prevents the transcription of viral mRNA of influenza A and B with a single dose. Clinical trial with Baloxavir Marboxil treatment showed significant reductions in influenza virus titer and symptoms in patients with uncomplicated influenza (O'Hanlon & Shaw, 2019; Uyeki, 2018).

The benefit of antiviral drug use in controlling the influenza pandemic was reduced after the onset of drug resistance strains of the virus (Barr et al., 2008; Barr et al., 2007a; Barr et al., 2007b; Deyde et al., 2007; Goldhill et al., 2018; Hayden & Jong, 2011; Li et al., 2015; Uehara et al., 2020). Vaccination against influenza is often recommended for high-risk groups, such as pregnant women, children and elderly and immune suppressed patients (Belot et al., 2017; Hayward, 2017; Ortiz & Neuzil, 2017; Rolfes et al., 2017). The seasonal trivalent influenza vaccines (TIV) and quadrivalent influenza vaccine (QIV) are currently employed which both comprise two IAV (H1 and H3) and a single B-strain or two B-strains (B/Victoria and B/Yamagata). The QIV is replacing TIV in some countries as it improved the protection against influenza B and is more cost effective (Crepey et al., 2020; Mennini et al., 2018; Tao et al., 2021).

Besides using whole or enveloped virus as above, using the epitopes corresponding to the immunogenic, conserved sequences of microbial proteins emerged as an alternative approach (Skwarcynski & Toth, 2016). The epitope-based vaccines (EVs) are focused on using the minimal fragment of proteins to activate the lymphocyte. Short peptides in

between 8-10 amino acids activate the cellular or T cells responses while longer regions activate the humoral or B cells responses (Kametani et al., 2015; Oyarzun & Kobe, 2015; Testa & Philip, 2012). The main benefit of immunization with an epitope-based vaccine is its ability to immunize with a minimal structure yet stimulate an effective specific immune response as well as avoiding potential undesirable effects such as autoimmunity.

Numerous EVs have been designed through *in silico* methods included *Lymphocytic choriomeningitis virus*, *Foot and mouth disease virus*, *Human coronavirus*, dengue, *E. coli*, *Epstein-Barr virus* and *Mers-Cov* (Ali et al., 2017; Alonso-padilla et al., 2017; Emran, 2014; Liu et al., 2017a; Mehla & Ramana, 2016; Sahrawat & Kaur, 2016; Shi et al., 2015). EVs of influenza have been demonstrated by incorporating epitopes from HA (HA1 and HA2), NA, NP, M1 and M2e (Table 2.3).

Table 2.3 Viral antigenic targets of influenza vaccines (Lee et al., 2014).

Viral proteins	Targeted site	Proposed mechanism(s) of protection
Hemagglutinin (HA1)	Receptor binding globular head domain	Strain specific neutralizing antibodies block the virus entry; generate? weak cellular immunity.
Hemagglutinin (HA2)	Stalk domain with fusion activity	Non-neutralizing antibodies, inhibition of fusion, maturation of the HA, and antibody dependent cell-mediated cytotoxicity.
Neuraminidase (NA)	Conserved sialidase active site	Non-neutralizing antibodies, Inhibition of virus release and virus spread.
Nucleoprotein (NP)	T cell epitopes	Cell lysis by $CD8^+$ cytotoxic T-lymphocytes (CTL), $CD4^+$ T lymphocyte mediated cytolysis.
Matrix (M1)	T cell epitopes	Cell lysis by $CD8^+$ CTL, $CD4^+$ T lymphocyte mediated cytolysis.
Matrix 2 ion channel (M2)	Ectodomain of M2 (M2e)	Non-neutralizing antibodies, antibody dependent natural killer cell activity, complement mediated lysis, antibody dependent cell-mediated cytotoxicity, $CD4^+$ and $CD8^+$ T cells mediated cytolysis.

Several plant viruses have been reported to express recombinant influenza proteins. PapMv has been used to express M1 epitope (amino acids 57-65), M2e epitope (amino acids 2-24 /6-14); NP epitope (amino acids 147-155), HA11 epitope (9 amino acids) of influenza A (Babin et al., 2013; Carignan et al., 2015; Denis et al., 2008; Hanafi et al., 2010; Leclerc et al., 2007; Rioux et al., 2012; Thérien et al., 2017). The PapMv coat protein harbouring a shortened M2e (amino acids 6–14, EVETPIRNE) (PapMv-sM2e) induced significant levels of M2e specific IgG and IgG2a antibodies in mice sera. The mice vaccinated with PapMV-sM2e not only survived the challenge with a sub-lethal dose of influenza but the morbidity and mortality of the mice were also reduced. The protection is dose-dependent and correlated with anti-M2e Ig2a antibody levels (Carignan et al., 2015). Bolduc and colleagues (2018) further combined the NP with the PapMV-M2e nanoparticles, which resulted in the protection of mice from infectious challenges of influenza strains H1N1 and H3N2 (Bolduc et al., 2018). On the other hand, chemical coupling of PapMv with NP and Sortase A induced significant level of humoral and CTL immune responses (Laliberté-Gagné et al., 2019).

NP epitope (amino acids 336-374) of influenza A was expressed by PVX and successfully activated specific $CD8^+$ cells (Lico et al., 2009). Likewise, *Malva mosaic virus* (MaMV) was used to express M2e peptide with OmpC adjuvant. This vaccine improved the protection in mouse against heterosubtypic strain of influenza and can be a potential vaccine for dogs (Leclerc et al., 2013). Another adjuvant vaccine reported using a TMV vector, Squalene-adjuvanted HA-TMV led to 100% protection against virus challenge in mice (Mallajosyula et al., 2014). In another study, mice immunized with a single 15µg dose of *Papaya ringspot virus* (PRSV) expressing the HA peptide (87-120) of Influenza A/H1N1 also led to 100% survival in a lethal virus challenge (Mallajosyula et al., 2014). Together, these studies suggest that epitope-based vaccine expressed using plant VNPs has the potential to be influenza vaccine.

2.7 *Tobamovirus* as plant virus vector

The genus *Tobamovirus* is a positive, sense, single stranded RNA viruses (Strauss and Strauss, 1988) in the family *Virgaviridae* (Adams et al., 2017). These rod shape viruses are around 18 nm in diameter and 300-310 nm in length. *Tobamovirus* genomes are linear and monopartite, around 6.3–6.5 kb encoding 4 proteins:125-130 kDa and 180-190 kDa replicase proteins of which the latter was expressed by readthrough of the leaky amber stop codon; a 30 kDa movement protein and a 17-18 kDa coat protein (Viral Zone, 2022). A methylated nucleotide cap (m7G5'pppG) is found at the 5' terminus while a tRNA-like structure is located at the 3' terminus.

Till now, there are 37 reported species of *Tobamoviruses* (Adams et al., 2017). Apart from CGMMV, CMV and TMV which have been constructed to use as 'smart vehicles' for diagnostic and therapeutic purposes (refer to section 2.2), as immunostimulators (refer to section 2.4) and as expression vectors for vaccines of infectious diseases and cancers (refer to session 2.5), other species including *Tobacco mild green mosaic virus* (TMGMV) and *Turnip vein clearing virus* (TVCV) have also been constructed to apply in agriculture, bone formation and protein purification.

TMGMV has been formulated to use as bioherbicide. It is commercially available by the name Solvinix, manufactured by BioProdex and used in the state of Florida, US to treat tropical soda apple (TSA) weed (Charudattan and Hiebert, 2007; Ferrell et al., 2008). Tested plants died between 20-50 days post inoculation with TMGMV (Charudattan and Hiebert, 2007). When TMGMV was mixed with synthetic herbicides for example with 2,4-D ester or amine, metsulfuron, or hexazinone, it increased the TSA control to 80%-100% (Ferrell et al., 2008).

Besides, TMGMV was also fabricated to deliver nematicides. TMGMV loaded with ~1500 copies of the anthelmintic drug, crystal violet (CV) to form cvTMGMV. The

treatment efficacy and solubility were compared between the cvTMGMV and CV alone. Although the treatment efficacy of cvTMGMV towards *Caenorhabditis elegans* nematode culture was slightly lower compared to CV alone, cvTMGMV enable to penetrate deep into the soil to deliver CV and killed the nematodes feeding on the roots of the plants (Chariou and Steinmetz, 2017).

TVCV coated with poly-d-lysine (PDL), a biocompatible polymer enables to improve bone formation. The coated nanoparticles proved to mediate the osteogenic differentiation of bone derived mesenchymal stem cells (BMSCs) by upregulation of osteogenic markers at gene and proteins levels (Metavarayuth et al., 2015). On the other hand, TVCV can also be used to purify antibody. A 133 amino acids fragment of protein A (an antibody-binding agent for IgG purification) can fused to the C' terminal of *Turnip vein clearing virus* (TVCV) through a flexible linker (GGGGS)3 or a helical linker (EAAAAK)3. By using this fusion technique, more than 2,100 copies of protein A can be packed in TVCV, forming an immunoadsorbent which can be used to purify the mABs in industry scale with high recovery yield and purity at 50% and >90% respectively (Werner et al., 2006).

2.8 Application CGMMV as expression vector

Cucumber green mottle mosaic virus (CGMMV) is an RNA plant virus which belongs to the genus *Tobamovirus*, in the family *Virgaviridae*. It was first reported in *Cucumis sativus* from the UK in 1935 (Ainsworth, 1935). Since then, several strains have been detected in Europe, Middle East, Asia and Australia (Dombrovsky et al., 2017). It is a single-stranded, positive sense RNA genome encapsidated in coat protein (CP) with a 5' methylated nucleotide cap (m7G5'pppG) and a 3' tRNA-like structure. These terminal structures protect the ends of their RNA strands from degradation (Ohno et al., 1972; Tan et al., 2000; Ugaki et al., 1991). The 6,424 nucleotides genome encodes for 4 proteins.

The 128 kDa and read-through 183 kDa RNA-dependent RNA polymerase (RdRp) proteins are essential for viral replication with the expression ratio of about 10:1 (128 to 183 kDa proteins) during infection (Watanabe et al., 1999). The 30 kDa cell-to-cell movement protein (MP) and the 17 kDa coat protein (CP) are translated from 3' co-terminal subgenomic RNAs (Kim et al., 2014) while its coat protein has 160 amino acids residue with a molecular mass of 17261Da (Figure 2.4).

Like other *Tobamoviruses*, CGMMV is a rod-shaped virus, approximately 300 nm long and 18 nm in diameter (Figure 2.5). An intact virion contains about 2,100 identical protein subunits, which form a rigid-handed helix of pitch close to 23 Å with 49 subunits in three turns. A single strand of RNA follows the protein helix at a radius of 40 Å and each coat protein binds three consecutive nucleotides (Lobert et al., 1987; Wang and Stubbs, 1994). CGMMV virus particle is stable and rigid. It can remain infectious in the sap for more than a year at room temperature and for 10 minutes at more than 90°C. Hence, killing infectious CGMMV requires heating the sap for several hours at temperature more 80°C (Scholthof, 2008). This character makes it a good nanoparticle candidate.

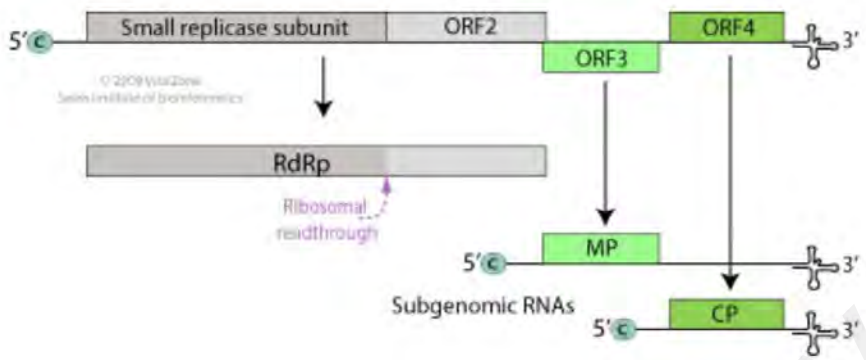

Figure 2.4: Structure and genome organisation of CGMMV. OFR, open reading frame; RdRP, RNA dependent RNA polymerase; MP, movement protein; CP, coat protein (Hulo et al., 2011).

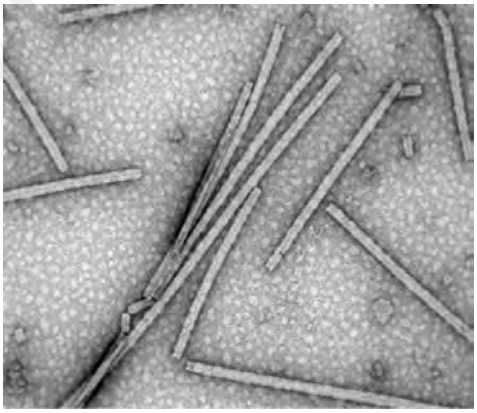

Figure 2.5: Electron micrograph of *Cucumber green mottle mosaic virus* (CGMMV) virions (Photo sourced from Dombrovsky et al., 2017).

To our best knowledge, there are currently 5 publications that reported the use of CGMMV as expression vector (Jailani et al., 2017; Ooi et al., 2006; Teoh et al., 2009; Tran et al., 2019; Zheng et al., 2015). Two studies used T7 promoters to *in vitro* transcribe the full length CGMMV into infectious RNA before inoculating the RNA onto the plants (Ooi et al., 2006; Teoh et al., 2009) while the other 3 studies used 35S promoter and agroinfiltration techniques to infect the plants (Jailani et al., 2017; Tran et al., 2019; Zheng et al., 2015). The differences between the studies above are the insertion location of foreign protein in CGMMV genome, with/without the read-through codon and the sequences of read-through codon. A binary vector of CGMMV with both 35S and T7 promoters was constructed by Park and colleagues (2017) but its function as expression vector for foreign protein was not studied (Park et al., 2017).

To express GFP in CGMMV nanoparticles, Zheng and colleagues (2015) were inserted the GFP genes in between the movement protein (MP) and coat protein (CP) and transcribed with the native subgenomic promoter via agroinfiltration. However, this strategy resulted in a very weak GFP expression in *Nicotiana benthamiana* (Zheng et al., 2015). In year 2017, Jalaini and colleagues (2017) were inserted the GFP genes at the 3' terminal of stop codon of CP without a read-through codon. In this case, formation of CGMMV virions as well as GFP proteins were detected in *N. benthamiana* at the initial stage but not stable over time (Jailani et al., 2017).

On the other hand, read-through codon strategy was used to express foreign proteins. Ooi and colleagues (2006) successfully expressed the 33 amino acids of *Hepatis B virus* surface antigen (HBsAg) in *Cucumis melo* var Earl favorite using T7 promoter. The HBsAg was placed after the read-through codon sequence (TCT-AAA-TAG-CAA-TTA). at the 3' terminal of CP (Ooi et al., 2006). However, similar strategy with one mutation at the first codon of the read-through sequence (TCC-AAA-TAG-CAA-TTA; from TCT to TCC without alter the amino acid residue) caused a deletion at 21 d.p.i. when Teoh and

colleagues (2009) used it to express dengue epitope of 44 amino acids in the same host (Teoh et al., 2009). In year 2019, Tran and colleagues (2019) performed a study using these two read-through codons and naming them as RT1 (TCT-AAA-TAG-CAA-TTA) and RT2 (TCC-AAA-TAG-CAA-TTA). The 9 amino acids of neutralizing epitope (NE) of PRRSV glycoprotein 5 (GP5) were cloned at the 5' terminal of RT 1 and RT2 to be expressed via agroinfiltration in cucumber and *N. benthamiana*. When the NE protein was expressed using RT1, the symptoms were very mild and unexpectedly, only the wild-type CGMMV was formed. In contrast, both wild-type and chimeric CGMMV-NE proteins expressed using RT2 were successfully detected when infected in cucumber but not in *N. benthamiana* (Tran et al., 2019).

Besides being used as an expression vector, CGMMV NP was constructed as a virus-induced gene silencing (VIGS) vector to carry a 69–300 nucleotides phytoene desaturase (PDS) gene and was successful in silencing the PDS gene in *N. benthamiana* and in cucurbits (watermelon, melon, cucumber and bottle gourd) (Liu et al., 2020). Notably, the silencing effect maintained for more than 2 months and could be passaged to the next generation making it useful to study gene function, restrict the spread of the viral pathogens and inducing resistance breeding in cucurbits (Liu et al., 2020).

In this study, we studied the *in vivo* characteristics of CGMMV nanoparticles in mice and its function as an immunostimulator *in vitro* in murine macrophages. Furthermore, we also engineered the CGMMV to be an expression vector for a series of HA and M1 epitopes of Influenza A/H1N1 virus using RT1 read-through stop codon strategy and tested their immune response in mice. Besides, we also explored the alternative propagation hosts from Malaysia melon varieties to substitute CGMMV original propagation host, *C. melo* var Earl favorite from Japan.

CHAPTER 3: METHODOLOGY

3.1 Propagation of CGMMV

3.1.1 Potential of local melon varieties as propagation hosts for CGMMV

Seeds of the *Cucumis melo* (*C. melo*) var Melon 3 (M3), Melon 4 (M4), Melon 5 (M5), Melon 6 (M6), WQ, PG and Yehe were purchased from Green World Genetics Sdn Bhd while seeds of *C. melo* var Earl favorite was contributed by Dr. Tan Siang Hee (CropLife Asia, Singapore). Plants were grown in a Sastec plant growth chamber (Segar Alatan Sains, Malaysia) at 28°C with full light for 12 hours and 25°C without light for 12 hours. The wild-type CGMMV-SH was a gift from Dr Tan Siang Hee. CGMMV-SH will be referred as CGMMV throughout this thesis. CGMMV nanoparticles were gently rubbed on the carborundum dusted cotyledon. The cotyledons were rinsed with distilled water 30 minutes after inoculation. Plants inoculated with 0.01 M potassium phosphate buffer were kept as negative controls. CGMMV VNPs were harvested at 10, 20 and 30 days post inoculation.

3.1.2 Detection of CGMMV nanoparticles via ELISA

Enzyme-linked immunosorbent assay (ELISA) was carried out using an ELISA kit from Agdia, USA. The procedures were carried out according to the manufacturer's protocol. Briefly, the 96-well microtitre plate was pre-coated with 100 µL of anti-CGMMV coating antibody, sealed with parafilm and incubated overnight at 4°C. The plate was then washed by emptying the wells and refilled till overflowing with 1× PBS with 0.1% Tween 20 (1× PBS-T). These washing steps were repeated for 4 to 8 times. After washing, the plate was tapped firmly on a folded paper towel to dry the wells.

One hundred milligrams of symptomatic leaf sample (upper new leaf) were freshly collected, wrapped with aluminium foil followed by rapid freezing in liquid nitrogen. The leaf was crushed in a chilled sterile pestle and mortar and transferred to a liquid nitrogen-

cooled 1.5 mL microcentrifuge tube. General extraction buffer was added to the tube before the sample was thawed following a ratio of 1:10 (tissue weight: extraction buffer volume). The sample was mixed thoroughly by vortexing and clarified through centrifugation at 8,000 g for 5 minutes. One hundred microlitres of each sample supernatant was then dispensed into sample wells following the loading diagram. A volume of 100 µL of the positive control supernatant (1:1 dilution) was dispensed into positive control wells; 100 µL of non-infected leaf sample supernatant was dispensed into the negative control wells while 100 µL of extraction buffer was dispensed into empty wells to act as blank. The plate was set inside the humid box and incubated for 2 hours at room temperature.

A few minutes before the incubation was completed, the enzyme conjugate (anti-CGMMV alkaline phosphatase conjugated antibody) was prepared according to the manufacturer's protocol. When incubation was completed, the plate was washed as described previously. After dispensing of the enzyme conjugate into the wells, the plate was incubated in the humid box for 2 hours at room temperature. The plate was then washed as described previously. The pNPP solution was prepared by dissolving one pNPP tablet into 5 mL of pNPP buffer. Wells were emptied and washed with 1× PBST before 100 µL of pNPP solution was dispensed into each well for color development. The plate was incubated for another 30-60 minutes in the humid box. The reaction was stopped by adding 50 µL of 3 M sodium hydroxide to each well. The wells were measured in a Tecan GENios Microplate Reader at 405 nm.

3.1.3 Extraction of CGMMV nanoparticles

Symptoms shown on the inoculated plants were recorded. CGMMV nanoparticles were extracted from inoculated plants at 30 days post-inoculation. The virus purification method was modified from Ooi et al., 2006. Two milliliters per gram (frozen plant

material) of potassium phosphate buffer (0.1 M, pH 7.0) containing 0.1% β-mercaptoethanol was added to the frozen plant material and then homogenized using a domestic blender. The mixture was separated by centrifugation at 10,000 g for 30 minutes at 4°C. The supernatant was sieved through two layers of muslin cloth. Subsequently, 4 g of sodium chloride (NaCl) and 4 g of PEG 6,000 were added to each 100 mL of the supernatant. The mixture was stirred until all the NaCl and the PEG 6,000 were dissolved entirely then stored overnight at 4°C.

After the incubation, the solution was centrifuged at 10,000 g for 30 minutes at 4°C. The virus pellet was then re-suspended in 20 mL of 0.01 M phosphate buffer (pH 7.0) for each 100 mL of initial plant extract. The virus suspension was then cleared by centrifugation at 6,000 g for 15 minutes 4°C. The supernatant was transferred to a new tube. NaCl and PEG 6,000 was added to the supernatant at a final concentration of 4%. The solution was centrifuged at 10,000 g for 30 minutes at 4°C. The pellet was dissolved again in 0.01 M phosphate buffer (pH 7.0). The solution was centrifuged at 6,000 g for 15 minutes 4°C. The clear supernatant was transferred to a new tube. The mixture was subjected to ultra-centrifugation at 110,000 g for 1 hour 30 minutes at 4°C for further purification. The purified virus nanoparticles were resuspended in 0.01M phosphate buffer (pH 7.0) and kept at 4°C for immediate use or at -20°C for long-term storage.

3.1.4 Transmission electron microscope (TEM)

The integrity of the virus nanoparticle was examined using TEM. Ten microlitres of virus particle in 0.01 M phosphate buffer (pH 7.0) was dropped onto a carbon grid and incubated for 15 minutes at room temperature. Excess liquid was removed using a filter paper. A drop of 2% uranyl acetate was dropped on the carbon grid and incubated for 5 minutes. Excess 2% uranyl acetate was removed by using filter paper. Grids were kept at room temperature at least three days before being examined using a transmission electron

microscope model, EFTEM Libra 120 (Carl Zeiss, AG, Germany) at a magnification of 31.50K.

3.1.5 UV/ visible absorbance

Total dry weight of virus nanoparticles in standard purified preparations was quantified by using a nanophotometer (Implen, Germany) to its extinction coefficient = 3.18 in dilute solution at 260 nm. A 260/A280 ratio of about 1:19 is expected for intact virus nanoparticles.

3.1.6 Polyacrylamide Gel Electrophoresis and Western Blotting

A fifteen percent (15%) polyacrylamide gel (SDS-PAGE) was prepared in a Mini-PROTEAN® Cell (Bio-Rad, USA) according to the manufacturer's protocols. Ten microlitres of virus coat protein were mixed with 10 µL of 2 × SDS sample buffer, boiled for 5 minutes followed by quick chilled on ice. The samples and protein marker (Thermo Scientific, USA) were spun down and loaded onto the SDS-PAGE gel. The gel was run at 180 V for one hour with 1 × running buffer.

After one hour, the gel was stained with Coomassie staining protocol. The gel was submerged in enough volume of fixation solution and was left to float freely in the tray by shaking using a rotary shaker for 30 minutes. The fixation solution was drained away and replaced by a Coomassie solution and shaken for 60 minutes. Then the gel was developed with de-staining buffer until the bands can be visualized and examined using a gel documentation system (Alpha Innotech AlphaImager Image Analysis System, USA).

A PVDF membrane was cut to size and soaked in methanol for 5 minutes. The membrane, filter paper and fiber pad were soaked in the protein transfer buffer for 30 minutes. After separating the protein samples by gel electrophoresis, the stacking gel was

removed. The electroblotting cassette of Mini Trans-Blot Electrophoresis Transfer Cell (Bio-Rad, USA) was assembled and placed between the electrodes in the blotting unit with cold transfer buffer, according to the manufacturer's protocol. The transfer process was carried out at 100 V for 1 hour and stirred with a cool pad.

After transfer, the membrane was removed from the cassette. The membrane was blocked for one hour at room temperature with 5% skim milk in 1 × TBS. After pouring off the blocking buffer, antibody buffer (1:100 dilution of anti-CGMMV-AP antibody in 2% skim milk dissolved in 1 × TBS) was added to the membrane and incubated at 4°C overnight. After the overnight incubation with antibody, the membrane was washed three times with TBS contained 0.1% Tween-20 (1 × TBS-T) washing buffer for 10 minutes each wash. Five milliliters of the Western Blue substrate (Promega, USA) were added to the membrane until the bands could be seen. The membrane was washed with distilled water and dried before image was captured using a scanner.

3.2 *In vivo* characteristics of CGMMV nanoparticles in mice

3.2.1 Animals

All animals used in this study were 6–8 weeks old female Balb/c mice obtained from Monash University (Sunway Malaysia Campus). Animals were used in compliance with IACUC approved protocols (Ethics approval reference no: 2015-181201/IBS/R/L/LWW).

3.2.2 Subcutaneous injection and samples collection

A total of 48 mice were divided into two groups. A group of 24 mice was inoculated with 100 µL of CGMMV nanoparticles (100 µg) via subcutaneous (sc) injection in the right thigh. Another 24 mice were inoculated with 100 µL sterile 0.01 M potassium phosphate buffer (pH 7.0) as mock- inoculation group. The thigh of the mouse was disinfected with 70% ethanol swap before injection. Each mouse was examined for

ruffled fur, tachypnea, dyspnea, seizure, lack of movement or sustained rapid movement around the cage 2 to 3 hours post s.c injection and as well as daily inspection over the 2 weeks of the experiment. The injection site (right thigh) was also examined for the redness, swelling, pus formation and rashes. The body weight of the mouse was measured pre-injection and dissection.

3.2.3 RNA Extraction and RT-PCR

To detect the presence of CGMMV in mice, total RNA was extracted using easy-BLUETM Total RNA Extraction Kit (Intron, Korea) following the manufacturer's protocol. Brain, bone marrow, duodenum, kidney, liver, lung, spleen and stomach tissues were ground to powder form using liquid nitrogen. Total RNA was treated with DNase I (Invitrogen, USA) at 37°C for 30 minutes. One microgram of RNA was mixed with 1 μM of 17K CP reverse primer, incubated at 70°C for 5 minutes and transferred to ice. The mixture and 0.25 μM of 17K CP forward primer were transferred to AccuPower® RT-PCR PreMix (Bioneer, Korea) and top up the volume to 20 μL follow manufacturer protocol. cDNA synthesis was performed at 42°C for 60 minutes and 95°C for 5 minutes followed by PCR amplification procedure as follows; 35 cycles of 1 minute denaturation at 95°C, 30 second annealing at 55°C, and 15 seconds extension at 72°C and ended with 5 minutes of final extension at 72°C, resulting in a 150 bp PCR product. The sequences of the primers are as listed in Appendix V. The PCR products were analyzed on a 2% agarose gel alongside a 100 bp DNA ladder (Thermo Fisher Scientific, USA), stained with ethidium bromide and visualized on gel documentation system (Alpha Innotech AlphaImager Image Analysis System, USA).

3.2.4 Preparation and characterization of CGMMV-488 nanoparticles

The Alexa-488 (A-488) NHS reactive ester fluorescent dye (Invitrogen, USA) was conjugated to purified CGMMV nanoparticles by mixing 200 μL (2 mg) of CGMMV

nanoparticles in 0.01 M phosphate buffer, pH 7.0 with 50 µL of 10mg/mL Alexa-488 and gentle agitated at room temperature for 24 hours. The conjugated VNPs were separated from free dye by precipitation with 4% PEG 6,000 and 4% NaCl overnight at 4°C. Two round of high-low centrifugations (10,000 g, 30 minutes; 6,000 g, 15 minutes) were performed at 4°C. The characteristics of conjugated (CGMMV-488 nanoparticles) and non-conjugated CGMMV nanoparticles (dissolved in 0.01 M phosphate buffer, pH 7.0) was analyzed using four methods: TEM (section 3.1.4), UV/visible absorbance (section 3.1.5), SDS-PAGE gel electrophoresis (section 3.1.6.) and size exclusion chromatography (section 3.2.5). The concentration of CGMMV-488 nanoparticles was determined by UV/visible spectroscopy based on the Beer-Lambert law specific extinction coefficients for CGMMV nanoparticles and A-488 (71,000 M−1cm−1 at 495 nm).

3.2.5 Size exclusion chromatography

All the buffers and solutions used with FPLC were filtered with 0.22 µM filter and degassed before used. One hundred microlitres loop was attached to injection valve and cleaned with 20% ethanol to remove air bubbles in the loop using a syringe in the injection valve. The Superdex 75 10/300GL was assembled on the ÄKTA FPLC (GE healthcare, USA). Pump wash step was executed by washing the column with 10 column volumes (cv) of distilled water and 10 cv of 0.01 M potassium phosphate buffer, pH 7.0 at a flow rate of 1 mL/min to equilibrate the column. One hundred microlitres of virus protein sample were injected into the loop and set the flow rate at 0.8 mL/min and ran with 0.01 M potassium phosphate buffer, pH 7.0. The UV channels (260 nm, 280 nm, and 488 nm) were turned on. When the run was completed, the column was washed with 5 cv of 0.01 M potassium phosphate buffer, pH 7.0, 5 cv of distilled water followed by 5 cv of 20% ethanol. The column was removed, re-capped and kept in 4ºC.

3.2.6 Pharmacokinetics and biodistribution studies

To determine the biodistribution of CMMV nanoparticles, a total of 48 Balb/c mice were divided into two groups. A group of 24 mice was inoculated with 100 µL CGMMV-488 nanoparticles (100 µg) via subcutaneous (s.c) injection in the right thigh. Another 24 mice were mock- inoculated with 100 µL sterile 0.01 M potassium phosphate buffer (pH 7.0) as negative control group. Four mice injected with CGMMV-488 nanoparticles and 4 mice from the negative control group were sacrificed at 1, 3, 5, 7, 10 and 14 days post-injection. All mice were sacrificed after anesthetization with an intraperitoneal injection of pentobarbitone. Seven tissues samples (brain, duodenum, kidney, liver, lung, spleen and stomach) were harvested from each mouse. Freshly harvested tissues were weighed, homogenized in 1× PBS and centrifuged at 10,000 g for 15 minutes at 4°C. A volume of 100 µL of supernatant from each tissue was dispensed into 96-well microtiter plate in triplicate. Fluorescence reading of blood and tissue samples were measured using Tecan Infinite M200 Pro Microplate Reader. The fluorescence intensity/gram was calculated and normalized against the tissues of mice injected with 0.01 M potassium phosphate buffer.

To measure the half-life of CGMMV nanoparticles in blood, blood was collected from the heart at 1, 3, 5, 7, 10 and 14 days post-injection, transferred into MiniCollect® Plasma Tubes (Greiner bio-one, Austria) and centrifuged for 10 minutes at 3,000 g to remove blood cells from plasma. A volume of 100 µL of plasma was dispensed into 96 wells microtiter plate in duplicate. Plasma spiked with known concentrations of CGMMV-488 (100 µg, 50 µg, 25 µg, 12.5 µg, 6.125 µg and 0 µg) was used as a standard curve. The concentration of CGMMV-488 nanoparticles in blood was measured and determined based on the standard curve.

3.2.7 Hemolysis assay

Blood was collected from the heart of four Balb/c mice, pooled and transferred into 1.5 microcentrifuge tubes to and centrifuged at 500 g for 10 minutes. The supernatant was removed and an equivalent volume of 1 × DPBS (without calcium and magnesium) was added to reach the previous volume. Centrifugation was repeated twice. The red blood cells (RBCs) were counted and diluted to 1×10^9 cells/mL with 1 × DPBS (without calcium and magnesium). Fifteen microlitres of 100 µg of CGMMV and CGMMV-488 nanoparticles (dissolved in 0.01 M phosphate buffer, pH 7.0) were pipetted into 96 wells round-bottom microtiter plate in triplicate. Sterile 1 × DPBS (without calcium and magnesium) was used as a negative control while 1% Triton X-100 was used as a positive control. The 96 -well plate was incubated in 37°C incubator for one hour. Plates were centrifuged at 1,000 g for 10 minutes. One hundred microliter of the supernatant was careful pipetted and transferred to a new flat bottom 96-well plate. The absorbance (abs) of the supernatant was measured using a Tecan GENios Microplate Reader at 540 nm. The percentage of hemolysis is calculated based on the formula as below:

$$\% \text{ hemolysis} = \frac{(\text{abs of sample}) - (\text{abs of negative control})}{(\text{abs of positive control}) - (\text{abs of negative control})}$$

3.2.8 H&E histology

A section of the spleen and liver samples (no more than 2-3 mm thick and 10 mm long) were kept in 10% formalin overnight prior to transfer to 70% ethanol. The tissues were then transferred to 85% ethanol and immersed for 30 minutes followed by 2 times immersions in 95% ethanol for 30 minutes for dehydration. After dehydration, the samples were proceeded to 2 times immersion in terpineol solution, 30 minutes for each immersion. Subsequently, the samples were transferred to tubes containing terpineol-

paraffin (1:1) mixture which was melted at 60°C before use. The tubes were left in the oven for 30 minutes or more.

Samples infiltrated with terpineol-paraffin mixture were transferred to a tube containing paraffin using heated forceps and kept in an oven (60°C) for one hour. The process was repeated twice, and the samples were ready for sectioning using a microtome at 10 µm thickness. The tissue sections were carefully transferred and spread onto the slides layered with Mayer's albumin and distilled water. The slides were placed on the slide warmer (40-45°C) until dried.

The slides were immersed into Coplin jars containing the solutions for nucleic acids and cytoplasm staining. The nucleic acid staining procedures were as follows: 3 minutes in Xylene (repeated 2 ×); 3 minutes in 95% ethanol (repeated 2 ×); 3 minutes in 70% ethanol; 3 minutes in distilled water; 15 seconds in alum harris haematoxylin; 3 minutes with running tap water; 2-3 seconds in hydrochloric acid; 1 minute rinse under running water; 2-3 seconds in 0.2% sodium bicarbonate and lastly 3 minutes rinse under running water.

After the nucleic acid staining was completed, the slides proceeded to cytoplasmic staining as follows: 1-2 minutes in eosin solution; quick rinse (~ 1 second) in 95% ethanol (repeated 2 ×); 3 minutes in 100% ethanol lastly 3 minutes in Xylene solution. The slides mounted with a coverslip and checked under a Zeiss Observer.Z1 inverted microscope (Carl Zeiss, Germany).

3.2.9 Detection of anti-CGMMV antibody in mouse serum

The 96-well microtitre plate was pre-coated with 100 µL of CGMMV nanoparticles (10 µg/mL) in bicarbonate buffer (pH 9.6) and incubated overnight at 4°C. The plate was washed with PBS with 0.1% Tween-20 (1 × PBS-T) and blocked with 100 µL of 1 ×

PBS-T with 2% BSA for 1 hour at room temperature. The plate was then washed with 1 × PBS-T for eight times. The serum samples diluted to 1:50 in 1 × PBS-T with 2% BSA and were added to the wells and incubated for 1 hour at room temperature. After the incubation, the plate was washed with 1 × PBS-T and tapped dried. Subsequently, 100 µL of alkaline peroxidase-conjugate goat anti-mouse IgG (Thermo Fisher Scientific, USA) diluted to 1:5,000 in 1 × PBS-T with 2% BSA was added to the well. The plate was incubated an hour at room temperature. After that, the plate was washed with 1 × PBS-T. One hundred microliters of the pNPP substrate were added to the well. Thirty minutes later, the absorbance was measured using Tecan GENios Microplate Reader at 405 nm. The absorbance of antibody from injected mice's sera was normalized against the sera of mice injected with 0.01 M potassium phosphate buffer.

3.2.10 Detection of IgG subclass in mouse serum

Sera were analyzed for IgG1, IgG2a, IgG2b and IgG3 by direct ELISA (Sigma, USA). ELISA plates were coated with 100 µL of per well of CGMMV nanoparticles (10 µg/mL) in 1 × carbonate-bicarbonate buffer (pH 9.6) (Agdia USA) overnight at 4°C. The well was then blocked for 1 hour at room temperature with 3% BSA containing 0.05% Tween-20. Plasma samples (1:50 dilutions with 1 × PBS-T) was added to the well and incubated for 2 hours at room temperature. Bound immunoglobulins were detected using isotype-specific anti-mouse antibodies conjugated to alkaline phosphatase. Samples were detected using pNPP and absorbance was measured using Tecan GENios Microplate Reader at 405 nm.

3.2.11 Re-Infectivity of CGMMV nanoparticles

The CGMMV nanoparticles was recovered from liver and spleen by precipitation with 4% PEG 6,000 and 4% NaCl. Whole blood samples were collected from healthy mice following a cardiac puncture and transferred to blood collection tubes (section 3.2.2).

Blood serum or plasma were transferred to a new tube and incubated with CGMMV nanoparticles (100 µg) in a 1:1 (v/v) ratio at 37°C for 30 minutes. Samples were inoculated onto the cotyledon of *C. melo* var Earl favorite dusted with carborundum. Positive control of Earl favorite was inoculated with purified CGMMV nanoparticles while negative control of Earl favorite was mock- inoculated with 0.01 M potassium phosphate buffer, pH 7.0. Formation of symptoms was observed and recorded. Inoculated and new leaves were harvested at 14 days. Total RNA was extracted, and RT-PCR was performed as described in section 3.2.3. The sequences of the primers are as listed in Appendix V.

3.3 *In vitro* immunostimulatory effect of CGMMV nanoparticles in macrophage

3.3.1 Macrophage cell culture (RAW264.7 cells)

Murine macrophage cell line, RAW264.7 cells (ATCC ®TIB-71™) from Abelson murine leukemia virus-induced tumor was kindly contributed by Dr. Ea Chee Kwee (UTSW Medical Center, Dallas, USA). The cell line was cultured using RPMI with 10% FBS and 1 × Pen/ Strep (Gibco, USA) in 37°C and 5% CO2.

3.3.2 CGMMV *in vitro* uptake and localization studies

A total of 1×10^6 of RAW264.7 cells were prepared as described in section 3.1 and treated in triplicate with a range of volume of CGMMV-488 particles for 2 hours at 37°C with 5% CO2. Uptake was first analyzed using fluorescence microscopy after washed the cell twice with 1 × PBS buffer. The *in vitro* uptake of CGMMV-488 was directly visualized using the Olympus IX73 fluorescence microscopy, and the image was captured by Olympus DP73 camera (Olympus, Japan). The cells were stained with 25 nM lysotracker for 15 minutes at room temperature in the dark, rinsed two times with 1x PBS followed by staining with DAPI (1:10,000) for 30 seconds at room temperature in the

dark. The cells were rinsed two times with 1 × PBS before visualized under fluorescence microscope.

Uptake of the cells was also analyzed using flow cytometry. Cells were spun down at 400 g for 10 minutes and washed two times with PBS, fixed with 2% formaldehyde and kept in 4°C (in the dark) before analyzed using Macs Quant Flow Cytometer and Macs Quantify software (Miltenyi Biotech, Germany).

3.3.3 Cytotoxicity assay

RAW264.7 cells were cultured in triplicate in 96-well culture plates at a concentration of 1×10^5 cells per well. Cells in each well were treated with various concentrations of CGMMV virus particles in triplicate. Untreated RAW264.7 cells were acted as a control. At day 0, 1, 2 and 3, a 50 µL of MTT solution (2 mg/mL) was added to the wells and incubated for 3 hours at 37°C with 5% CO2. After incubation, media and MTT solution were discarded, and 100 µL of DMSO was added into the wells followed by gently swirling of the plate. The absorbance of each well was measured by an Tecan Infinite M200 Pro Microplate Reader at 570 nm.

3.3.4 Induction of gene expression

CGMMV-488 was added into the 2.5×10^5 of RAW264.7 cells in a 24-well cell culture plate and treated for 2, 4, 6,12 and 24 hours. Zero hours (0 hours) was used as a control. Total RNA was extracted from raw cells using GeneJET RNA extraction kit (Thermo Fisher Scientific, USA). One microgram of RNA was used as a template for cDNA synthesis by using M-MuLV reverse transcriptase (NEB, USA), RNase Inhibitor (NEB, USA) and random primer (Invitrogen, USA) in a total volume of 20 µL. Subsequently, real time-PCR was carried out using 3 µL of cDNA (1:5 dilution), 1 × Lo-Rox SyBr Green premix (Bioline, UK), 0.1 µM of forward and reverse primers and performed with ABI 7500 (Applied Biosystem, USA). A three steps cycle was carried out: initial

denaturation at 95°C for 2 minutes; 40 cycles of denaturation at 95°C for 5 seconds, annealing at 60°C for 10 seconds and extension at 72°C for 10 seconds. The sequences of the primers are as listed in Appendix V. The RPL32 primer was acted as an endogenous control. Relative comparison of fold change of the genes was calculated using $2^{(-\Delta\Delta Ct)}$.

3.3.5 Cytokine detection

Cytokines (IL-6, IL-12, and TNF-α) were measured from RAW264.7 cell's supernatants after 2, 4, 6, 12 and 24 hours post-treatment with CGMMV using an ELISA kit (Thermo Fisher Scientific, USA) following the manufacturer's protocols. Zero hours was used as a control.

3.3.6 *In vitro* activation of RAW264.7 cells

RAW264.7 cells (1×10^6) were treated with 75 µg of CGMMV. Cells were collected at 6 hours, 12 hours and 24 hours, washed and stained with anti-CD54-PerCP, anti-CD40-APC and anti-CD86-PE (Miltenyi Biotech, Germany). Zero hours was used as a control. Ten thousand cells were analyzed using flow cytometry (Miltenyi Biotech, Germany). The experiment was repeated twice.

3.3.7 Protection of RAW264.7 cells from virus infection

An amount of 75 µg of CGMMV nanoparticles was treated with 2.5×10^5 of RAW264.7 cells for 6 hours. Then, multiplicity of infection (MOI) of 1.0 of recombinant *Vesicular stomatitis virus* tagged with green fluorescence protein (VSV-GFP) was added to the wells. After 12 hours, the GFP of the cells was analyzed with an Olympus IX73 inverted microscope and photographed using an Olympus DP73 digital camera and Cellsens standard software. The cells were later harvested for total RNA extraction. The experiment was repeated by using 150 HAU/mL of *Sendai virus* (SeV) and the cells were harvested at 14 hours post infection with SeV. To quantify the mRNA level, total RNA

was extracted using GeneJET RNA extraction kit (Thermo Scientific, USA). An amount of 1 µg of total RNA was used as template for cDNA synthesis using random hexamer (Invitrogen, USA).

To determine the virus load (vRNA), total RNA was harvested at 2 hours post infection with VSV or SeV. Next, cDNA was synthesized using the forward primer of GFP and SeV coat protein primer sets as well as the reverse primer of RPL32. Quantitative qRT-PCR was performed using 3 µL of cDNA (1:5 dilution), 1× Lo-Rox SyBr Green premix (Bioline, UK), 0.1 µM of forward and reverse primers and performed with ABI 7500 (Applied Biosystem, USA). A three steps cycle was carried out: initial denaturation at 95°C for 2 minutes; 40 cycles of denaturation at 95°C for 5 seconds, annealing at 60°C for 10 seconds and extension at 72°C for 10 seconds. The sequences of the primers are as listed in Appendix V. The *RPL32* primer acted as an endogenous control. Relative comparison of fold change of the genes was calculated using $2^{(-\Delta\Delta Ct)}$.

3.4 Construction of chimeric CGMMV vectors with influenza epitopes

3.4.1 Identification of B and T cell epitopes of HA and M1 proteins

The B cell and T cell epitopes of HA and M1 proteins were identified from the Immune Epitopes Database (IEDB) (Vita etal., 2018). Epitopes which had shown positive immune response were pre-selected. A read-through amber stop codon (asc) with sequences of SKLQL and the selected epitopes were fused at the 3' terminal of the CGMMV coat protein. The glutamic acid was added to adjust the pI of the protein to or nearer to 5.08.

3.4.2 *In vitro* modelling of coat protein and RNA secondary structure

The chimeric CGMMV virus coat proteins were predicted using homology modeling from iterative threading assembly refinement (I-TASSER) (Xu et al., 2015; Zhang, 2008). The crystallized structure of CGMMV coat protein, 1cgm (3.4 Å) (Wang and Stubbs,

1994) and 1Ei7 (2.4 Å) (Bhyravbhatla et al., 1998) was downloaded from RCSB Protein Database (Berman et al., 2000) and used as a template.

One hundred models of each chimeric CGMMV coat protein were generated with loop and side chain refinement. Three models with the lowest energy were validated using PROCHECK (Laskowski et al., 1993). The model with the average highest confident score was chosen as the model of the respective chimeric CGMMV. The 3D structure of protein models was viewed using VMD viewer (Humphrey et al., 1996).

As the influenza epitopes were inserted at the 3' terminal of the coat protein, the looping pattern of the structures was analyzed to compare the RNA secondary structure between wild-type and chimeric which encoded the coat protein (RNA 4). The RNA secondary structures were predicted using Vienna RNA secondary prediction server (Lorenz et al., 2011).

3.4.3 Gene synthesis

The amber stop codon (asc) and selected epitopes DNA sequences were sent to AIT, Singapore for gene synthesis. HindIII and SphI restriction enzymes sequence were added at the 5' and 3' terminal of epitopes. Epitopes were cloned into pUC 57 vector and sent in the lyophilized form. Fifty microlitres of distilled water were added to dissolve the plasmid.

3.4.4 Construction of chimeric CGMMV vectors

The plasmid CGMMV 1410 was constructed from pCGHB3110803 (Ooi et al., 2006) by first digesting the Hepatitis B surface antigen sequence from the plasmid using Hind III and Sph I restriction enzyme. The pUC 57 vector (10 µg) containing HA and M epitopes was digested with Hind III and Sph I restriction enzymes. Digested epitopes

were cloned into CGMMV 1410 to create the chimeric CGMMV vectors. Plasmids were extracted and subjected to sequencing.

Full-length chimeric CGMMV genome (with the T7 promoter and influenza epitopes) were amplified using T7doubleG forward primer and CGMMV 3'UTR reverse primer. PCR was carried out in 0.2 µL of thin wall tubes with the following components: 1 × PCR buffer, 0.2 mM of dNTP, 0.2 µM of gene-specific primer forward and reverse primer, 50 ng of plasmid and 2.5 U of Velocity Polymerase (Bioline, Germany). The mixture was then topped up with distilled water to a final volume of 20 µL. Initial denaturation at 98°C for 10 minutes; 35 cycles of denaturation at 98°C for 30 seconds, annealing at 63°C for 30 seconds and extension at 72°C for 3 minutes; final extension at 72°C for 10 minutes and then the PCR samples was held at 20°C. The sequences of the primers are as listed in Appendix V. The PCR product was purified before proceeding to *in vitro* transcription.

3.4.5 *In vitro* transcription of chimeric CGMMV RNAs

In vitro transcription was performed using the mMessager mMachine® High Yield Capped RNA Transcription kit (Ambion, USA) following the protocol provided by the manufacturer. The reaction was performed by mixing 1 µg of linear DNA template with 1 × NTP/CAP mix, 1 × reaction buffer and 2 µL of enzyme mix in the final volume of 20 µL. The mixture was gently mixed by pipetting and briefly centrifuged to collect the content. The mixture was then incubated at 37°C for 2 hours. Transcribed-RNA was treated with TURBO DNase by incubated at 37°C for 15 minutes.

3.4.6 Northern blotting

The inserted HA and M epitopes in transcribed RNA were confirmed using Northern Blots. The DNA probes were labeled using DIG DNA labeling and detection kit (Roche, USA) according to manufacturer's protocols. The yield of probes was quantified according to manufacturer's protocols before hybridization.

Capillary transfer by upward flow was carried out overnight (~ 12 to 16 hours) in alkaline transfer buffer to transfer RNA from gel to membrane. The membrane was then hybridized following the kit manual. After hybridization, the membrane was developed with Anti-Digoxigenin-AP antibody and detected with NBT/BCIP substrate until the band could be seen. The membrane was washed with distilled water and dried before image-capture using the scanner.

3.4.7 Inoculation of RNAs and detection of CGMMV nanoparticles

The *in vivo* transcribed RNA (wild-type and chimeric) was used to inoculate on the cotyledon of *C. melo* var Earl favorite. Distilled water was used as the negative control. Excess RNA inoculum was washed off 30 minutes post-inoculation. The plants were maintained in a growth chamber under condition as described in section 3.1.1. Symptoms that developed on the leaves were recorded. ELISA was carried on samples from the upper new leaves to detect the active CGMMV virus infection (section 3.1.2).

3.4.8 Detection of inserted HA and M1 epitopes

Chimeric CGMMV nanoparticles with inserted HA and M1 were detected through RT-PCR. Total RNA was extracted from inoculated and non-inoculated *C. melo* var Earl favorite. One microgram of RNA was used as a template for first strand cDNA and was synthesized using a Maxime RT PreMix (Random Primer) (Intron, Korea). The mixture was then topped up with distilled water to a final volume of 20 µL. The cDNA synthesis reaction was as follows: 45°C for 60 minutes and 95°C for 5 minutes. Two microlitres of the first strand cDNA were then used in a PCR reaction with 0.2 µM of epitope forward primers and epitope reverse primer listed in Appendix V. The mixture was then topped up with distilled water to final volume of 20 µL. Amplification was carried out under the following condition: initial denaturation at 94°C for 2 minutes; 30 cycles of denaturation

at 94°C for 20 seconds, annealing at 55°C for 10 seconds and extension at 72°C for 20 seconds. A final extension at 72°C for 2 minutes and hold the PCR samples at 20°C.

Virus nanoparticles (wild-type and chimeric) were extracted and analyzed using TEM and Western blot as described in section 3.1.4 and 3.1.6.

3.4.9 In-gel digestion and mass spectrometry

Chimeric and wild-type CGMMV coat proteins were excised from the SDS-PAGE gel stained with Coomassie blue. In-gel digestion was performed using Trypsin Gold (Promega, USA) following manufacturer's protocol. Briefly, the gel was placed in a microcentrifuge tube prewashed twice with 50% acetonitrile (ACN)/0.1% trifluoroacetic acid (TFA). The gel was de-stained twice with 0.2 mL of 100 mM NH4HCO3/50% ACN for 45 minutes at 37°C followed by dehydration with 100 µL of 100% ACN for 5 minutes at room temperature. Gel slices were dried before 10 µL of Trypsin Gold (resuspended in 1 µg/µL in 50 mM acetic acid, then diluted in 40 mM NH4HCO3/10% ACN to 20 µg/mL) was added and incubated at room temperature for 1 hour. The gel was covered with digestion buffer (40 mM NH4HCO3/10% ACN) and incubated overnight at 37°C. Next, 150 µL of NANOpure® water was added in the tube with frequent vortex mixing for 10 minutes. The liquid was saved in a new tube. The gel was then extracted twice with 50 µl of 50% ACN/5% TFA (with mixing) for 60 minutes at room temperature. The liquids (NANOpure® water and 50% ACN/5% TFA) were pooled and dried with a Speed Vac at room temperature for 2-4 hours, concentrated with ZipTip® pipette tips before subjected to mass spectrometric analysis.

Digested samples were analyzed with a Thermo Orbitrap Fusion Tribrid mass spectrometer (Thermo Fisher Scientific, USA) equipped with a Thermo EASY-nanoLC system (Thermo Fisher Scientific, USA) and a nanoelectrospray source. Five microliters of sample were injected into an Acclaim™ PepMap™ 100 C18 LC Column (Thermo

Fisher Scientific, USA) and separated with the Thermo EASY-nanoLC system loaded with a Thermo Scientific™ EASY-Spray™ C18 LC Column (Thermo Fisher Scientific, USA) (2 m, 75 µm × 50 cm). The samples were separated at a flow rate of 250 nL/min over 65 minutes with a gradient from 5% to 95% buffer B (99.9% Acetonitrile/0.1% formic acid). The raw data were collected continuously with a mass spectrometer in a data-dependent manner. A survey scan was recorded in the Orbitrap analyzer with a 240,000 resolution over a mass range between m/z 100-2,000 Da and an automatic gain control (AGC) target at 4.0^{e5}. Then, it was followed by the second stage isolation mode with quadrupole and detected with IonTrap at a resolution of 3,0000. The scan range was between 350-1,400 (m/z) with an AGC target of 1^{e3} and 35% of collision-induced dissociation (CID) collision energy. Charge state was assigned to focus at ions that have a charge state of +2 to +7.

The raw files generated from the mass spectrometer were analyzed with a MaxQuant software package (Cox & Mann, 2008) and scanned against the protein sequence of wild-type and chimeric CGMMV.

3.5 Analysis of chimeric CGMMV with mice

3.5.1 Peptide synthesis

The peptides were synthesized through solid phase and purified by HPLC (peptide purity > 96%) (GenScript, USA). The peptides were characterized by amino acid analysis and mass spectroscopy.

3.5.2 Immunization of mice

All animals used in this study were 6–8 weeks old female Balb/c mice obtained from Monash University (Sunway Malaysia Campus). Animals were used in compliance with IACUC approved protocols (ethics reference no: 2014-08-05/CEBAR/R/LWW).

Three groups of Balb/c mice (4 mice each group) were vaccinated three times at 14-day intervals. The first group of mice were injected subcutaneously into the upper left thigh with 100 µL (1 µg/µL) purified chimera CGMMV diluted in 0.01 M phosphate buffer (pH 7.4). The second and third groups of mice consisted of positive and negative controls of mice receiving 100 µL (1 µg/µL) of wild-type CGMMV and 100 µL of 0.01 M phosphate buffer (pH 7.4), respectively. The serum of mice from each group was collected via tail-bleed two weeks after the second booster.

3.5.3 Detection of anti-CGMMV antibody and anti-epitopes antibody

ELISA 96-well plates were coated with 100 µL of either wild-type CGMMV or peptide (10 µg/mL) diluted in 1 × carbonate coating buffer (pH 9.6) (Agdia, USA) and incubated overnight at 4ºC. The wells were then blocked for 1 hour at room temperature with 3% BSA containing 0.05% Tween-20. Serum samples were diluted in PBS containing 0.05% Tween 20 (PBST)/3% BSA, added to blocked wells and incubated for 2 hours at room temperature. Bound immunoglobulins were detected using anti-mouse IgG antibodies conjugated to alkaline phosphatase (Thermo Fisher Scientific, USA) in 1:5000 dilution. The label was detected using pNPP and absorbance was measured using Tecan GENios Microplate Reader at 405 nm.

3.5.4 Proliferation assay

Two weeks after the final immunization, four mice of each group were sacrificed. The proliferation of splenocytes was determined by MTT. Briefly, splenocytes isolated from four mice of each group were cultured in triplicate in 96-well culture plates at a concentration of 1×10^5 cells per well in RPMI-1640 culture medium containing 1-glutamine (2 mM), penicillin-streptomycin (500 U and 50 µg/ml) final concentration, sodium pyruvate (0.1 mM), monothioglycerol (0.02%) and foetal calf serum (10%). Cells in each well were stimulated with 10 µg/mL antigen (wild-type CGMMV or epitopes

peptide) or 5 µg/mL concanavalin A (Con A) (Sigma, USA) and were incubated for 72 hours. Fifty microlitres of MTT solution (2 mg/mL) was added to each well and then cultured for an additional 3 hours. Subsequently, 100 µL of MTT lysis buffer (10% SDS, 45% dimethylformamide, adjusted to pH 4.5 by glacial acid) was added to the wells, incubated overnight and read at 570 nm.

3.5.5 Statistical analysis

The data were analyzed using data analysis tool from Microsoft Excel. F test was carried out to determine the equality of variance. Data are presented as mean values ± standard deviation (SD) and the unpaired Student t-test with calculations of a two-tailed p-value were calculated to determine significance; differences with a p-value of 0.05 and above were considered significant.

CHAPTER 4: RESULTS

4.1 Determination of CGMMV susceptible hosts of Malaysia and Japan melon

Cucumber green mottle mosaic virus (CGMMV) infects *Cucurbitaceous* crops such as watermelon and cucumber. An identified host of CGMMV for propagation is the *C. melo* var Earl favorite from Japan. To investigate the possibility of using alternative localised hosts, seven Malaysia melon varieties, *C. melo* var M3, M4, M5, M6, WQ, PG and Yehe were used to test their susceptibility for CGMMV propagation and virus yield. Among the 7 tested melon varieties, M4, M5, and Yehe showed typical mosaic and mottle symptoms on the upper new leaf about 10-14 days post inoculation (d.p.i) with CGMMV nanoparticles which were similar but less significant (milder) (Figure 4.1C-E) than the control (Earl favorite) (Figure 4.1B). On the other hand, variety M3, M6, WQ and PG remained symptomless up to 30 d.p.i. (Figure 4.1F-I). Table 4.1 summarised the susceptibility of melon varieties toward CGMMV based on the symptoms observed. The result was verified with ELISA by detecting CGMMV antigen from the inoculated plants. The ELISA results confirmed that M3, M6, WQ, and PG are resistant to CGMMV while M4, M5 and Yehe were susceptible to the CGMMV (Table 4.2; Appendix A).

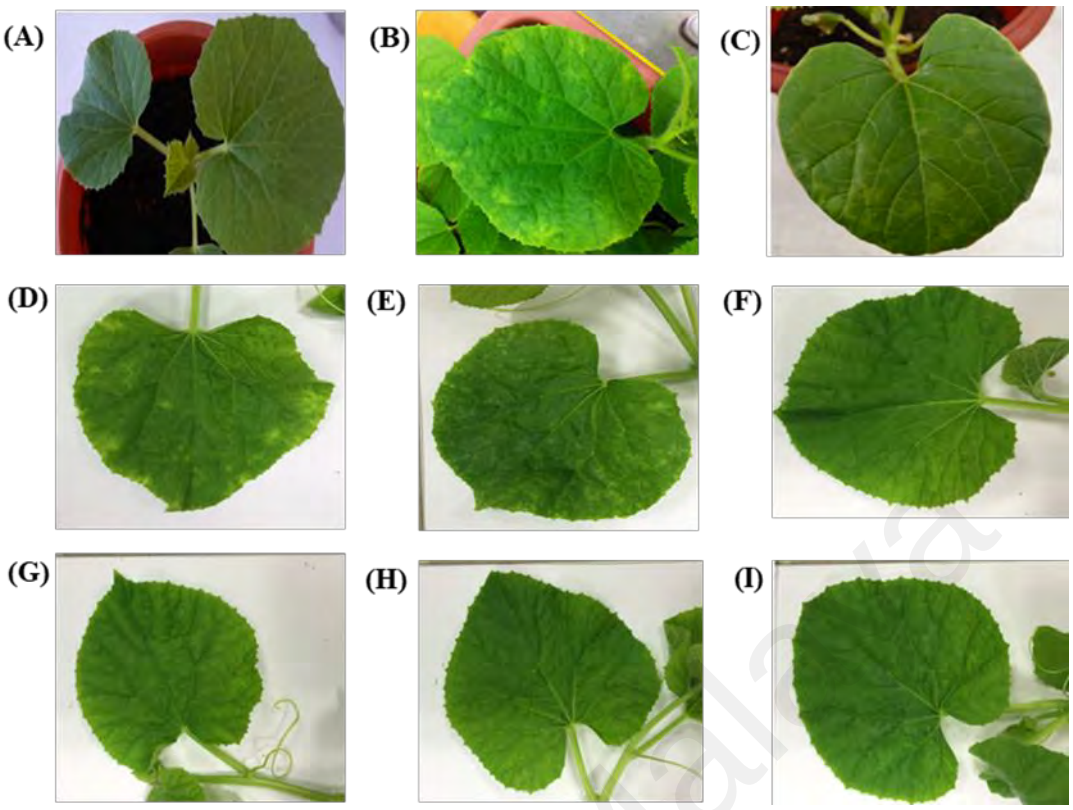

Figure 4.1: Visual inspection of mottle and mosaic symptoms on CGMMV nanoparticles-inoculated Malaysian and Japan melons. Typical mottle and mosaic signs were observed on upper new leave of (B) *C. melo* var Earl favorite, (C) M4, (D) M5 and (E) Yehe at 10-14 d.p.i. However, there were no symptom seen on (F) M3, (G) M6, (H) WQ and (I) PQ until 30 d.p.i. Image (A) represents the mock-inoculated plant which acts as a negative control.

Table 4.1: CGMMV susceptibility test of Malaysia melon varieties. The number of plants which showed mosaic and mottle symptoms on the upper new leaves at 30 d.p.i (or earlier) was recorded. M4, M5 and Yehe showed mild symptoms while M3, M6, WQ, and PG did not. The susceptibility test was repeated three times with 6 replicates in each trial. *C. melo* var Earl favorite act as a positive control.

Hosts	1st trial	2nd trial	3rd trial
M3	0/6	0/6	0/6
M4	6/6	6/6	6/6
M5	6/6	6/6	6/6
M6	0/6	0/6	0/6
Yehe	6/6	6/6	6/6
WQ	0/6	0/6	0/6
PQ	0/6	0/6	0/6
Earl favorite	6/6	6/6	6/6

Table 4.2: Detection of CGMMV on the inoculated melon varieties using ELISA. Three upper new leaves with or without symptoms from each variety were pooled in a group and tested. Data represent the mean ± SD after normalized to blank (buffer only) (n = 3 biological replicates). '+' represents positive; '-' represents negative.

Hosts	Absorbance (405 nm)	Interpretation
M3	0.07040±0.00029	-
M4	0.77073±0.00105	+
M5	0.72377±0.00143	+
M6	0.07510±0.00067	-
Yehe	0.78430±0.00437	+
WQ	0.06160±0.00040	-
PG	0.07363±0.00036	-
Earl favorite	0.97940±0.01439	+
Negative control	0.06427±0.00110	-
Positive control	1.23143±0.00972	+

Next, the virus yield from 4 susceptible melon varieties was determined. The concentration of CGMMV nanoparticles in the plant extracts was determined by UV/visible spectroscopy using the extinction coefficient of 3.0 mg^{-1} ml^{-1} cm^{-1}. The purity of the CGMMV nanoparticles was confirmed based on the spectrophotometry measurement of A260:A280 ratio whereby a ratio of 1.9 was obtained indicating pure and Fintact CGMMV nanoparticles. Based on the results, the yield of the CGMMV nanoparticles from 4 susceptible melons: M4, M5, Yehe and Earl favorite were in the range of 0.2-0.6 mg and varied from batch to batch (Figure 4.2; Appendix B). The yield of CGMMV nanoparticles from Malaysia melons: M4, M5, and Yehe (0.21-0.26 mg/g) were relatively lower than Earl favorite (0.57 mg/g). Transmission electron microscopy (TEM) examination showed that the shape, structure and the dimension of the CGMMV nanoparticles extracted from M4, M5 and Yehe remained the same as those extracted from its original host, Earl favorite with some degradation observed in dimension which was possibly due to the isolation process (Figure 4.3). The size of the CGMMV coat protein from the M4, M5 and Yehe was as expected, 17 kDa (Figure 4.4).

These results showed that Earl favorite originating from Japan remained the most efficient host for CGMMV nanoparticles production and was used for propagation and subsequent tests for this research. The Malaysia melon varieties could be used to propagate CGMMV nanoparticles which would be useful for production upscaling in the future. However, more Malaysia melons or cucumber varieties can be tested to identify a suitable propagation host for CGMMV nanoparticles production in Malaysia.

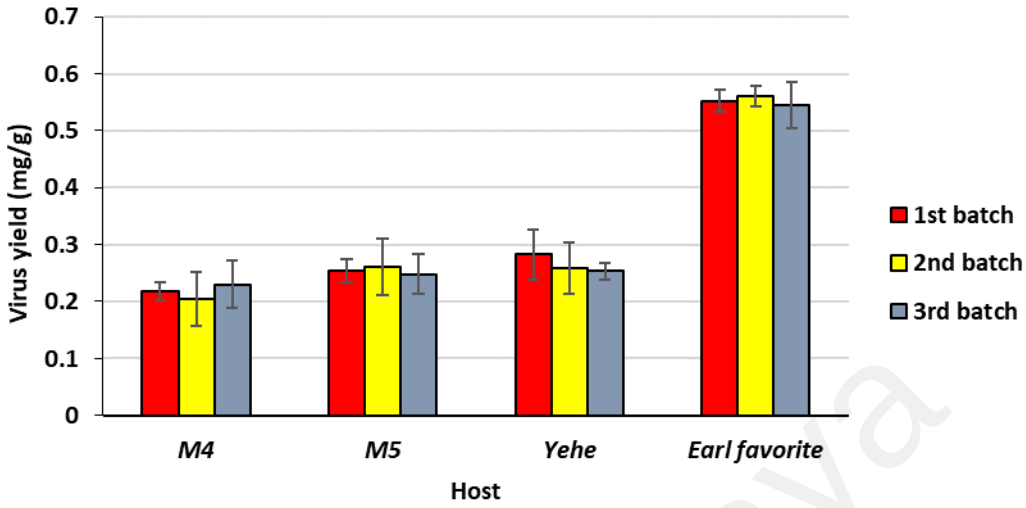

Figure 4.2: The yield of CGMMV nanoparticles from susceptible Malaysia melons and Japan melon varieties. Ten grams of sample was used to extract the virus. Data represents the mean ± SD, n = 3 biological replicates.

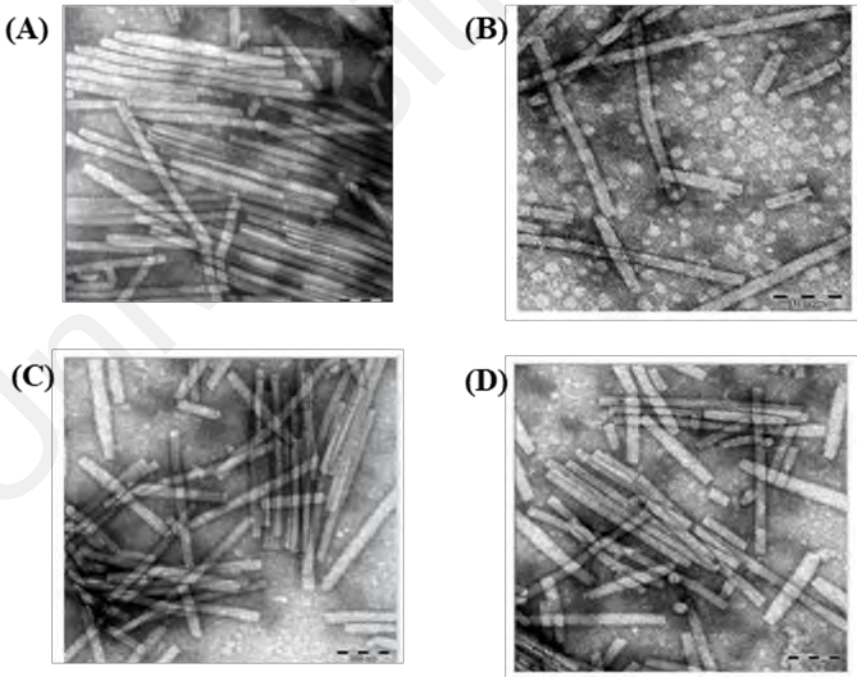

Figure 4.3: Detection of CGMMV nanoparticles extracted from susceptible melon varieties. Transmission electron microscopy captured images of viruses extracted from (A) *C. melo* var Earl favorite, (B) M4, (C) M5 and (D) Yehe. The shape and structure of virus extracted from M4, M5 and Yehe remained intact with the same dimensions and shape as extracted from Earl favorite.

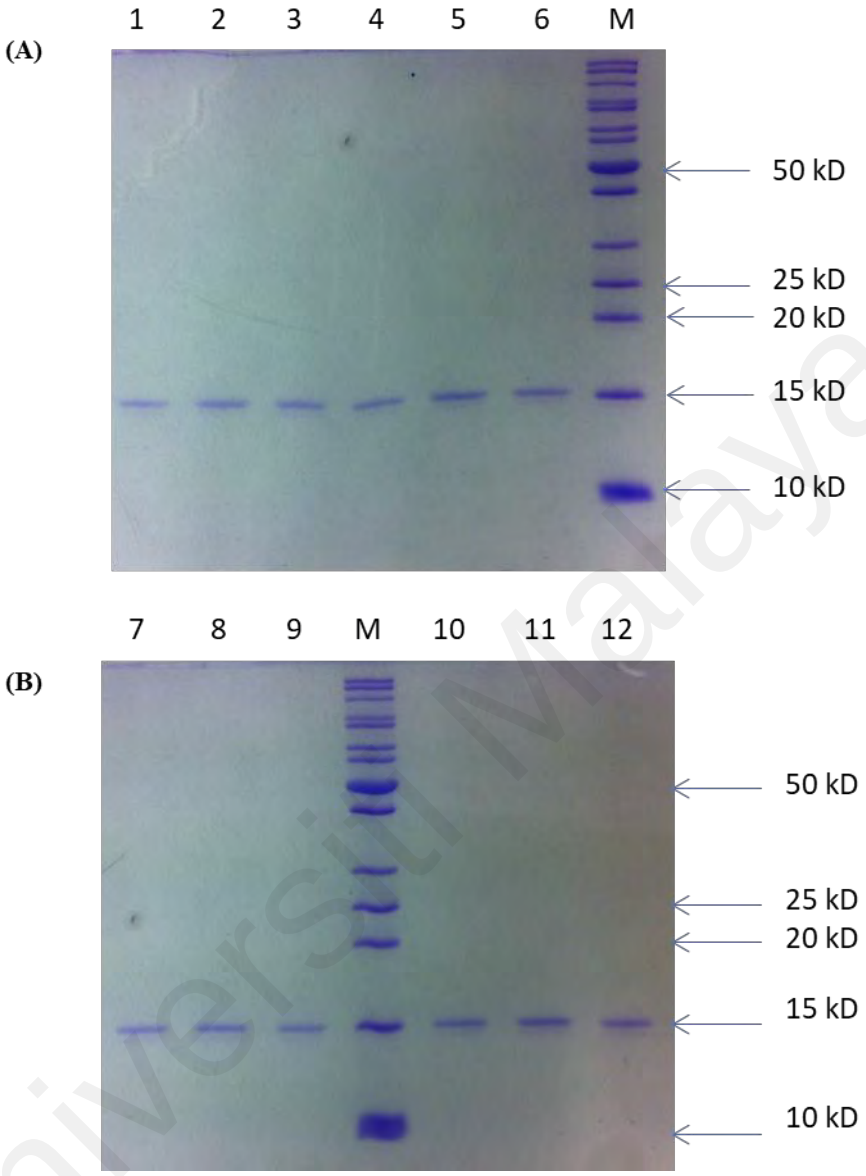

Figure 4.4: Detection of CGMMV coat protein. Coat protein of CGMMV extracted from 4 susceptible varieties of 3 different batches were analyzed using SDS-PAGE. Gel (A) showed samples extracted from M4 (Lane 1-3) and M5 (Lane 4-6) while gel (B) showed samples extracted from Yehe (Lane 7-9) and Earl favorite (Lane 10-12). All the coat proteins detected are of the expected size of 17kDa. Lane M represents a PageRuler unstained protein marker (Thermo Scientific, USA).

4.2 *In vivo* characteristic of CGMMV nanoparticles in mice

4.2.1 Detection of CGMMV nanoparticles in broad range of mice tissues

The *in vivo* characteristics of the purified CGMMV nanoparticles isolated from *C. melo* var Earl favorite were studied in Balb/c mice. Initial analysis involved identifying the biodistribution of CGMMV nanoparticles in the mouse's tissues. A dose of 100 µg of CGMMV nanoparticles was introduced into the right thigh of the mouse through subcutaneous (SC) injection. The presence of CGMMV nanoparticles in mouse tissues was determined by detecting for the presence of its RNA through RT-PCR at 1, 3, 5, 7, 10 and 14 days post injection. As shown in Figure 4.5, CGMMV RNA was detected in bone marrow, duodenum, kidney, liver, spleen, and stomach of all 4 inoculated mice at all the harvesting timepoints post-inoculation except for the brain and lung tissues. Whereas the presence of CGMMV RNA can only be detected in the brain of 2 mice at 7 days post injection and 1 mouse at day-14 (Table 4.3), CGMMV RNA can only be detected in the lung of 2 mice at 10 days post injection and only 1 mouse at day-14 (Table 4.3). This result showed the bands were diminished in the last two time points in brain and lung. No amplification of CGMMV-specific PCR products was detected in mock-inoculated mice (Figure 4.5; Table 4.3). Based on the results, we can conclude that CGMMV nanoparticles shows broad tissues distribution in mice administrated through subcutaneous injection and persisted for 14 days in the mice.

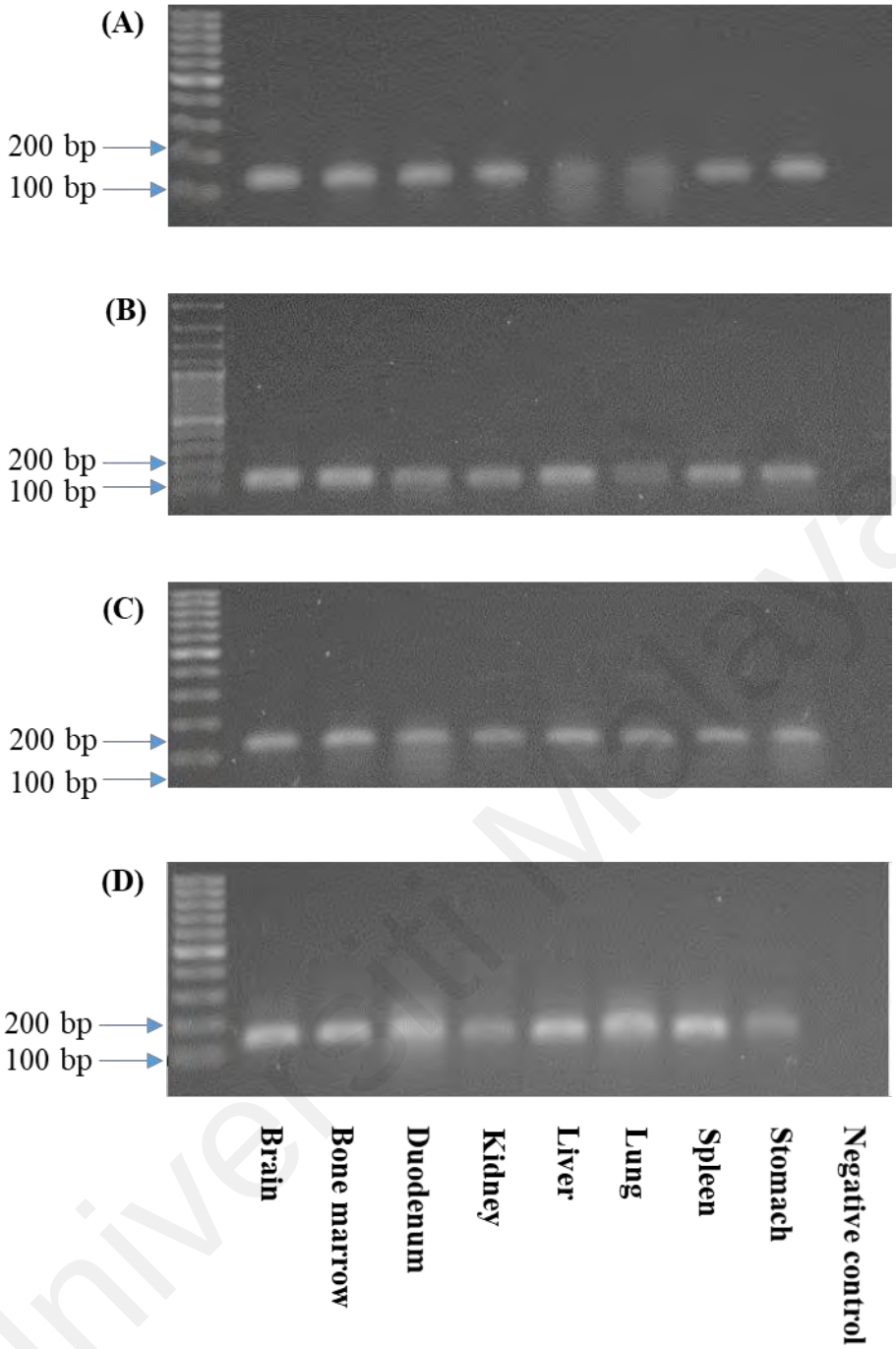

Figure 4.5: Agarose gel electrophoresis of RT-PCR products for the detection of CGMMV RNA in mouse tissues. (A) Day 1, (B) Day 3, (C) Day 5, (D) Day 7, (E) Day 10 and (F) Day 14 post subcutaneous injection with 100 µg of CGMMV nanoparticles. CGMMV RNA was detected in brain, bone marrow, duodenum, kidney, liver, lung, spleen, and stomach of the mouse. Mock-inoculated mouse act as a negative control. Each gel represents the RT-PCR result of the tissues harvested from a mouse from a group of 4 mice. Refer to next page for figure E and F.

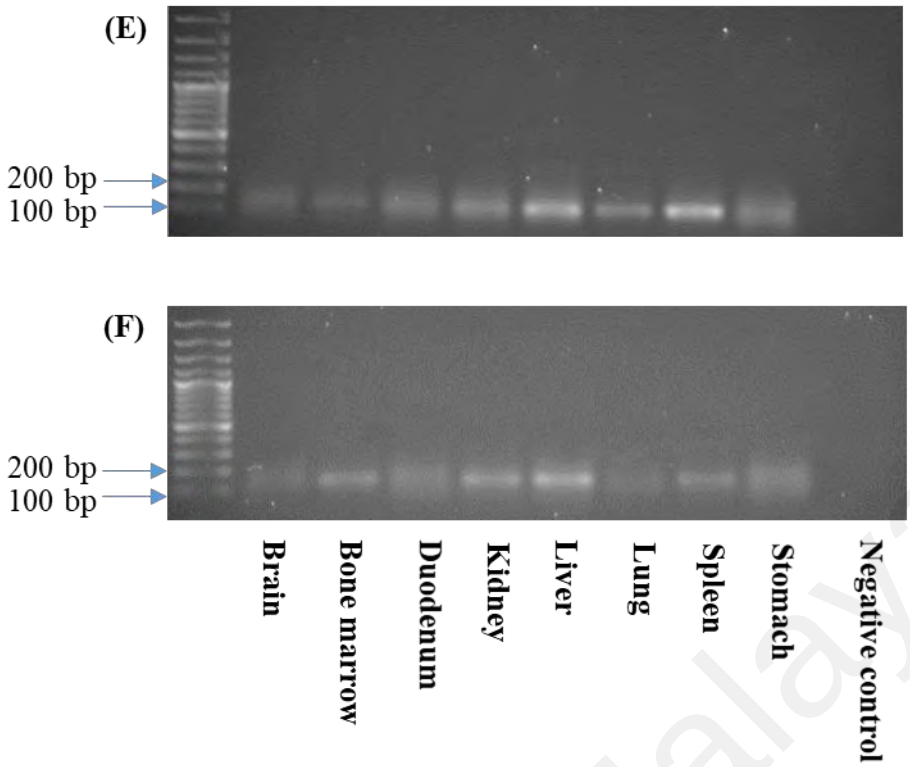

Figure 4.5, continued.

Table 4.3: Detection of CGMMV RNA in tissues of mice injected with CGMMV nanoparticles. Four mice were injected with 100 µg of CGMMV nanoparticles and the presence of CGMMV RNA was investigated over 14 days post-injection.

Tissues	Days post injection						Mock-inoculation
	1	3	5	7	10	14	
Brain	4/4	4/4	4/4	2/4	1/4	1/4	0/4
Bone marrow	4/4	4/4	4/4	4/4	4/4	4/4	0/4
Duodenum	4/4	4/4	4/4	4/4	4/4	4/4	0/4
Kidney	4/4	4/4	4/4	4/4	4/4	4/4	0/4
Liver	4/4	4/4	4/4	4/4	4/4	4/4	0/4
Lung	4/4	4/4	4/4	4/4	2/4	1/4	0/4
Spleen	4/4	4/4	4/4	4/4	4/4	4/4	0/4
Stomach	4/4	4/4	4/4	4/4	4/4	4/4	0/4

4.2.2 Biodistribution and clearance of CGMMV nanoparticles in mouse

To study the relative abundance and clearance of CGMMV nanoparticles in mice, fluorescent conjugated CGMMV nanoparticle samples were prepared. The CGMMV capsid has four reactive lysine residues on the surface of the coat protein (Figure 4.6A). We conjugated these reactive lysines with Alexa-488, an amine reactive ester of fluorescent dye. The size, concentration, labelling efficiency, binding and integrity of the fluorescent viruses (CGMMV-488) were monitored by four methods: SDS-PAGE, size exclusion chromatography, TEM and UV absorbance. SDS-PAGE showed a band of expected size with the native CGMMV and CGMMV-488 nanoparticles at the size of approximately 17 kDa and 17.5 kDa respectively (Figure 4.6B). Further confirmation was carried out using size-exclusion chromatography. Intact virions were detected at retention times of approximately 10 min, at an elution rate of 0.8 mL/min. The CGMMV-488 nanoparticles demonstrated a single excitation at 495 nm that indicated the covalent conjugation of Alexa-488 onto the coat protein which is not shown in the native CGMMV nanoparticles (Figure 4.6C and 4.6D). Subsequently, TEM imaging showed that the CGMMV-488 nanoparticles maintained their structural integrity and filamentous shape post conjugation when compared to the native CGMMV nanoparticles (Figure 4.6E and 4.6F). In addition, UV/visible spectroscopy showed a degree of labelling at 24%, which is equivalent to 504 copies of dye per nanoparticle. These results showed that the CGMMV nanoparticles were successfully conjugated with Alexa-488 without altering its structure, shape and dimension.

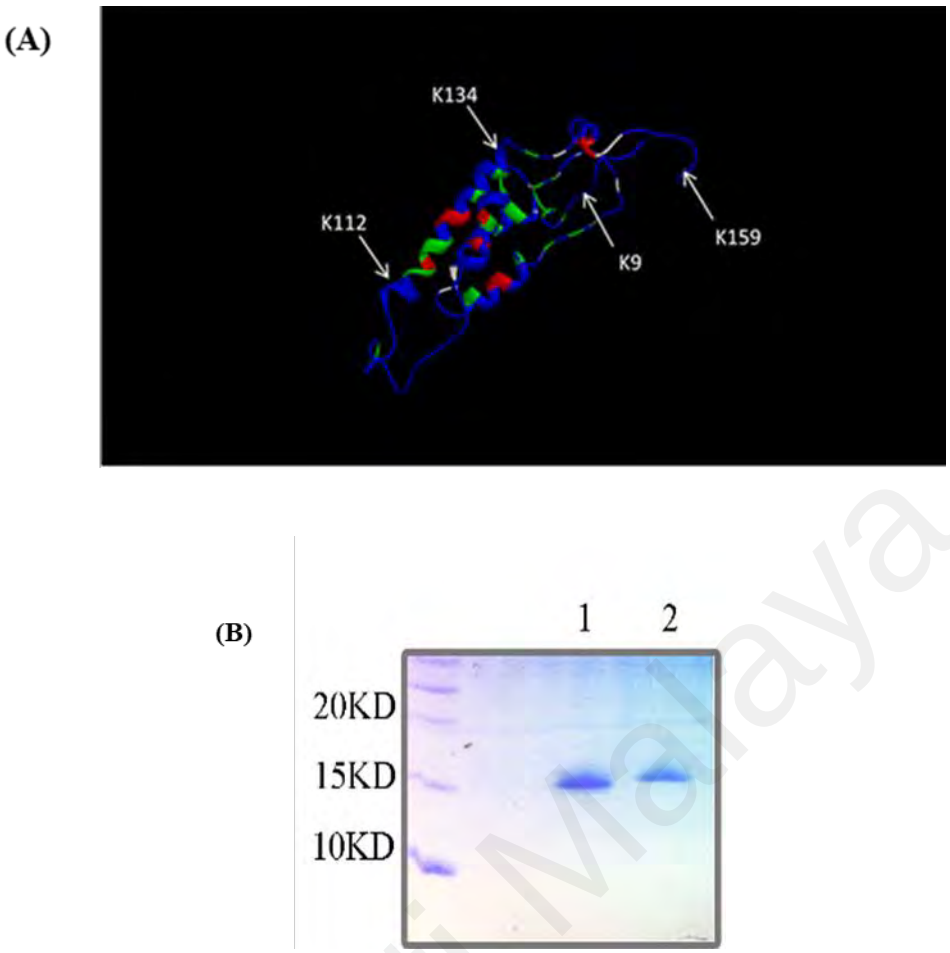

Figure 4.6: Characteristics of native CGMMV and CGMMV-488 nanoparticles. (A) CGMMV coat protein structure (1cgm.pdb). Arrows indicate the four lysine residues (K9, K112, K134 and K159) exposed to solvent (B) A 15% SDS-PAGE gel electrophoresis was used to detect the native CGMMV and CGMMV-488 coat proteins. The molecular weight of two coat protein products were about 17kD for native CGMMV coat protein (lane 1) and 17.5kD for CGMMV-488 coat protein (lane 2) respectively. (C-D) Confirmation was carried out using size-exclusion chromatography. The elution time of (C) CGMMV and (D) CGMMV-488 nanoparticles is 10 minutes at flow rate of 0.8mL/minute using 0.01M potassium phosphate buffer. The peak at 495 nm showed that the Alexa-488 (pink peak) was successfully bonded at the surface of the CGMMC coat protein. The blue peak represents signal detected by the 280 nm laser while the red peak represents the signal detected by the 260 nm laser. (E-F) The structure, shape and size of the (E) CGMMV and (F) CGMMV-488 nanoparticles were maintained as confirmed by transmission electron microscopy. Refer to next page for figure C, D, E and F.

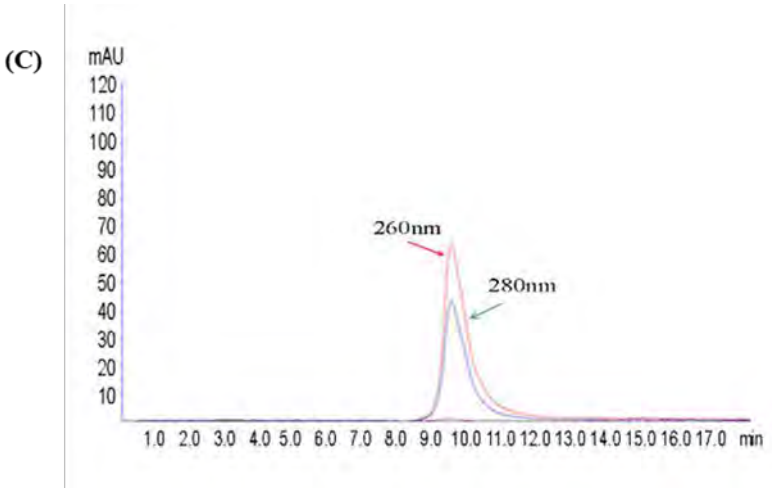

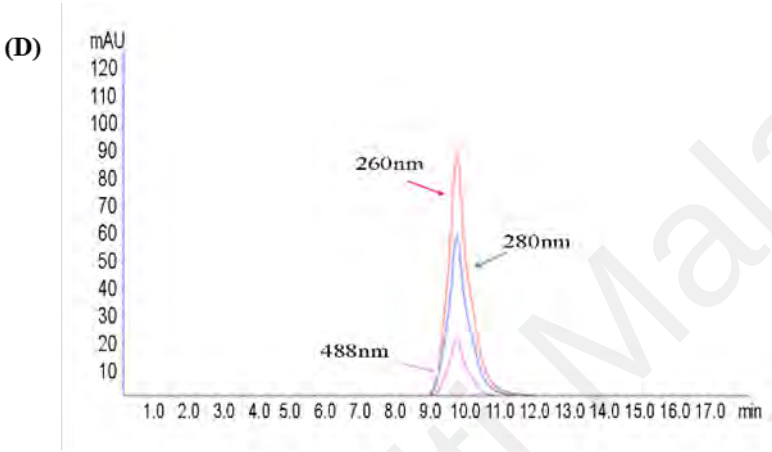

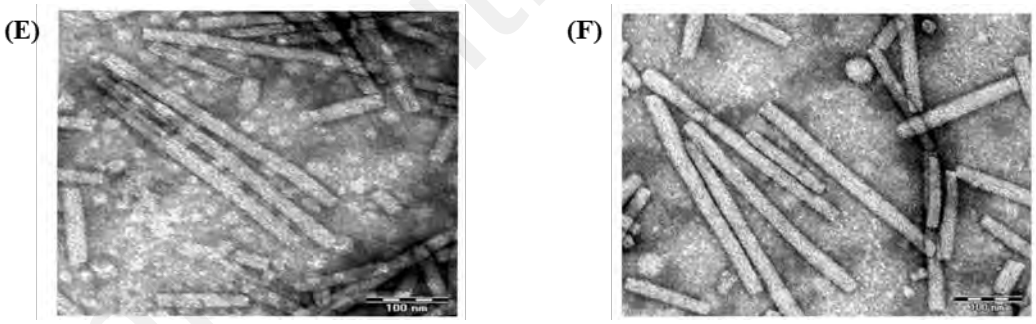

Figure 4.6, continued.

Next, the relative abundance of CGMMV nanoparticles in mice was determined by measuring the fluorescent dye intensity in each tissue. Supernatant of homogenized tissues were measured using fluorescence reader in triplicate at 495 nm excitation and 595 nm emission wavelengths. Tissues from brain, duodenum, kidney, liver, lung, spleen and stomach were included in this test. The fluorescence intensity per gram of tissue weight was calculated and normalized against the same tissues from the mouse injected with phosphate buffer (Appendix C).

Figure 4.7 showed the biodistribution of CGMMV nanoparticles in the mice tissues after subcutaneous injection. Low level of fluorescence signal detected at 1 day post-injection indicated that the CGMMV nanoparticles needed extended time to diffuse from the interstitial subcutaneous fluid and then absorbed into the vascular system before being found in the tissues compared to intravenous injection. Fluorescent signals were highest in between 3-5 days post injection before slowly decreasing to low level at day-14 indicating that the CGMMV nanoparticles was slowly being cleared from the mice system. Although there is some degree of variability between mice, the overall trend indicates that CGMMV nanoparticles accumulated the most in the spleen > liver > kidney> duodenum > stomach. (Figure 4.7). Weak signals were noted in the brain, lung and kidney.

The results suggested that the intact CGMMV nanoparticles had passed through the subcutaneous area, entered the vascular system, penetrated to the endothelium and parenchyma cells of the tissues above before being slowly cleared from the tissues. However, CGMMV VNPs might remaining in the circulation. Finally, the fluorescence result is consistent with the RT-PCR results in section 4.5.

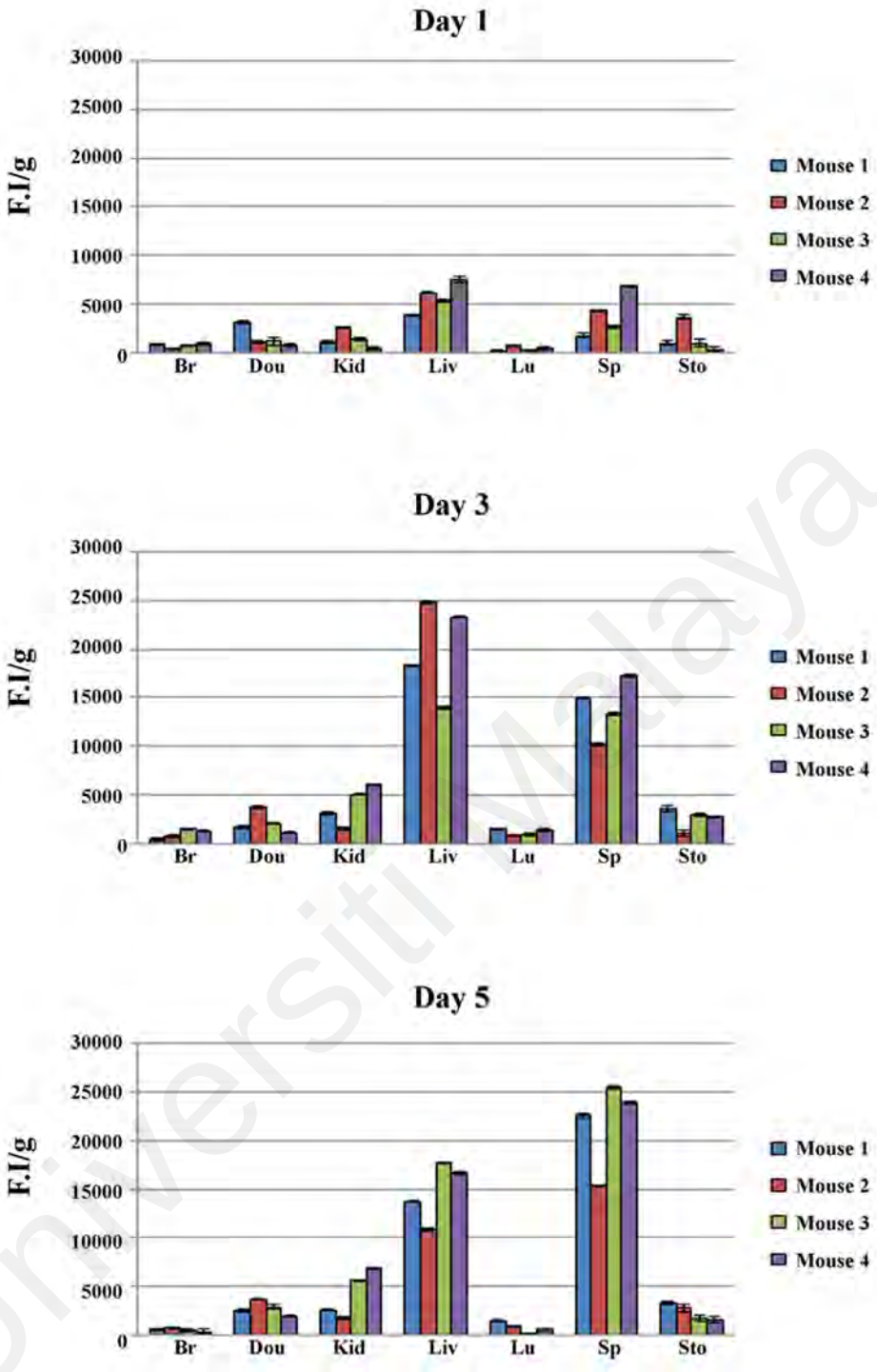

Figure 4.7: Biodistribution of CGMMV-488 nanoparticles in Balb/c mice. The reading is represented by fluorescence intensity (F.I) per gram tissue weights at 1, 3, 5, 7, 10 and 14 days post-subcutaneous injection. Br: Brain; Duo: Duodenum; Kid: Kidney; Liv: Liver; Lu: Lung; Sp: Spleen; Sto: Stomach. Data represents the mean ± SD, n = 4 biological replicates. Refer to next page for figure 7, 10 and 14 days post-subcutaneous injection.

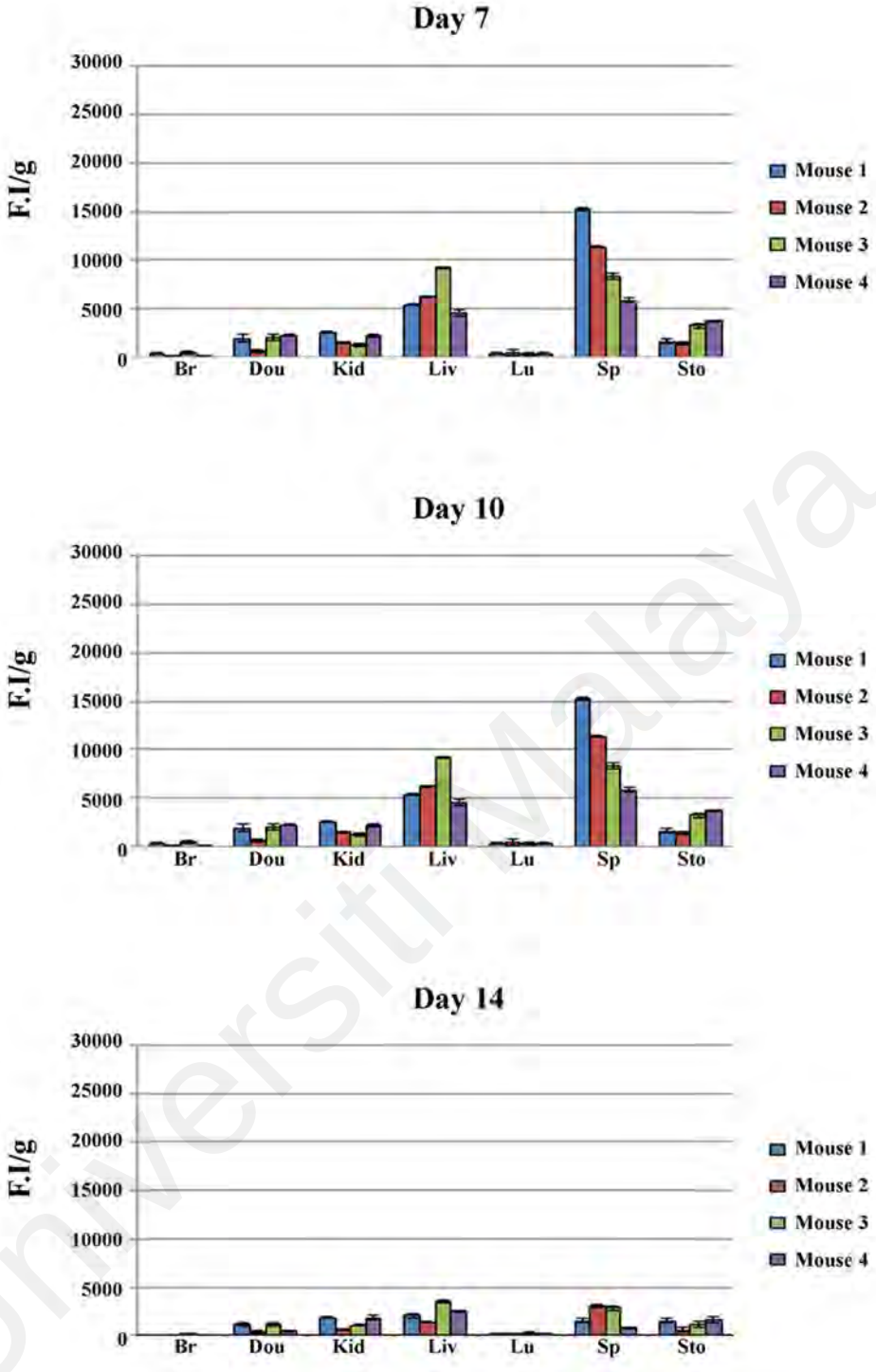

Figure 4.7, continued.

4.2.3 Pharmacokinetics, blood biocompatibility and toxicity

The experiments were continued to study the half-life, blood compatibility and toxicity of CGMMV nanoparticle in mice. The half-life of CGMMV nanoparticles in plasma circulation of Balb/c mice after subcutaneous injection was determined. A fluorescence standard curve was plotted with plasma spiked with different concentration of CGMMV-488 nanoparticle. Injection dose (ID) in the circulation of 100% was equivalent to 100 µg of CGMMV-488 nanoparticles. From the results, it was showed that about 70% of the CGMMV-488 nanoparticles detected in the bloodstream of 1 day post injection. The half-life of CGMMV nanoparticles in serum is 3.3 days (Figure 4.8A; Appendix D).

The blood compatibility of CGMMV nanoparticles was tested using the red blood cell (RBC) disruption (hemolysis) method by incubating purified RBCs with CGMMV and CGMMV-488 nanoparticles. The mixtures were pelleted after one-hour incubation and the supernatant that contained hemoglobin content released after RBC lysis was measured at 540 nm (Figure 4.8B; Appendix E). Data indicated that neither CGMMV nor CGMMV-488 nanoparticles induced RBC hemolysis.

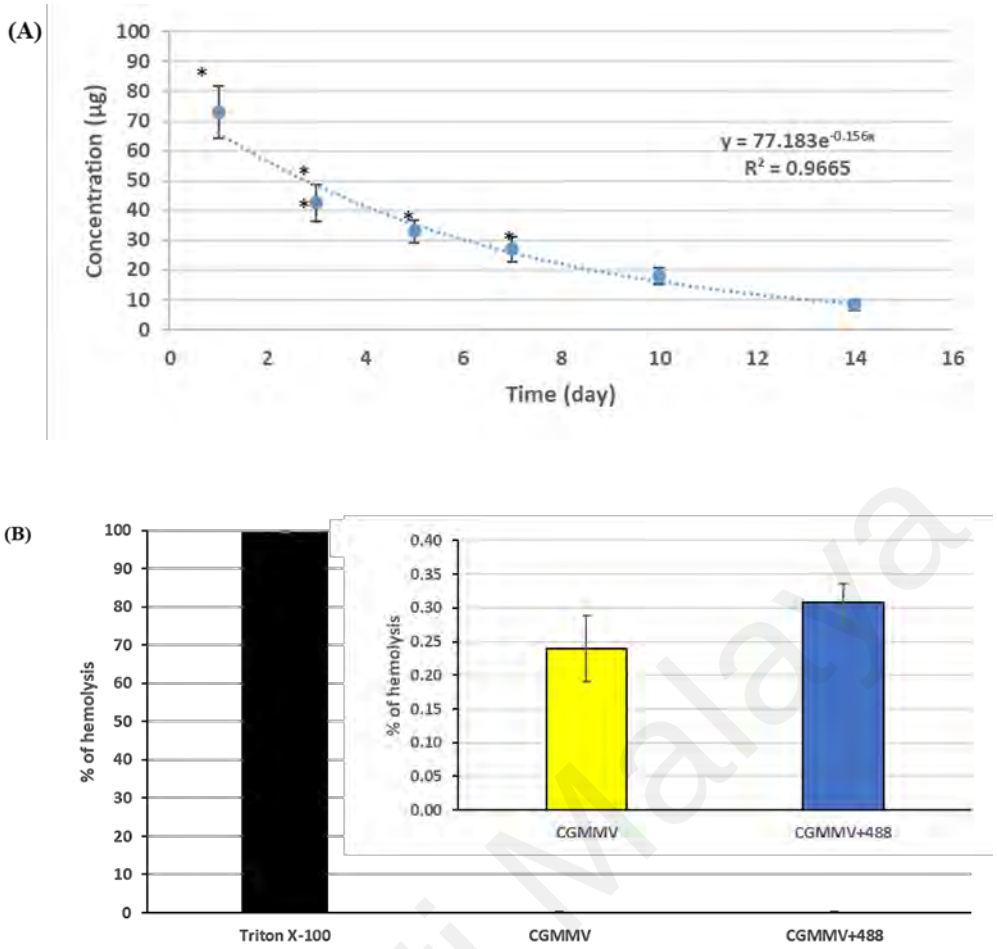

Figure 4.8: Half-life and blood biocompatibility of CGMMV nanoparticles in mice serum. (A) The half-life of CGMMV nanoparticles was about 3.3 days. Percentage of CGMMV-488 nanoparticles in mice serum was calculated based on a CGMMV-488 nanoparticle standard curve. One hundred percentage is equivalence to 100 µg of CGMMV-488 nanoparticles. (B) Blood biocompatibility of CGMMV via red blood cell (RBC) hemolysis assay. The inset bar graph showed zoomed in RBC hemolysis assay for purified RBCs treated with CGMMV and CGMMV-488. Both showed neither CGMMV nanoparticles nor CGMMV-488 nanoparticles lyses RBCs. Readings are reported as a percentage of CGMMV-488 and percentage of hemolysis. Purified RBCs treated with neat triton X-100 act as positive control for complete RBC lysis. Data represents the mean ± SD, n = 4 biological replicates. **, $p < 0.01$; *, $p < 0.05$.

Next, the toxicity effect of CGMMV nanoparticles in mice was examined. In this experiment, all mice were injected subcutaneously either with CGMMV nanoparticles or 0.01 M potassium phosphate buffer as a control. There were no clinical signs observed throughout the 14 days of study. There were no rashes, swelling, redness and pus formation at the injection sites underneath the skin as well as no weight loss was recorded (Appendix F). The behaviours of the mice were normal.

From section 4.2.2, two tissues with the most abundant CGMMV nanoparticles accumulated, liver and spleen were sectioned and H&E stained. Based on the histological study, no significant signs of tissue degeneration nor necrosis were observed in both the liver (Figure 4.9) and spleen (Figure 4.10) compared to PBS injected mice, suggesting that that CGMMV nanoparticles were not toxic to the mice.

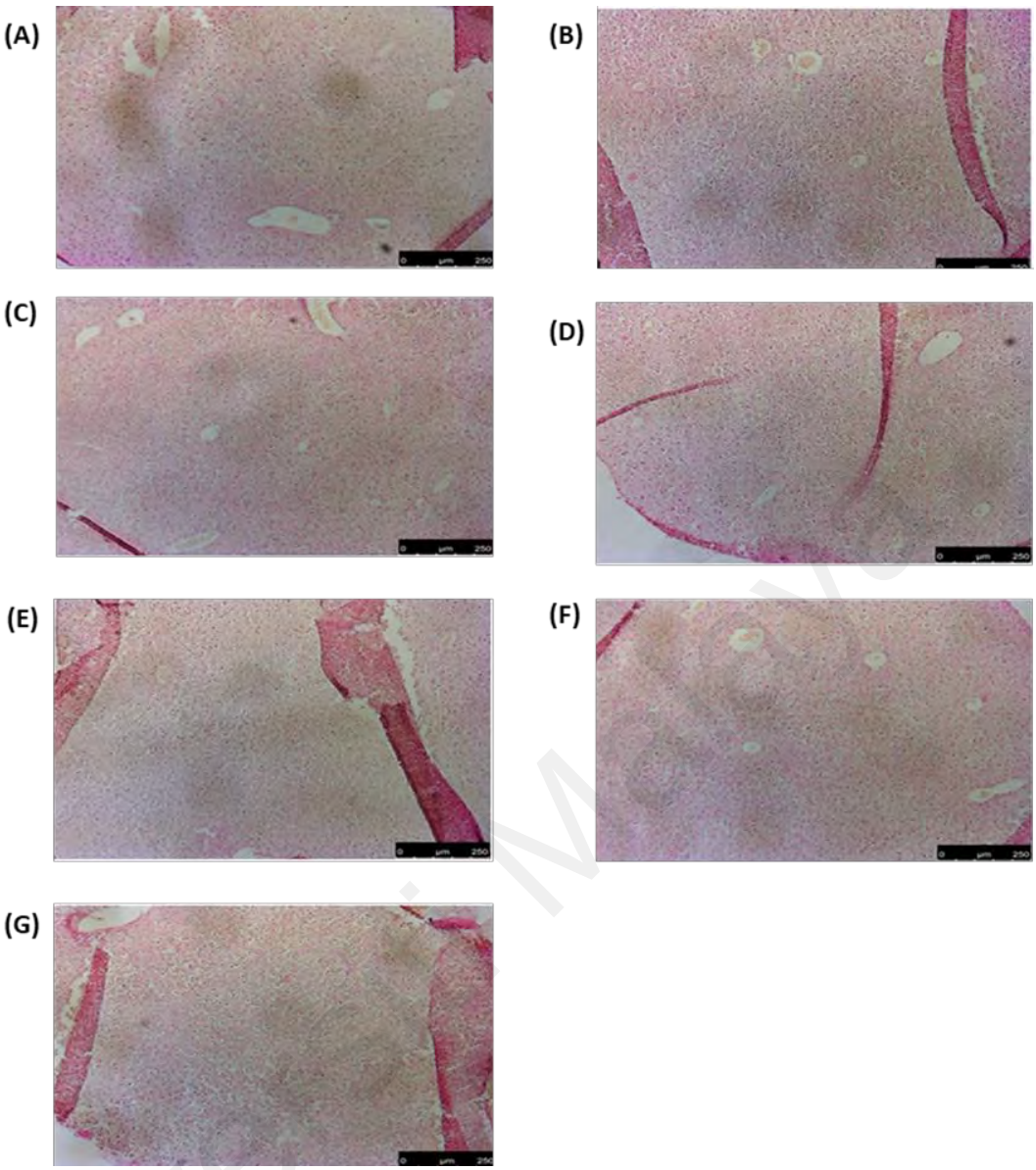

Figure 4.9: Histological examination of spleen tissues. Hematoxylin and eosin-stained sections of spleen from mouse injected with 100 µg of CGMMV nanoparticles harvested on (A) Day 1, (B) Day 3, (C) Day 5, (D) Day 7, (E) Day 10 and (F) Day 14 post-injection. (G) Spleen tissue from mouse injected with 0.01 M potassium phosphate (pH 7.0) act as a negative control.

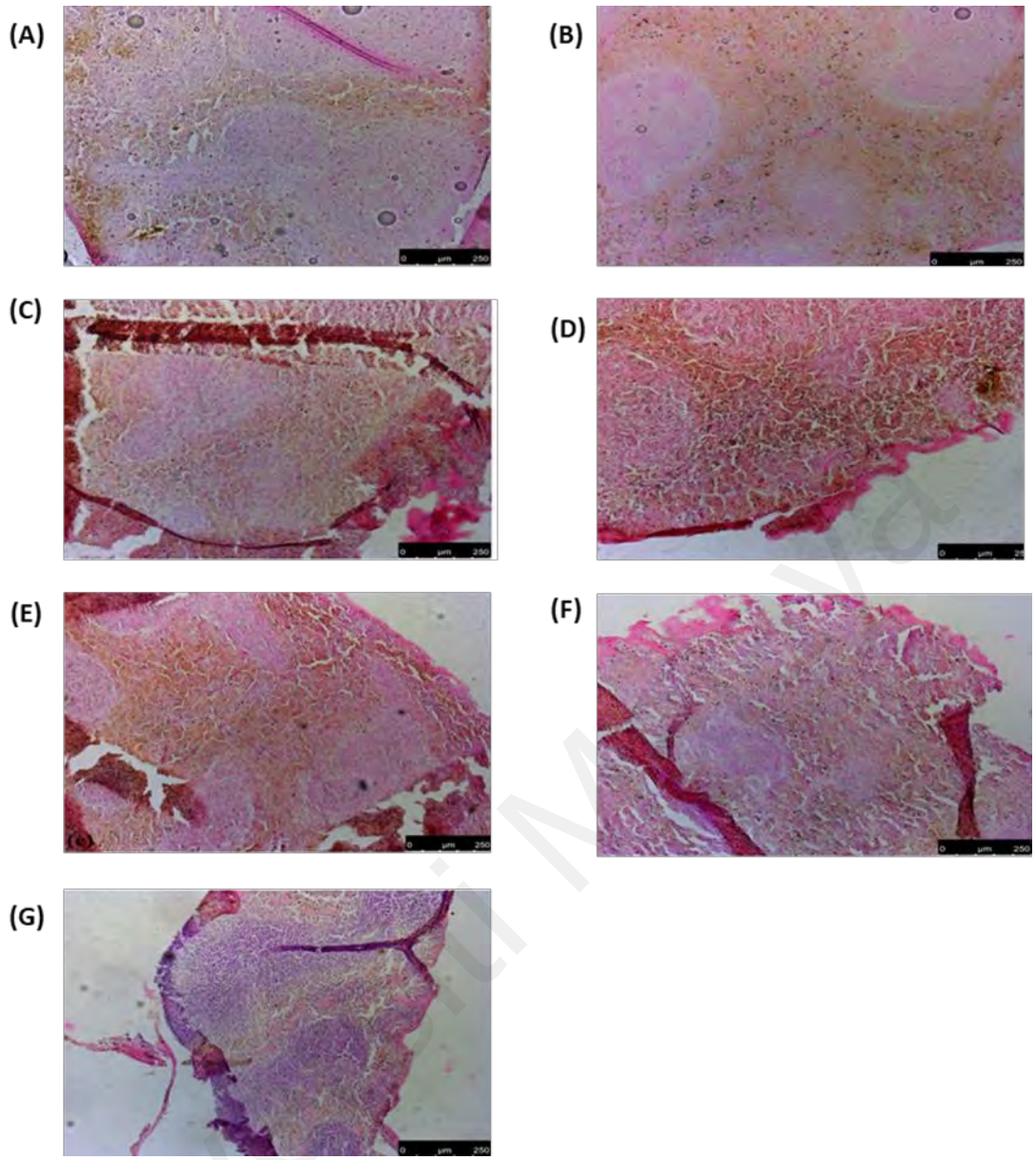

Figure 4.10: Histological examination of liver tissues. Hematoxylin and eosin-stained sections of liver from mouse injected with 100 µg of CGMMV harvested on (A) Day 1 day, (B) Day 3, (C) Day 5, (D) Day 7, (E) Day 10 and (F) Day 14 post-injection. (G) Liver tissue from mouse injected with 0.01 M potassium phosphate, pH 7.0 act as a negative control.

4.2.4 Detection of anti-CGMMV IgG in mouse serum

In order to study the immunogeneicity of CGMMV nanoparticles in mice, serum antibody against CGMMV and IgG subclasses were measured using ELISA. At 5 days post-injection, anti-CGMMV antibody can be detected in mouse serum and the level continued to increase over time (Figure 4.11A; Appendix G). This result showed that the CGMMV nanoparticles is immunogenic and induced antibody production even without the presence of an adjuvant. At the end of the study period (14 days post injection), the anti-CGMMV antibody was still present at a high level suggesting the production of anti-CGMMV antibody might sustain for a longer period.

Besides, CGMMV nanoparticles also induced changes in the Th1-Th2 balance based on the immunoglobulin G subclasses isotyping. In mice, IgG1 is related with a Th2-like response, while IgG2a, IgG2b, and IgG3 antibodies are related to a Th1-like response. Based on the results, mouse serum contained a higher level of IgG1 and IgG2a subclass than IgG2b and IgG3 (Figure 4.11B; Appendix H). All the different IgG levels showed increase over time. A Th1:Th2 index was calculated for each injection group by comparing the Th1 IgG (IgG2a, IgG2b, and IgG3) subclasses to the Th2 (IgG1) subclass. The results indicated that CGMMV was more skewed towards a Th1 response (Th1:Th2 ratio <1) (Table 4.4).

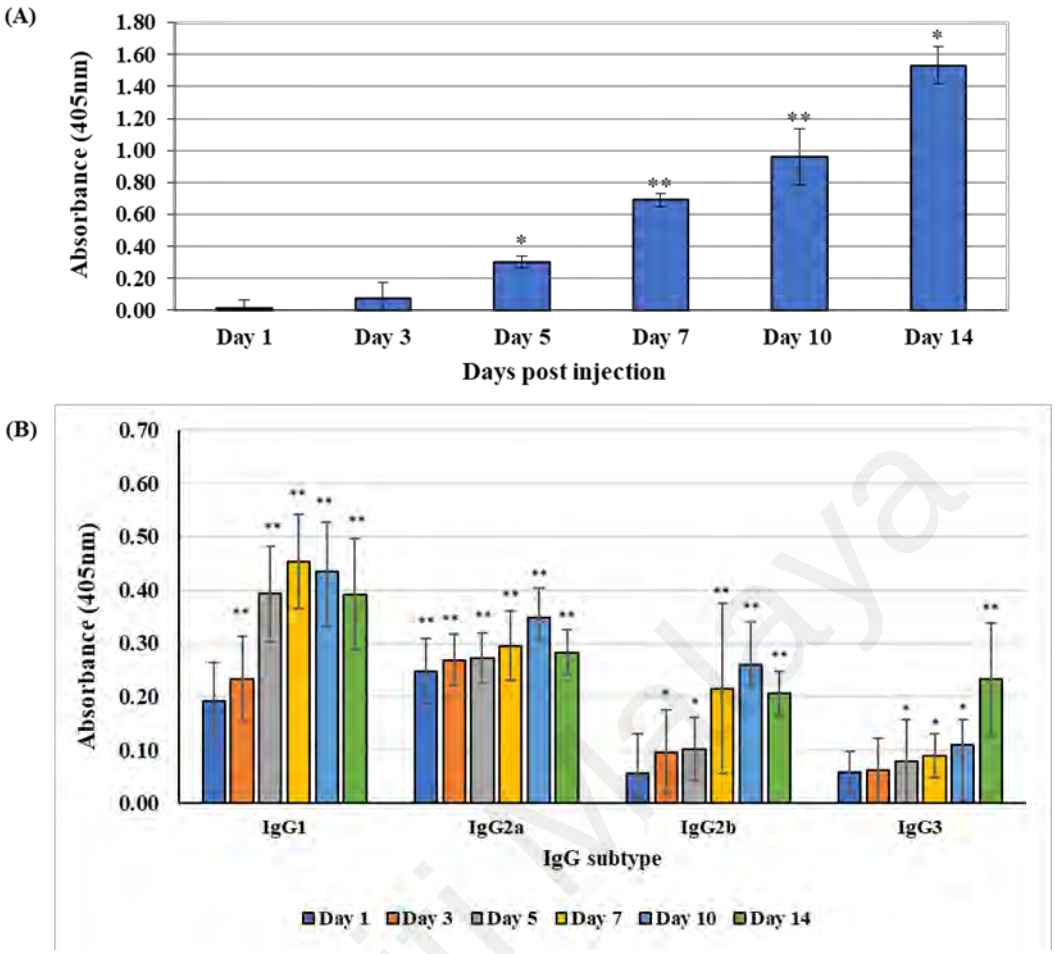

Figure 4.11: Humoral responses of CGMMV nanoparticle injection in mice. Relative quantification of anti-CGMMV antibody in serum of Balb/c mice at 1, 3, 5, 7, 10 and 14 days post-subcutaneous injection. (A) Anti-CGMMV antibody was detected after five days post-injection and increased over time. (B) IgG isotyping detected high-level of IgG1 and IgG2a compared to IgG2b and IgG3. Data was normalized to control and represents the mean ± SD and in relative to control, n = 4 biological replicates. **, $p < 0.01$; *, $p < 0.05$.

Table 4.4: Th1:Th2 index table post CGMMV nanoparticles subcutaneous injection. Th1:Th2 was calculated as (average of IgG2a, IgG2b and IgG3)/(IgG1). Data represents the mean, n = 4 biological replicates.

Day post injections	IgG1	IgG2a	IgG2b	IgG3	Th1	Th2	Th1:Th2
Day 1	0.1927	0.2485	0.0556	0.0580	0.1207	0.1927	0.6262
Day 3	0.2335	0.2688	0.0970	0.0614	0.1421	0.2335	0.6083
Day 5	0.3932	0.2725	0.1007	0.0786	0.1506	0.3932	0.3830
Day 7	0.4540	0.2958	0.2156	0.0887	0.2000	0.4540	0.4406
Day 10	0.4348	0.3486	0.2599	0.1102	0.2396	0.4348	0.5510
Day 14	0.3923	0.2833	0.2061	0.2326	0.2406	0.3923	0.6133

4.2.5 Infectivity of recovered CGMMV nanoparticles

Based on the section 4.2.2, CGMMV nanoparticles were most abundant in liver and spleen and are compatible with blood with no signs of RBC hemolysis. To investigate whether the recovered CGMMV nanoparticles from mice tissues were infectious to plants, supernatant from spleen and liver of mice were pooled and inoculated onto the cotyledon of *C. melo* var Earl favorite. At the same time, the effect of components within the blood towards the infectivity of CGMMV nanoparticles were also determined by incubating CGMMV nanoparticles with plasma and serum for 30 min at 37 ºC before inoculation as mentioned above.

Based on the results in section 4.1.1, Earl favorite showed mottle and mosaic symptoms on secondary new leave at day 10-14 post inoculation. However, it was observed that there was no symptom observed on the upper new leaves of Earl favorite inoculated with CGMMV nanoparticles extracted from the spleen or liver as well as from serum or plasma (Figure 4.12A-D). As expected, mottle symptom was seen on the upper new leave of Earl favorite inoculated with native CGMMV nanoparticles (Figure 4.12F).

Next, RT-PCR was performed to detect the CGMMV RNA. RT-PCR products were detected from inoculated and upper new leaves (Figure 4.12G). The results suggested the presence of viral RNA in the inoculum and that the virus has replicated and spread to the new leaves. However, the amount of CGMMV nanoparticles extracted from the mice tissues might be too low, or the nanoparticle were less infectious and were unable to initiate infection in plants as no symptoms were observed (Figure 4.12A-D). Thus, we hypothesized that the enzymatic activities in the liver and spleen, as well as the blood components, may have contributed to the reduced infectivity of CGMMV nanoparticles.

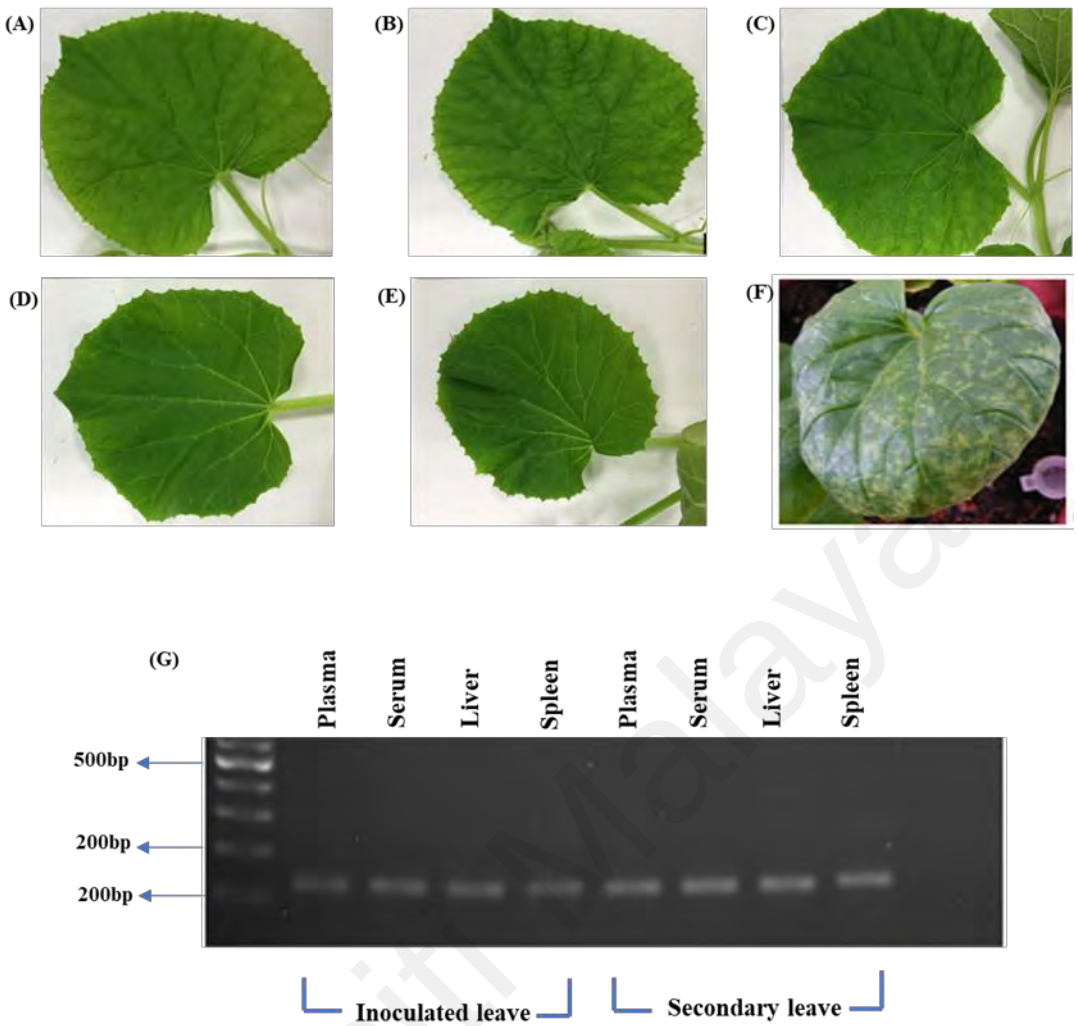

Figure 4.12: Detection of CGMMV on inoculated and upper new leaves. Cotyledon of Earl favorite was inoculated with the CGMMV nanoparticles recovered from mice tissues, blood and serum. Results showed no visible symptoms on upper new leaves of plants inoculated with virus particles extracted from (A) serum (B) plasma (C) liver (D) spleen and (E) negative control. (F) Earl favorite inoculate with CGMMV showing mottle and mosaic symptoms (positive control). (G) Agarose gel electrophoresis of RT-PCR demonstrated the presence of CGMMV genome in both inoculated and upper new leaves.

4.3 CGMMV nanoparticles as an immunostimulator

4.3.1 *In vitro* uptake of CGMMV nanoparticles by murine macrophage

Toll-like receptors (TLRs) are part of the innate immunity. Several pVNPs have been proven as an effective immunostimulator including PapMV, TMV and CPMV (refer to section 2.4). CGMMV is also a ssRNA virus. Thus, in this part of research, the immunostimulatory function of CGMMV nanoparticles was studied to determine whether CGMMV nanoparticles could induced an innate response in RAW264.7 cells and provide protection towards virus infection.

This study utilised the RAW264.7 cells, a murine macrophage cell line to study the capability of CGMMV nanoparticles to induce an innate response. Prior to this, the concentration of CGMMV nanoparticles uptake by RAW264.7 cells was determined by using CGMMV-488 nanoparticles. Based on the results of a fluorescence microscopy and flow cytometry, the uptake of 5%, 50% and 100% of CGMM-488 by RAW264.7 cells (cells fluoresce green) were achieved by 0.75 µg, 7.5 µg and 15 µg of CGMMV nanoparticles at 2 hours post incubation time respectively (Figure 4.13A and 4.13B). Localization of CGMMV-488 nanoparticles within acidic vesicles was confirmed by staining with Lysotracker (red) and DAPI (for nucleus staining) which started as early as 2 hours post incubation (Figure 4.13C) In addition, there was no cytotoxicity effect detected toward RAW264.7 cells treated with by CGMMV-488 nanoparticles with concentration as high as 75 µg (5 × higher than the 100% uptake) for three days, indicating that CGMMV nanoparticles is not toxic and does not inhibit the growth of RAW264.7 cells (Figure 4.14; Appendix I).

Taken together, the results showed that the 15 µg of CGMMV-488 nanoparticles was internalized by 1×10^6 RAW264.7 cells into the endolysosome compartment at 2 hours post incubation time without causing any toxicity effect.

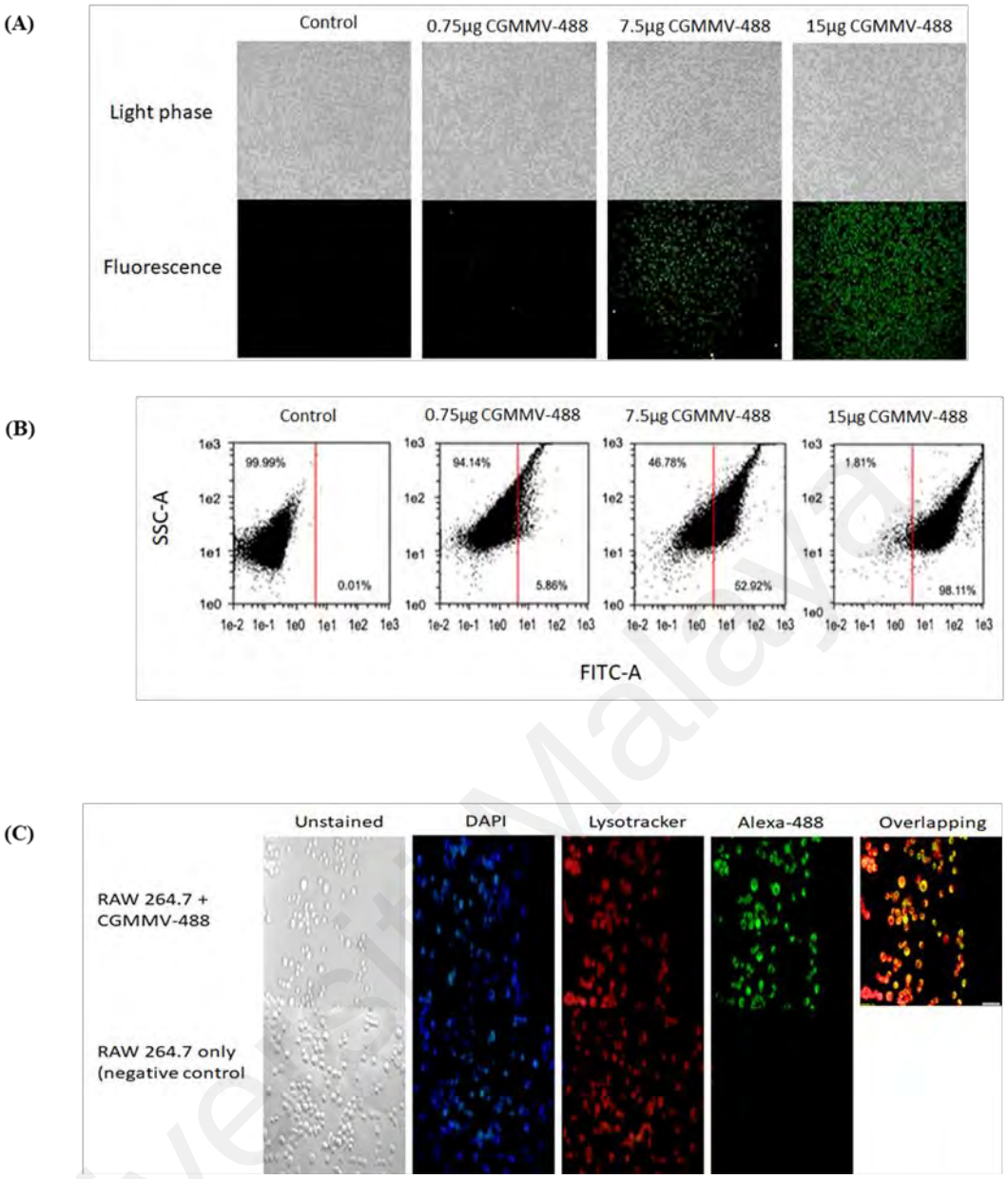

Figure 4.13: CGMMV-488 nanoparticles were taken by and localized in the macrophage. RAW264.7 cells were seeded in a 24 wells plate and treated with different concentrations of CGMMV. (A) After 2 hours, cells were visually examined on an Olympus IX73 inverted and photographed using an Olympus DP73 digital camera and analyzed using Cellsens standard software and FACS. (B) The percentage of CGMMV-488 uptake was determined by using flow cytometry. Amount of 5%, 50% and 100% of CGMMV update were equivalent to 0.75 µg, 7.5 µg and 15 µg of CGMMV nanoparticles. (C) CGMMV-488 nanoparticles co-localized to the acidic endosomes upon uptake. RAW264.7 cells were incubated with 7.5 µg of CGMMV-488 for two hours. Cells were washed with PBS then stained with Lysotracker red (for vesicles) and DAPI (for nuclei). The cells were visualized by fluorescence microscopy in light phase (grey), with DAPI (blue), with Lysotracker (red) and A488 (green).

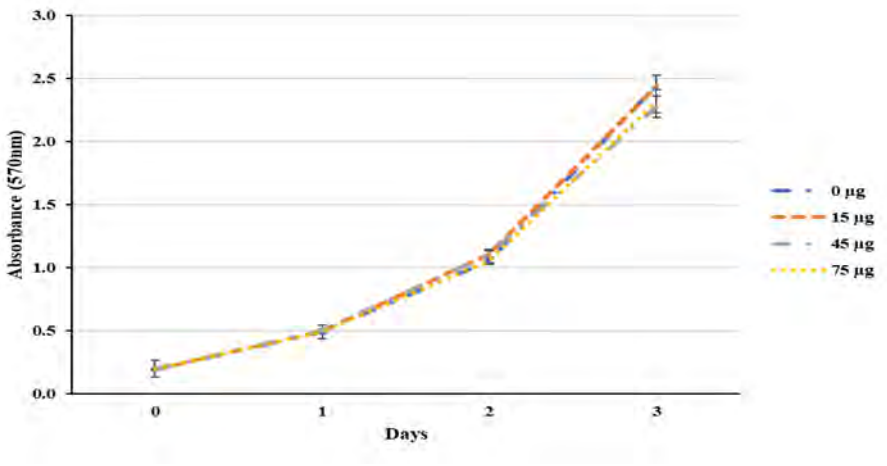

Figure 4.14: CGMMV-488 showed no cytotoxic effect in RAW264.7 cells. RAW264.7 cells were incubated with 15 µg, 45 µg, and 75 µg of CGMMV-488 nanoparticles for three days and measured for mitochondrial dehydrogenase activity (MTT assay). There is no significant difference between control (0 µg) and RAW264.7 cells treated with different concentration of CGMMV-488 nanoparticles. Data represent the means ± SD, n = 2 biological replicates. **, $p < 0.01$; *, $p < 0.05$.

4.3.2 CGMMV nanoparticles induces innate immune response

To prevent the Alexa-488 interfering with the real-time PCR and flow cytometry signals, native CGMMV nanoparticles instead of CGMMV-488 nanoparticles were used in this and subsequent experiments. Upon virus infection, macrophages will mount a type I interferon response to produce Interferon-stimulated genes (ISGs) and proinflammatory cytokines including tumour necrosis factor alpha (TNF-α) as the first line of defence to control virus replication. We tested 15 µg of CGMMV nanoparticles (100% uptake) and another with 5 folds higher concentration of CGMMV nanoparticles (75 µg) to test whether CGMMV nanoparticles treatment can induce an innate immune response in the RAW264.7 cells. The mRNA expression level of a list of genes involved in the nuclear factor kappa B (NF-κB) pathway and Type I interferon signalling were tested.

Based on the results, the expression level of genes (*TNF-α*, *IFN-β*, *IFIT-2*, *IFIT-3*, *OAS-2* and *OAS-3*) were upregulated as early as 2 hours post incubation with 15 µg CGMMV (Figure 4.15; Appendix J) and 75 µg of CGMMV and reached the peak between 4-6 hours post incubation before gradually reducing. The expression level of the genes was higher when treated with 75 µg of CGMMV nanoparticles than with 15 µg of CGMMV nanoparticles (Figure 4.16; Appendix K) suggesting that the effect was dose dependent.

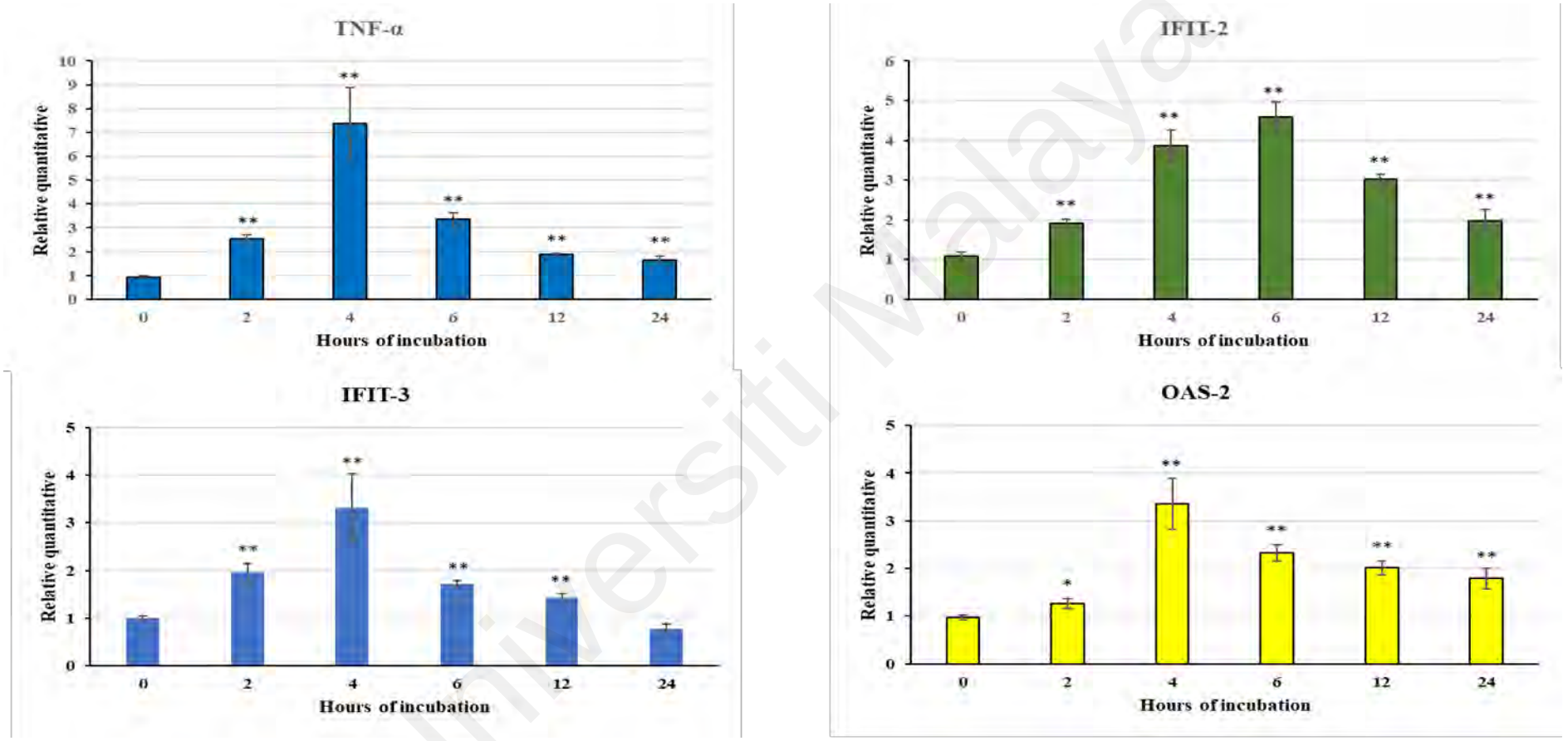

Figure 4.15: CGMMV upregulates the expression of interferon-β, ISGs and inflammatory genes at concentration of 15 µg. *TNF-α*, *IFIT-2*, *IFIT-3*, *OAS-2*, *OAS-3* and *IFN-β* of RAW264.7 cells was upregulated after treated with CGMMV for 2, 4, 6,12 and 24 hours. Data represent the mean and ± SD, n = 2 biological replicates. Data was normalized to RPL32 and shown in relative to 0 hours of CGMMG control **, $p < 0.01$; *, $p < 0.05$. Refer to next page for *OAS-3* and *IFN-β*.

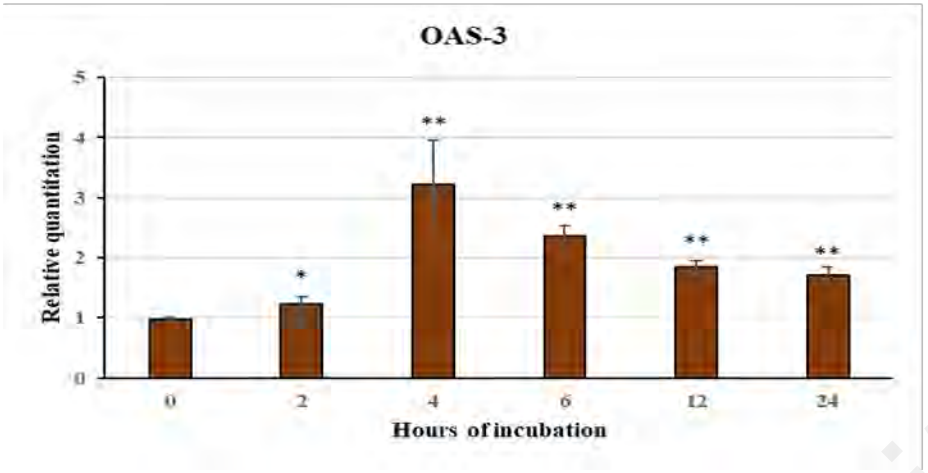

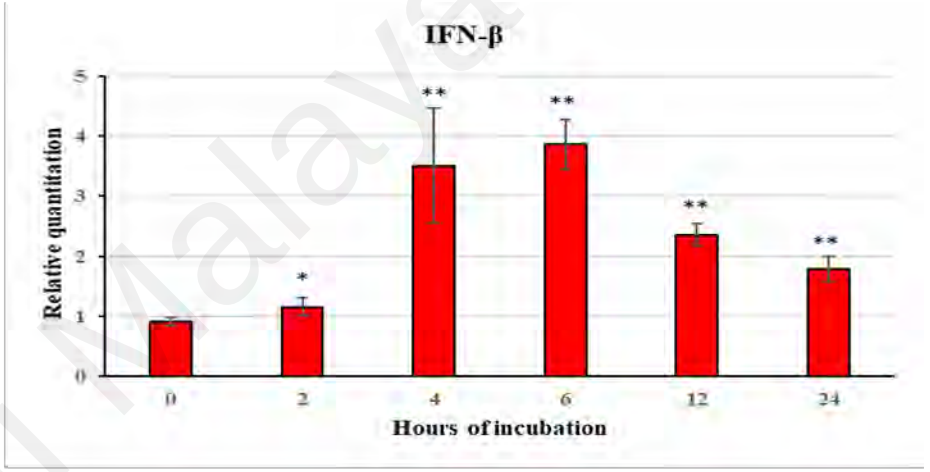

Figure 4.15, continued.

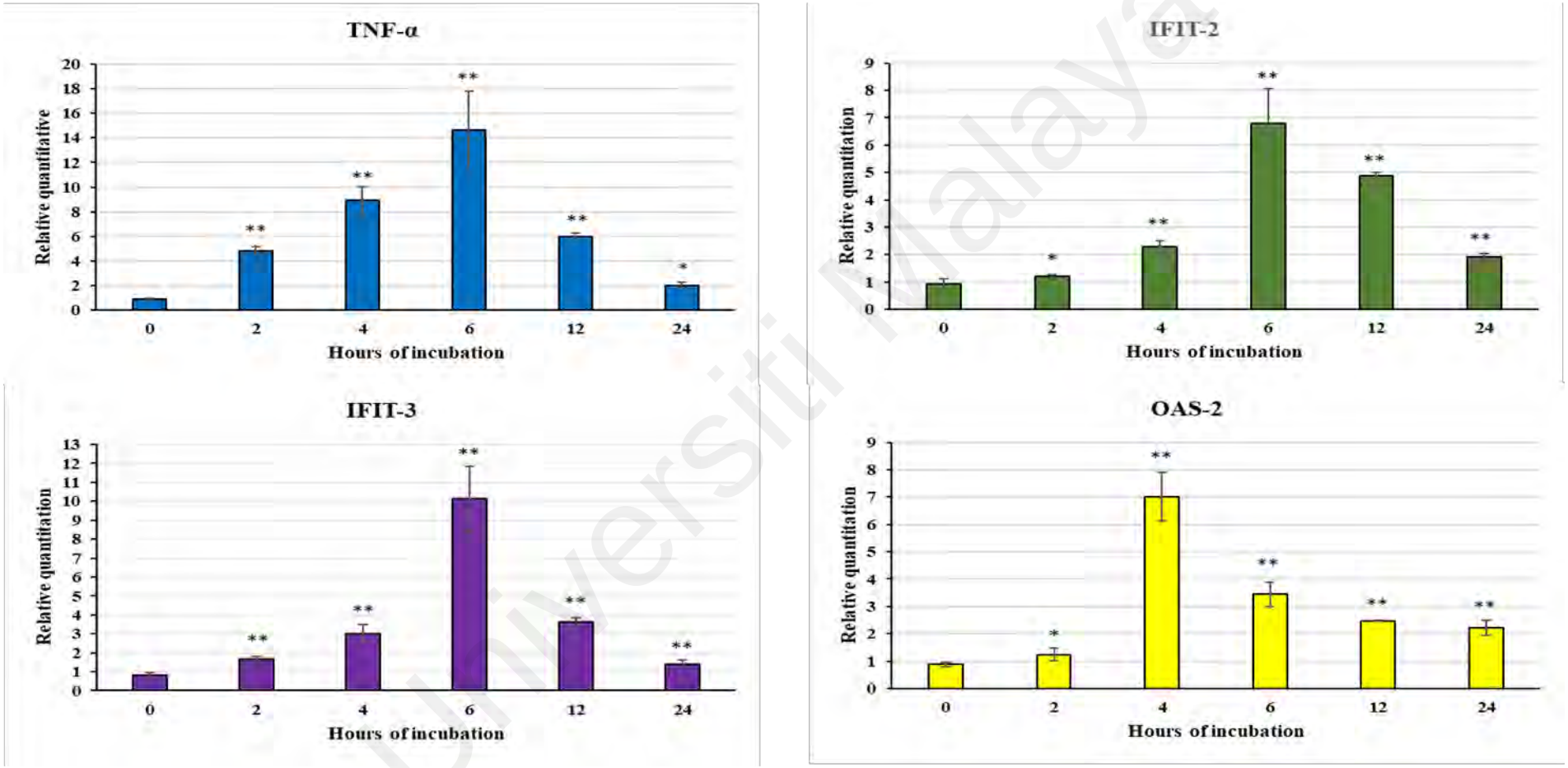

Figure 4.16: CGMMV upregulates the expression of interferon-β, ISGs and inflammatory genes at concentration of 75 µg. *TNF-α*, *IFIT-2, IFIT-3*, *OAS-2*, *OAS-3* and *IFN-β* of RAW264.7 cells was upregulated after treated with CGMMV for 2, 4, 6,12 and 24 hours. Data represent the mean and ± SD, n = 2 biological replicates. **. Data was normalized to RPL32 and shown in relative to 0 hours of CGMMG control, $p < 0.01$; *, $p < 0.05$. Refer to next page for *OAS-3* and *IFN-β.*

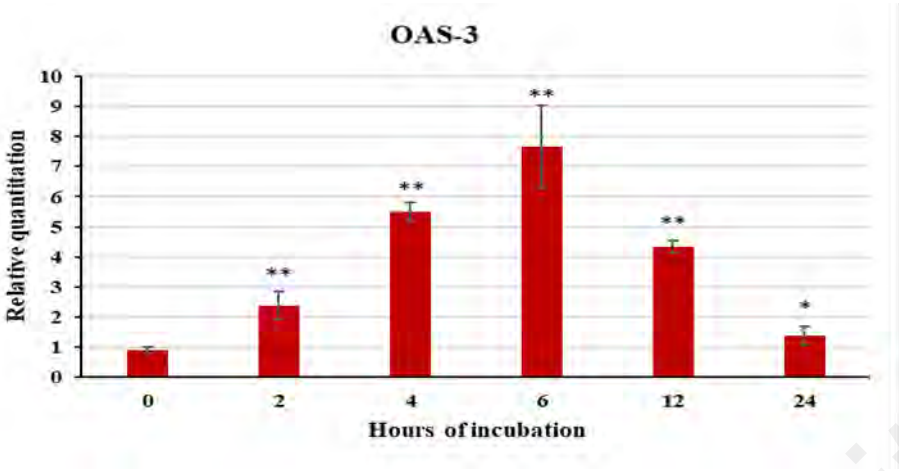

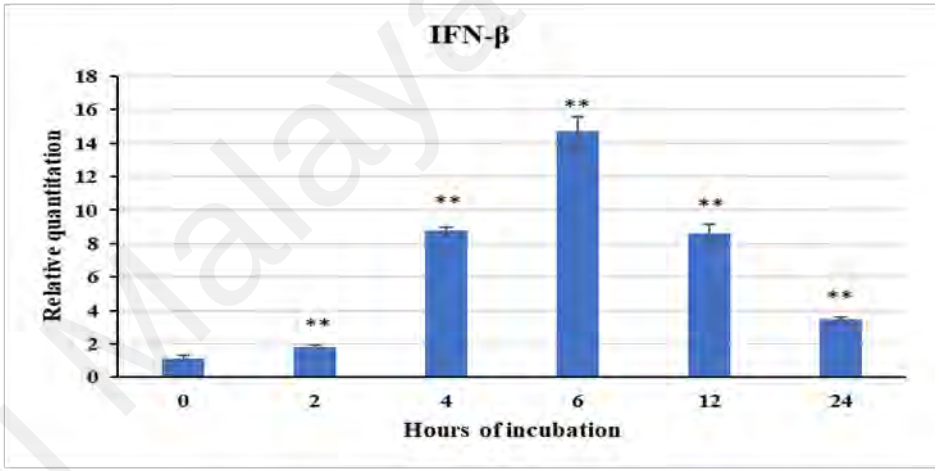

Figure 4.16, continued.

Subsequently, the level of pro-inflammatory cytokines (TNF-α, IL-6 and IL-12) were determined by ELISA. Based on the results, inflammatory cytokines produced as early as 2 hours post incubation and it was also dose dependent (Figure 4.17; Appendix L). Taken together, these results suggest that CGMMV nanoparticles can induce innate response via NF-κB pathway and Type I interferon signalling in RAW264.7 cells and the expression level was dose dependent.

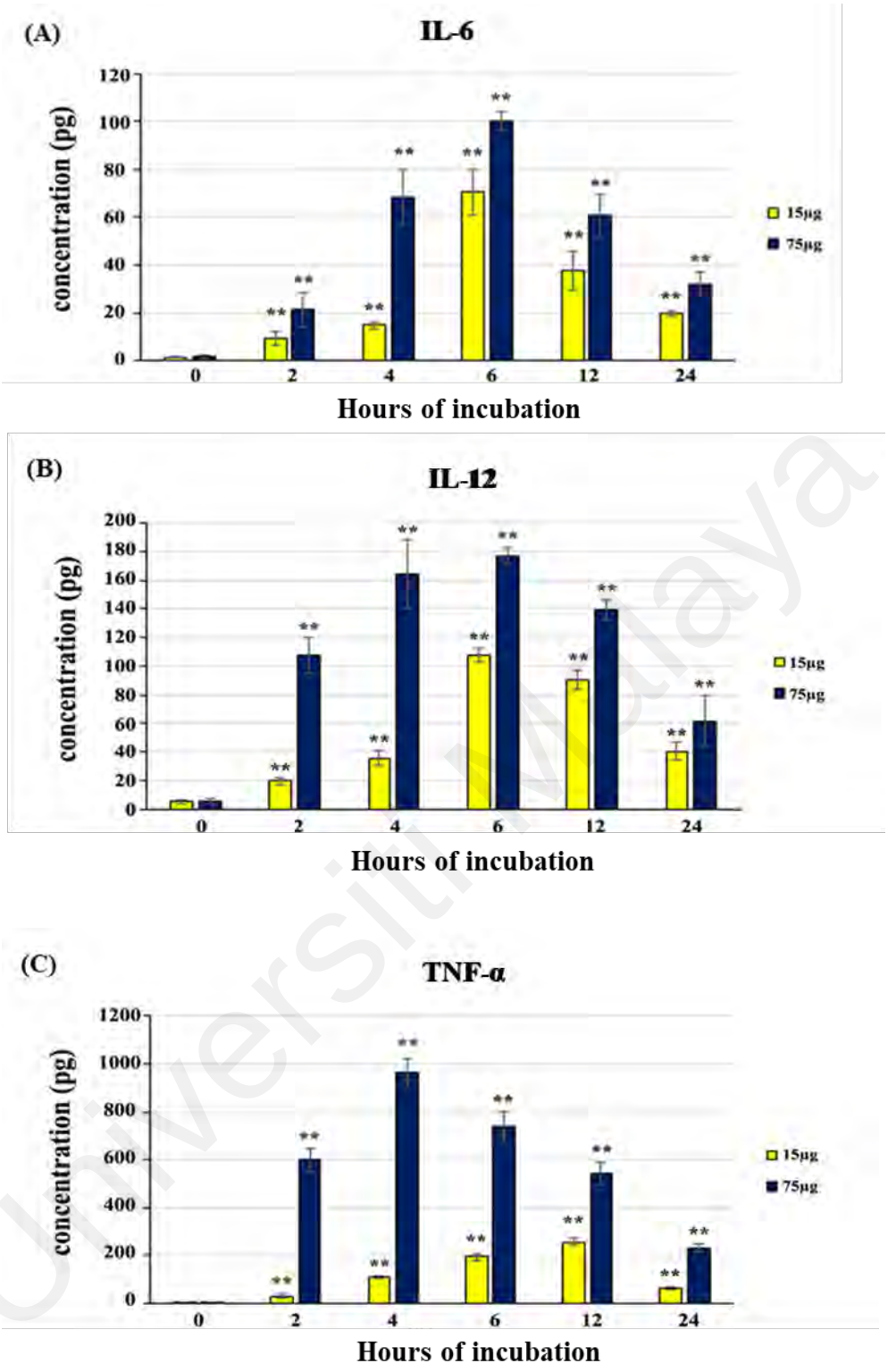

Figure 4.17: CGMMV nanoparticles induced the production of pro-inflammatory cytokines. Cytokine production of (A) IL-6, (B) IL-12 and (C) TNF-α in murine macrophages RAW264.7 cells treated with 15 µg and 75 µg of CGMMV nanoparticles for 2, 4, 6, 12 and 24 hours. A standard curve was plotted, and the concentration of the cytokines was calculated based on the equation with $R2 > 0.99$ and plotted. Data represent the mean and ± SD, n = 2 biological replicates. **, $p < 0.01$; *, $p < 0.05$.

4.3.3 Upregulation of CD54, CD40 and CD86

To gain an insight into the *in vitro* antigen-specific T cells induction properties of CGMMV nanoparticles, the signs of activated macrophages through the expression of cell surface markers on RAW264.7 cells treated with 75 µg CGMMV nanoparticles over a 24 hours' time course was analyzed. As shown in Figure 4.18, the T cells interaction molecule CD54 (a.k.a. ICAM-1), used by macrophages to bind non-specifically to passer-by T cells for the purpose of T cells receptor sampling, was significantly up-regulated. CD40, needed for crosstalk and stimulation of T cells via CD40L binding, was also significantly increased. Similarly, higher amounts of the co-stimulatory molecule CD86, required for potent $CD4^+$ and $CD8^+$ T cells activation was also observed. These results indicate that not only was CGMMV nanoparticles efficiently taken up by the macrophage but it also facilitated macrophage activation, indicating a potential for antigen-specific T cells proliferation.

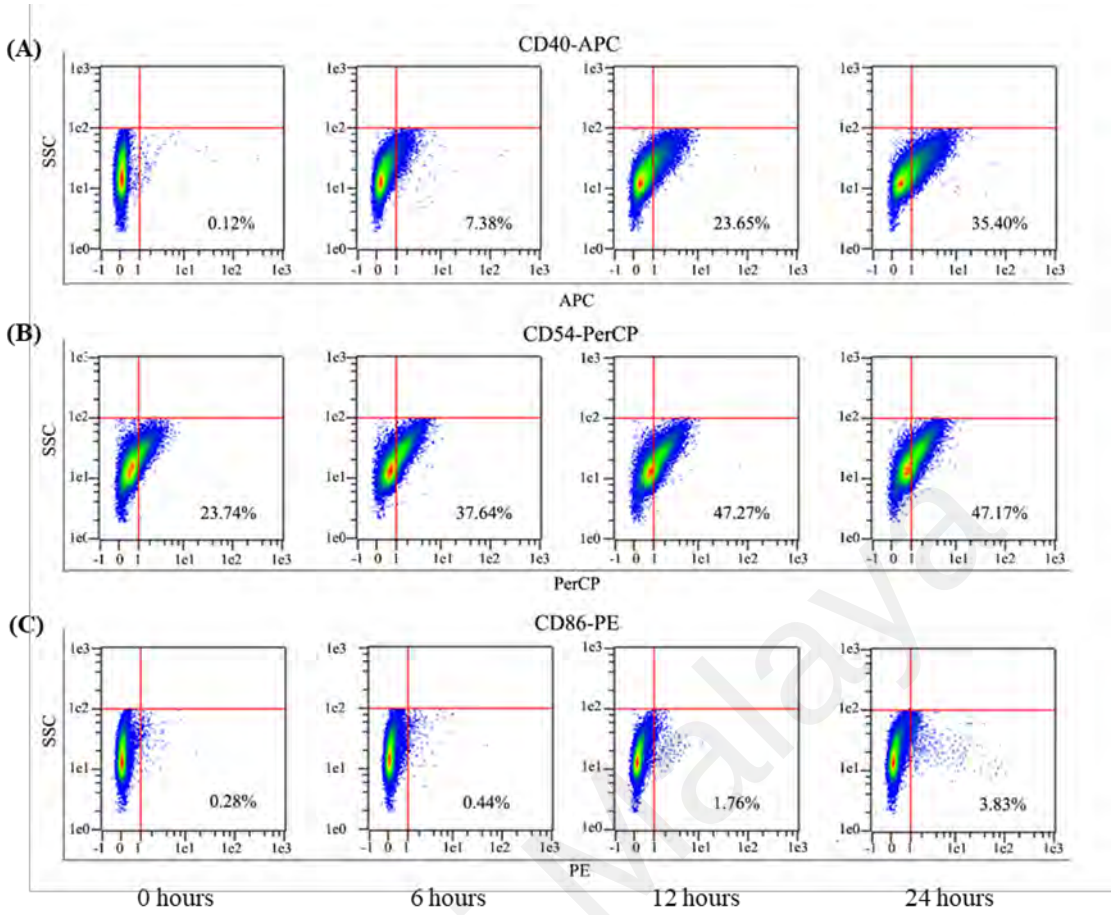

Figure 4.18: CGMMV nanoparticles induces RAW264.7 cells activation *in vitro* as indicated by cell surface marker expression upregulation. Single cell suspension was stained with (A) anti-CD40-APC, (B) anti-CD54-PerCP and (C) anti-CD80-PE. Ten thousand cells were analyzed via flow cytometry.

4.3.4 CGMMV nanoparticles confer protection against virus infection

Since CGMMV nanoparticles can stimulate innate immune response in RAW264.7 cells, it was further tested whether pre-treatment of RAW264.7 cells with CGMMV nanoparticles can confer protection against virus infections. The RAW264.7 cells pre-treated with 75 µg CGMMV nanoparticles for 6 hours was infected with an MOI of 1 of VSV-GFP for 12 hours.

In comparison to the control, RAW264.7 cells pre-treated with CGMMV nanoparticles showed a reduction of infection by VSV-GFP (Figure 4.19A). The GFP mRNA in CGMMV nanoparticles-exposed cells was reduced by approximately 80% as measured by qRT-PCR (Figure 4.19B, Appendix M). To determine if the GFP signal reduction was due to an inhibition at the virus entry or transcription step, we measured the expression of negative strand vRNAs (vGFP) at 2 hours post infection after being pre-treated with 75 µg CGMMV nanoparticles. As shown in Figure 4.19C, there were no significant changes observed in the level of vGFP in both VSV-GFP and VSV-GFP + CGMMV-treated cells indicating similar viral load and VSV infection rate (Appendix M).

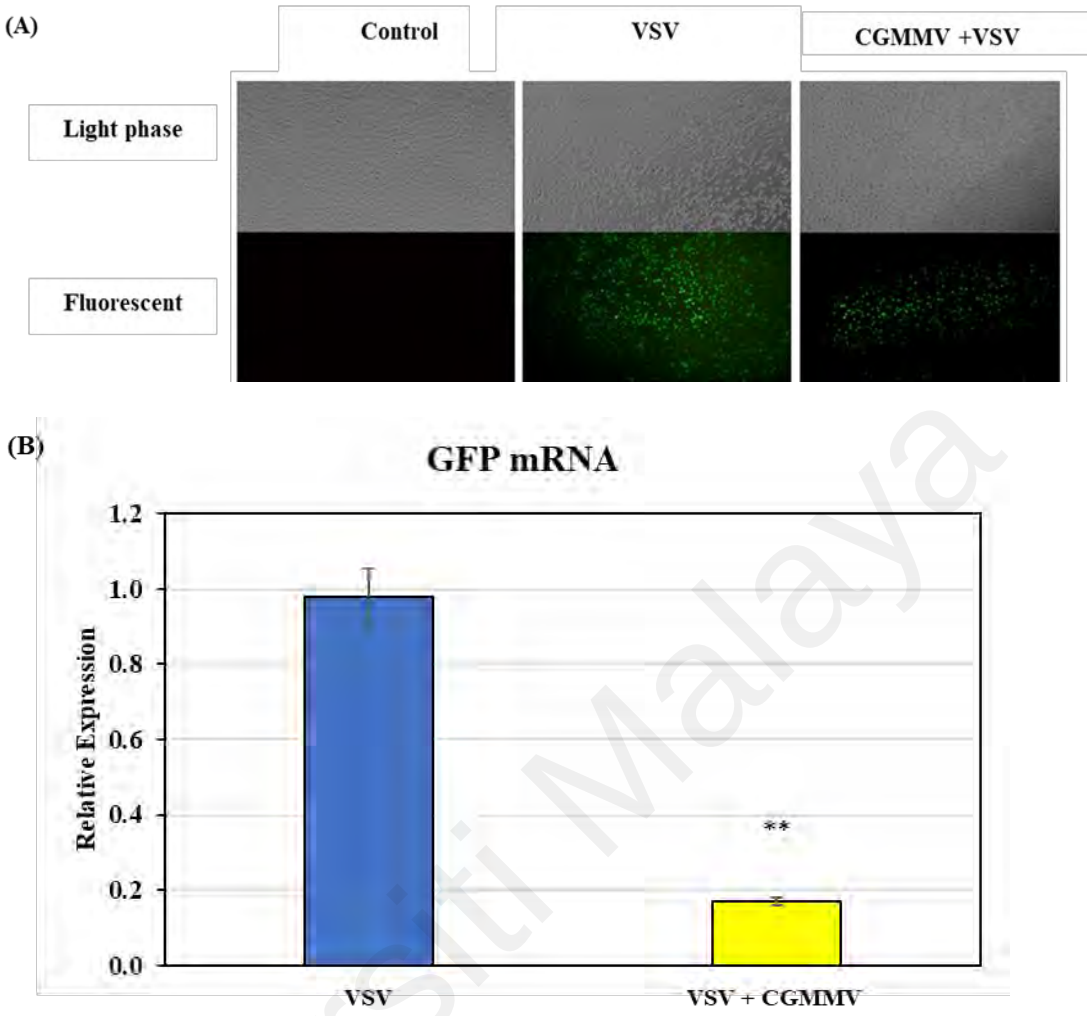

Figure 4.19: CGMMV nanoparticles pre-treatment reduced VSV-GFP replication in RAW264.7 cells. (A) The GFP fluorescence signal of VSV-GFP in the RAW264.7 cells was significantly reduced after treated with CGMMV nanoparticles as shown by fluorescence microscopy. (B) Relative expression of GFP mRNA measured using qRT-PCR in VSV-GFP infected cells pre-treated with or without CGMMV nanoparticles as measured by qRT-PCR. (C) The viral load as measured by the vGFP vRNA in both treatments (with or without CGMMV nanoparticles). Data was normalized to RPL32, in relative to RAW264.7 cells + VSV and represent the mean and ± SD, n = 2 biological replicates. **, $p < 0.01$; *, $p < 0.05$. Refer to next page for figure (C).

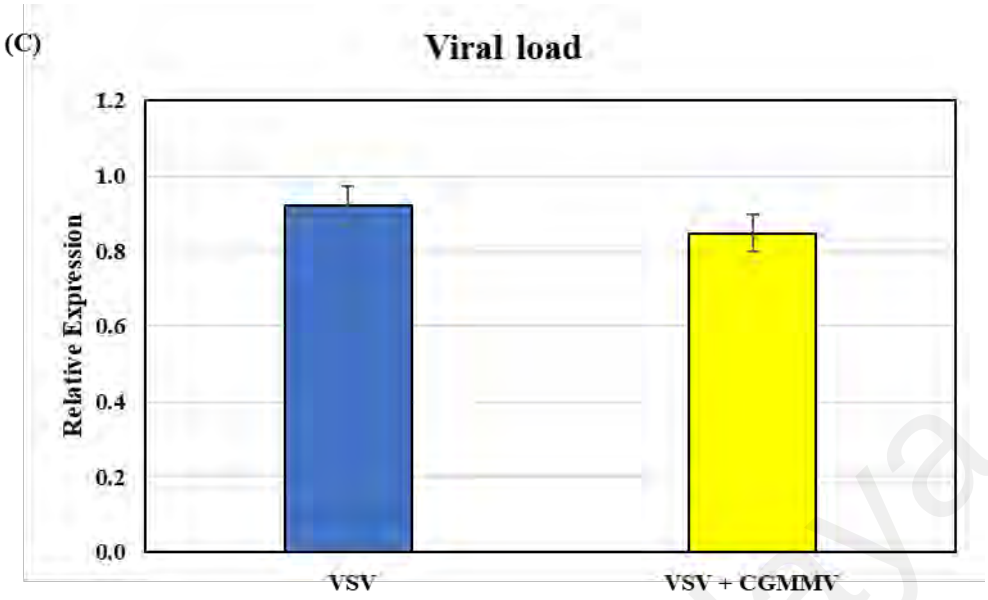

Figure 4.19, continued.

To determine if the CGMMV nanoparticles conferred protection is specific to VSV-GFP, similar experiment was carried out on another negative single-stranded RNA virus which is *Sendai virus* (SeV) from the *Paramyxoviridae* family. The RAW264.7 cells pre-treated with 75 µg CGMMV nanoparticles for 6 hours was infected with a 150 HAU of SeV for 2 hours and 14 hours to measure the vRNA and mRNA expression of SeV coat protein respectively. Similar protection was observed in the RAW264.7 cells infected with SeV whereby CGMMVV pre-treatment significantly reduced the SeV replication by 75% without affecting the SeV entry into the cells (Figure 4.20; Appendix N).

Together, these data suggest that the treatment of RAW264.7 cells with CGMMV nanoparticles significantly reduced VSV and SeV replication.

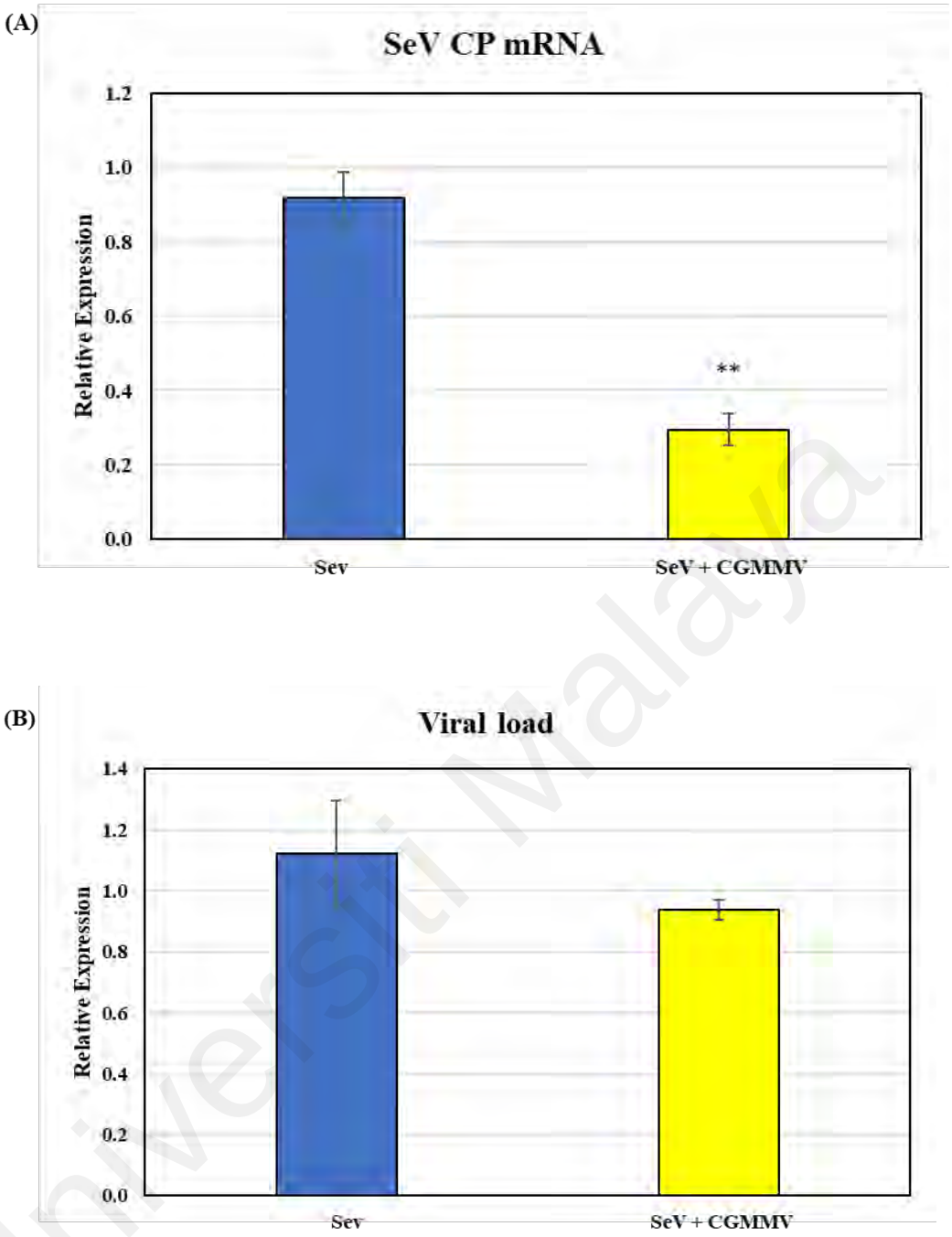

Figure 4.20: CGMMV nanoparticles pre-treatment reduced SeV replication in RAW264.7 cells. (A) The expression of CP mRNA (B) vRNA (viral load) of SeV coat protein gene in RAW264.7 cells treated with or without CGMMV nanoparticles pre-treatment. Data was normalized to RPL32, in relative to RAW264.7 cells + SeV and represent the mean and ± SD, n = 2 biological replicates. **, $p < 0.01$; *, $p < 0.05$.

4.4 Construction of CGMMV as expression vector of influenza epitopes

4.4.1 Selection of the hemagglutinin (HA) and matrix (M1) epitopes

In this section of study, a CGMMV vector was constructed to express the influenza epitopes comprising of the HA and M1 proteins. The Immune epitope database which contains experimental data on antibody and T cell epitopes related to nearly 92% of infectious diseases including influenza was used to search for usable HA and M1 epitopes (Vita et al., 2010, 2015, 2019). By referring to this database, epitopes from HA and M1 proteins of influenza with positive results of T cell ($CD8^+$ or $CD4^+$) and B cell responses were selected.

Thus, a total of 11 HA and 4 M1 epitopes with promising experimental results were selected (Appendix O and P). These epitopes are either able to induce cell proliferation with or without the release of interferon gamma (IFN-γ) and interleukin 2 (IL-2) (indicator for T cells activation and proliferation), reduce the virus titer in lung, antigen/antibody binding or increase the survival rate in tested animal models after challenged with influenza virus. The size of T cell epitopes that target the T cells is in the range of 8-10 amino acids due to the structure of MHC binding cleft that can only present a limited number of the amino acids. However, there is no limitation for B cell epitopes as the antibody mainly recognizes the structure formed by the epitopes than its sequence (Sanchez-Trincado et al., 2017).

Next, to express the HA and M1 epitopes on the coat protein of CGMMV, we followed the read-through strategy developed by the Ooi and colleagues, 2006 by adding the amber stop codon (asc) of CGMMV with the sequence of 'TCT-AAA-TAG-CAA-TTA' (SKLQL) at the N terminal of the coat protein before fused with HA and M1 epitopes. With this strategy, wild-type as well as chimeric CGMMV nanoparticles with the foreign epitopes can be formed (Ooi et al., 2006). The isoelectric point (pI) value of the chimeric

CGMMV coat protein was adjusted to be close to or lower than the value of the wild-type CGMMV to maintain the stability of the virus particles and the epitopes expressed on the surface of CGMMV coat protein (Bendahmane et al., 1999). The pI value of the wild-type CGMMV coat protein was 5.08 as predicted using Protein calculator v3.3 (http://www.scripps.edu/~cdputnam/protcalc.html). Glutamic acid was added at the C terminal of epitopes to adjust the pI value of recombinant CGMMV nearer to 5.08. For the chimeric CGMMV coat protein which showed the pI value lower than 5.08, no adjustment was made. As a result, ten epitopes (6 from HA and 4 from M1) were selected to be cloned into CGMMV vector. The name of the chimeric constructs, name of epitopes with the amino acids sequences as well as molecular weight and pI of chimeric CGMMVs were summarized in Table 4.5. The number in the chimeric constructs and name of epitopes referred to the position of amino acids in the HA and M1 protein. To avoid confusion, M1 will be written as M when mentioned as the name of the chimeric construct and epitope.

Table 4.5: Chimeric CGMMV constructs with asc and HA or M1 epitopes. The chimeric constructs were adjusted by two or less glutamic acids. The sequence and length of amino acids, molecular weight and pI are as listed.

Constructs name	Epitope name	Inserted sequence	Inserted size (aa)	Predicted Molecular weight (kD)	Predicted pI
Wild-type CGMMV 1410		-	-	17.394	5.08
CGMMVasc (CGMMV+amber stop codon)		S*KLQL*	5	17.964	5.27
CGMMVasc+HA127-137	HA127-137	S*KLQL*SLERFEIFPKEA	17	19.411	5.15
CGMMVasc+HA166-175	HA166-175	S*KLQL*WLTKKGDSYPEEA	18	19.469	5.15
CGMMVasc+HA331-354	HA331-354	S*KLQL*VTGLRNIPSIQSRGLFGAIAGFIEGEEA	32	20.849	5.15
CGMMVasc+HA344-354	HA344-354	S*KLQL*GLFGAIAGFIEA	17	19.111	5.10
CGMMVasc+HA461-469	HA461-469	S*KLQL*LYEKVKSQLEEA	17	19.382	5.15
CGMMVasc+HA532-540	HA532-540	S*KLQL*IYSTVASSLEA	16	19.086	5.10
CGMMVasc+ M58-66	M58-66	S*KLQL*GILGFVFTLEA	16	19.112	5.10
CGMMVasc+M83-100	M83-100	S*KLQL*ALNGNGDPNNMDKAVKLYEA	25	20.080	5.15
CGMMVasc+ M128-135	M128-135	S*KLQL*MGLIYNRMEEA	16	19.272	5.12
CGMMVasc+M220-236	M220-236	S*KLQL*GTHPSSSAGLKNDLLENEA	24	19.886	5.15

4.4.2 *In silico* modelling and secondary prediction

Subsequently, we modelled the chimeric CGMMV coat protein carrying the influenza epitope using the iterative threading assembly refinement (I-TASSER) server to predict the model of chimeric CGMMV coat protein. This server was chosen as it has been ranked as the best method for the automated protein structure prediction in the past 8 CASP experiments, a community-wide critical assessment of protein structure prediction in between 2006-2020 (Yang et al., 2015; Zhang, 2008).

The structure templates used for prediction are crystalized CGMMV (1cgm at 3.4Å) (Wang and Stubbs, 1994) and crystalized TMV (1Ei7 at 2.4 Å) (Bhyravbhatla et al., 1998) from the protein database (PDB) (Figure 4.21).

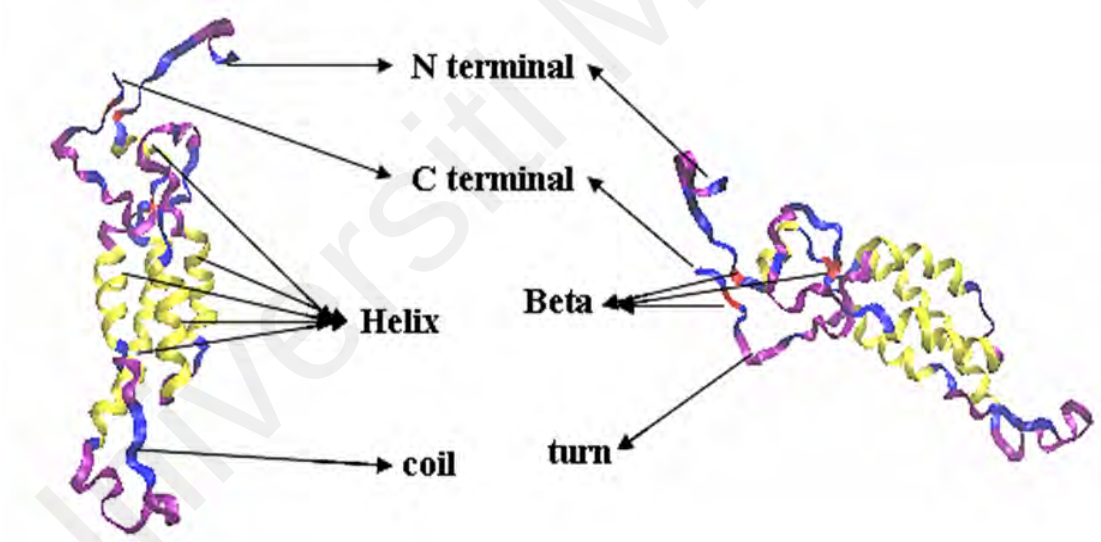

Figure 4.21: Crystal structures of CGMMV and TMV coat proteins. (Left) 1cgm and (right) 1iE7 from PDB. Both structures consist of alpha helix (yellow), beta sheets (red) and coils (blue) and turns (purple).

Figure 4.22 showed that the predicted models of chimeric CGMMV coat proteins generated by I-TASSER. All the models predicted showed high quality with correct fold and topology as the C-score and TM score are fall in the acceptable range (Table 4.6). C-score is a confidence score for estimating the quality of predicted models by I-TASSER. It is calculated based on the significance of threading template alignments and the convergence parameters of the structure assembly simulations. C-score is typically in the range of [-5 to 2], where a C-score of higher value signifies a model with a high confidence and vice-versa. The models with C-score more >-1.5 have a correct fold. A TM-score >0.5 indicates a model of correct topology.

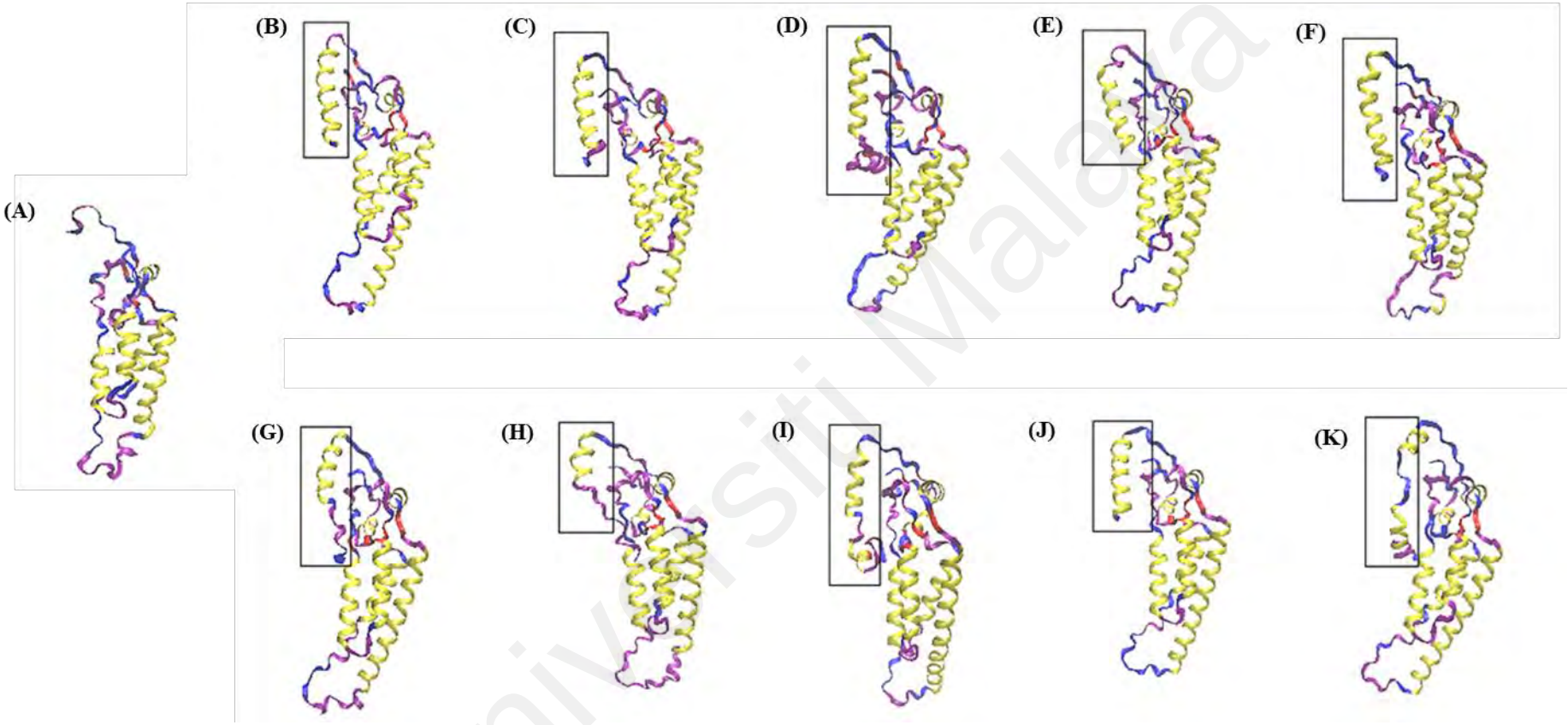

Figure 4.22: The 3D structure of wild-type CGMMV and chimeric CGMMV coat protein generated by I-TASSER. The structure in the rectangle box represents the structure of inserted epitope. (A) Wild-type CGMMV coat protein, (B) CGMMVasc+HA127-137, (C) CGMMVasc+HA166-175, (D) CGMMVasc+HA331-354, (E) CGMMVasc+HA344-354, (F) CGMMVasc+HA461-469, (G) CGMMVasc+HA532-540, (H) CGMMVasc+M58-66, (I) CGMMVasc+M81-100, (J) CGMMVasc+M128-135 and (K) CGMMVasc+M220-236.

Table 4.6: The value/scores of the chimeric CGMMV coat protein models predicted by I-TASSER.

Name of construct	TM scores	C scores
CGMMVasc+HA166-175	0.71±0.12	-0.04
CGMMVasc+HA344-354	0.73±0.11	0.102
CGMMVasc+HA331-354	0.67±0.13	-0.322
CGMMVasc+HA127-137	0.71±0.12	-0.14
CGMMVasc+HA532-540	0.73±0.11	0.101
CGMMVasc+HA461-469	0.72±0.11	0.077
CGMMVasc+M58-66	0.72±0.11	-0.069
CGMMVasc+M128-135	0.71±0.12	-0.041
CGMMVasc+M83-100	0.69±0.12	-0.208
CGMMVasc+M220-236	0.71±0.12	-0.041

The predicted models were further validated using PROCHECK, a program that checks the stereochemical quality of a protein structure by analysing the residue-by-residue geometry and overall structure geometry (Table 4.7). A good quality model would be expected to have over 90% residues in the most favored regions based on the structures of resolution of at least 2.0 Angstroms. However, based on the results, the amino acids residue in the most favored region of all the chimeric models were in the range of 70.4% to 90.2%. It might be due to the quality the templates used rather than the error in prediction method as the PROCHECK value of 1cgm and 1Ei7 was 63.9% and 83.1%.

Table 4.7: PROCHECK validation result of chimeric CGMMV, CGMMV (1cgm) and TMV (1Ei7).

Constructs	Residues in most favored regions	Residues in additional allowed regions	Residues in generously allowed regions	Residues in disallowed regions
CGMMVasc+HA127-137	87.2	9.9%	2.3%	0.6%
CGMMVasc+HA166-175	87.6%	11.2%	1.2%	0.0%
CGMMVasc+HA331-354	82.6%	12.2%	2.3%	2.9%
CGMMVasc+HA344-354	86.2%	13.8%	0.0%	0.0%
CGMMVasc+HA461-469	81.6	14.7%	2.5%	1.2%
CGMMVasc+HA532-540	90.1	8.1%	1.2%	0.6%
CGMMVasc+M58-66	70.4	22.6%	5.7%	1.3%
CGMMVasc+M83-100	84.4	12.6%	2.4%	0.6%
CGMMVasc+M128-135	87.5	11.2%	1.2%	0.0%
CGMMVasc+M220-236	81.3	15.7%	1.8%	1.2%
CGMMV (1cgm)	63.9%	32.6%	3.5%	0.0%
TMV (1Ei7)	83.1%	11.3%	4.2%	1.4%

Since the epitope was inserted at the 3' terminal of RNA that encodes the coat protein, the RNA secondary structure was also predicted using Vienna secondary structure prediction server to compare the stability and the structure of chimeric CGMMV with the wild-type CGMMV (Figure 4.23). The minimum energy (ME) of all chimeric RNAs were slightly lower than the ME of the wild-type CGMMV which showed that the stability of the chimeric constructs was similar with the wild-type RNA 4 of CGMMV. In terms of structure, the wild-type RNA secondary structure possessed a few asymmetrical hairpin loops in the structure with one major loop at the middle of the structure. The RNA secondary structure of CGMMVasc+HA331-354 (RNA4+HA331-354), CGMMVasc+HA344-354 (RNA4+HA344-354) and CGMMVasc+HA32-540 (RNA4+HA532-540) were highly similar to the wild CGMMV (wild-type RNA) in terms of pattern and topology. The RNA secondary structure of CGMMVasc+HA461-469 (RNA4+HA461-469), CGMMVasc+M58-66 (RNA4+M58-66), CGMMVasc+M83-100 (RNA4+M83-100) and CGMMVasc+M220-266 (RNA4+M220-266) was also similar with the wild-type CGMMV except the asymmetrical loop at the middle of the structure is smaller. The topology of the CGMMVasc+M128-135 (RNA4+M128-135) is slightly different where there were more loops structure at the left and bottom of the structure.

In addition, the RNA secondary structure of two chimeric constructs were very different with the others: CGMMVasc+HA127-137 (RNA4+HA 127-137) and CGMMVasc+HA166-175. Their structure is horizontal compared to the rest which were vertical. The 5' and the 3' termini (circle in red) of RNA which are initially located at the upper (top) of the structure of wild-type CGMMV and other chimeric constructs were shifted to the middle of the structure.

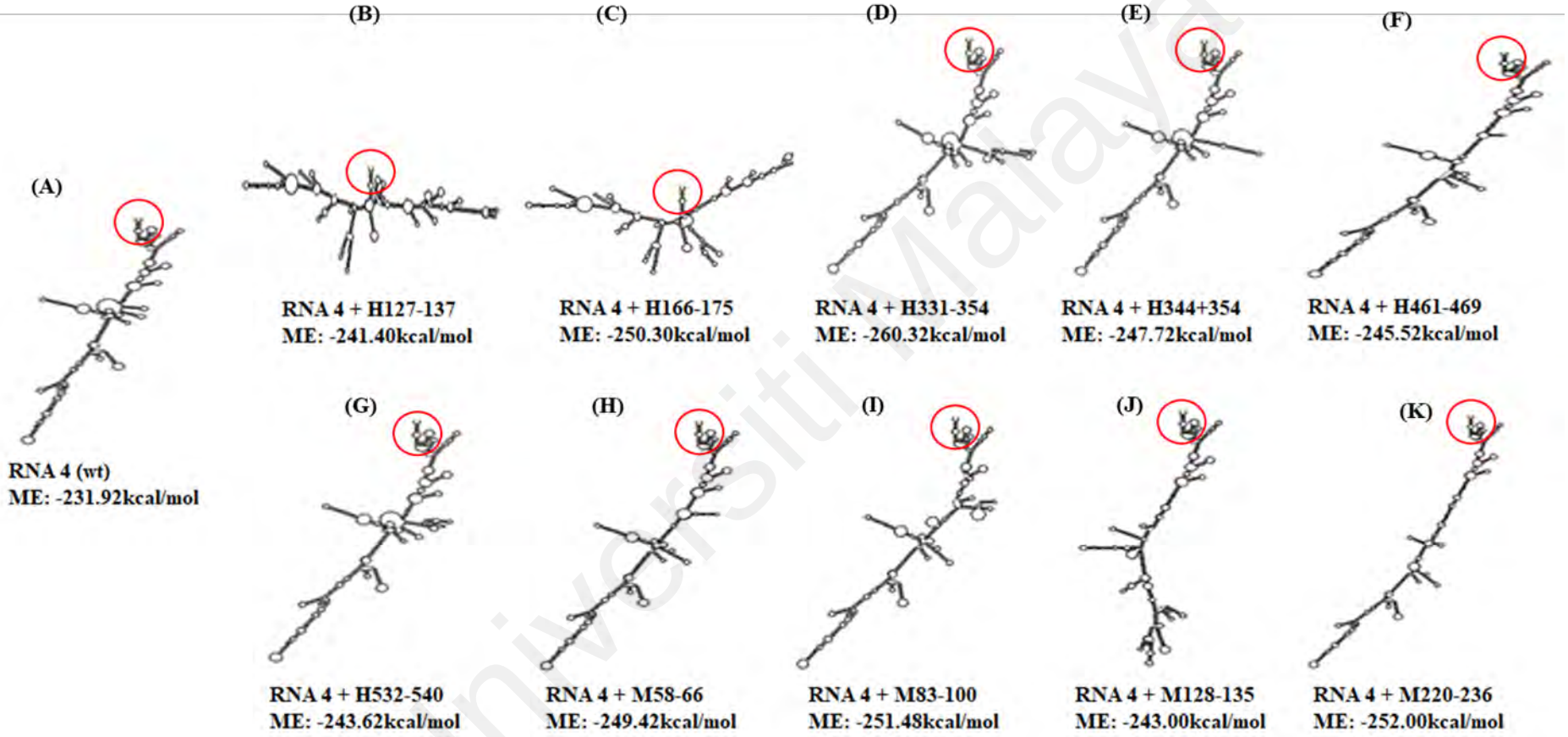

Figure 4.23: Predicted RNA secondary of wild-type and chimeras of newly synthesis RNA 4. The infectious chimeras possessed similar structure patterns with lower ME compared with the (A) wild-type except the (B) RNA4+HA127-137, and (C) RNA4+HA66-175, (D) RNA4+HA331-354, (E) RNA4+HA344-354, (F) RNA4+HA461-469, (G) RNA4+HA532-540, (H) RNA4+M58-66, (I) RNA4+M81-100, (J) RNA4+M128-135 and (K) RNA4+M220-236.

As the chimeric coat protein and RNA structures showed above were generated using the computer software, the actual effect of the inserted epitopes toward the topology and structure of coat protein and RNA were further verified by lab wet in the following sections.

4.3.3 Construction of chimeric CGMMV vectors

CGMMV 1410 vector was constructed based on the pCGHB310803 vector by removing the Hepatitis B surface antigen (Ooi et al 2006). As the sequences of the selected epitopes are relatively short (~ 11 to 28 amino acids, equivalent to ~33 to 84 bp), PCR is not applicable to amplify the segments. Therefore, the sequence encoding the read through amber stop codon, selected epitopes, as well as the 3' non translated region of CGMMV, was designed with Hind III restriction digestion site added at the 5' terminal of the amber stop codon and Sph I restriction digestion site added at the 3' terminal of the non-translated region and sent for gene synthesis to synthesise the entire sequence which were then cloned into pUC57 vector. The sequences were then subcloned from pUC57 vector into the CGMMV 1410 vector (Figure 4.24 and Figure 4.25).

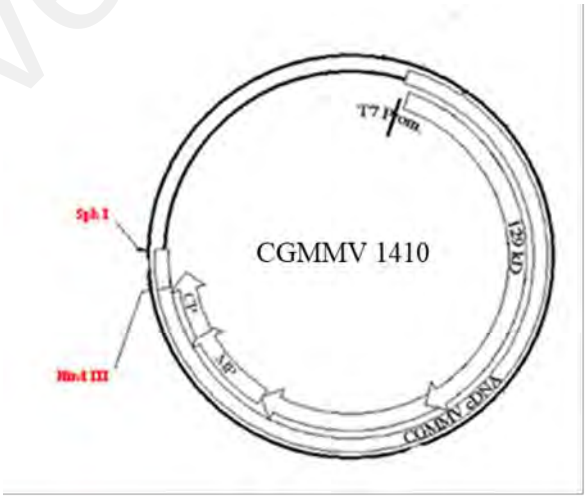

Figure 4.24: The map of CGMMV 1410 vector. The custom-designed selected epitopes were cloned into Hind III and Sph I restriction sites to form chimeric vectors.

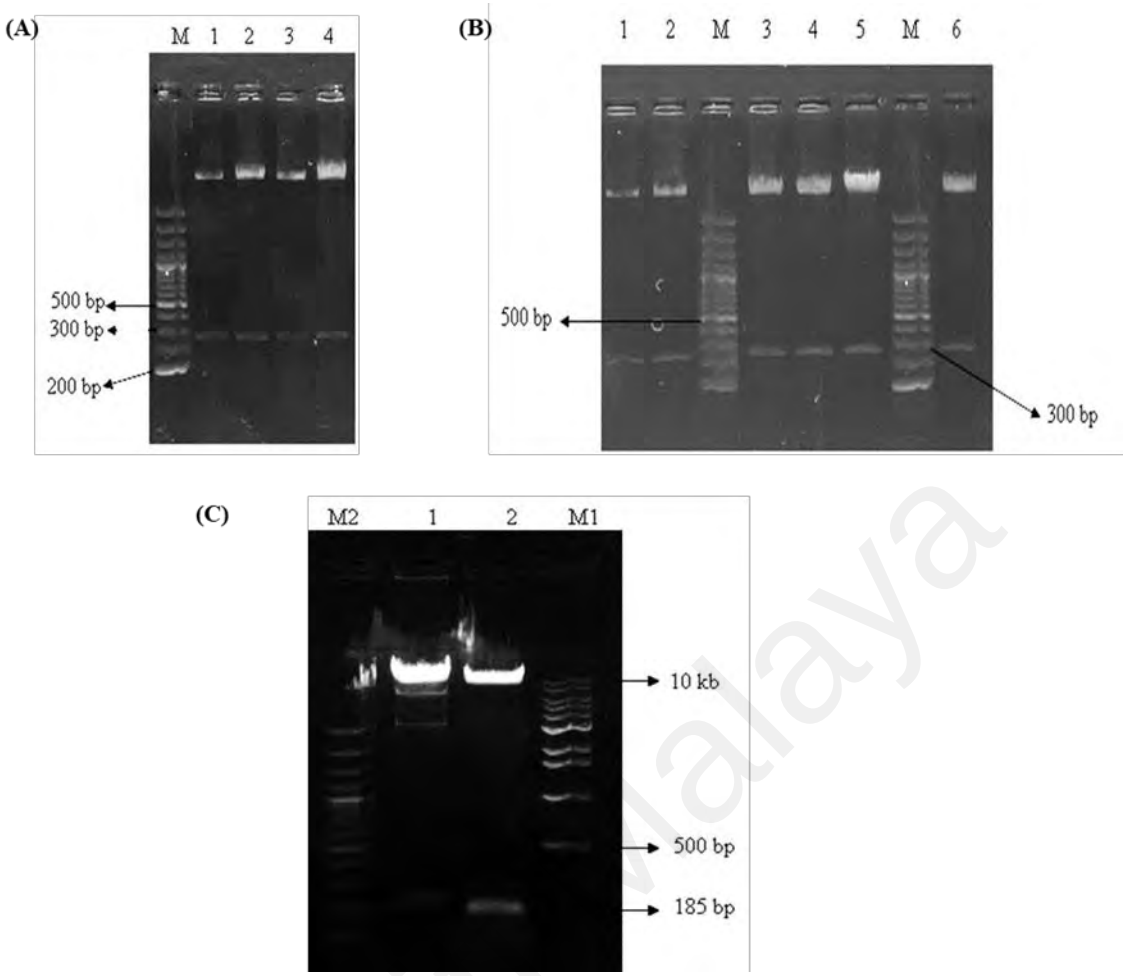

Figure 4.25: Restriction digestion of genes from pUC57 and pCGHB310803 vectors. Double digestion was carried out using Hind III and Sph I on pUC57 vector was shown as a gel (A) and (B). In the gel (A), lanes 1, 2, 3 and 4 represent the epitopes of H532-540 (237 bp), M58-66 (237 bp), M128-135 (237 bp) and H127-137 (240bp). As in gel (B), lanes 1, 2, 3, 4, 5 and 6 represent the epitopes of H344-354 (240 bp), H461-469 (240 bp), H166-175 (243 bp), M220-236 (261 bp), M83-100 (264 bp) and H331-354 (290 bp). Gel (C) represents restriction digestions of pCGHB310803with Hind III and Sph I restriction enzymes (lane 2). Lane 1 was undigested CGMMV 1410 while M1 and M2 represent 100 bp (Fermentas, USA) and 1 kb DNA marker (NEB, USA) respectively.

The chimeric plasmids with the correct insert of influenza epitopes were used as a template to amplify the full-length DNA using the T7doubleG and CGMMV3'UTR primers (Listed in Appendix V). The CGMMV 1410 vector was used as the wild-type control. The full-length DNA of the wild-type and the chimeric CGMMV were purified and used as template for *in vitro* transcription (Figure 4.26).

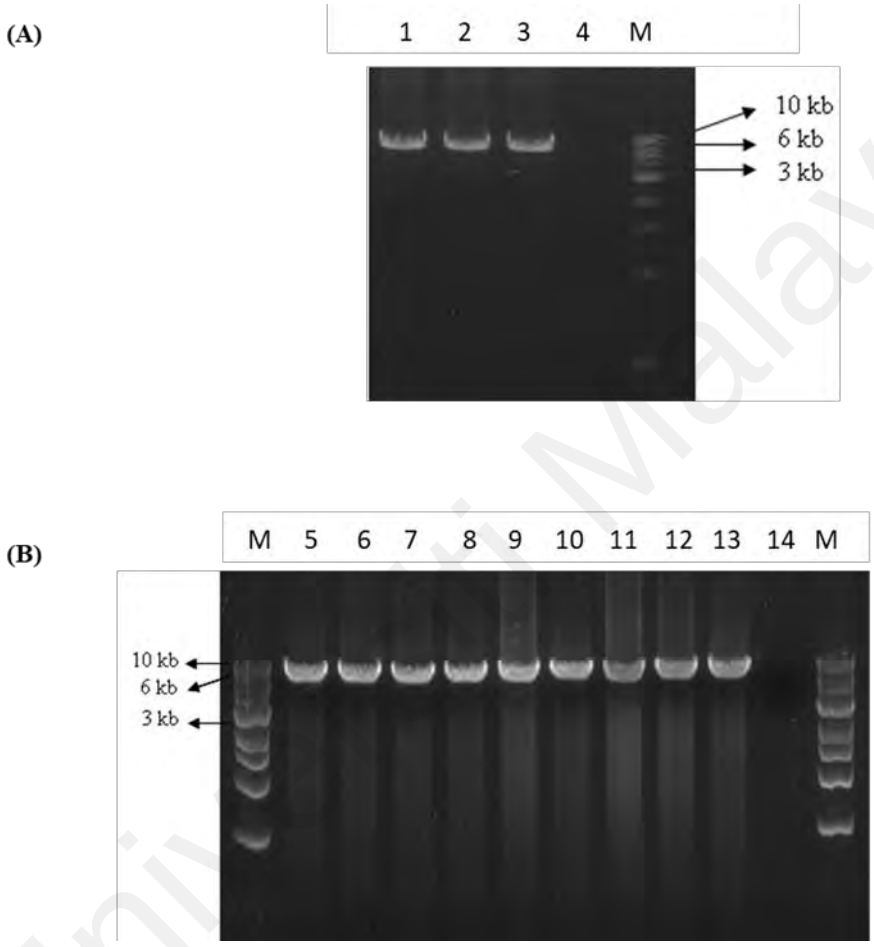

Figure 4.26: Amplification of full length wild-type CGMMV DNA with the T7 promoter sequences. Lane 1 to 13 of gel (A) and (B) represent the full length of wild-type and chimeric CGMMV. (Lane 2) CGMMVasc+HA127-137, (Lane 3) CGMMVasc+HA166-175, (Lane 5) CGMMVasc+HA331-354, (Lane 6) CGMMVasc+HA344-354, (Lane 7) CGMMVasc+HA461-469, (Lane 8) CGMMVasc+HA532-540, (Lane 9) CGMMVasc+M58-66, (Lane 10) CGMMVasc+M83-100, (Lane 11) CGMMVasc+M128-135 and (Lane 12) CGMMVasc+M220-236. Lane 1 and 13 of gel (A) and (B) represent full length of wild-type CGMMV. Lane 4 and Lane 14 represent the negative control (without template). Lane M represents 1 kb DNA marker (NEB, USA). The size of the PCR product is about 6.4 kb.

Upon confirmation of the presence of influenza epitopes, the full-length amplified DNA of wild-type and chimeric CGMMV were *in vitro* transcribed into RNAs. The results showed that the transcribed wild-type and chimeric RNA was at the correct size (about 6.4 kb) and without degradation (Figure 4.27). Next, Northern Blotting was carried out to verify the presence of the inserted epitope's RNA using the DNA probes synthesis based on the inserted epitopes sequence. Based on the results, all the transcribed RNA contained the inserted HA or M epitopes (Figure 4.28).

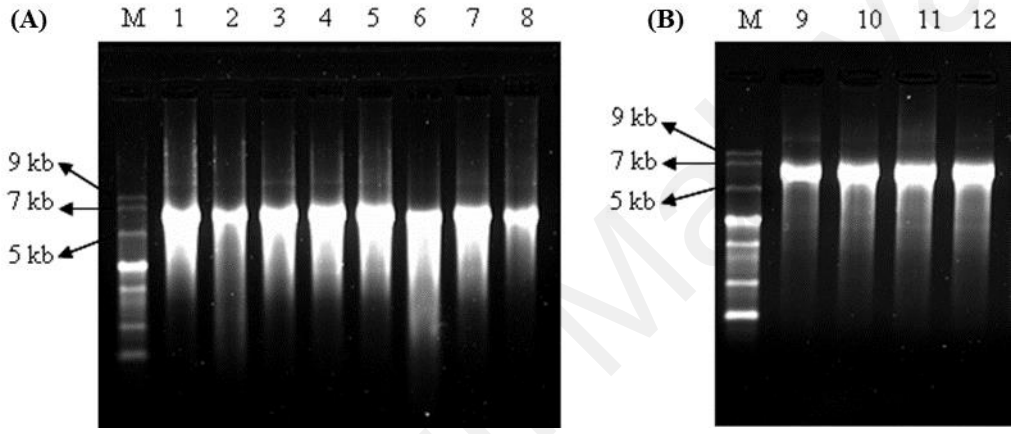

Figure 4.27: Gel electrophoresis analysis of *in vitro* transcribed RNA products from purified full length CGMMV (wild-type and chimeric CGMMV). Lane 2 to 11 of gel (A) and (B) represent RNA of (Lane 2) CGMMVasc+HA127-137, (Lane 3) CGMMVasc+HA166-175, (Lane 4) CGMMVasc+HA331-354, (Lane 5) CGMMVasc+HA344-354, (Lane 6) CGMMVasc+HA461-469, (Lane 7) CGMMVasc+HA532-540, (Lane 8) CGMMVasc+M58-66, (Lane 9) CGMMVasc+M83-100, (Lane 10) CGMMVasc+M128-135 and (Lane 11) CGMMVasc+M220-236. Lanes 1 and 12 represent the RNAs of CGMMV 1410. Lane M is ssRNA marker (NEB, USA). The size of the RNA is about 6.4 kb.

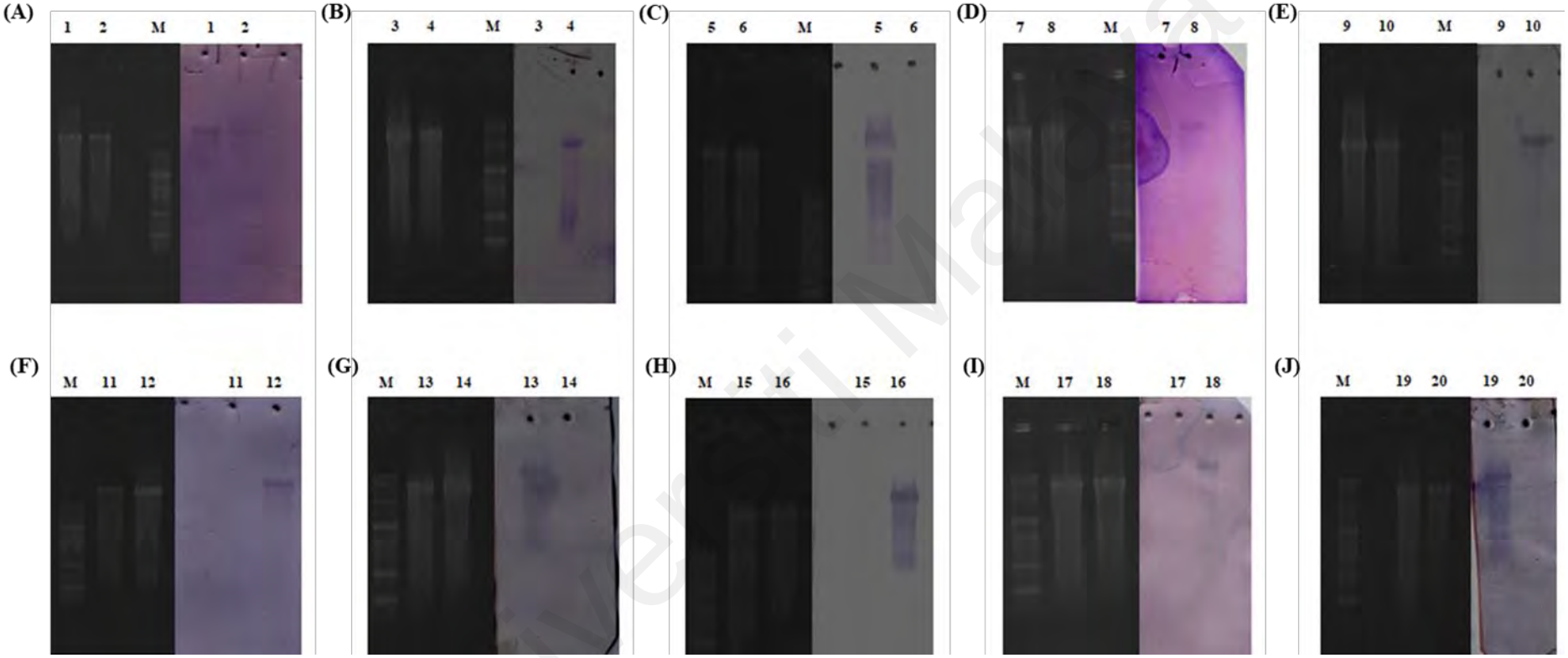

Figure 4.28: Northern blotting to confirm the presence of inserted epitope's RNA in the *in vitro* transcribed RNA. Lanes 1, 4, 5, 8, 9, 10, 12, 13,16, 18 and 19 represent the RNA of (A) CGMMVasc+HA127-137, (B) CGMMVasc+HA166-175, (C) CGMMVasc+HA331-354, (D) CGMMVasc+HA344-354, (E) CGMMVasc+HA461-469, (F) CGMMVasc+HA532-540, (G) CGMMVasc+M58-66, (H) CGMMVasc+M83-100, (I) CGMMVasc+M128-135 and (J) CGMMVasc+M220-236. Lanes 2, 3, 6, 7, 9, 11, 14, 15, 17 and 20 represent RNA of CGMMV 1410 (control). Lane M is ssRNA marker (NEB, USA).

The full length *in vitro* transcribed RNAs were inoculated on the cotyledon of *C. melo* var Earl favorite. Approximately twenty-one days post inoculation (d.p.i), symptoms began to be produced from the upper new leaves (Figure 4.29) Eight out of ten chimeric CGMMV developed symptoms of mild mosaic, mosaic, edge lesion and leave wrinkle (CGMMVasc+HA331-354; CGMMVasc+HA344-354; CGMMVasc+HA461-469; CGMMVasc+HA532-540; CGMMVasc+M58-66; CGMMVasc+M83-100; CGMMVasc+M128-135 and CGMMVasc+M220-236) (Figure 4.29E-L). Two of the chimeric CGMMV: CGMMVasc+HA127-137 and CGMMVasc+HA166-175 did not induce any symptom on Earl favorite even up till 30 days post inoculation (Figure 4.29C-D). On the other hand, wild-type CGMMV induced severe mosaic and mottle on Earl favorite at 10-14 days post inoculation (Figure 4.29B). ELISA detection of CGMMV was recorded from the upper new leaves (with or without symptoms) at 30 days post inoculation and were consistent with the presence of symptoms. (Table 4.8). Taken together, 8 out of 10 chimeric CGMMV constructs with HA and M1 epitopes successfully induced mild symptoms in Earl favorite about a week later than wild-type CGMMV.

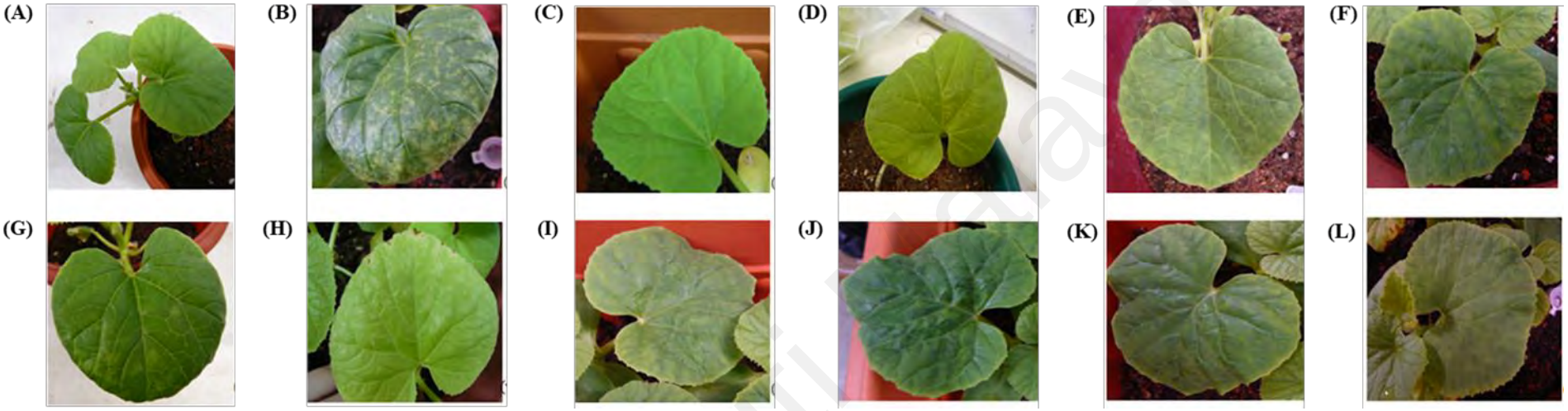

Figure 4.29: Mosaic and mottle symptoms of the Earl favorite at 21 d.p.i. Earl favorite was inoculated with (A) phosphate buffer (negative control), (B) wild-type CGMMV (positive control), (C) CGMMVasc+HA127-137, (D) CGMMVasc+HA166-175, (E) CGMMVasc+HA331-354, (F) CGMMVasc+HA344-354, (G) CGMMVasc+HA461-469, (H) CGMMVasc+HA532-540, (I) CGMMVasc+M58-66, (J) CGMMVasc+M83-100, (K) CGMMVasc+M128-135 and (L) CGMMVasc+M220-23.

Table 4.8: Detection of CGMMV in Earl favorite plants at 30 d.p.i. using ELISA. The readings shown represent the average reading of three Earl favorite replicates from three experiments. The positive control is provided by the kit (Agdia, USA). Negative control represents Earl favorite that was inoculated with distilled water while blank represents the test well with grinding buffer only. Samples with a reading fivefold more than the negative control were considered as infected samples. '+' represents positive; '-' represents negative.

Samples	Absorbance (405nm)	Interpretation
Positive Control	1.2031±0.0150	+
Negative control	0.0771±0.0185	-
CGMMV 1410	0.9124±0.0307	+
CGMMVasc+HA127-137	0.0824±0.0149	-
CGMMVasc+HA166-175	0.0835±0.0177	-
CGMMVasc+HA331-354	0.7681±0.0209	+
CGMMVasc+HA344-354	0.7214±0.0180	+
CGMMVasc+HA461-469	0.5517±0.0332	+
CGMMVasc+HA532-540	0.5734±0.0134	+
CGMMVasc+M58-66	0.7111±0.0255	+
CGMMVasc+M83-100	0.4972±0.0094	+
CGMMVasc+M128-135	0.7104±0.0137	+
CGMMVasc+M220-236	0.6234±0.0224	+

The 8 plants inoculated with chimeric CGMMV nanoparticles that induced mosaic and mottle symptoms together with significant ELISA readings were subjected to total RNA extraction and RT-PCR to detect for the presence of the influenza epitopes using specific primers (Appendix V). Figure 4.30 confirmed the presence of the inserted HA and M1 epitopes sequence in the plants inoculated with chimeric CGMMV nanoparticles.

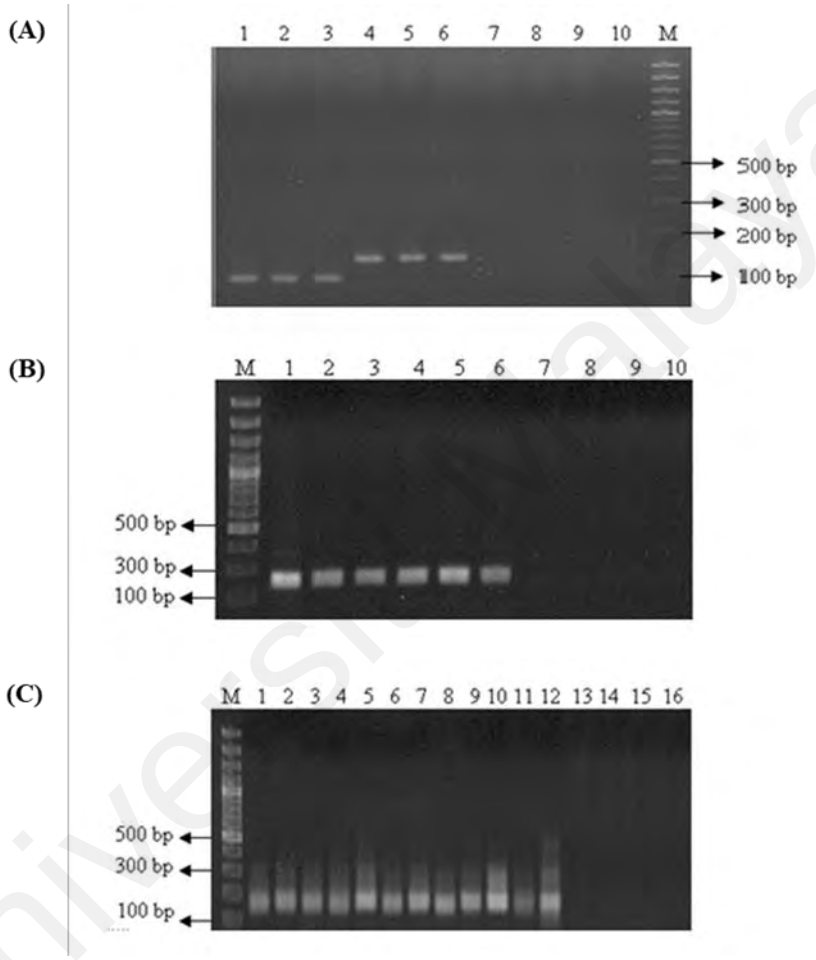

Figure 4.30: Agarose gel electrophoresis of RT-PCR products for the detection of influenza epitopes in chimeric CGMMV-inoculated plants. In gel (A), lane 1 to 3 and lane 4 to 6 showed the presence of epitopes of M58-66 and HA331-354, respectively while in gel (B), lane 1 to 3 and lane 4 to 6 showed the presence of epitopes of M220-236 and M83-100, respectively. In gel (C) Lane 1-3, 4-6, 7-9 and 10-12 showed the presence of epitopes HA344-354, HA461-469, HA532-540, and M128-135. Lane 7 to 9 in gel (A) and (B) and lane 13 to 15 in gel (C) represent the results of plant inoculated with phospahte buffer while lane 10 in gel (A) and (B) and lane 16 in gel (C) represent the negative control of RT-PCR (without template). Lane M is 100 bp DNA marker (Fermentas, USA).

4.4.4 Confirmation of inserted epitopes in chimeric CGMMV nanoparticles

Virus particles were extracted from the 8 symptomatic *C. melo* var Earl favorite and observed under the TEM to confirm the presence of CGMMV nanoparticles. In all eight, the rod shape of CGMMV nanoparticles were observed (Figure 4.4.11). The coat protein of CMMG nanoparticles were further analyzed with Western blotting. Western blotting results showed the presence of the wild-type CGMMV and the chimeric CGMMV (Figure 4.32) using anti-CGMMV antibody. Taken together, the results suggest that both wild-type CGMMV and chimeric CGMMVs (CGMMVasc+HA331-354, CGMMVasc+HA344-354, CGMMVasc+HA461-469, CGMMVasc+HA532-540, CGMMVasc+M58-66, CGMMVasc+M83-100, CGMMVasc+M128-135 and CGMMVasc+M220-23) were expressed in the plants and were intact viruses.

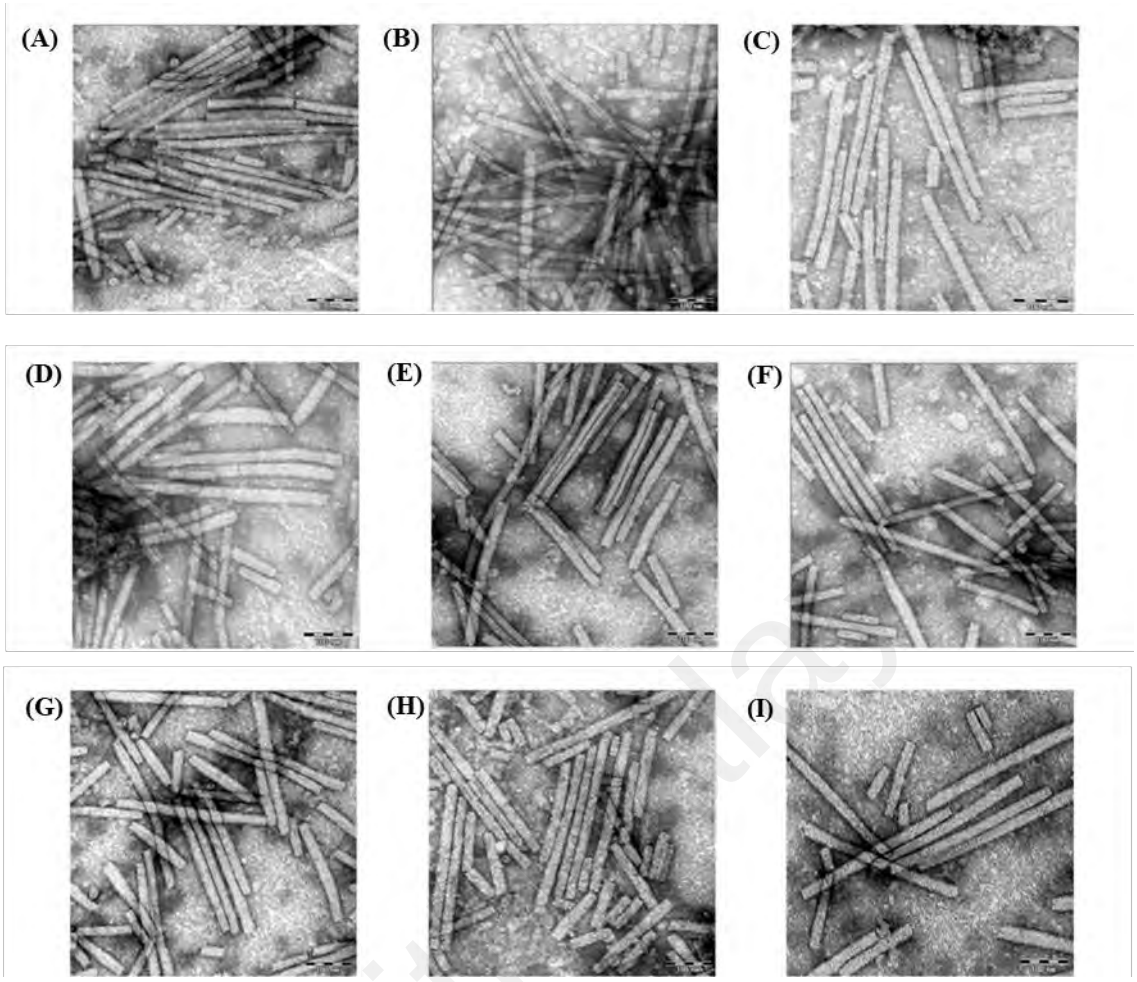

Figure 4.31: Observation of wild-type and chimeric CGMMV nanoparticles under TEM. The virus structure was visualized under a magnification of 31.50K. (A) CGMMVasc+HA331-354, (B) CGMMVasc+HA344-354, (C) CGMMVasc+HA461-469, (D) CGMMVasc+HA532-540, (E) CGMMVasc+M58-66, (F) CGMMVasc+M83-100, (G) CGMMVasc+M128-135, (H) CGMMVasc+M220-236 and (I) wild-type CGMMV. Partial degradation was noticed in wild-type and chimeric viruses that probably resulted from the extraction process.

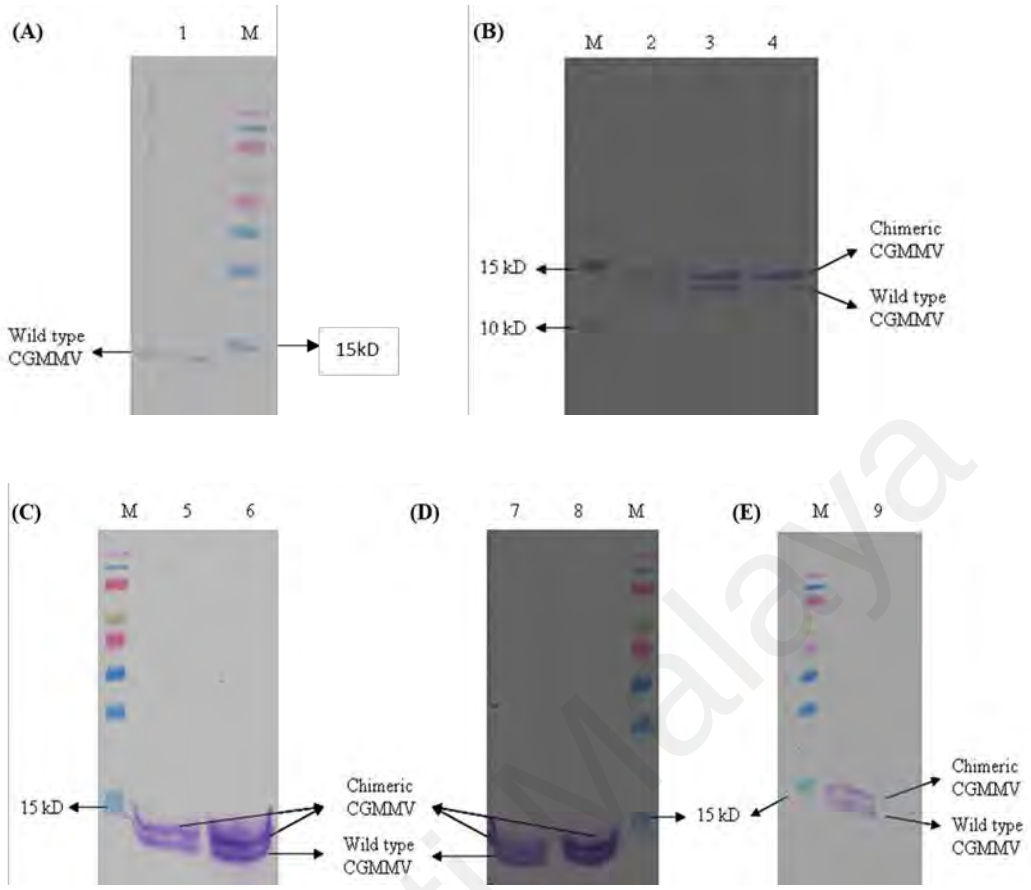

Figure 4.32: Detection of wild-type and chimeric CGMMV coat protein by anti-CGMMV antibody conjugate with alkaline phosphatase. (A) Lane 1 represents the coat protein of CGMMV extracted from Earl favorite inoculated with wild-type CGMMV. (B) Lanes 2, 3 and 4 represent the coat protein of CGMMV (wild-type and chimeric) extracted from Earl favorite inoculated with CGMMVasc+HA344-354, CGMMVasc+HA461-469, CGMMVasc+HA532-543. (C) Lanes 5 and 6 represent the coat protein of CGMMV (wild-type and chimeric) extracted from Earl favorite inoculated with CGMMVasc+M128-135 and CGMMVasc+HA331-3547. (D) Lanes 7 and 8 represent the coat protein of CGMMV (wild-type and chimeric) extracted from Earl favorite inoculated with CGMMVasc+M83-100 and CGMMVas+M58-66 while (E) lane 9 represents the coat protein of CGMMV (wild-type and chimeric) extracted from Earl favorite inoculated with CGMMVasc+M220-236. Lane M represents the multi color pre-stained protein marker (Fermentas, USA).

In this section, the presence of complete amino acid sequence of HA and M1 epitopes were subsequently further verified using LC/MS/MS. The band of the protein was excised from the PAGE-gel and proceeded to in-gel trypsin digestion and analyzed using mass spectrophotometry.

The raw file (Table 4.9, 4.10, 4.11 and 4.12) generated from the mass spectrometer were analyzed with a MaxQuant software (Cox & Mann, 2008). The A2 is level confidence achieved with the peptide sequence which can be categorized by high confidence, medium confidence, or low confidence. Only the high-confidence data are presented. #PSMs represents the total number of identified peptide sequences (PSMs) that matched the protein. The PSMs score can be higher than the number of peptides as it includes those repeatedly identified. The higher the #PSMs, the more reliable the results are. Xcorr (cross correlation) is a search-dependent score. The higher the score, the closer the peptide fragments to theoretical spectra. The charge of the peptide is always greater than 1 (can be 2, 3 or 4). MH+(Da) is the molecular weight of the peptide and is calculated by m/z of the peptide where z = 1 while the RT (min) is the peptide's retention time during chromatographic separation. Met oxidation is the dynamic modification of methionine in the peptide.

The LC/MS/MS results that were high in confidence level, #PMSs score and Xcorr were further analyzed with Blast against the database containing CGMMV coat protein and influenza epitope amino acid sequences. Based on the results, only the sequence of the wild-type coat protein and 3 chimeric constructs (CGMMVasc+M83-100, CGMMVasc+M128-135 and CGMMVasc+M220-236) can be detected and there were no mutations or truncation in between the peptides as shown in Table 4.9, 4.10, 4.11 and 4.12 and Figure 4.33, 4.34, 4.35 and 4.36. The epitopes of the other constructs (CGMMVasc+HA331-354; CGMMVasc+HA344-354; CGMMVasc+HA461-469, CGMMVasc+HA532-540 and CGMMVasc+M58-66) were failed to be detected.

Table 4.9: LC/MS/MS results of CGMMV wild-type coat protein.

A2	Sequence	# PSMs	Modifications	XCorr	Charge	MH+ [Da]	RT [min]
High	VIEVVDPSNPTTAESLNAVK	501		7.59	3	2083.09092	19.73
High	TLLNFLVASQGTAFQTQAGR	501		7.29	3	2123.12528	43.62
High	FPDAGFYAFLNGPVLRPIFVSLLSSTDTR	18		6.45	3	3200.67734	28.78
High	ASFEAAFSVVWSEATTSK	481		6.40	3	1917.92319	42.76
High	LIAFSASYVPVRTLLNFLVASQGTAFQTQAGR	13		6.20	3	3426.85471	28.09
High	NRVIEVVDPSNPTTAESLNAVK	3		6.20	3	2353.23465	16.03
High	DSFRESLSALPSSVVDINSR	11		5.86	3	2179.09842	19.69
High	ESLSALPSSVVDINSR	304		5.69	3	1673.86924	18.52
High	AEIDNLIESISKGFDVYDR	11		5.16	3	2184.07578	25.45
High	TLLNFLVASQGTAFQTQAGRDSFR	3		5.10	3	2628.35318	22.15
High	AEIDNLIESISK	276		5.08	2	1331.70500	42.16
High	LIAFSASYVPVR	504		4.66	3	1322.74564	35.31
High	RTDDASTAAR	15		3.88	2	1063.51238	4.69
High	ASFEAAFSVVWSEATTSKASK	3		3.88	3	2204.06687	31.59
High	MAYNPITPSK	1		3.38	2	1121.56536	12.59
High	mAYNPITPSK	7	M1(Oxidation)	3.33	2	1137.56096	11.13
High	TDDASTAAR	10		3.03	2	907.41051	4.66
High	VIEVVDPSNPTTAESLNAVKR	68		3.01	2	2239.19316	16.30
High	GFDVYDR	316		2.59	2	871.39287	12.47
High	VIEVVDPSNPTTAESLNAVKRTDDASTAAR	1		2.43	4	3127.59194	14.72
High	TDDASTAARAEIDNLIESISK	1		1.82	4	2220.09853	17.52

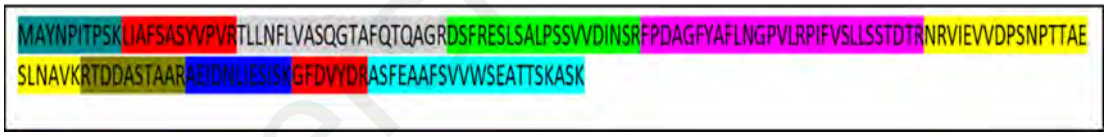

Figure 4.33: Summary of the LC/MS/MS data of CGMMV wild-type full length amino acid sequence. The fragments digested with trypsin were assembled (color coding) and corresponded to the position of peptide in the wild-type CGMMV coat protein.

Table 4.10: LC/MS/MS results of CGMMVasc+M83-100 coat protein. Red circle represented the amino acids sequence of epitope M83-100.

A2	Sequence	# PSMs	Modifications	XCorr	Charge	MH+ [Da]	RT [min]
High	VIEVVDPSNPTTAESLNAVK	509		7.52	3	2083.09128	19.77
High	TLLNFLVASQGTAFQTQAGR	543		7.47	3	2123.12546	48.69
High	NRVIEVVDPSNPTTAESLNAVK	6		7.37	3	2353.23301	16.08
High	FPDAGFYAFLNGPVLRPIFVSLLSSTDTR	6		6.44	3	3200.67990	28.91
High	ASFEAAFSVVWSEATTSK	437		6.32	3	1917.92301	32.34
High	LIAFSASYVPVRTLLNFLVASQGTAFQTQAGR	6		6.24	3	3426.85288	28.08
High	ESLSALPSSVVDINSR	315		6.19	3	1673.86942	18.59
High	DSFRESLSALPSSVVDINSR	10		5.74	3	2179.09879	19.89
High	VIEVVDPSNPTTAESLNAVKRTDDASTAAR	2		5.59	4	3127.58462	15.67
High	AEIDNLIESISK	237		5.05	2	1331.70561	41.25
High	AEIDNLIESISKGFDVYDR	6		5.03	3	2184.07999	25.58
High	LIAFSASYVPVR	449		4.78	2	1322.74724	52.26
High	TLLNFLVASQGTAFQTQAGRDSFR	2		4.39	3	2628.35355	22.09
High	RTDDASTAAR	18		4.03	2	1063.51323	4.65
High	mAYNPITPSK	9	M1(Oxidation)	3.61	2	1137.56096	11.45
High	VIEVVDPSNPTTAESLNAVKR	50		3.50	3	2239.19382	17.69
High	ASFEAAFSVVWSEATTSKASK	2		3.45	3	2204.06522	31.40
High	MAYNPITPSK	2		3.42	2	1121.56536	12.68
High	TDDASTAAR	13		3.19	2	907.41100	4.90
High	GFDVYDR	308		2.51	2	871.39427	52.00
High	AVKLYEA	13		2.31	2	793.44005	6.97
High	ASKLQLALNGNGDPNNmDKAVK	1	M17(Oxidation)	2.06	3	2314.17459	34.88

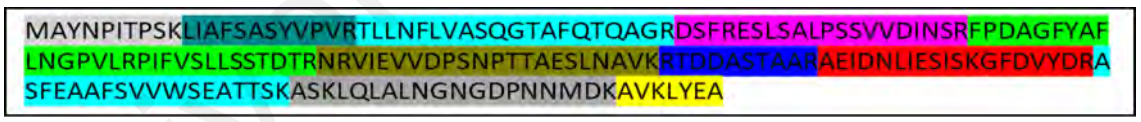

Figure 4.34: Summary of the LC/MS/MS data of CGMMVasc+M83-100, chimeric coat protein sequence full length amino acids sequence. The fragments digested with trypsin were assembled (color coding) and corresponded to the position of peptide in the chimeric CGMMV coat protein.

Table 4.11: LC/MS/MS results of CGMMVasc+M128-135 coat protein. Red circle represented the amino acids sequence of epitope M128-135.

A2	Sequence	# PSMs	Modifications	XCorr	Charge	MH+ [Da]	RT [min]
High	VIEVVDPSNPTTAESLNAVK	501		7.59	3	2083.09092	19.73
High	TLLNFLVASQGTAFQTQAGR	501		7.29	3	2123.12528	43.62
High	FPDAGFYAFLNGPVLRPIFVSLLSSTDTR	18		6.45	3	3200.67734	28.78
High	ASFEAAFSVVWSEATTSK	481		6.40	3	1917.92319	42.76
High	LIAFSASYVPVRTLLNFLVASQGTAFQTQAGR	13		6.20	3	3426.85471	28.09
High	NRVIEVVDPSNPTTAESLNAVK	3		6.20	3	2353.23465	16.03
High	DSFRESLSALPSSVVDINSR	11		5.86	3	2179.09842	19.69
High	ESLSALPSSVVDINSR	304		5.69	3	1673.86924	18.52
High	AEIDNLIESISKGFDVYDR	11		5.16	3	2184.07578	25.45
High	TLLNFLVASQGTAFQTQAGRDSFR	3		5.10	3	2628.35318	22.15
High	AEIDNLIESISK	276		5.08	2	1331.70500	42.16
High	LIAFSASYVPVR	504		4.66	3	1322.74564	35.31
High	RTDDASTAAR	15		3.88	2	1063.51238	4.69
High	ASFEAAFSVVWSEATTSKASK	3		3.88	3	2204.06687	31.59
High	MAYNPITPSK	1		3.38	2	1121.56536	12.59
High	mAYNPITPSK	7	M1(Oxidation)	3.33	2	1137.56096	11.13
High	TDDASTAAR	10		3.03	2	907.41051	4.66
High	VIEVVDPSNPTTAESLNAVKR	68		3.01	2	2239.19316	16.30
High	GFDVYDR	316		2.59	2	871.39287	12.47
High	VIEVVDPSNPTTAESLNAVKRTDDASTAAR	1		2.43	4	3127.59194	14.72
High	TDDASTAARAEIDNLIESISK	1		1.82	4	2220.09853	17.52

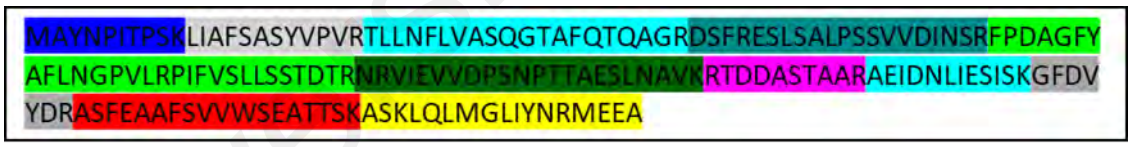

Figure 4.35: Summary of the LC/MS/MS date of CGMMVasc+M128-135, chimeric coat protein sequence full length amino acids sequence. The fragments digested with trypsin were assembled (color coding) and corresponded to the position of peptide in the chimeric CGMMV coat protein.

Table 4.12: LC/MS/MS results of CGMMVasc+M220-236 coat protein. Red circle represented the amino acids sequence of epitope M220-236.

A2	Sequence	# PSMs	Modifications	XCorr	Charge	MH+ [Da]	RT [min]
High	RTDDASTAAR	14		4.07	2	1063.51238	4.86
High	TDDASTAAR	9		3.04	2	907.41100	4.53
High	TLLNFLVASQGTAFQTQAGRDSFR	5		4.82	3	2628.35208	21.58
High	mAYNPITPSK	12	M1(Oxidation)	3.27	2	1137.56108	10.73
High	GFDVYDR	290		2.56	2	871.39360	33.33
High	MAYNPITPSK	2		3.40	2	1121.56560	12.14
High	VIEVVDPSNPTTAESLNAVKR	50		2.64	4	2239.19130	15.48
High	NRVIEVVDPSNPTTAESLNAVK	5		6.64	3	2353.23520	15.79
High	VIEVVDPSNPTTAESLNAVK	467		7.52	3	2083.08854	19.06
High	ESLSALPSSVVDINSR	292		5.76	3	1673.86997	16.44
High	VIEVVDPSNPTTAESLNAVKRTDDASTAAR	2		5.87	4	3127.58486	15.43
High	LIAFSASYVPVR	436		4.75	2	1322.74724	49.69
High	AEIDNLIESISK	267		5.01	2	1331.70561	45.66
High	DSFRESLSALPSSVVDINSR	13		5.53	2	2179.09917	19.67
High	TDDASTAARAEIDNLIESISK	2		5.55	3	2220.09739	23.88
High	TLLNFLVASQGTAFQTQAGR	559		7.30	3	2123.12546	50.29
High	AEIDNLIESISKGFDVYDR	15		5.57	3	2184.08182	25.16
High	ASFEAAFSVVWSEATTSK	413		6.46	3	1917.92282	30.64
High	LIAFSASYVPVRTLLNFLVASQGTAFQTQAGR	6		5.97	3	3426.85764	27.92
High	FPDAGFYAFLNGPVLRPIFVSLLSSTDTR	13		6.56	3	3200.67661	28.85
High	ASFEAAFSVVWSEATTSKASK	2		3.56	3	2204.06559	30.99
High	ASKLQLGTHPSSSAGLKNDLLENEA	10		3.27	3	2580.32060	14.50

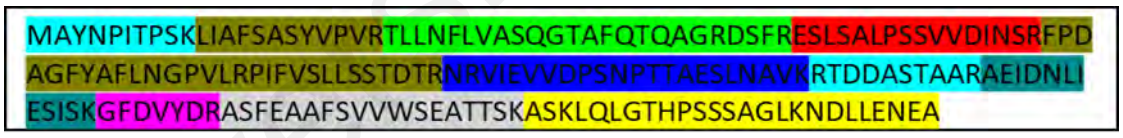

Figure 4.36: Summary of the LC/MS/MS date of CGMMVasc+M220-236, chimeric coat protein sequence full length amino acids sequence. The fragments digested with trypsin were assembled (color coding) and corresponded to the position of peptide in the chimeric CGMMV coat protein.

The infectivity, mosaic and mottle symptoms caused and the presence of influenza epitopes of CGMMV nanoparticles were summarised in Table 4.13. As a summary, CGMMVasc+HA127-137 and CGMMVasc+HA166-175 failed to induce any symptoms and produced either wild-type or chimeric CGMMV on the Earl favorite. This result is consistent with the changes of their RNA structures after inserted with HA epitopes (refer to Figure 4.23). Although CGMMVasc+HA331-354, CGMMVasc+HA344-354, CGMMVasc+HA461-469, CGMMVasc+HA532-540, CGMMVasc+M58-66, CGMMVasc+M83-100, CGMMVasc+M128-135 and CGMMVasc+M220-236 constructs managed to cause symptoms on the Earl favorite and their wild-type and chimeric CGMMV coat protein were detectable using Western Blotting (Figure 4.32). However, the only the complete inserted amino acids sequences of epitopes M83-100, M128-135 and M220-236 of CGMMVasc+M83-100, CGMMVasc+M128-135 and CGMMVasc+M220-236 were managed to detect using LC/MS/MS (Table 4.10, 4.11 and 4.12; Figure 4.34, 4.35 and 4.36).

Table 4.13: Summary of the characteristics of chimeric CGMMV nanoparticles. The summary is made based on the results of three repeated experiments with six replicates of samples. '+' represents positive; '-' represents negative.

Name of constructs	Infectivity	Symptoms	Present of wild-type and chimeric CGMMV coat protein (western blot)	Presence of CGMMV coat protein with influenza epitopes (LC/MS/MS)
Wild-type CGMMV 1410	6/6	Mottle, mosaic	+	-
CGMMVasc+HA127-137	0/6	No	-	-
CGMMVasc+HA166-175	0/6	No	-	-
CGMMVasc+HA331-354	6/6	Mottle, mosaic	+	-
CGMMVasc+HA344-354	6/6	Mottle, mosaic	+	-
CGMMVasc+HA461-469	5/6	Mild mosaic	+	-
CGMMVasc+HA532-540	5/6	Edge lesion	+	-
CGMMVasc+M58-66	6/6	Mottle, mosaic	+	-
CGMMVasc+M83-100	5/6	Leave wrinkle	+	+
CGMMVasc+M128-135	6/6	Mottle, mosaic	+	+
CGMMVasc+M220-236	6/6	Mottle, mosaic	+	+

4.4.5 Immune response of chimeric CGMMV nanoparticles in mice

Based on the results of LC/MS/MS, only 3 chimeric CGMMV nanoparticles with inserted M1 epitopes namely CGMMVasc+M83-100, CGMMVasc+M28-135 and CGMMVasc+M220-236 were further tested for inducing the immune response in mouse. Three doses of 100 μg of wild-type and chimeric CGMMV nanoparticles were administrated subcutaneously into the mice. Mice mock injected with phosphate buffer acted as negative control. Anti-CGMMV and anti-epitope antibodies in sera extracted from mice were tested after the 3rd injection. Subcutaneous immunization with wild-type and chimeric CGMMV nanoparticles efficiently induced antibody against CGMMV nanoparticles (Figure 4.37; Appendix Q). No anti-CGMMV antibodies were found in the sera of the mice immunized with phosphate buffer. However, only low levels of anti-M83-100 and anti-M220-236 antibodies could be detected in the sera of mice injected with CGMMVasc+M83-100 and CGMMVasc+M220-236 nanoparticles at a dilution factor of 1:25 of which the level was not significant ($P>0.05$). On the other hand, mice immunized with CGMMVasc+M128-135 nanoparticles failed to induce any anti-M128-135 antibody (Figure 4.38; Appendix R, S and T).

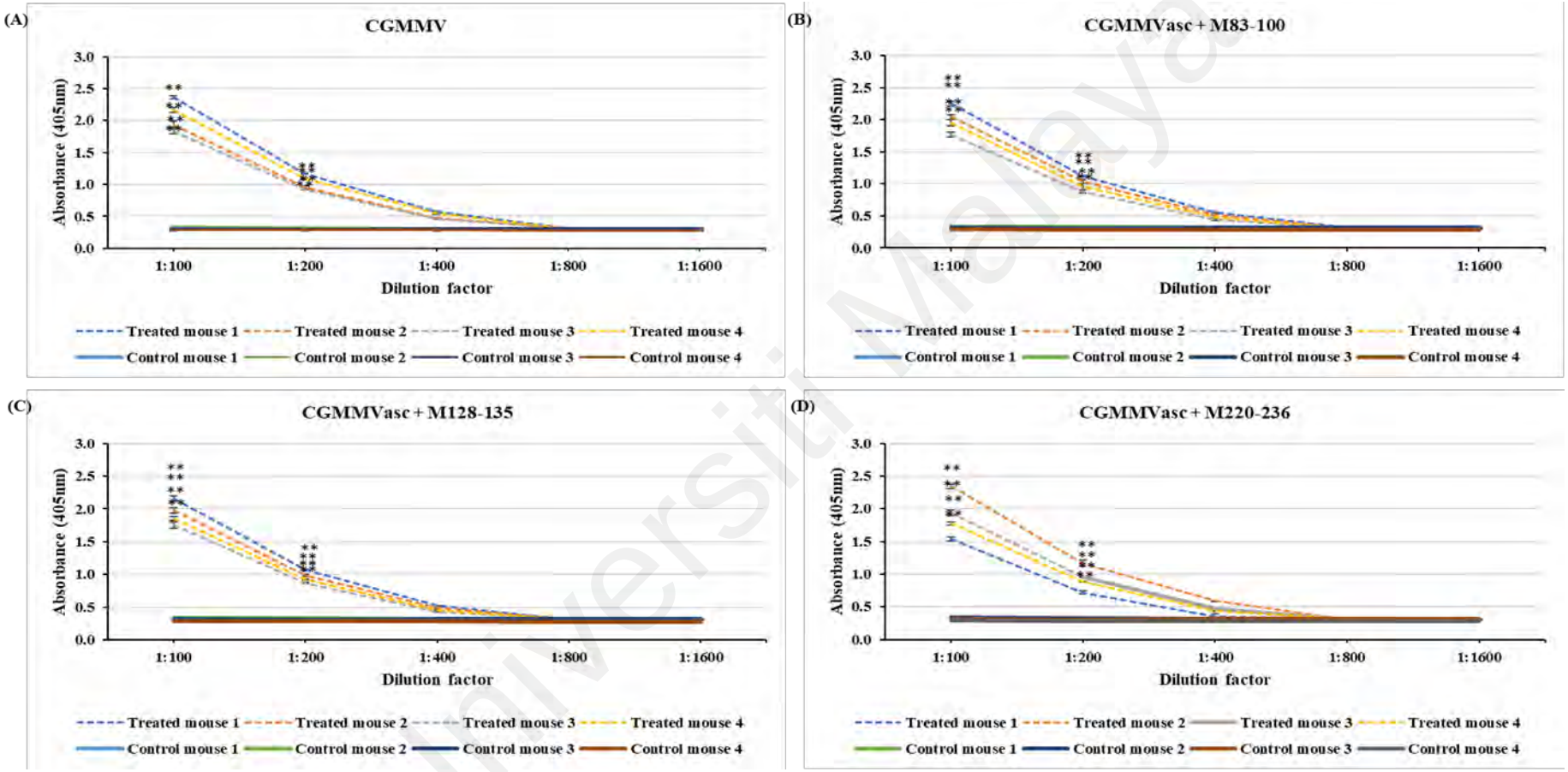

Figure 4.37: Detection of anti-CGMMV antibody in mice sera after 3rd injections. Anti-CGMMV antibody was detected in mice injected with (A) wild-type CGMMV, (B) CGMMVasc+M83-100, (C) CGMMVasc+M128-135 and (D) CGMMVasc+M220-236 nanoparticles at 1:100 and 1:200 dilution factors. Mice injected with phosphate buffer act as the negative control. Data represent the mean and ± SD, n = 4 biological replicates (**, $p < 0.01$; *, $p < 0.05$).

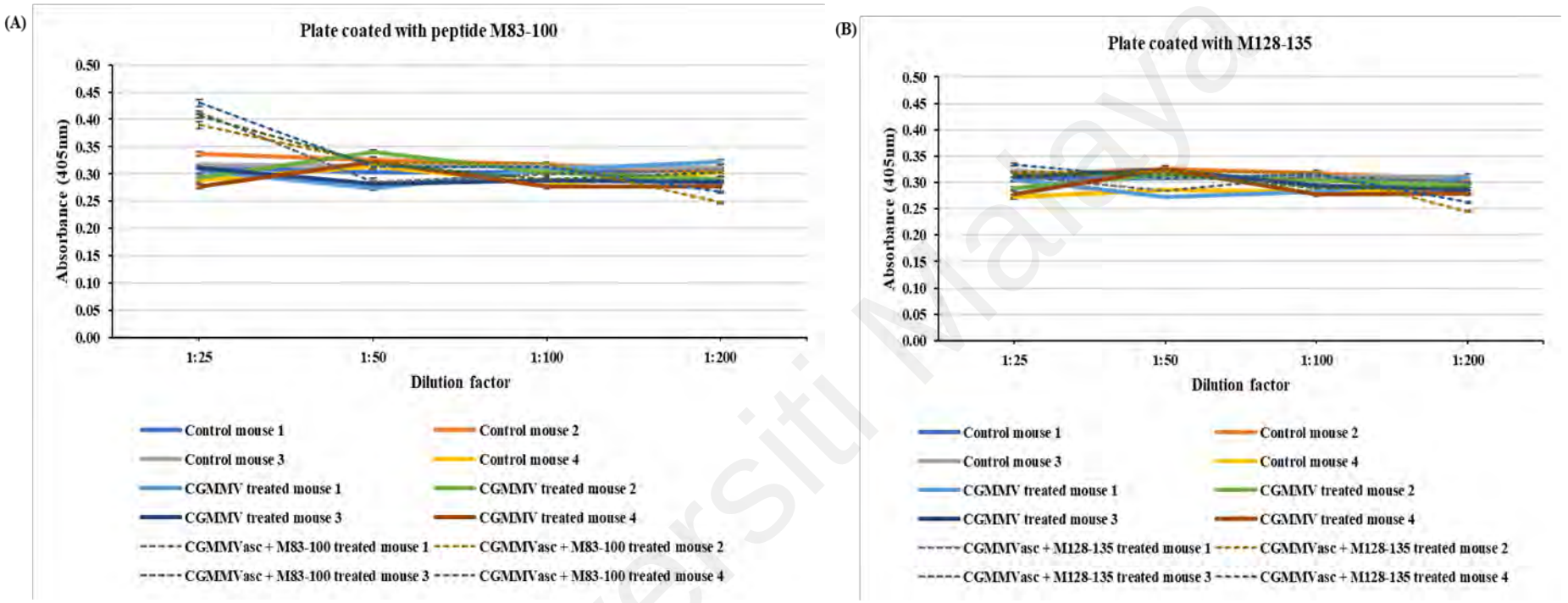

Figure 4.38: Detection of anti-epitopes antibody in mice sera after 3rd injections. Plate was coated with (A) peptide M83-100, (B) peptide M128-135 and (C) peptide M220-236 and tested with mice sera injected with CGMMV, CGMMVasc+M83-100, CGMMVasc+M128-135 or CGMMVasc+M220-236 nanoparticles. There was no significant level of anti-M83-126, anti-M128-135 and anti-M220-236 antibody detected in mice injected with wild-type CGMMV or chimeric CGMMV nanoparticles (CGMMVasc+M83-100, CGMMVasc+M128-135 and CGMMVasc+M220-236) at dilution factors as high as 1:25. Mice injected with phosphate buffer act as negative control. Data represent the mean and ± SD, n = 4 biological replicates (**, $p < 0.01$; *, $p < 0.05$). Refer to next page for figure (C).

(C)

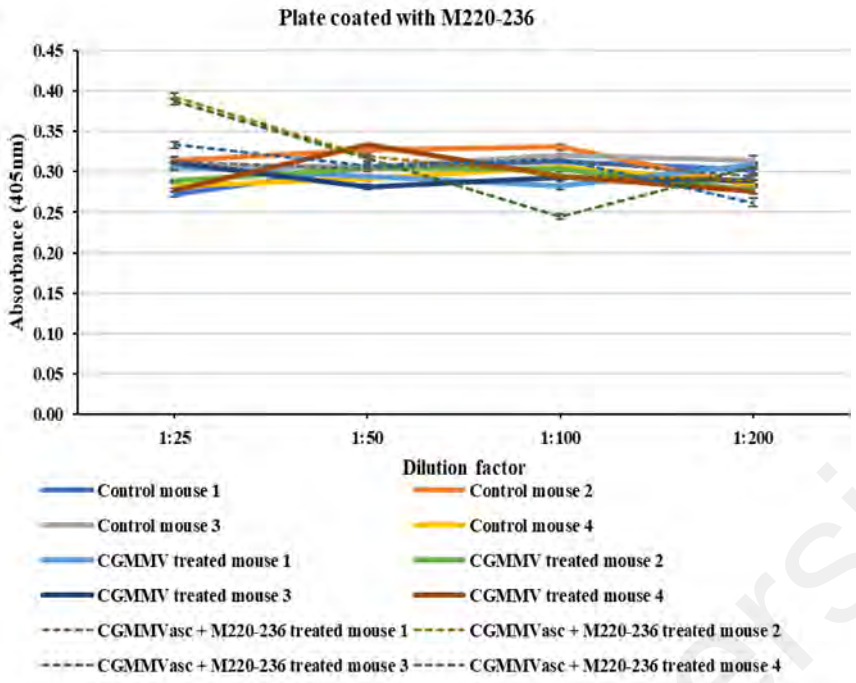

Figure 4.38, continued.

Next, we proceed to study the proliferation effect of spleen towards the wild-type and chimeric CGMMV nanoparticles. Spleens were harvested at 5 days post 3rd injection from mice injected with 100 µg wild-type CGMMV, CGMMVasc+M83-100, CGMMVasc+M128-135 and CGMMVasc+M220-236 nanoparticles. The spleen cells were cultured and challenged with wild-type CGMMV, M83-100, M128-135 and M220-236 epitopes. Concavalin A (ConA) treated cells acts as the positive control. Whereas the spleen cells proliferated significantly when induced with CGMMV nanoparticles, no proliferation was observed in response to influenza epitopes of M83-100; M128-135 and M220-236 challenges (Figure 4.39; Appendix U). This result suggested that the mice immune response only recognized CGMMV nanoparticle as foreign subject and induced antibody as well as T cells against it but not the inserted M1 epitopes. From the combined antibody detection and spleen proliferation results, we concluded that the influenza M1 epitopes (M83-100, M128-135 and M220-236) expressed on the surface CGMMV nanoparticle failed to induce any immune response in mice (Figure 4.37, 4.38 and 4.39).

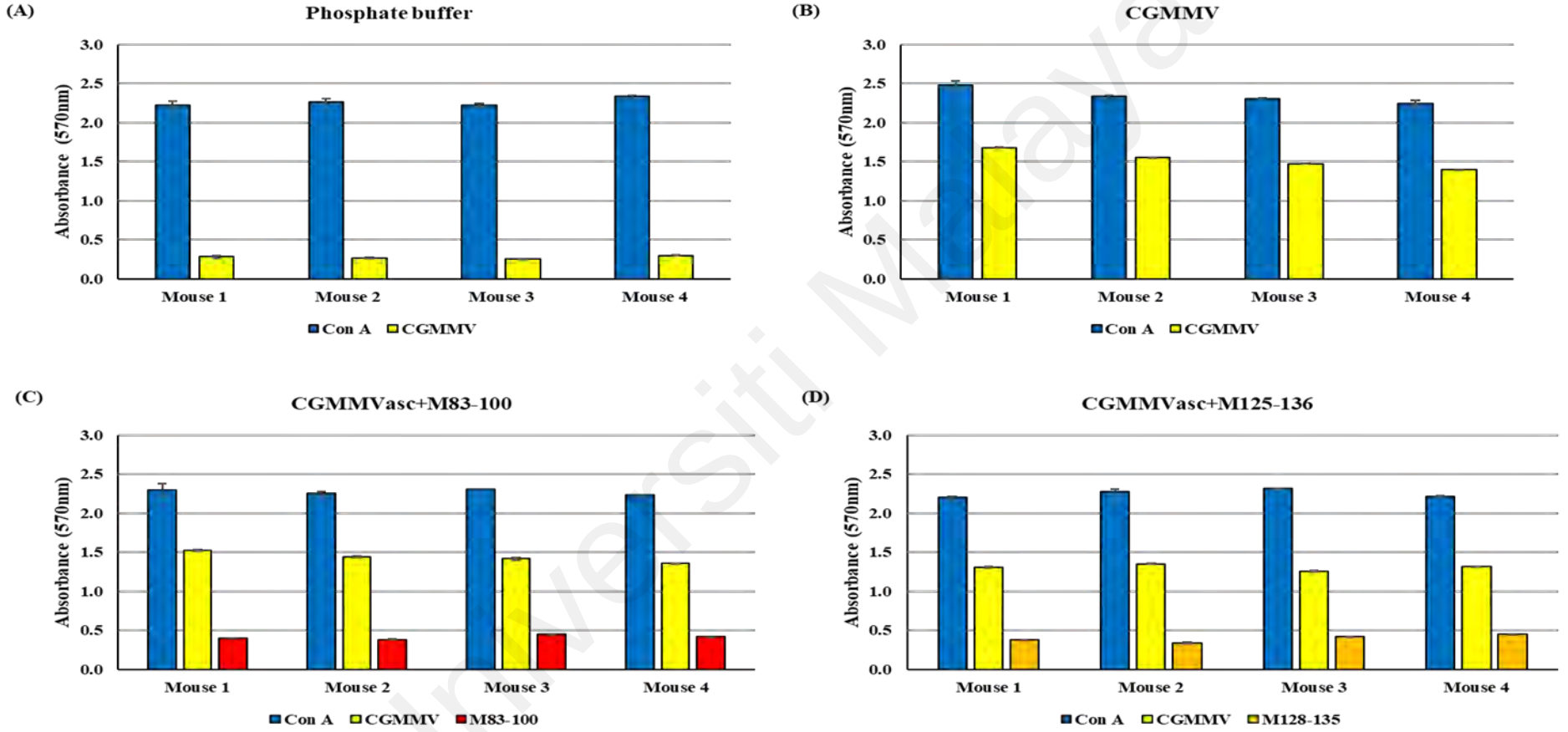

Figure 4.39: Proliferation rate of mouse spleen cells after 3rd injection. Mice were injected with (A) phosphate buffer, (B) CGMMV, (C) CGMMVasc+M83-100, (D) CGMMVasc+M125-136 and (E) CGMMVasc+M220-236 nanoparticles. Significant level of proliferation was detected when spleen was challenged with Con A (positive control) and wild-type CGMMV. However, there is no significant level of proliferation induced with peptide M83-100, M128-135 and M220-236. Data represent the mean and ± SD, n = 4 biological replicates. (**, $p < 0.01$; *, $p < 0.05$). Refer to next page for figure (E).

(E)

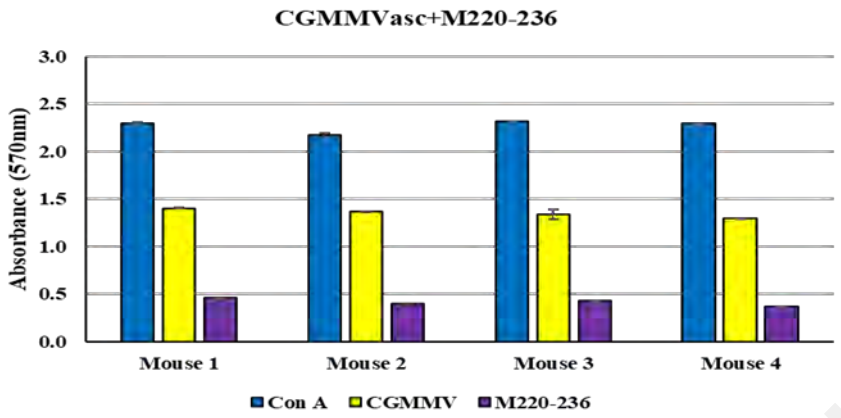

Figure 4.39, continued.

Chapter 5: DISCUSSION

5.1 Potential of CGMMV nanoparticles for biomedical applications

Plant virus nanoparticles (pVNPs) are recognised as promising platforms for application in biomedicine due to their small size, high symmetry, biocompatibility and degradability in the mammalian system as well as the ease to produce with high yield in their plant hosts. Plant VNPs including icosahedral viruses (CCMV, HCRSV, CPMV, BMV, RCNMV), rod shape viruses (TMV) and filamentous shapes (PVX) have been widely used in biomedical imaging, drug delivery, therapeutic protein and vaccines applications (Abrahamian et al., 2020; Alvandi et al., 2021; Dang & Guan, 2020; Eiben et al., 2019; Santoni et al., 2020; Shahgolzari & Pazhouhandeh, 2020; Shoeb & Hefferon, 2019). Other recent applications include functioning as a nanocarrier for siRNA targeting Akt1 by BMV for anti-cancer purposes (Nuñez-Rivera et al., 2020) and MRP-14 (also known as S100A9) by CPMV and TMV which proved to enhance not only the deep vein thrombosis diagnostics and therapeutics but also prognosis (Jooneon Park et al., 2021).

In this project, the *in vivo* characteristics of CGMMV nanoparticles, its ability as an adjuvant in a murine macrophage model and as an expression vector for influenza epitopes were investigated. As a potential pVNP for biopharmaceutical applications, CGMMV has been successfully used to express HBsAg and the results of *in vitro* studies have highlighted its promising potential (Ooi et al, 2006). However, *in vivo* characteristics of CGMMV nanoparticles when presented in a mammalian model system has not yet been fully studied. Every plant VNP has its own unique characteristics *in vivo* depending on their physical and chemical properties as well as route of administration, which could lead to different patterns in biodistribution, pharmacokinetics and pharmacodynamics (Bruckman et al., 2013; Li & Huang, 2008; Longmire et al., 2008; Rae, Khor, et al., 2005). Studies have shown that rod VNPs which possess high aspect ratio surfaces had advantages over spherical VNP in endothelial targeting and circulation time (Decuzzi et

al., 2010; Decuzzi & Ferrari, 2006; Gentile et al., 2008; Lee et al., 2009). CGMMV as a rod shape VNP is proposed as another potential candidate in addition to other reported pVNPs.

5.2 Propagation of CGMMV nanoparticles

At the onset, the study explored alternative hosts that could facilitate efficient production of the CGMMV VNPs in Malaysia's tropical climate for the subsequent experiments of this study. In the long run this may contribute to the economic cost of production, particularly if the localised plants could be grown easily and do not need controlled environment facilities. The advantages of using local resources as biofactories and its economic implications have been discussed by (Bamogo et al., 2019) in the context of Africa and other least developed countries. In this study the potentially susceptible hosts of CGGMV nanoparticles from local cucumber cultivars were investigated.

The most widely used propagation host of the CGMMV nanoparticles is *Cucumis melo* var Earl favorite originating from Japan as reported previously (Ooi et al., 2006; Teoh et al., 2009b). However, as these seeds are difficult to obtain, require importation and can incur high costs, the study proceeded to test several local melon species as an alternative. Three out of the seven local cultivars (M4, M5 and Yehe) tested showed potential to be the host as they were susceptible to CGMMV in which similar symptoms upon infection was observed and was able to produce the expected intact virus particles. Despite so, they were not the ideal propagation host as the yield of virus was only 40% of the yield of Earl favourite. As a consequence, the *C. melo* var Earl favorite was used as the propagation host throughout this entire project. In the future however, other potential local hosts should be explored in downstream studies to ensure production is economical, accessible and sustainable.

Although there are numerous factors that could contribute to the differences in the virus yield, factors such as growing condition, harvesting, storage and extraction methods can be ruled out as the same conditions and procedures were applied to all the hosts tested. (Nichols et al., 2002; Phelps et al., 2007). The structure of the CGMMV nanoparticles extracted from the *C. melo* var Earl favorite appeared to be the most intact compared to the VNPs extracted from M4, M5 and Yehe in this study. This may be due to Earl favorite being the natural host possibly has co-evolved with the virus resulting in adaptations to its pathogen defense system (Allen et al., 2004; Fonseca & Mysore, 2019). This creates a conducive and susceptible system for infection, replication and structural integrity of the virus making it an ideal host for propagation of the CGMMV nanoparticles.

Host resistance to virus infection can be caused by several mechanisms including inhibition of virus replication (Ishibashi et al., 2009), translation inhibition of viral genome due to mismatch of viral factors with the host's plant factors (Nieto et al., 2011) and RNA interference (RNAi)-mediated silencing (Jaubert et al., 2011). Plant viruses need plant factors to replicate, transcribe and translate its genome (Liu & Nelson, 2013). It is reported that lack of these factors can lead to non-host resistance (Nieto et al., 2011). Example was observed in *Cauliflower mosaic virus* (CaMV). CaMV is highly susceptible in *Brassica rapa* but less susceptible to another Brassica species due to lack of specific transcription factors which consequently lead to the reduced of virus multiplication (Covey et al., 1990). Cellular eukaryotic translation initiation factors including eukaryotic translation factor eIF (iso) 4E and eIF4G are essential for gene expression and movement of *potyviruses*, *bymoviruses* and *poleroviruses* (Niehl, et al., 2016b; Truniger & Aranda, 2009). However, the lack of interaction or incompatibility between virus proteins and the translation factor can hinder the viral replication and virus movement (Léonard et al., 2000; Nieto et al., 2011; Sanfaçon, 2015). Thus, it can be speculated that varieties M4,

M5 and Yehe of Malaysia melon might also lack of specific plant proteins that resulted in the decrease of CGMMV yield compared to Earl favorite.

On the other hand, RNA silencing mechanism might be the reason for the resistance of M3, M6, WQ and PG towards CGMMV. The viral RNAs of CGMMV nanoparticles consist of stem loops (Ugaki et al., 1991). These dsRNA can be recognised by Dicer-like (DCL) enzymes and small RNAs (siRNAs)-containing complex to degrade it resulting in an antiviral defense (Pumplin & Voinnet, 2013). The ability of PVX to infect dcl2 dcl3, dcl4 triple mutant and ago2 mutant *Arabidodsis thaliana* in which the native plant is a non-host plant of PVX confirm the function of RNAi silencing mechanism in non-host resistance (Jaubert et al., 2011). Additionally, a series of CGMMV-responsive miRNAs in watermelon has also been identified. These miRNAs are mainly involved in cell-wall modulation, plant hormone signaling and defense-related protein induction (Sun et al., 2017). Further study of these identified miRNAs in Malaysia melon varieties could help us to understand the susceptibility response towards CGMMV nanoparticles in these plants. Nonetheless, non-host resistance may involve multi-layered and broad-spectrum of mechanisms. Therefore, a more comprehensive series of studies need to be conducted in the future to fully elucidate the underlying mechanisms.

Lastly, the yield of CGMMV nanoparticles from Earl favorite ranged between 0.5-0.6 mg per gram of leaf harvested within a month which is comparable with reported yields from other pVNPs such as PVX, CPMV and CCMV (0.5-1.0 mg, 0.5-2.0 mg and 0.1-0.2 mg per gram of infected leaf respectively) but lesser than TMV nanoparticles which has been reported to be up to 4.5 mg per gram (Bruckman et al., 2013; Gopinath et al., 2000; Liepold et al., 2005; Porta et al., 2003; S Shukla et al., 2014a; Yasawardene et al., 2003).

5.3 *In vivo* characteristics of CGMMV nanoparticles in mouse

In this study we analyzed the behavior of CGMMV nanoparticles following subcutaneous injection in mice. The biodistribution of VNPs were verified by qualitative or quantitative methods. Qualitative method was performed by detecting the presence of CGMMV RNA using RT-PCR. However, as the assay may not be able to differentiate between the presence of RNA that might not represent the intact form of the CGMV nanoparticles, a quantitative experiment was needed to study the biodistribution of CGMMV VNPs in the tissue. There are several methods to track and quantify the biodistribution of VNPs for examples using high-performance liquid chromatography (HPLC), positron emission tomography (PET), spectroscopy/mass spectroscopy, radio-labelling and lanthanide metals gadolinium (Gd) or terbium (Tb) (Artzi et al., 2011; Ocampo-García et al., 2011; Oliveira et al., 2011; Rojas et al., 2011; Shukla et al., 2014a; Singh et al., 2007; Vasquez et al., 2011). These methods are either costly or are hazardous to carry out.

In this study, Alexa-488 which was used to label CMPV nanoparticles (Rae et al., 2005) and TMV nanoparticles (McCormick et al., 2006b) to study their biodistribution in mouse tissue was also used to label CGMMV nanoparticles for the same purpose. This method is a safe, rapid and inexpensive method using fluorescence-dyes including A647 and Cy5 as alternatives (Bruckman et al., 2014; Le et al., 2019; Shukla et al., 2014a). The labelling efficiency of Alexa-488 in CGMMV nanoparticles was better than CMPV nanoparticles with 504 dyes and 71.33 dyes per particle respectively (Gonzalez et al., 2009). Most importantly, the structure of CGMMV-488 nanoparticles remain intact after the fluorescence dye labelling.

To date, the biodistribution of one rod-shape virus (TMV), 2 filamentous viruses (PVX and PepMV [*Pepino mosaic virus*]) and 3 icosahedral viruses (CPMV, CCMV and

TBSV) as well as one spherical virus thermally developed from TMV (Bruckman et al., 2014; Kaiser et al., 2007; Le et al., 2019; Lico et al., 2016; Rae et al., 2005; Shukla et al., 2013; Shukla et al., 2014a; Singh et al., 2007) have been documented. Like the plant VNPs mentioned above, CGMMV nanoparticles were widely found in the organs of mice post subcutaneous injection. Administration by subcutaneous injection results in delivery to the interstitial area underlying the dermis of the skin which is then absorbed to the vascular or lymphatic capillaries in the systemic circulation (McLennan et al., 2005). The slower adsorption rate resulting in longer retention times in the system (up to 14 days) is preferred compared to the intravenous route which acts almost immediately after injection (generally cleared after 48 to 72 hours) (Kaiser et al., 2007; Rae et al., 2005; Shukla et al., 2014a). The longer half-life in the tissues also allows for the distribution and effects of CGMMV nanoparticles in mice to be studied in a greater detail. One limitation of subcutaneous injection may be that some CGMMV nanoparticles might be trapped or degraded at the subcutaneous layer of the mouse compared to intravenous injection.

The low abundance of CGMMV nanoparticles detected in the brain is encouraging and suggested that the CGMMV nanoparticles are small enough and/or highly lipid soluble enabling it to pass through the blood-brain barrier though perhaps not efficiently. The blood-brain barrier (BBB) is a highly impermeable barrier that prevents invasion of infectious organism and toxic substances (Chen & Liu, 2012). However, this barrier also hampers the treatment of brain or central nervous-related disease. Among the nanoparticles developed so far, only the amphiphilic molecule-formed liposomes and polymeric nanoparticles are more widely studied for brain drug delivery. With proper modification such as PEGylation or coating with serum albumin to enhance solubility and stability, CGMMV and other VNPs can be developed as potential nanoparticles for brain drug delivery and imaging purposes (Bruckman et al., 2014; Pitek et al., 2016).

CGMMV nanoparticles are found in the reticuloendothelial system organs which are the liver and spleen that also function to clear these VNPs. Liver and spleen are organs of mononuclear phagocyte system (MPS) which can interact with foreign materials by phagocytosis thus further protecting the systemic circulation by clearing the harmful substances. Thus, the accumulation of CGMMV nanoparticles in the spleen and liver is expected. Unlike PVX or CPMV nanoparticles which mainly accumulated in the spleen and liver respectively (Shukla et al., 2013, 2014a), Like TMV, CGMMV nanoparticles were found abundant in liver and spleen. This might be due to both CGMMV and TMV nanoparticles originated from same genus (*Tobamoviruses*) and share similar shape and size (300nm × 18nm).

Besides clearance by the reticuloendothelial system organs (the spleen and liver), CGMMV nanoparticles also appears to have undergone renal clearance as they are also found in small amount in the kidneys. As CGMMV is a rod shape plant VNP with 18nm in diameter, it can flow in the blood stream through the glomerular structure which only allows particles less than 20 nm to pass through. It is followed by absorption within the tubes as previously observed with PVX nanoparticles and synthetic particles such as carbon nanotubes (Shukla et al., 2015; Ruggiero et al., 2010). Additionally, a small number of broken CGMMV nanoparticle fragments that could be in between 30-80 nm might have flowed to the kidneys as well as lungs. This is due to the spherical nanoparticles with the size more than 80 nm showed high tendency to be trapped in spleen and liver while those in between 30-80 nm are mostly caught in the lungs (Lunov et al., 2011; Maldiney et al., 2011).

In this study, CGMMV nanoparticles administered through subcutaneous injection prolongs its retention in the mouse systemically. Longer retention time however, increases the concern of toxicity effects including inflammation and apoptosis (Khlebtsov & Dykman, 2011). Although CGMMV nanoparticles remained in the mouse for 14 days,

it showed no significant weight loss or visibly concerned clinical signs observed at the injection site and overt pathology on the mice's liver and spleen after subcutaneous injection. The half-life of CGMMV nanoparticles in blood was 3.3 days and is also biocompatible with the red blood cells (without causing hemolysis effect) which is an important factor for its use as VNPs *in vivo* (Albanese et al., 2012; Geng et al., 2007). Although the blood clotting effects was not investigated in this study due to the lack of equipment needed, we postulate that blood clotting will not occur. This is due to hemolysis and blood clotting did not occur in mice injected with TMV nanoparticles that are from the same genus with similar shape and dimension as CGMMV nanoparticles (Bruckman et al., 2014). Furthermore, H&E- stain of livers and spleens tissues did not reveal signs of obvious toxicity and inflammation, such as tissue degeneration, apoptosis or necrosis suggested that no sign of tissue damage observed in the liver and spleen.

Immunofluorescence imaging of liver- and spleen-sections to further prove the localisation and association of CGMMV nanoparticles with a specific cell type was not performed in this study. However, based on the reported data from TMV (Bruckman et al., 2014), we can postulate that CGMMV nanoparticles might co-localized with macrophage in the liver which is consistent with clearance via the mononuclear phagocytotic system (MPS). On the other hand, CGMMV nanoparticles might also co-localized with marginal zone of spleen cells which consists of macrophages and B-cells as shown in TMV nanoparticles (Bruckman et al., 2014). This statement was supported by the production of anti-CGMMV antibodies in mice after 5 days of subcutaneous injection.

Like others plant VNPs, the highly ordered and repetitive structure of CGMMV nanoparticles facilitates recognition by the immune system and induces B cell activation through B cell receptor cross-linking (Batista & Harwood, 2009). At the early stages of injection, it elicited mainly IgG1 and IgG2a subclass antibodies with IgG2b and IgG3

subclasses represented at lower titre. Increasing levels of IgG2b and IgG3 after 7 days of injection proved the balanced profile of Th1/Th2 has started to skew towards Th1. Th1 drives the type I pathway to produce more anti-CGMMV IgG1 and IgG3 antibodies to clear it from the system.

Lastly, CGMMV nanoparticles recovered from the mouse liver, spleen, serum and plasma failed to initiate symptoms in its original melon host, Earl favorite indicating that the prolonged exposure in the *in vivo* mammalian cell environment including the enzymatic activities in liver and spleen, as well as interaction with blood components, may have contributed to the reduced infectivity of CGMMV nanoparticles. Studies on CPMV nanoparticles recovered from spleen, kidney, serum and plasma also reported no symptoms on the inoculated leaves and secondary leaves (Rae et al., 2005). The advantage of this effect is it highly reduces the risk of CGMMV nanoparticles contamination to the environment.

In conclusion, CGMMV nanoparticles are distributed in a wide range of mouse tissues without causing any toxicity effect. By using fluorescent tag, CGMMV nanoparticles were found in high abundance in liver and spleen and minimal amount in brain, duodenum, kidney, lung and stomach. CGMMV nanoparticles were cleared out from mouse system within 14 days post subcutaneous injection by RES system. The disassembled and unassembled Alexa 488-conjugate coat protein might also contribute to the fluorescent reading. Thus, more tests need to be done in future to validate this preliminary result. In term of immune response, CGMMV nanoparticles induced the production anti-CGMMV antibodies that was inclined towards to the Th1 profile. Finally, the re-infectivity of CGMMV nanoparticles was greatly reduced after extracting from mouse tissues and blood.

5.4 CGMMV nanoparticles as a potential immunostimulatory

The potential of plant VNPs to be used as a natural immunostimulator has been demonstrated in several studies (review in Evtushenko et al., 2020). In this study, we have demonstrated the potential of CGMMV nanoparticles as an immunostimulator using the murine macrophage model, RAW264.7 cells. CGMMV nanoparticles can be taken up by the murine macrophages and was able to induce the innate response by up-regulating the genes involved in the nuclear factor kappa B (NF-κB) and Type I interferon signalling pathways followed by the expression of inflammatory cytokines. Treatment with CGMMV nanoparticles can also activate the murine macrophages to express the T cells activation cell surface markers. Importantly, pre-treatment of RAW264.7 cells with CGMMV nanoparticles was able to confer protection against virus infections.

To date, the knowledge on the use of VNPs or VLPs as immunostimulators came from studies in DCs (Lebel et al., 2014; Ole Kemnade et al., 2014). Except for the study of CPMV nanoparticles uptake pathway (Plummer & Manchester, 2013), the ability of pVNPs to stimulate an immune response in macrophages has not been reported. Macrophages are important innate immune cells in the defence against invading pathogens. RAW264.7 cells are known to express several TLRs (TLR 1-9, MyD88) as well as RIG-I receptor that play important roles in the innate immune response making these cells the ideal model for immune-related study (Applequist et al., 2002; Melchjorsen et al., 2005; Palazzo et al., 2008; Meyer et al., 2012).

Here we show that the internalization of the CGMMV nanoparticles by RAW264.7 cells is probably through the lysosomes and/or endolysosomes. A possible route of entry may be facilitated by the receptor-mediated endocytosis and micropinocytosis, which travels through the endosome and then en route to the lysosome as shown by the CPMV nanoparticles (Plummer & Manchester, 2013). In our finding, RAW264.7 cells uptake

reached 5% and 50% within 2 hours with 0.75 µ and 7.5 µg of CGMMV nanoparticles respectively. Compared with another finding with TMV which only 1.5% of 2 µg of TMV nanoparticles was taken up by the DCs within an hour and only reached 40% uptake after 24 hours (Ole Kemnade et al., 2014). Notably, the internalization efficiency of CGMMV nanoparticles by RAW264.7 cells was better compared to other VNPs or VLPs reported in DCs.

CGMMV nanoparticles consist of ssRNA which was encapsulated inside the coat protein. These CGMMV ssRNA has the potential to act as one of the TLR 7/8 ligand upon endocytosis (Crozat & Beutler, 2004; Diebold et al., 2004; Tanji et al., 2015). Inside the endosome/endolysosome, the CGMMV coat protein will be degraded and ssRNA released (Heil et al., 2004; Jensen & Thomsen, 2012; Lund et al., 2004). The upregulation of *TNF-α*, together with the secretion of proinflammatory cytokines as well as interferon genes and interferon stimulated genes (ISGs) in GCMMV-treated RAW264.7 cells suggested that the CGMMV ssRNA was able to trigger the endosomal TLR 7/8 pathway that leads to the activation of NF-κB pathway and type-I interferons (*IFN*) response (Kaisho & Akira, 2006; Kawai & Akira, 2010). Similar cytokine profile was detected when PapMV was added to the DCs which suggest that both PapMV and CGMMV nanoparticles are TLR7 agonist with strong immunostimulatory properties (Lebel et al., 2014). Added to the DCs, RAW264.7 cells treated with CGMMV expressed cell surface markers that is specific to T cells activations suggesting that CGMMV nanoparticles was also capable of inducing T cells responses (McCormick et al., 2006a, Ole Kemnade et al., 2014).

Notably, we showed that the innate response induced by CGMMV nanoparticles pre-treatment protected RAW264.7 cells from VSV-GFP and SeV infections. Based on the vRNA load results which show similar amount of vRNA at the early phase of virus infection regardless of the CGMMV pre-treatment status, CGMMV nanoparticles pre-

treatment did not inhibit the VSV-GFP and SeV virus entry into the host cells but prohibited the viral replication of the VSV and SeV after the entry of virus. Our data agrees with PapMV-induced innate immune response which protects DC from *Listeria Monocytigen* infection (Lebel et al., 2014).

Taken together the *in vitro* results in RAW264.7 cells, we propose that CGMMV nanoparticles have the potential to function as an immunostimulator which can be potentially used in adjuvant studies. However, further experiments using other potential APCs for example DCs can be included for comparison. Furthermore, the uptake of CGMMV nanoparticles *in vivo* and interaction with APCs as well as the effect towards T cells activation can be investigated in the future.

5.5 CGMMV nanoparticles as expression vector of influenza epitopes

In the field of vaccine development, new options to traditional immunization approaches are constantly being explored. Utilizing short synthetic peptides presents an exciting possibility to replace whole protein or inactivated virus vaccines. However, without the addition of powerful adjuvants, synthetic epitope-based vaccines are not highly immunogenic (Afrough et al., 2019; Patricio Oyarzun & Kobe, 2016). As discussed in section 5.3 and 5.4, CGMMV nanoparticles possesses an immunostimulatory characteristic which enables it to induce adaptive immunity by eliciting anti-CGMMV antibodies as well as triggering innate immunity. We therefore proceeded to construct the CGMMV vector to express a series of T and B cell epitopes from HA and M proteins of influenza as potential vaccine candidates.

A chimeric CGMMV based system expressing *Hepatitis B virus* surface antigen was successfully developed by Ooi and co-workers in 2006 (Ooi et al., 2006). The system expresses CGMMV with fusion epitopes in parallel with the wild-type CGMMV coat protein at an approximate ratio of 1:1 and can induce specific antibody reaction towards

the fused epitope (Ooi et al., 2006). It was further used to express high amount of chimeric CGMMV nanoparticles carrying neutralizing epitope (NE) of PRRSV glycoprotein 5 (GP5) on the surface of coat protein in cucumber (Tran et al., 2019). This proves the capability of CGMMV nanoparticles to be used as a potential nanoparticle candidate in vaccine development. In this study, the same strategy from Ooi and colleagues was applied in constructing the vector to express influenza epitopes. An amber read-through codon sequence was fused at the 5' terminal of influenza epitopes before being inserted at the 3' terminal of coat proteins. By using this strategy, 8 out of 10 constructs successfully expressed both wild-type and chimeric CGMMV nanoparticles carrying HA or M1 epitopes at the surface of coat proteins. However, plants inoculated with these eight chimeric CGMMV's RNA showed a milder and delayed onset of symptoms. Additionally, deletion of inserted epitope sequences was observed in 5 out of 8 chimeric CGMMV nanoparticles with 4 carrying HA epitopes and 1 carrying M1 epitope. Thus, only 3 chimeric CGMMV nanoparticles with M1 epitopes were subsequently tested for humoral and adaptive immune response in mice but unfortunately the immune responses towards theses 3 chimeric CGMMVs nanoparticles were not significant in inducing epitopes-specific antibodies and proliferation of spleen cells of which the latter is an indicator of T cells proliferation.

As the severity, onset of the symptoms and virus formation were different among these 10 chimeric CGMMV nanoparticles with 2 constructs failing to induce symptoms and virus formation at all, we try to understand the reasons behind this by comparing the length of insert, amino acids content and pI of each construct. Upon inoculation of the chimaeras onto the propagation host, the delay of the symptoms and reduction of virus titer were as expected and is consistent with TMV and CPMV nanoparticles carrying foreign sequences (Bendahmane et al., 1999; Porta et al., 2003). The insertion of the

foreign peptide appears to have impaired the rate of systemic movement of the virus hence the delay in symptoms as shown in this study and as reported for CMV nanoparticles.

Upon comparing the properties and yield of chimaeras with different inserts, it was difficult to determine if the size, amino acid content and pI is/are the factor/factors that contributed to the virus production and stability. The length of insert as short as 17 and 18 amino acids (HA127-137 and HA166-175) can impair the virus formation while the insert with 33 amino acids (HA331-354) did not show any side effects towards virus formation. There are studies reporting that certain amino acids for example, cysteine and tryptophan can affect the stability of *Tobacco mosaic virus* (Li et al., 2007) and virus formation of *Potato virus X* (Lico et al., 2006). However in our study, there was no cysteine residue in any of the peptide while the effect of tryptophan towards virus formation was inconclusive as both the infectious and non-infectious chimaera contained one tryptophan residue. The importance of the foreign peptides pI towards virus formation was reported for *Tobacco mosaic virus* (Bendahmane et al., 1999), *Cowpea mosaic virus* (Porta et al., 2003), *Potato virus X* (Uhde-Holzem et al., 2007) and *Hepatitis A virus* (Kusov et al., 2007). However, this property is not fully applicable to the CGMMV although it is a member of *Tobamovirus* as the pI of all constructs have been adjusted as near as possible to the pI of wild-type CGMMV by adding glutamic acids. Hence, the amino acid content, insert length and pI factors could not provide conclusive answers for the mild and delayed virus symptoms observed,

The chimeric virus structure was also studied through computer modelling to study the effect of adding the different influenza short epitopes to the virus coat protein's structure. Based on the results, the additional peptides at the 3' non translated region of coat protein did not affect the overall virus coat protein structure regardless of their secondary structures. It was proposed by Kusov et al (2007) that glutamic acid and leucine are good α-helix forming residues that could allow the folding of an extended and stable α-helix

(Kusov et al., 2007). Thus, it was noticed the inserted epitopes tend to form helix structure as there were 1 or 2 glutamic acids added at the 5' terminal of epitopes. It was also suggested by Kusov et al (2007) that glycine and serine will interrupt the formation of a rigid secondary structure coat protein but this phenomenon did not occur with the CGMMV coat protein although there are multiple glycine and serine residues in the epitope peptide (Kusov et al., 2007). It therefore suggests that the CGMMV nanoparticles is relatively flexible in accommodating any amino acid without disrupting its natural structure.

During the RNA secondary structure analysis of the chimeric vectors, we noticed that RNA secondary structure of 2 constructs namely, CGMMVas+HA127-137 and CGMMVasc+HA166-175 were totally different from the wild-type and the other chimeric vectors. It was later shown that these 2 constructs failed to induce any symptoms and virus formations. Due to the changes of the RNA structure, RNA dependent RNA polymerase (RdRp) might not be able to bind to the tRNA-like 3' end of RNA 4 causing RdRp to enter a transient, catalytically inactive state known as transcriptional pauses (Zhang & Landick, 2016). As a result, none or a lesser amount of minus strand RNA will be synthesized leading to none or lesser template to synthesize plus-strand genomic RNAs needed for protein translation. Without the newly synthesized coat protein, there is no virus particle formed and the RNA is easily degraded by the host enzymes resulting in the loss of infectivity.

There are 2 sets of amber read-through stop codons namely RT1, "TCT-AAA-TAG-CAA-TTA" and RT2, "TCC-AAA-TAG-CAA-TTA" being used in CGMMV to express foreign epitopes (Ooi et al., 2006; Othman et al., 2009; Tran et al., 2019). Ooi and colleagues (2006) using RT1 read-through stop codon successfully expressed both wild-type and chimeric CGMMV nanoparticles carrying Hep B sAg at 1:1 ratio without deletion (Ooi et al., 2006). RT1 read-through stop codon also used in this study but to

express influenza epitopes. There are 8 chimeric constructs which formed CGMMV nanoparticles and seem to express chimeric CGMMV with influenza epitopes. However, upon analyzing the peptide sequence with LC/MS/MS, only 3 chimera constructs with complete amino acid sequence of wild-type coat protein as well as inserted epitope were detected. Our result was similar with the finding in a study carried out by Tran and colleagues (2019) to express neutralizing epitope (NE) of PRRSV glycoprotein 5 (GP5) using CGMMV. The construct with RT1, "TCT-AAA-TAG-CAA-TTA" successfully produced the wild-type CGMMV nanoparticles but not the CP fusion protein (CP-NE) although RT-PCR results confirmed the presence of chimeric CGMMV nanoparticles in all symptomatic cucumber and *N. benthmiana* plants (Tran et al., 2019). This suggests that not all plants with symptoms and the presence of chimeric RT-PCR products will lead to the formation of chimeric proteins. Even though the chimeric proteins were detected using Western blotting using anti-CGMMV antibody, the deletion or absence of inserted sequences can only be detected using mass spectrometry at 30 d.p.i.

When Tran and colleagues repeated the experiment using the RT 2 read-through codon, both wild-type and chimeric CGMMVs (CP-NE) nanoparticles were detected in cucumber but not *N. benthmiana* (Tran et al., 2019a). However, the expression level decreased dramatically at 50 d.p.i suggested that deletion might happened. This result was similar with the findings of Teoh and colleagues (2009) who expressed dengue epitopes but the deletion was observed much earlier which was at 21 d.p.i (Teoh et al., 2009b).

As the inserted sequence and the inoculated plants are different between our study and the research carried out by Ooi et al., (2006), Teoh et al., and Tran et al., 2019, it remains inconclusive whether the RT1 or RT 2 is a more effective read-through codon. But based on the finding above, we can postulate that the read-through codon might be sequence and host specific and might not be stable for prolonged propagation. However, further

studies are needed to verify this hypothesis. Earlier harvesting time might be able to prevent the deletion of inserted epitope from happening. Further experiment is needed to determine the optimal harvesting time that balances between the yield of virus and the loss of inserted sequence.

CGMMVasc+M83-100 and CGMMVasc+M220-236 failed to induce epitope specific antibody in mice when injected subcutaneously. Only anti-CGMMV antibody was detected which was similar with the results seen in section 5.3 with the native virus. Although CGMMV nanoparticles were proved to have immunostimulatory function, it might still not be enough to induce immune response toward M83-100 and M220-236. The HA and M1 epitopes chosen to be expressed on the coat protein of CGMMV nanoparticles were selected from IEDB through a series of assays supporting their antigenic roles (refer to Appendix O and P). The M83-100 and M220-236 epitopes were identified as epitopes recognized by B cells (Bucher, et al. 1989). When purified M1 protein were injected intravenously with Freund's complete adjuvant into Balb/c mice, it induced panels of monoclonal antibodies. Among them, there are 2 panels that recognized peptides M83-100 and M220-236 through antibody/antigen binding (Bucher, et al. 1989). However, to date, there are no reported studies of direct immunisation of the mouse using these 2 epitopes alone. This might be due to the possibility that the epitopes alone are not immunogenic enough to induce antibodies by itself and might explain our negative results.

Thus, to further boost the immunogenicity of the M83-100 and M220-236 epitopes, adjuvants can be injected together with CGMMVasc+M83-100 and CGMMVasc+M220-236 into the mice. Adjuvants are compound that can augment the specific immune response to antigens (Coler et al., 2009; Reed et al., 2009). It was shown that when mice were immunized with Ov-103 and Ov-RAL-2 recombinant antigens only, these antigens did not induce a significant antibody response. However, positive antibody responses

were detected when Ov-103 and Ov-RAL-2 were injected together with alum, Advax 1, Advax 2, CpG oligonucleotide (CpG), and MF59 adjuvants (Hess et al., 2016). Similar finding was also showed recently in a phase 1 randomized trial of a plant-derived virus-like particle (VLP) vaccine for COVID-19. The immunogenicity of VLP with AS03 or CpG1018 adjuvant was stronger compared to VLP alone. The neutralising antibody, protein-specific interferon-γ and interleukin-4 cellular responses were higher in people vaccinated with Covid VLP +adjuvants (AS03 or CpG1018) (Ward et al., 2021). This study proves the need and effects of adjuvants to elicit immunity.

On the other hand, the M128-135 epitope was identified as a subdominant H2-kb recognized by T cells by IFN-γ production and presented on MHC-I during *in vivo* infection (Belz et al., 2000; Vitiello et al., 2020; Ting Wu et al., 2019; Zhong et al., 2003). It can elicit $CD8^+$ T cells when the peptide was pulsed in dendritic cells (Crowe et al., 2006). The M128-135 epitopes of A/California/4/09 (CA/09) was expressed by the modified *Vaccinia virus Ankara* (MVA-M1) and used to immunize AAD mice intramuscularly (i.m.) twice, three weeks apart, with 10^7 pfu of the MVA-M1. The result proved that MVA-M1 can induced $CD8^+$ T cells responses and generated protection against lethal influenza virus challenge with 72% survival rate (Di Mario et al., 2017). Unexpectedly, it was also reported that when MVA-M1 was injected into Balb/c mice, no M128-135 specific antibodies or $CD4^+$ and $CD8^+$ cells were detected and subsequently no protection against influenza viruses was observed (Hessel et al., 2014) which is consistent with our result when it was immunized with CGMMVasc+M128-135, there was also no significant spleen cells proliferation response detected. Therefore, it is suspected that the M128-135 epitope immunogenicity might be mouse species specific. To address this possibility, further experiments can be done by injecting CGMMVasc+M128-135 intramuscularly into AAD mice and to observe the immune responses.

Other than the epitopes from the HA and M1 proteins, there are other potential epitopes from PA, NP, PB1, M2e, NS1 of H1N1 or other strains that can be potentially expressed using the CGMMV vector (Eickhoff et al., 2019; Sheikh et al., 2016; Ye Wang et al., 2018, 2020). Polymerase epitope (PA224–233) in nanofiber format generated greater antigen-specific $CD8^+$ T cells responses in the lung-draining lymph nodes by intranasal immunization and promote more lung-resident memory $CD8^+$ T cells (Si et al., 2018). Modified *Vaccinia virus Ankara* expressing the nucleoprotein epitope (MVA-NP147-155) induced influenza-specific antibodies and protected the AAD mice against lethal influenza virus challenge (Di Mario et al., 2017; Hessel et al., 2014). On the other hand, four tandem copies of the ectodomain of matrix protein 2 (M2e) and fusion of M2e with HA2 on a flagellin carrier induced vaccine antigen-specific humoral immune responses and fully protected against lethal doses of influenza virus challenge (Deng et al., 2017). Last but not least, the M2e coupled with helper T cell epitopes also induced significant production of M2e antibodies in Balb/c mice and C57BL/6 mice and protected mice from lethal influenza virus challenge (Jeong-Ki Kim et al., 2019).

All in all, although the CGMMVasc+M83-100, M126-135 and CGMMVasc+M220-236 chimeric VNPs failed to induce significant immune response in Balb/c mice, it does not negate the fact that CGMMV nanoparticles is a potential expression vector that could be developed further. With more studies and optimization, CGMMV vector could express epitopes with higher yield and stability.

CHAPTER 6: CONCLUSION

This work provides the foundation on the potential of CGMMV nanoparticles in nanomedicine applications including its *in vivo* characteristics, *in vitro* immunostimulatory property and as a chimeric expression vector to elicit immune response against influenza virus *in vivo*. In addition, this study also demonstrated that *C. melo* var Earl favorite is a better host to propagate CGMMV nanoparticles compared to the local host.

Our preliminary study of the biodistribution, clearance mechanism, re-infectivity and immunogenicity of CGMMV nanoparticles enable us to understand its fate *in vivo*, an integral part of vaccine or therapeutic candidate study. CGMMV nanoparticles were distributed in a wide range of tissues and can induce antibody production without causing toxicity, suggesting that CGMMV is a potential nanoparticle with biomedical applications. In the future, mice can be immunised with the plant's extract in addition to phosphate buffer saline to rule out any possibility of non-specific and cross-reactive antibody reactions. In addition, blood tests and marker of inflammation can be carried out to further confirm the non-toxicity of CGMMV nanoparticles s. Although the viral infectivity of CGMMV nanoparticles is reduced following *in vivo* passage, this could be due to many reasons such as adsorption of serum proteins to the VNPs which might block planta infection. Further work is required to confirm this hypothesis or identify other possible reasons.

In the *in vitro* study using RAW264.7 cells that phenotypically and functionally resemble the macrophages, we tested the potential of CGMMV nanoparticles to function as an immune stimulator. The results showed that CGMMV nanoparticles can induce innate immunity, activate macrophage and thus confer protection against virus infection.

Further experiments are needed to delineate the molecular mechanism of how CGMMV nanoparticles can activate TLR in macrophages and other APC populations in the future.

In this study, CGMMV nanoparticles were successfully utilized to express a range of influenza epitopes from HA and M1 proteins. Selected epitopes were fused at 3' terminal of CGMMV CP together with amber stop codon and expressed using read through strategy. Eight out of ten chimeric CGMMVs nanoparticles induced mild mottle and mosaic symptoms on the host. However, only three chimeric CGMMVs nanoparticles carried M1 epitopes showed the complete amino acids sequences.

Immunization of Balb/c mice with the 3 validated chimeric CGMMV nanoparticles carrying M1 epitopes unfortunately did not induce any significant immune response. This is in spite of the *in vitro* modelling and pI adjustment that were carried out before proceeding for vector construction and expression. It is possible that there are still some underlying unknown factors that needs to be understood to ensure the expression and stability of epitopes expressed at the surface of CGMMV coat protein especially those that might restrain the conformation of epitopes. Further experiments, such as immuno-gold labelling transmission electron microscopy (TEM) using gold-conjugated anti-influenza virus proteins can be carried on the chimeric CGMMV nanoparticles to examine if the epitopes are properly displayed on the surface of the nanoparticles.

Adjuvants like alum can be introduced with chimeric CGMMV nanoparticles to boost the immune response as well. Besides, non-fused epitopes only can also be included to immunise mice (with or without the adjuvants) to confirm the effectiveness of selected epitopes in inducing immune response in mice. Finally, newly identified epitopes from influenza virus expressed proteins like NA and M2 should also be included in the future in order to create a potential universal influenza vaccine using CGMMV nanoparticles.

REFERENCES

Abrahamian, P., Hammond, R. W., & Hammond, J. (2020). Plant virus–derived vectors: Applications in agricultural and medical biotechnology. *Annual Review of Virology*, *8*(23), 1–23.

Adams, M. J., Adkins, S., Bragard, C., Gilmer, D., Li, D., MacFarlane, S. A., … Ryu, K.H., (2017). ICTV virus taxonomy profile: Virgaviridae. *The Journal of general virology*, *98*(8), Article#1999.

Afrough, B., Dowall, S., & Hewson, R. (2019). Emerging viruses and current strategies for vaccine intervention. *Clinical & Experimental Immunology*, *196*(2), 157–166.

Ahmad, S., Munir, S., Zeb, N., Ullah, A., Khan, B., Ali, J., … Salman, S. M. (2019). Green nanotechnology: A review on green synthesis of silver nanoparticles - An ecofriendly approach. *International Journal of Nanomedicine*, *14*, Article#5087.

Ahmadi, M. H., Ghazvini, M., Alhuyi Nazari, M., Ahmadi, M. A., Pourfayaz, F., Lorenzini, G., & Ming, T. (2019). Renewable energy harvesting with the application of nanotechnology: A review. *International Journal of Energy Research*, *43*(4), 1387–1410.

Ahmed, S., Chaudhry, S. A., & Ikram, S. (2017). A review on biogenic synthesis of ZnO nanoparticles using plant extracts and microbes: A prospect towards green chemistry. *Journal of Photochemistry and Photobiology B: Biology*, *166*, 272–284.

Ainsworth, G. C. (1935). Mosaic diseases of the cucumber. *Annals of Applied Biology*, *22*(1), 55–67.

Akhtar, S., Shahzad, K., Mushtaq, S., Ali, I., Rafe, M. H., & Fazal-ul-Karim, S. M. (2019). Antibacterial and antiviral potential of colloidal Titanium dioxide (TiO2) nanoparticles suitable for biological applications. *Materials Research Express*, *6*(10), Article#105409.

Akira, S., & Takeda, K. (2004). Toll-like receptor signalling. *Nature Reviews Immunology*, *4*(7), 499–511.

Albakri, M. M., Veliz, F. A., Fiering, S. N., Steinmetz, N. F., & Sieg, S. F. (2020). Endosomal toll-like receptors play a key role in activation of primary human monocytes by cowpea mosaic virus. *Immunology*, *159*(2), 183–192.

Albanese, A., Tang, P. S., & Chan, W. C. W. (2012). The Effect of nanoparticle size , shape , and surface chemistry on biological systems. *European Journal of Pharmaceutics and Biopharmaceutics*, *14*(1), 1–16.

Alemzadeh, E., Dehshahri, A., Izadpanah, K., & Ahmadi, F. (2018). Plant virus nanoparticles: Novel and robust nanocarriers for drug delivery and imaging. *Colloids and Surfaces B: Biointerfaces*, *167*, 20-27.

Ali, M., Pandey, R. K., Khatoon, N., Narula, A., & Mishra, A. (2017). Exploring dengue genome to construct a multi-epitope based subunit vaccine by utilizing immunoinformatics approach to battle against dengue infection. *Scientific Reports*,*7*(1), 1–13.

Aljabali, A. A., Al Zoubi, M. S., Al-Batanyeh, K. M., Al-Radaideh, A., Obeid, M. A., Al Sharabi, A., ... Evans, D. J. (2019). Gold-coated plant virus as computed tomography imaging contrast agent. *Journal of Nanotechnology*, *10*, 1983–1993.

Allen, R. L., Bittner-Eddy, P. D., Grenville-Briggs, L. J., Meitz, J. C., Rehmany, A. P., Rose, L. E., & Beynon, J. L. (2004). Host-parasite coevolutionary conflict between Arabidopsis and downy mildew. *Science*, *306*(5703), 1957–1960.

Alonso-padilla, J., Lafuente, E. M., & Reche, P. A. (2017). Computer-aided design of an epitope-based vaccine against Epstein-Barr virus. *Journal of Immunology Research*, *2017*.

Alvandi, N., Rajabnejad, M., Taghvaei, Z., & Esfandiari, N. (2021). New generation of viral nanoparticles for targeted drug delivery in cancer therapy. *Journal of Drug Targeting*, *30*(2), 151-165.

Amato, R., Dal Monte, M., Lulli, M., Raffa, V., & Casini, G. (2018). Nanoparticle-mediated delivery of neuroprotective substances for the treatment of diabetic retinopathy. *Current Neuropharmacology*, *16*(7), 993–1003.

Amudhavalli, N. K., & Ravi, C. (2019). A review on nanotechnology in concrete. *International Journal of Civil Engineering and Technology (IJCIET)*, *10*(03), 1953–1960.

Applequist, S. E., Wallin, R. P., & Ljunggren, H. G. (2002). Variable expression of Toll-like receptor in murine innate and adaptive immune cell lines. *International Immunology*, *14*(9), 1065–1074.

Arazi, T., Huang, P. L., Huang, P. L., Zhang, L., Shiboleth, Y. M., Gal-On, A., & Lee-Huang, S. (2002). Production of antiviral and antitumor proteins MAP30 and GAP31 in cucurbits using the plant virus vector ZYMV-AGII. *Biochem Biophys Res Commun*, *292*(2), 441–448.

Arnaboldi, P. M., Sambir, M., D'Arco, C., Peters, L. A., Seegers, J. F. M. L., Mayer, L., … Dattwyler, R. J. (2016). Intranasal delivery of a protein subunit vaccine using a Tobacco mosaic virus platform protects against pneumonic plague. *Vaccine*, *34*(47), 5768–5776.

Artzi, N., Oliva, N., Puron, C., Shitreet, S., Artzi, S., bon Ramos, A., Groothuis, A., Sahagian, G., & Edelman, E. R. (2011). In vivo and in vitro tracking of erosion in biodegradable materials using non-invasive fluorescence imaging. *Nature Materials*, *10*(9), 704–9.

Atabekov, J., Nikitin, N., Arkhipenko, M., Chirkov, S., & Karpova, O. (2011). Communication thermal transition of native Tobacco mosaic virus and RNA-free viral proteins into spherical nanoparticles. *Journal of General Virology*, *92*, 453–456.

Autio, K. A., Dreicer, R., Anderson, J., Garcia, J. A., Alva, A., Hart, L. L., … Graf, R. P. (2018). Safety and efficacy of BIND-014, a docetaxel nanoparticle targeting prostate-specific membrane antigen for patients with metastatic castration-resistant prostate cancer: A phase 2 clinical trial. *JAMA Oncology*, *4*(10), 1344–1351.

Azizgolshani, O., Garmann, R. F., Cadena-Nava, R., Knobler, C. M., & Gelbart, W. M. (2013). Reconstituted plant viral capsids can release genes to mammalian cells. *Virology*, *441*(1), 12–17.

Babin, C., Majeau, N., & Leclerc, D. (2013). Engineering of papaya mosaic virus (PapMV) nanoparticles with a CTL epitope derived from influenza NP. *Journal of Nanobiotechnology*, *11*(1), 1–8.

Balke, I., & Zeltins, A. (2020). Recent advances in the use of plant virus-like particles as

Vaccines. *Viruses*, *12*, 1–16.

Bamogo, P. K. A., Brugidou, C., Sérémé, D., Tiendrébéogo, F., Djigma, F. W., Simpore, J., & Lacombe, S. (2019). Virus-based pharmaceutical production in plants: An opportunity to reduce health problems in Africa. *Virology Journal*, *16*(1), 1–16.

Banik, S., Mansour, A. A., & Suresh, R. V. (2015). Development of a Multivalent Subunit Vaccine against Tularemia Using Tobacco mosaic virus (TMV) Based Delivery System. *PLoS ONE*, *10*(6), 1–22.

Barbalat, R., Ewald, S. E., Mouchess, M. L., & Barton, G. M. (2011). Nucleic acid recognition by the innate immune system. *Annual Review of Immunology*, *29*, 185–214.

Barr, I. G., Deng, Y. M., Iannello, P., Hurt, A. C., & Komadina, N. (2008). Adamantane resistance in Influenza A (H1) viruses increased in 2007 in South East Asia but decreased in Australia and some other countries. *Antiviral Research*, *80*, 200–205.

Barr, I. G., Hurt, A. C., Deed, N., Iannello, P., Tomasov, C., & Komadina, N. (2007a). The emergence of adamantane resistance in Influenza A (H1) viruses in Australia and regionally in 2006. *Antiviral Research*, *75*, 173–176.

Barr, I. G., Hurt, A. C., Iannello, P., Tomasov, C., Deed, N., & Komadina, N. (2007b). Increased adamantane resistance in Influenza A (H3) viruses in Australia and neighbouring countries in 2005. *Antiviral Research*, *73*, 112–117.

Batista, F. D., & Harwood, N. E. (2009). The who, how and where of antigen presentation to B cells. *Nature Reviews Immunology*, *9*(1), 15–27.

Beatty, P. H., & Lewis, J. D. (2019). Cowpea mosaic virus nanoparticles for cancer imaging and therapy. *Advanced Drug Delivery Reviews*, *145*, 130–144.

Belanger, H., Fleysh, N., Cox, S., Bartman, G., Deka, D., Trudel, M., Koprowski, H., & Yusibov, V. (2000). Human respiratory syncytial virus vaccine antigen produced in plants. *FASEB Journal*, *14*(14), 2323–2328.

Belot, A., Lopez, A., Mariette, X., Bonnotte, B., Hachulla, E., Lahfa, M., … Peyrin-biroulet, L. (2017). Vaccination recommendations for the adult immunosuppressed patient: A systematic review and comprehensive field synopsis. *Journal of Autoimmunity*, *80*, 10-27.

Belz, G. T., Xie, W., Altman, J. D., & Doherty, P. C. (2000). A previously unrecognized H-2Db-restricted peptide prominent in the primary Influenza A virus-specific CD8+ T-cell response is much less apparent following secondary challenge. *Journal of Virology*, *74*(8), 3486–3493.

Ben-Akiva, E., Witte, S. E., Meyer, R. A., Rhodes, K. R., & Green, J. J. (2019). Polymeric micro-and nanoparticles for immune modulation. *Biomaterials Science*, *7*(1), 14–30.

Bendahmane, M., Koo, M., Karrer, E., & Beachy, R. N. (1999). Display of epitopes on the surface of tobacco mosaic virus: impact of charge and isoelectric point of the epitope on virus-host interactions. *Journal of Molecular Biology*, *290*(1), 9–20.

Bennett, A., Rodriguez, D., Lister, S., Boulton, M., McKenna, R., & Agbandje-McKenna, M. (2018). Assembly and disassembly intermediates of Maize streak geminivirus. *Virology*, *525*, 224–236.

Berman, H. M., Westbrook, J., Feng, Z., Gilliland, G., Bhat, T. N., Weissig, H., …

Bourne, P. E. (2000). The Protein Data Bank. *Nucleic Acids Research*, *28*(1), 235–242.

Blandino, A., Lico, C., Baschieri, S., Barberini, L., Cirotto, C., Blasi, P., & Santi, L. (2015). In vitro and in vivo toxicity evaluation of plant virus nanocarriers. *Colloids and Surfaces B: Biointerfaces*, *129*, 130–136.

Bolduc, M., Baz, M., Laliberté-Gagné, M. È., Carignan, D., Garneau, C., Russel, A., … Leclerc, D. (2018). The quest for a nanoparticle-based vaccine inducing broad protection to influenza viruses. *Nanomedicine: Nanotechnology, Biology and Medicine*, *14*(8), 2563–2574.

Brennan, F. R., Bellaby, T., Helliwell, S. M., Jones, T. D., Kamstrup, S., Dalsgaard, K., … Hamilton, W. D. (1999). Chimeric plant virus particles administered nasally or orally induce systemic and mucosal immune responses in mice. *Journal of Virology*, *73*(2), 930–938.

Brennan, F. R., Jones, T. D., Gilleland, L. B., Bellaby, T., Xu, F., North, P. C., … Gilleland, H. E. (1999). Pseudomonas aeruginosa outer-membrane protein F epitopes are highly immunogenic in mice when expressed on a plant virus. *Microbiology*, *145*(1), 211–220.

Brodzik, R., Bandurska, K., Deka, D., Golovkin, M., & Koprowski, H. (2005). Advances in Alfalfa mosaic virus-mediated expression of anthrax antigen in planta. *Biochemical and Biophysical Research Communications*, *338*(2), 717–722.

Bruckman, M. A., Czapar, A. E., VanMeter, A., Randolph, L. N., & Steinmetz, N. F. (2016). Tobacco mosaic virus-based protein nanoparticles and nanorods for chemotherapy delivery targeting breast cancer. *Journal of Controlled Release*, *231*, 103–113.

Bruckman, M. A., Hern, S., Jiang, K., Flask, C. A., Yu, X., & Steinmetz, N. F. (2013). Tobacco mosaic virus rods and spheres as supramolecular high-relaxivity MRI contrast agents. *Journal of Materials Chemistry. B*, *1*(10), 1482–1490.

Bruckman, M. A., Randolph, L. N., VanMeter, A., Hern, S., Shoffstall, A. J., Taurog, R. E., & Steinmetz, N. F. (2014). Biodistribution, pharmacokinetics, and blood compatibility of native and PEGylated Tobacco mosaic virus nano-rods and-spheres in mice. *Virology*, *449*, 163–173.

Bruckman, M. A., & Steinmetz, N. F. (2014). Chemical modification of the inner and outer surfaces of Tobacco mosaic virus (TMV). In *Virus Hybrids as Nanomaterials* (pp. 173-185). Humana Press, Totowa, NJ.

Brumeanu, T. D., Bot, A., Bona, C. A., Dehazya, P., Wolf, I., & Zaghouani, H. (1996). Engineering of doubly antigenized immunoglobulins expressing T and B viral epitopes. *Immunotechnology*, *2*(2), 85–95.

Brumfield, S., Willits, D., Tang, L., Johnson, J. E., Douglas, T., & Young, M. (2004). Heterologous expression of the modified coat protein of Cowpea chlorotic mottle bromovirus results in the assembly of protein cages with altered architectures and function. *Journal of General Virology*, *85*(4), 1049–1053.

Brunotte, L., Beer, M., Horie, M., & Schwemmle, M. (2016). Chiropteran influenza viruses : Flu from bats or a relic from the past ? *Current Opinion in Virology*, *16*, 114–119.

Bucher, D., Popple, S., Baer, M'Mikhail, A., Gong, Y. ., Whitaker, C., Paoletti, E., &

Judd, A. (1989). M Protein (M1) of influenza virus: Antigenic analysis and intracellular localization with monoclonal antibodies. *Journal of Viirology*, *63*(9), 3622–3633.

Burleigh, L. M., Calder, L. J., Skehel, J. J., & Steinhauer, D. A. (2005). Influenza A viruses with mutations in the M1 helix six domain display a wide variety of morphological phenotypes. *Journal of Virology*, *79*(2), 1262–1270.

Burnett, J. R., & Hooper, A. J. (2009). Alipogene tiparvovec, an adeno-associated virus encoding the Ser (447) X variant of the human lipoprotein lipase gene for the treatment of patients with lipoprotein lipase deficiency. *Current Opinion in Molecular Therapeutics*, *11*(6), 681–691.

Cabral-Miranda, G., Heath, M. D., Mohsen, M. O., Gomes, A. C., Engeroff, P., Flaxman, A., … Skinner, M. A. (2017). Virus-like particle (VLP) plus microcrystalline tyrosine (MCT) adjuvants enhance vaccine efficacy improving T and B cell immunogenicity and protection against Plasmodium berghei/vivax. *Vaccines*, *5*(2), Article#10.

Cachau, R., Fritts, M., Topol, I., Burt, S., Gonzalez-Nilo, F., & Matties, M. (2007). Structural analysis of nanobioparticles. *MRS Online Proceedings Library (OPL)*, *1019*.

Cai, H., Shukla, S., Wang, C., Masarapu, H., & Steinmetz, N. F. (2019). Heterologous prime-boost enhances the antitumor immune response elicited by plant-virus-based cancer vaccine. *Journal of the American Chemical Society*, *141*(16), 6509–6518.

Calder, L. J., Wasilewski, S., Berriman, J. A., & Rosenthal, P. B. (2010). Structural organization of a filamentous Influenza A virus. *Proceedings of the National Academy of Sciences*, *107*(23), 10685–10690.

Carignan, D., Herblot, S., Laliberté-Gagné, M. È., Bolduc, M., Duval, M., Savard, P., & Leclerc, D. (2018). Activation of innate immunity in primary human cells using a plant virus derived nanoparticle TLR7/8 agonist. *Nanomedicine: Nanotechnology, Biology and Medicine*, *14*(7), 2317–2327.

Carignan, D., Thérien, A., Rioux, G., Paquet, G., Gagné, M. È. L., Bolduc, M., ... Leclerc, D. (2015). Engineering of the PapMV vaccine platform with a shortened M2e peptide leads to an effective one dose influenza vaccine. *Vaccine*, *3351*, 7245-7253.

Center for Disease Control and Prevention. (2020). Image of H1N1 influenza. Retrieved on 26th, September, 2020, from https://www.cdc.gov/h1n1flu/images.htm?s_cid=cs_001.

Chariou, P. L., Ortega-Rivera, O. A., & Steinmetz, N. F. (2020). Nanocarriers for the delivery of medical, veterinary, and agricultural active ingredients. *ACS Nano*, *14*(3), 2678–2701.

Chariou, P.L., & Steinmetz, N.F. (2017). Delivery of pesticides to plant parasitic nematodes using tobacco mild green mosaic virus as a nanocarrier. *ACS Nano*, *11*, 4719–4730.

Charudattan, R., & Hiebert, E. (2007). A plant virus as a bioherbicide for tropical soda apple, Solanum viarum. *Outlooks Pest Manag*ement, *18*, Article#167.

Chen, T., Chen, T., Hu, C., Liao, J., Lee, C., Liao, J., … Hsu, Y. (2012). Induction of protective immunity in chickens immunized with plant-made chimeric Bamboo mosaic virus particles expressing very virulent Infectious bursal disease virus

antigen. *Virus Research*, *166*, 109–115.

Chen, T. H., Hu, C. C., Liao, J. T., Lee, Y. L., Huang, Y. W., Lin, N. S., … Hsu, Y. H. (2017). Production of Japanese encephalitis virus antigens in plants using Bamboo mosaic virus-based vector. *Frontiers in Microbiology*, *8*, Article#788.

Chen, W., Calvo, P. A., Malide, D., Gibbs, J., Schubert, U., Bacik, I., … Yewdell, J. W. (2001). A novel Influenza A virus mitochondrial protein that induces cell death. *Nature Medicine*, *7*(12), 1306–1312.

Chen, Y., & Liu, L. (2012). Modern methods for delivery of drugs across the blood-brain barrier. *Advanced Drug Delivery Reviews*, *64*(7), 640–665.

Chichester, J. A., Green, B. J., Jones, R. M., Shoji, Y., Miura, K., Long, C. A., … Streatfield, S. J. (2018). Safety and immunogenicity of a plant-produced Pfs25 virus-like particle as a transmission blocking vaccine against malaria: A Phase 1 dose-escalation study in healthy adults. *Vaccine*, *36*(39), 5865–5871.

Cho, C. F., Yu, L., Nsiama, T. K., Kadam, A. N., Raturi, A., Shukla, S., … Lewis, J. D. (2017). Viral nanoparticles decorated with novel EGFL7 ligands enable intravital imaging of tumor neovasculature. *Nanoscale*, *9*(33), 12096–12109.

Chou, T. C., Hsu, W., Wang, C. H., Chen, Y. J., & Fang, J. M. (2011). Rapid and specific influenza virus detection by functionalized magnetic nanoparticles and mass spectrometry. *Journal of Nanobiotechnology*, *9*(1), Article#52.

Clemente, M., Curilovic, R., Sassone, A., Zelada, A., Angel, S. O., & Mentaberry, A. N. (2005). Production of the main surface antigen of Toxoplasma gondii in tobacco leaves and analysis of its antigenicity and immunogenicity. *Molecular Biotechnology*, *30*(1), 41–50.

Coler, R. N., Carter, D., Friede, M., & Reed, S. G. (2009). Adjuvants for malaria vaccines. *Parasite Immunology*, *31*(9), 520–528.

Collin, E. A., Sheng, Z., Lang, Y., Ma, W., & Hause, B. M. (2015). Cocirculation of two distinct genetic and antigenic lineages of proposed Influenza D virus in cattle. *Journal of virology*, *89*(2), 1036-1042.

Contreras, J. E., Rodriguez, E. A., & Taha-Tijerina, J. (2017). Nanotechnology applications for electrical transformers - A review. *Electric Power Systems Research*, *143*, 573–584.

Covey, S. N., Turner, D. S., Lucy, A. P., & Saunders, K. (1990). Host regulation of the Cauliflower mosaic virus multiplication cycle. *Proceedings of the National Academy of Sciences*, *87*(5), 1633–1637.

Cox, J., & Mann, M. (2008). MaxQuant enables high peptide identification rates, individualized ppb-range mass accuracies and proteome-wide protein quantification. *Nature Biotechnology*, *26*(12), 1367–72.

Crepey, P., Redondo, E., Díez-Domingo, J., Ortiz de Lejarazu, R., Martinón-Torres, F., Gil de Miguel, Á., ... Solozabal, M. (2020). From trivalent to quadrivalent influenza vaccines: Public health and economic burden for different immunization strategies in Spain. *PLoS One*, *15*(5), Article#e0233526.

Crowe, S. R., Miller, S. C., & Woodland, D. L. (2006). Identification of protective and non-protective T cell epitopes in influenza. *Vaccine*, *24*(4), 452-456.

Crozat, K., & Beutler, B. (2004). TLR7: A new sensor of viral infection. *Proceedings of*

the National Academy of Sciences, *101*(18), 6835–6836.

Dalsgaard, K., Uttenthal, A., Jones, T. D., Xu, F., Merryweather, A., Hamilton, W. D., … Rodgers, P. B. (1997). Plant-derived vaccine protects target animals against a viral disease. *Nature Biotechnology*, *15*(3), 248–252.

Dang, Y., & Guan, J. (2020). Nanoparticle-based drug delivery systems for cancer therapy. *Smart Materials in Medicine, 1*, 10-19.

Daniel, M., Tsvetkova, I. B., Quinkert, Z. T., Murali, A., De, M., Rotello, V. M., … Dragnea, B. (2010). Role of surface charge density in nanoparticle-templated assembly of bromovirus protein cages. *ACS Nano*, *4*(7), 3853–3860.

Dawood, F. S., Iuliano, A. D., Reed, C., Meltzer, M. I., Shay, D. K., Cheng, P., … Katz, M. A. (2012). Estimated global mortality associated with the first 12 months of 2009 pandemic Influenza A H1N1 virus circulation: A modelling study. *The Lancet Infectious Diseases*, *12*(9), 687–695.

Decuzzi, P., & Ferrari, M. (2006). The adhesive strength of non-spherical particles mediated by specific interactions. *Biomaterials*, *27*(30), 5307–5314.

Decuzzi, P., Godin, B., Tanaka, T., Lee, S. Y., Chiappini, C., Liu, X., & Ferrari, M. (2010). Size and shape effects in the biodistribution of intravascularly injected particles. *Journal of Controlled Release*, *141*(3), 320–327.

Deng, L., Kim, J. R., Chang, T. Z., Zhang, H., Mohan, T., Champion, J. A., & Wang, B. (2017). Protein nanoparticle vaccine based on flagellin carrier fused to influenza conserved epitopes confers full protection against Influenza A virus challenge. *Virology*, *509*, 82–89.

Denis, J., Acosta-Ramirez, E., Zhao, Y., Hamelin, M. E., Koukavica, I., Baz, M., … Leclerc, D. (2008). Development of a universal Influenza A vaccine based on the M2e peptide fused to the Papaya mosaic virus (PapMV) vaccine platform. *Vaccine*, *26*(27–28), 3395–3403.

Denis, J., Majeau, N., Acosta-Ramirez, E., Savard, C., Bedard, M. C., Simard, S., … Leclerc, D. (2007). Immunogenicity ofPpapaya mosaic virus-like particles fused to a Hepatitis C virus epitope: Evidence for the critical function of multimerization. *Virology*, *363*(1), 59–68.

Desai, N. (2012). Challenges in development of nanoparticle-based therapeutics. *The AAPS Journal*, *14*(2), 282–295.

Deyde, V. M., Xu, X., Bright, R. A., Shaw, M., Smith, C. B., Zhang, Y., … Klimov, A. I. (2007). Surveillance of resistance to adamantanes among Influenza A (H3N2) and A (H1N1) viruses isolated worldwide. *The Journal of Infectious Diseases*, *196*, 249–257.

Di Mario, G., Sciaraffia, E., Facchini, M., Gubinelli, F., Soprana, E., Panigada, M., … Castrucci, M. R. (2017). Protective immunity against influenza in HLA-A2 transgenic mice by modified vaccinia virus Ankara vectored vaccines containing internal influenza proteins. *Pathogens and Global Health*, *111*(2), 1–7.

Diebold, S. S., Kaisho, T., Hemmi, H., Akira, S., & Sousa, C. R. (2004). Innate antiviral responses by means of TLR7-mediated recognition of single-stranded RNA. *Science*, *303*(5663), 1529–1531.

Ding, S., Khan, A. I., Cai, X., Song, Y., Lyu, Z., Du, D., … Lin, Y. (2020). Overcoming

blood–brain barrier transport: Advances in nanoparticle-based drug delivery strategies. *Materials Today*, *37*, 112–125.

Dombrovsky, A., Tran-nguyen, L. T. T., & Jones, R. A. C. (2017). Cucumber green mottle mosaic virus: Rapidly increasing global distribution, etiology, epidemiology and management. *Annual Review of Phytopathology*, *55*, 1–26.

Draz, M. S., & Shafiee, H. (2018). Applications of gold nanoparticles in virus detection. *Theranostics*, *8*(7), Article#1985.

Dudhipala, N., & Gorre, T. (2020). Neuroprotective effect of ropinirole lipid nanoparticles enriched hydrogel for parkinson's disease: In vitro, ex vivo, pharmacokinetic and pharmacodynamic evaluation. *Pharmaceutics*, *12*(5), Article#448.

Dunning, J., Baillie, J. K., Cao, B., & Hayden, F. G. (2014). Antiviral combinations for severe influenza. *The Lancet infectious diseases*, *14*(12), 1259-1270.

Durrani, Z., McInerney, T. L., McLain, L., Jones, T., Bellaby, T., Brennan, F. R., & Dimmock, N. J. (1998). Intranasal immunization with a plant virus expressing a peptide from HIV-1 gp41 stimulates better mucosal and systemic HIV-1-specific IgA and IgG than oral immunization. *Journal of Immunological Methods*, *220*(1–2), 93–103.

Ehlerding, E. B., Grodzinski, P., Cai, W., & Liu, C. H. (2018). Big potential from small agents: Nanoparticles for imaging-based companion diagnostics. *ACS Nano*, *12*(3), 2106–2121.

Eiben, S., Koch, C., Altintoprak, K., Southan, A., Tovar, G., Laschat, S., … Wege, C. (2019). Plant virus-based materials for biomedical applications: Trends and prospects. *Advanced Drug Delivery Reviews*, *145*, 96–118.

Eickhoff, C. S., Terry, F. E., Peng, L., Meza, K. A., Sakala, I. G., Van Aartsen, D., … Buller, R. M. (2019). Highly conserved influenza T cell epitopes induce broadly protective immunity. *Vaccine*, *37*(36), 5371–5381.

Eisfeld, A. J., Neumann, G., Kawaoka, Y., & Project, I. H. R. (2015). At the centre: Influenza A virus ribonucleoproteins. *Nature Reviews Microbiology*, *13*(1), 28–41.

Emran, A. (2014). Design of an epitope-based peptide vaccine against spike protein of human coronavirus : An in silico approach. *Drug Design, Development and Therapy*, *8*, 1139–1149.

Esfandiari, N., Arzanani, M. K., & Soleimani, M. (2015). A new application of plant virus nanoparticles as drug delivery in breast cancer. *Tumor Biology*, *37*(1), 1229–1236.

Evans, D. J. (2008). The bionanoscience of plant viruses: Templates and synthons for new materials. *Journal of Materials Chemistry*, *18*(32), 3746–3754.

Everts, M., Saini, V., Leddon, J. L., Kok, R. J., Stoff-khalili, M., Preuss, M. A., … Curiel, D. T. (2006). Covalently linked Au nanoparticles to a viral vector : Potential for combined photothermal and gene cancer therapy. *Nano letters*, *6*(4), 587-591.

Evtushenko, E. A., Ryabchevskaya, E. M., Nikitin, N. A., Atabekov, J. G., & Karpova, O. V. (2020a). Plant virus particles with various shapes as potential adjuvants. *Scientific Reports*, *10*(1), 1–10.

Fernández-Fernández, M. Rosario, Martínez-Torrecuadrada, J. L., Casal, J. I., & García, J. A. (1998). Development of an antigen presentation sytem based on Plum pox

potyvirus. *FEBS Letters*, *427*(2), 229–235.

Fernández-Fernández, M R, Mouriño, M., Rivera, J., Rodríguez, F., Plana-Durán, J., & García, J. a. (2001). Protection of rabbits against Rabbit hemorrhagic disease virus by immunization with the VP60 protein expressed in plants with a potyvirus-based vector. *Virology*, *280*(2), 283–291.

Ferrell, J., Charudattan, R., Elliott, M., & Hiebert, E. (2008). Effects of selected herbicides on the efficacy of Tobacco mild green mosaic virus to control tropical soda apple (Solanum viarum). *Weed Sciene*, *56*, 128–132.

Feynman, R. P. (1961). There's plenty of room at the bottom: An invitation to enter a new field of physics. *Miniaturization, Reinhold*.

Fonseca, J. P., & Mysore, K. S. (2019). Genes involved in nonhost disease resistance as a key to engineer durable resistance in crops. *Plant Science*, *279*, 108–116.

França, R., Zhang, X., Veres, T., Yahia, L. H., & Sacher, E. (2013). Core-shell nanoparticles as prodrugs: Possible cytotoxicological and biomedical impacts of batch-to-batch inconsistencies. *Journal of Colloid Nd Interface Sciences*, *389*, 292–297.

Franconi, R., Di Bonito, P., Dibello, F., Accardi, L., Muller, A., Cirilli, A., … Giorgi, C. (2002). Plant-derived human papillomavirus 16 E7 oncoprotein induces immune response and specific tumor protection. *Cancer Research*, *62*(13), 3654–3658.

Fromen, C. A., Robbins, G. R., Shen, T. W., Kai, M. P., & Ting, J. P. Y. (2015). Controlled analysis of nanoparticle charge on mucosal and systemic antibody responses following pulmonary immunization. *Proceedings of the National Academy of Sciences*, *112*(2), 488–493.

Fujiyama, K., Saejung, W., Yanagihara, I., Nakado, J., Misaki, R., Honda, T., … Seki, T. (2006). In planta production of immunogenic poliovirus peptide using Tobacco mosaic virus-based vector system. *Journal of Bioscience and Bioengineering*, *101*(5), 398–402.

Gallucci, S., & Matzinger, P. (2001). Danger signals: SOS to the immune system. *Current Opinion in Immunology*, *13*(1), 114–119.

Gannagé, M., Schmid, D., Albrecht, R., Dengjel, J., Torossi, T., Rämer, P. C., … Münz, C. (2009). Matrix protein 2 of Influenza A virus blocks autophagosome fusion with lysosomes. *Cell Host & Mirobe*, *6*, 367–380.

Gellért, Á., Salánki, K., Tombácz, K., Tuboly, T., & Balázs, E. (2012). A Cucumber mosaic virus based expression system for the production of porcine circovirus specific vaccines. *PLoS ONE*, *7*(12), 1–10.

Geng, Y., Dalhaimer, P., Cai, S., Tsai, R., Tewari, M., Minko, T., & Discher, D. E. (2007). Shape effects of filaments versus spherical particles in flow and drug delivery. *Nature Nanotechnology*, *2*(4), 249–55.

Gentile, F., Ferrari, M., & Decuzzi, P. (2008). The transport of nanoparticles in blood vessels: The effect of vessel permeability and blood rheology. *Annals of Biomedical Engineering*, *36*(2), 254–261.

Gerhard, W., Haberman, A. N. N. M., Scherle, P. A., Taylor, A. H., Palladino, G., & Caton, A. J. (1991). Identification of eight determinants in the hemagglutinin molecule of Influenza virus A / PRI8 / 34 (HlN1) which are recognized by class II-

restricted T cells from Balb/c mice. *Journal of Virology*, *65*(1), 364–372.

Gibbs, A. J., Wood, J., Garcia-arenal, F., Ohshima, K., & Armstrong, J. S. (2015). Tobamoviruses have probably co-diverged with their eudicotyledonous hosts for at least 110 million years. *Virus Evolution*, *1*(1), 1–9.

Gilleland Jr., H. E., Gilleland, L. B., Staczek, J., Harty, R. N., Garcia-Sastre, A., Engelhardt, O. G., & Palese, P. (2000). Chimeric animal and plant viruses expressing epitopes of outner membranes protein F as a combined vaccine agaisnt Pseudomanas auruginos lung infection. *FEMS Immunology and Medical Micobiology*, *27*, 291–301.

Goldhill, D. H., Te Velthuis, A. J. W., Fletcher, R. A., Langat, P., Zambon, M., Lackenby, A., & Barclay, W. S. (2018). The mechanism of resistance to favipiravir in influenza. *Proceedings of the National Academy of Sciences*, *115*(45), 11613–11618.

Gomez-Puertas, P., Albo, C., Perez-Pastrana, E., Vivo, A., & Portela, A. (2000). Influenza virus matrix protein is the major driving force in virus budding. *Journal of Virology*, *74*(24), 11538–11547.

Gonzalez, M. J., Plummer, E. M., Rae, C. S., & Manchester, M. (2009). Interaction of Cowpea mosaic virus (CPMV) nanoparticles with antigen presenting cells in vitro and in vivo. *PLoS ONE*, *4*(11), Article#e7981.

Gopinath, K., Wellink, J., Porta, C., Taylor, K. M., Lomonossoff, G. P., & van Kammen, A. (2000). Engineering Cowpea mosaic virus RNA-2 into a vector to express heterologous proteins in plants. *Virology*, *267*(2), 159–73.

Goraya, M. U., Wang, S., Munir, M., & Chen, J. (2015). Induction of innate immunity and its perturbation by influenza viruses. *Protein & Cell*, *6*(10), 712-721.

Gould, K. G., Scotney, H., & Brownlee, G. G. (1991). Characterization of two distinct major histocompatibility complex class I Kk-restricted T-cell epitopes within the Influenza A/PR/8/34 virus hemagglutinin. *Journal of Virology*, *65*(10), 5401–5409.

Gulati, N. M., Pitek, A. S., Czapar, A. E., Stewart, P. L., & Steinmetz, N. F. (2018). The in vivo fates of plant viral nanoparticles camouflaged using self-proteins: Overcoming immune recognition. *Journal of Materials Chemistry B*, *6*(15), 2204–2216.

Gupta, N., Regar, H., Verma, V. K., Prusty, D., Mishra, A., & Prajapati, V. K. (2020). Receptor-ligand based molecular interaction to discover adjuvant for immune cell TLRs to develop next-generation vaccine. *International Journal of Biological Macromolecules*, *152*, 535–545.

Haase, G., Kennel, P., Pettmann, B., Vigne, E., Akli, S., Revah, F., … Kahn, A. (1997). Gene therapy of murine motor neuron disease using adenoviral vectors for neurotrophic factors. *Nature Medicine*, *3*(4), 429–436.

Hajipour, M. J., Fromm, K. M., Ashkarran, A. A., de Aberasturi, D. J., de Larramendi, I. R., Rojo, T., ... & Mahmoudi, M. (2012). Antibacterial properties of nanoparticles. *Trends in Biotechnology*, *30*(10), 499–511.

Hale, B. G., Randall, R. E., Ortin, J., & Jackson, D. (2008). The multifunctional NS1 protein of Influenza A viruses. *Journal of General Virology, 89*(10), 2359–2376.

Halstead, E. S., Mueller, Y. M., Altman, J. D., & Katsikis, P. D. (2002). In vivo stimulation of CD137 broadens primary antiviral CD8 + T cell responses. *Nature*

Immunology, *3*(6), 536–541.

Hanafi, L. A., Bolduc, M., Gagné, M. È. L., Dufour, F., Langelier, Y., Boulassel, M. R., … Lapointe, R. (2010). Two distinct chimeric potexviruses share antigenic cross-presentation properties of MHC class I epitopes. *Vaccine*, *28*(34), 5617–5626.

Hause, B. M., Collin, E. A., Liu, R., Huang, B., Sheng, Z., Lu, W., ... & Li, F. (2014). Characterization of a novel influenza virus in cattle and swine: Proposal for a new genus in the Orthomyxoviridae family. *MBio*, *5*(2), Article#e00031-14.

Hayden, F. G., & Jong, M. D. (2011). Emerging influenza antiviral resistance threats. *Journal of Infectious Diseases*, *203*(1), 6-10.

Hayward, A. C. (2017). Influenza vaccination of healthcare workers is an important approach for reducing transmission of influenza from staff to vulnerable patients. *PLoS ONE*, *12*, Article#e0169023.

Hefferon, K. (2017). Plant virus expression vectors: A powerhouse for global health. *Biomedicines*, *5*(3), Article#44.

Heil, F., Hemmi, H., Hochrein, H., Ampenberger, F., Kirschning, C., Akira, S., … Bauer, S. (2004). Species-specific recognition of single-stranded RNA via toll-like receptor 7 and 8. *Science*, *303*(5663), 1526–1529.

Held, G., Luescher, I. F., Neumann, F., Papaioannou, C., Schirrmann, T., Sester, M., … Pfreundschuh, M. (2015). MHC/peptide-specific interaction of the humoral immune system: A new category of antibodies. *The Journal of Immunology*, *195*(9), 4210–4217.

Hess, J. A., Zhan, B., Torigian, A. R., Patton, J. B., Petrovsky, N., Zhan, T., … Lustigman, S. (2016). The immunomodulatory role of adjuvants in vaccines formulated with the recombinant antigens Ov-103 and Ov-RAL-2 against Onchocerca volvulus in mice. *PLoS Neglected Tropical Diseases*, *10*(7), Article#e0004797.

Hessel, A., Savidis-Dacho, H., Coulibaly, S., Portsmouth, D., Kreil, T. R., Crowe, B. A., … Falkner, F. G. (2014). MVA vectors expressing conserved influenza proteins protect mice against lethal challenge with H5N1, H9N2 and H7N1 viruses. *PloS ONE*, *9*(2), Article#e88340.

Horváth, A., Tóth, G. K., Gogolák, P., Nagy, Z., Kurucz, I., Pecht, I., & Rajnavölgyi, É. (1998). A hemagglutinin-based multipeptide construct elicits enhanced protective immune response in mice against Influenza A virus infection. *Immunology Letters*, *60*(2–3), 127–136.

Hsu, C. H., Lin, S. S., Liu, F. L., Su, W. C., & Yeh, S. D. (2004). Oral administration of a mite allergen expressed by Zucchini yellow mosaic virus in cucurbit species downregulates allergen-induced airway inflammation and IgE synthesis. *Journal of Allergy and Clinical Immunology*, *113*(6), 1079–1085.

Hu, J., Li, S., Li, Z., Li, H., Song, W., Zhao, H., … Zhang, Y. (2019). A Barley stripe mosaic virus-based guide RNA delivery system for targeted mutagenesis in wheat and maize. *Molecular Plant Pathology*, *20*(10), 1463–1474.

Huang, X., Zhu, J., & Yang, Y. (2005). Protection against autoimmunity in nonlymphopenic hosts by CD4+ CD25+ regulatory T cells is antigen-specific and requires IL-10 and TGF-β. *The Journal of Immunology*, *175*(7), 4283–4291.

Hulo, C., De Castro, E., Masson, P., Bougueleret, L., Bairoch, A., Xenarios, I., & Le

Mercier, P. (2011). ViralZone: a knowledge resource to understand virus diversity. *Nucleic acids research*, *39*(suppl_1), D576-D582.

Humphrey, W., Dalke, A., & Schulten, K. (1996). VMD: visual molecular dynamics. *Journal of Molecular Graphics*, *14*(1), 33–38.

Hyung, J., Kwon, S., Lee, M., Chung, H., Kim, J., Kim, Y., … Young, S. (2006). Self-assembled nanoparticles based on glycol chitosan bearing hydrophobic moieties as carriers for doxorubicin: In vivo biodistribution and anti-tumor activity. *Biomaterials*, *27*, 119–126.

Irvine, D. J., Swartz, M. A., & Szeto, G. L. (2013). Engineering synthetic vaccines using cues from natural immunity. *Nature Materials*, *12*(11), 978–990.

Ishibashi, K., Naito, S., Meshi, T., & Ishikawa, M. (2009). An inhibitory interaction between viral and cellular proteins underlies the resistance of tomato to non adapted tobamoviruses. *Proceedings of the National Academy of Sciences*, *106*(21), 8778–8783.

Jailani, A. A. K., Solanki, V., Roy, A., Sivasudha, T., & Mandal, B. (2017). A CGMMV genome-replicon vector with partial sequences of coat protein gene efficiently expresses GFP in Nicotiana benthamiana. *Virus Research*, *233*, 77–85.

Jain, V., Kumar, H., Anod, H. V, Chand, P., Gupta, N. V., Dey, S., & Kesharwani, S. S. (2020). A review of nanotechnology-based approaches for breast cancer and triple-negative breast cancer. *Journal of Controlled Release*, *326*, 628-647.

Jaubert, M., Bhattacharjee, S., Mello, A. F. S., Perry, K. L., & Moffett, P. (2011). ARGONAUTE2 mediates RNA-silencing antiviral defenses against Potato virus X in Arabidopsis. *Plant Physiology*, *156*(3), 1556–1564.

Jeevanandam, J., Pal, K., & Danquah, M. K. (2019). Virus-like nanoparticles as a novel delivery tool in gene therapy. *Biochimie*, *157*, 38–47.

Jensen, S., & Thomsen, A. R. (2012). Sensing of RNA viruses: A review of innate immune receptors involved in recognizing RNA virus invasion. *Journal of Virology*, *86*(6), 2900–2910.

Jia, D., Rahbar, R., Chan, R. W. Y., Lee, S. M. Y., Chan, M. C. W., Xuhao, B., … Fish, E. N. (2010). Influenza virus non-structural protein 1 (NS1) disrupts interferon signaling. *PLoS ONE*, *5*(11), Article#e13927.

Jiang, L., Li, Q., Li, M., Zhou, Z., Wu, L., Fan, J., … Xu, Z. (2006). A modified TMV-based vector facilitates the expression of longer foreign epitopes in tobacco. *Vaccine*, *24*(2), 109–115.

JináLee, S., MináSeok, J., HeeáLee, J., DooáKim, W., KeunáKwon, I., & AáPark, S. (2018). In situ gold nanoparticle growth on polydopamine-coated 3D-printed scaffolds improves osteogenic differentiation for bone tissue engineering applications: In vitro and in vivo studies. *Nanoscale*, *10*(33), 15447–15453.

Joelson, T., Åkerblom, L., Oxelfelt, P., Strandberg, B., Tomenius, K., & Morris, T. J. (1997). Presentation of a foreign peptide on the surface of Tomato bushy stunt virus. *Journal of General Virology*, *78*(6), 1213–1217.

Jones, R. M., Chichester, J. A., Manceva, S., Gibbs, S. K., Musiychuk, K., Shamloul, M., … Yusibov, V. (2015). A novel plant-produced Pfs25 fusion subunit vaccine induces long-lasting transmission blocking antibody responses. *Human Vaccines &*

Immunotherapeutics, *11*(1), 124–132.

Jones, R. M., Chichester, J. A., Mett, V., Jaje, J., Tottey, S., Manceva, S., … Yusibov, V. (2013). A plant-produced Pfs25 VLP malaria vaccine candidate induces persistent transmission blocking antibodies against Plasmodium falciparum in immunized mice. *PLoS ONE*, *8*(11), Article#e79538

Jordan, A., Scholz, R., Maier-Hauff, K., van Landeghem, F. K., Waldoefner, N., Teichgraeber, U., ... Felix, R. (2006). The effect of thermotherapy using magnetic nanoparticles on rat malignant glioma. *Journal of Neuro-Oncology*, *78*, 7–14.

Jung, H. E., & Lee, H. K. (2020). Host protective immune responses against Influenza A virus infection. *Viruses*, *12*(5), Article#504.

Kaiser, C. R., Flenniken, M. L., Gillitzer, E., Harmsen, A. L., Harmsen, A. G., Jutila, M. A., … Young, M. J. (2007). Biodistribution studies of protein cage nanoparticles demonstrate broad tissue distribution and rapid clearance in vivo. *International Journal of Nanomedicine*, *2*(4), 715–733.

Kaisho, T., & Akira, S. (2006). Toll-like receptor function and signaling. *Journal of Allergy and Clinical Immunology*, *117*(5), 979–987.

Kalyane, D., Raval, N., Maheshwari, R., Tambe, V., Kalia, K., & Tekade, R. K. (2019). Employment of enhanced permeability and retention effect (EPR): Nanoparticle-based precision tools for targeting of therapeutic and diagnostic agent in cancer. *Materials Science and Engineering: C*, *98*, 1252–1276.

Kametani, Y., Miyamoto, A., Tsuda, B., & Tokuda, Y. (2015). B Cell Epitope-based vaccination therapy. *Antibodies*, *4*, 225–239.

Karagoz, S., Kiremitler, N. B., Sarp, G., Pekdemir, S., Salem, S., Goksu, A. G., … Ozkara, E. S. (2021). Antibacterial, antiviral, and self-cleaning mats with sensing capabilities based on electrospun nanofibers decorated with ZnO nanorods and Ag nanoparticles for protective clothing applications. *ACS Applied Materials & Interfaces*, *13*(4), 5678–5690.

Karasev, A. V., Foulke, S., Wellens, C., Rich, A., Shon, K. J., Zwierzynski, I., … Reitz, M. (2005). Plant based HIV-1 vaccine candidate: Tat protein produced in spinach. *Vaccine*, *23*(15), 1875–1880.

Kawai, T., & Akira, S. (2010). The role of pattern-recognition receptors in innate immunity: update on Toll-like receptors. *Nature Immunology*, *11*(5), 373–84.

Kawasaki, T., & Kawai, T. (2014). Toll-like receptor signaling pathways. *Frontiers in Immunology*, *5*, Article#461.

Kerstetter-Fogle, A., Shukla, S., Wang, C., Beiss, V., Harris, P. L. R., Sloan, A. E., & Steinmetz, N. F. (2019). Plant virus-like particle in situ vaccine for intracranial glioma immunotherapy. *Cancers*, *11*(4), Article#515.

Khan, I., Saeed, K., & Khan, I. (2019). Nanoparticles: Properties, applications and toxicities. *Arabian Journal of Chemistry*, *12*, 908–931.

Khandelwal, N., Kaur, G., Kumar, N., Tiwari, A., Gandhi, R., & Vishwavidyalaya, P. (2014). Application of silver nanoparticles in viral inhibition: A new hope for antivirals. *Digest Journal of Nanomaterials and Biostructures*, *9*(1), 175–186.

Khlebtsov, N., & Dykman, L. (2011). Biodistribution and toxicity of engineered gold nanoparticles: a review of *in vitro* and *in vivo* studies. *Chemical Society Reviews*,

40(3), 1647–1671.

Khor, C., Sam, I., Hooi, P., Quek, K., & Chan, Y. (2012). Epidemiology and seasonality of respiratory viral infections in hospitalized children in Kuala Lumpur, Malaysia: A retrospective study of 27 years. *BMC Pediatrics*, *12*(1), Article#32.

Kim, J. K., Cheong, S., & Lee, M. K. (2019). Evaluation of protective immunity of peptide vaccines composed of a 15-mer N-terminal matrix protein 2 and a helper T-cell epitope derived from Influenza A virus. *Immune Network*, *19*(4).

Kim, M. ., Na, H. ., Kim, Y. ., Ryoo, S. ., Cho, H. ., Lee, K. ., … Min, D. (2011). Facile synthesis of monodispersed mesoporous silica nanoparticles with ultralarge pores and their application in gene delivery. *ACS Nano*, *5*(5), 3568–3576.

King, A. M., Lefkowitz, E., Adams, M. J., & Carstens, E. B. (Eds.). (2011). *Virus taxonomy: Ninth report of the International Committee on Taxonomy of Viruses* (Vol. 9). Elsevier.

Kirtane, A. R., Verma, M., Karandikar, P., Furin, J., Langer, R., & Traverso, G. (2021). Nanotechnology approaches for global infectious diseases. *Nature Nanotechnology*, *16*(4), 369–384.

Klem, M. T., Willits, D., Young, M., & Douglas, T. (2003). 2-D Array formation of genetically engineered viral cages on Au surfaces and imaging by atomic force microscopy. *Journal of American Chemical Society*, *125*, 10806–10807.

Konstantin, B. O., Yoko, M., Jessica, S., & Alpuche-solı, G. (2015). Engineering and expression of a RhoA peptide against respiratory syncytial virus infection in plants. *Planta*, *243*(2), 451–458.

Koo, M., Bendahmane, M., Lettieri, G. A., Paoletti, A. D., Lane, T. E., Fitchen, J. H., ... & Beachy, R. N. (1999). Protective immunity against Murine hepatitis virus (MHV) induced by intranasal or subcutaneous administration of hybrids of Tobacco mosaic virus that carries an MHV epitope. *Proceedings of the National Academy of Sciences*, *96*(14), 7774–7779.

Kumar, P., Mahajan, P., Kaur, R., & Gautam, S. (2020). Nanotechnology and its challenges in the food sector: A review. *Materials Today Chemistry*, *17*, Article#100332.

Kumar, S., Ochoa, W., Singh, P., Hsu, C., Schneemann, A., Manchester, M., … Reddy, V. (2009). Tomato bushy stunt virus (TBSV), a versatile platform for polyvalent display of antigenic epitopes and vaccine design. *Virology*, *388*(1), 185–190.

Kumari, S., Tyagi, M., & Jagadevan, S. (2019). Mechanistic removal of environmental contaminants using biogenic nano-materials. *International Journal of Environmental Science and Technology*, *16*(11), 7591–7606.

Kushnir, N., Streatfield, S. J., & Yusibov, V. (2012). Virus-like particles as a highly efficient vaccine platform: Diversity of targets and production systems and advances in clinical development. *Vaccine*, *31*(1), 58–83.

Kusov, Y., Gauss-Müller, V., & Morace, G. (2007). Immunogenic epitopes on the surface of the Hepatitis A virus capsid: Impact of secondary structure and/or isoelectric point on chimeric virus assembly. *Virus Research*, *130*(1–2), 296–302.

La-Beck, N. M., & Gabizon, A. A. (2017). Nanoparticle interactions with the immune system: Clinical implications for liposome-based cancer chemotherapy. *Frontiers in*

Immunology, *8*, Article#416.

Laliberté-Gagné, M. È., Bolduc, M., Thérien, A., Garneau, C., Casault, P., Savard, P., … Leclerc, D. (2019). Increased immunogenicity of full-length protein antigens through sortase-mediated coupling on the PapMV vaccine platform. *Vaccines*, *7*(2), Article#49.

Lam, P., & Steinmetz, N. F. (2019). Delivery of siRNA therapeutics using Cowpea chlorotic mottle virus-like particles. *Biomaterials Science*, *7*(8), 3138–3142.

Langeveld, J. P. M., Brennan, F. R., Martínez-Torrecuadrada, J. L., Jones, T. D., Boshuizen, R. S., Vela, C., … Hamilton, W. D. O. (2001). Inactivated recombinant plant virus protects dogs from a lethal challenge with canine parvovirus. *Vaccine*, *19*(27), 3661–3670.

Laskowski, R. A., MacArthur, M. W., Moss, D. S., & Thornton, J. M. (1993). PROCHECK: a program to check the stereochemical quality of protein structures. *Journal of Applied Crystallography*, *26*(2), 283–291.

Lavelle, L., Gingery, M., Phillips, M., Gelbart, W. M., Knobler, C. M., & Obrego, A. V. (2009). Phase diagram of self-assembled viral capsid protein polymorphs. *Journal of Physical Chemistry B*, *113*, 3813–3819.

Le, D. H. T., Hu, H., Commandeur, U., & Steinmetz, N. F. (2017). Chemical addressability of Potato virus X for its applications in bio/nanotechnology. *Journal of Structural Biology*, *200*(3), 360–368.

Le, D. H. T., Méndez-L pez, E., Wang, C., Commandeur, U., Aranda, M. A., & Steinmetz, N. F. (2019). Biodistribution of filamentous plant virus nanoparticles: Pepino mosaic virus versus Potato virus X. *Biomacromolecules*, *20*(1), 469–477.

Lebel, M. È., Daudelin, J. F., Chartrand, K., Tarrab, E., Kalinke, U., Savard, P., … Lamarre, A. (2014). Nanoparticle adjuvant sensing by TLR7 enhances CD8+ T cell-mediated protection from Listeria monocytogenes infection. *The Journal of Immunology*, *192*(3), 1071–1078.

Lebel, M. È., Chartrand, K., Tarrab, E., Savard, P., Leclerc, D., & Lamarre, A. (2016). Potentiating cancer immunotherapy using Papaya mosaic virus-derived nanoparticles. *Nano Letters*, *16*(3), 1826–1832.

Leclerc, D., Beauseigle, D., Denis, J., Morin, H., Paré, C., Lamarre, A., & Lapointe, R. (2007). Proteasome-independent major histocompatibility complex class I cross-presentation mediated by papaya mosaic virus-like particles leads to expansion of specific human T cells. *Journal of Virology*, *81*(3), 1319–1326.

Leclerc, D., Rivest, M., Babin, C., López-Macias, C., & Savard, P. (2013). A novel M2e based flu vaccine formulation for dogs. *PLoS One*, *8*(10), Article#e77084.

Lee, K. L., Murray, A. A., Le, D. H. T., Sheen, M. R., Shukla, S., Commandeur, U., … Steinmetz, N. F. (2017). Combination of plant virus nanoparticle-based in situ vaccination with chemotherapy potentiates antitumor response. *Nano Leters*, *17*, 4019–4028.

Lee, K. L., Shukla, S., Wu, M., Ayat, N. R., El Sanadi, C. E., Wen, A. M., … Dubyak, G. R. (2015). Stealth filaments: Polymer chain length and conformation affect the in vivo fate of PEGylated Potato virus X. *Acta Biomaterialia*, *19*, 166–179.

Lee, K. L., Uhde-Holzem, K., Fischer, R., Commandeur, U., & Steinmetz, N. F. (2014).

Genetic engineering and chemical conjugation of Potato virus X. In *Virus Hybrids as Nanomaterials* (pp. 3-21). Humana Press, Totowa, NJ.

Lee, N., & Ison, M. G. (2012). Diagnosis , management and outcomes of adults hospitalized with influenza. *Antiviral Therapy*, *17*, 143–157.

Lee, S. Y., Ferrari, M., & Decuzzi, P. (2009). Design of bio-mimetic particles with enhanced vascular interaction. *Journal of Biomechanics*, *42*(12), 1885–1890.

Lee, Y., Kim, K., Ko, E., Lee, Y., Kim, M., Kwon, Y., … Cho, M. (2014). New vaccines against influenza virus. *Clinical and Experimental Vaccine Research*, *3*, 12–28.

Léonard, S., Plante, D., Wittmann, S., Daigneault, N., Fortin, M. G., & Laliberté, J. F. (2000). Complex formation between potyvirus VPg and translation eukaryotic initiation factor 4E correlates with virus infectivity. *Journal of Virology*, *74*(17), 7730–7737.

Li, Q., Jiang, L., Li, M., Li, P., Zhang, Q., Song, R., & Xu, Z. (2007). Morphology and stability changes of recombinant TMV particles caused by a cysteine residue in the foreign peptide fused to the coat protein. *Journal of Virological Methods*, *140*(1–2), 212–217.

Li, S. D., & Huang, L. (2008). Pharmacokinetics and biodistribution of nanoparticles. *Molecular Pharmaceutics*, *5*(4), 496–504.

Li, T. C. M., Chan, M. C. W., & Lee, N. (2015). Clinical implications of antiviral resistance in influenza. *Viruses*, *7*, 4929–4944.

Lico, C., Capuano, F., Renzone, G., Donini, M., Marusic, C., Scaloni, A., … Baschieri, S. (2006). Peptide display on Potato virus X: molecular features of the coat protein-fused peptide affecting cell-to-cell and phloem movement of chimeric virus particles. *Journal of General Virology*, *87*(10), 3103–3112.

Lico, C., Giardullo, P., Mancuso, M., Benvenuto, E., Santi, L., & Baschieri, S. (2016). A biodistribution study of two differently shaped plant virus nanoparticles reveals new peculiar traits. *Colloids and Surfaces B: Biointerfaces*, *148*, 431–439.

Lico, C., Mancini, C., Italiani, P., Betti, C., Boraschi, D., Benvenuto, E., & Baschieri, S. (2009). Plant-produced Potato virus X chimeric particles displaying an influenza virus-derived peptide activate specific CD8+ T cells in mice. *Vaccine*, *27*(37), 5069–5076.

Liepold, L. O., Revis, J., Allen, M., Oltrogge, L., Young, M., & Douglas, T. (2005). Structural transitions in Cowpea chlorotic mottle virus (CCMV). *Physical Biology*, *2*(4), S166–S172.

Lin, T., & Johnson, J. E. (2003). Structures of picorna-like plant viruses: Implications and applications. *Advances in Virus Research*, *62*, 167–241.

Liu, C., & Nelson, R. S. (2013). The cell biology of Tobacco mosaic virus replication and movement. *Frontiers in Plant Science*, *4*, Article#12.

Liu, H., Qu, C., Johnson, J. E., & Case, D. A. (2003). Pseudo-atomic models of swollen CCMV from cryo-electron microscopy data. *Journal of Structural Biology*, *142*, 356–363.

Liu, M., Liang, Z., Aranda, M. A., Hong, N., Liu, L., Kang, B., & Gu, Q. (2020). A Cucumber green mottle mosaic virus vector for virus-induced gene silencing in cucurbit plants. *Plant Methods*, *16*(1), 1-13.

Liu, X., Wu, F., Tian, Y., Wu, M., Zhou, Q., Jiang, S., & Niu, Z. (2016). Size dependent cellular uptake of rod-like bionanoparticles with different aspect ratios. *Scientific Reports*, *6*(1), 1–10.

Liu, Y., Lin, C., & Hong, H. (2017a). In silico design , synthesis and potency of an epitope-based vaccine against Foot-and-mouth disease virus. *International Journal of Pharmacology*, *13*(2), 122–133.

Liu, Y., Hardie, J., Zhang, X., & Rotello, V. (2017b). Effects of engineered nanoparticles on the innate immune system. In *Seminars in immunology* (Vol. 34, pp. 25-32). Academic Press.

Liu, Z., Qiao, J., Niu, Z., & Wang, Q. (2012). Natural supramolecular building blocks: From virus coat proteins to viral nanoparticles. *Chemical Society Reviews*, *41*(18), 6178–6194.

Lobert, S., Heil, P.D., Namba, K., & Stubbs, G. (1987). Preliminary X-ray fiber diffraction studies of cucumber green mottle mosaic virus, watermelon strain. *Journal of Molecular Biology*, *196*(4), 935–938.

Longmire, M., Choyke, P. L., & Kobayashi, H. (2008). Clearance properties of nano-sized particles and molecules as imaging agents: Considerations and caveats. *Nanomedicine*, *3*(5), 703–17.

Look, M., Bandyopadhyay, A., Blum, J. S., & Fahmy, T. M. (2010). Application of nanotechnologies for improved immune response against infectious disease in the developing world. *Advanced Drug Delivery Reviews*, *62*(4–5), 378–393.

Lorenz, R., Bernhart, S. H., Höner, C., Tafer, H., & Flamm, C. (2011). ViennaRNA Package 2.0. *Algorithms for Molecular Biology*, *6*(26), 1–14.

Lund, J. M., Alexopoulou, L., Sato, A., Karow, M., Adams, N. C., Gale, N. W., … Flavell, R. A. (2004). Recognition of single-stranded RNA viruses by Toll-like receptor 7. *Proceedings of the National Academy of Sciences*, *101*(15), 5598–5603.

Lunov, O., Syrovets, T., Loos, C., Beil, J., Delacher, M., Tron, K., … Simmet, T. (2011). Differential uptake of functionalized polystyrene nanoparticles by human macrophages and a monocytic cell line. *ACS Nano*, *5*(3), 1657–1669.

Lux, F., Tran, V. L., Thomas, E., Dufort, S., Rossetti, F., Martini, M., … Denat, F. (2019). AGuIX® from bench to bedside - Transfer of an ultrasmall theranostic gadolinium-based nanoparticle to clinical medicine. *The British Journal of Radiology*, *92*(1093),Article#,20180365.

Ma, W., García-sastre, A., & Schwemmle, M. (2015). Expected and unexpected features of the newly discovered bat Influenza A-like viruses. *PLoS Pathogens*, *11*(6), Article#e1004819.

Madden, A. J., Oberhardt, B., Lockney, D., Santos, C., Vennam, P., Arney, D., … Gehrig, P. (2017). Pharmacokinetics and efficacy of doxorubicin-loaded plant virus nanoparticles in preclinical models of cancer. *Nanomedicine*, *12*(20), 2519–2532.

Maier, H. J., Kashiwagi, T., Hara, K., & Brownlee, G. G. (2008). Differential role of the Influenza A virus polymerase PA subunit for vRNA and cRNA promoter binding. *Virology*, *370*, 194–204.

Maldiney, T., Richard, C., Seguin, J., Wattier, N., Bessodes, M., & Scherman, D. (2011). Effect of core diameter , surface coating , and PEG chain length on the

biodistribution of persistent luminescence nanoparticles in mice. *ACS Nano*, *5*(2), 854–862.

Mallajosyula, J. K., Hiatt, E., Hume, S., Johnson, A., Jeevan, T., Chikwamba, R., … Mccormick, A. A. (2014). Single-dose monomeric HA subunit vaccine generates full protection from influenza challenge. *Human vaccines & immunotherapeutics*, *10*(3), 586-595.

Mansour, A. A., Banik, S., Suresh, R. V, Kaur, H., Malik, M., McCormick, A. A., & Bakshi, C. S. (2018). An improved tobacco mosaic virus (TMV)-conjugated multiantigen subunit vaccine against respiratory tularemia. *Frontiers in Microbiology*, *9*, Article#1195.

Marconi, G., Albertini, E., Barone, P., De Marchis, F., Lico, C., Marusic, C., … Porceddu, A. (2006). In planta production of two peptides of the Classical swine fever virus (CSFV) E2 glycoprotein fused to the coat protein of Potato virus X. *BMC Biotechnology*, *6*, Article#29.

Mardanova, E. S., Kotlyarov, R. Y., Kuprianov, V. V, Stepanova, L. A., Tsybalova, L. M., Lomonosoff, G. P., & Ravin, N. V. (2015). Rapid high-yield expression of a candidate influenza vaccine based on the ectodomain of M2 protein linked to flagellin in plants using viral vectors. *BMC Biotechnology*, *15*(42), 1–10.

Marusic, C., Rizza, P., Lattanzi, L., Mancini, C., Spada, M., Belardelli, F., … Capone, I. (2001). Chimeric plant virus particles as immunogens for inducing murine and human immune responses against Human immunodeficiency virus type I. *Journal of Virology*, *75*(18), 8434–8439.

Matrosovich, M. N., Matrosovich, T. Y., Gray, T., Roberts, N. A., & Klenk, H. (2004). Neuraminidase is important for the initiation of influenza virus infection in human airway epithelium. *Journal of Virology*, *78*(22), 12665–12667.

Matzinger, P. (1994). Tolerance, danger, and the extended family. *Annual Review of Immunology*, *12*(1), 991–1045.

McCormick, A. A., Corbo, T. A., Wykoff-Clary, S., Nguyen, L. V., Smith, M. L., Palmer, K. E., & Pogue, G. P. (2006a). TMV-peptide fusion vaccines induce cell-mediated immune responses and tumor protection in two murine models. *Vaccine*, *24*(40–41), 6414–6423.

McCormick, A. A., Corbo, T. A., Wykoff-Clary, S., Palmer, K. E., & Pogue, G. P. (2006b). Chemical conjugate TMV-Peptide bivalent fusion vaccines improve cellular immunity and tumor protection. *Bioconjugate Chemistry*, *17*(5), 1330–1338.

McLennan, D. N., Porter, C. J. H., & Charman, S. A. (2005). Subcutaneous drug delivery and the role of the lymphatics. *Drug Discovery Today: Technologies*, *2*(1), 89–96.

Medhi, R., Srinoi, P., Ngo, N., Tran, H.-V., & Lee, T. R. (2020). Nanoparticle-based strategies to combat COVID-19. *ACS Applied Nano Materials*, *3*(9), 8557–8580.

Mehla, K., & Ramana, J. (2016). Identification of epitope-based peptide vaccine candidates against enterotoxigenic Escherichia coli: A comparative genomics and immunoinformatics approach. *Molecular Biosystems*, *12*(3), 890–901.

Melchjorsen, J., Jensen, S. B., Malmgaard, L., Rasmussen, S. B., Weber, F., Bowie, A. G., … Paludan, S. R. (2005). Activation of innate defense against a paramyxovirus is mediated by RIG-I and TLR7 and TLR8 in a cell-type-specific manner. *Journal*

of Virology, *79*(20), 12944–12951.

Mennini, F. S., Bini, C., Marcellusi, A., Rinaldi, A., & Franco, E. (2018). Cost-effectiveness of switching from trivalent to quadrivalent inactivated influenza vaccines for the at-risk population in Italy. *Human Vaccines & Immunotherapeutics*, *14*(8), 1867–1873.

Metavarayuth, K., Sitasuwan, P., Luckanagul, J.A., Feng, S., & Wang, Q. (2015). Virus nanoparticles mediated osteogenic differentiation of bone derived mesenchymal stem cells. *Advanced Science*, *2*(10), Article#1500026.

Metlay, J., Atlas, S. J., & Singer, D. (1998). Time course of symptom resolution pneumonia in patients with community-acquire pneumonia. *Respiratory Medicine*, *92*, 1137–1142.

Meyer, I. De, Martinet, W., & Schrijvers, D. M. (2012). Toll-like receptor 7 stimulation by imiquimod induces macrophage autophagy and inflammation in atherosclerotic plaques. *Basic research in cardiology*, *107*(3), 1-13.

Miller, R. A., Presley, A. D., & Francis, M. B. (2007). Self-assembling light-harvesting systems from synthetically modified Tobacco mosaic virus coat proteins. *Journal of American Chemical Society*, *129*, 3104–3109.

Milligan, G. N., Morrison, L. A., Gorka, J., Braciale, V. L., & Braciale, T. J. (1990). The recognition of a viral antigenic moiety by class I MHC-restricted cytolytic T lymphocytes is limited by the availability of the endogenously processed antigen. *The Journal of Immunology*, *145*(10), 3188–3193.

Mitchell, M. J., Billingsley, M. M., Haley, R. M., Wechsler, M. E., Peppas, N. A., & Langer, R. (2021). Engineering precision nanoparticles for drug delivery. *Nature Reviews Drug Discovery*, *20*(2), 101–124.

Modelska, A, Dietzschold, B., Sleysh, N., Fu, Z. F., Steplewski, K., Hooper, D. C., … Yusibov, V. (1998). Immunization against rabies with plant-derived antigen. *Proceedings of the National Academy of Sciences*, *95*(5), 2481–2485.

Mohsen, M. O., Heath, M. D., Cabral-Miranda, G., Lipp, C., Zeltins, A., Sande, M., … Zha, L. (2019). Vaccination with nanoparticles combined with micro-adjuvants protects against cancer. *Journal for Immunotherapy of Cancer*, *7*(1), 1–12.

Moore, L., Gatica, M., Kim, H., Osawa, E., Ho, D., & Bone, N. P. (2013). Multi-protein Delivery by nanodiamonds promotes bone formation. *Journal of Dental Research*, *92*(11), 976–981.

Mulder, A., Eijsink, C., Kester, M. G. D., Franke, M. E. I., Kardol, M. J., Heemskerk, M. H. M., … Koning, F. (2005). Impact of peptides on the recognition of HLA class I molecules by human HLA antibodies. *The Journal of Immunology*, *175*(9), 5950–5957.

Murray, A. A., Wang, C., Fiering, S., Steinmetz, N. F., & States, U. (2018). In Situ vaccination with Cowpea vs Tobacco mosaic virus against melanoma. *Molecular pharmaceutics*, *15*(9), 3700-3716.

Narayanan, K. B., & Han, S. S. (2017). Icosahedral plant viral nanoparticles-bioinspired synthesis of nanomaterials/nanostructures. *Advances in Colloid and Interface Science*, *248*, 1–19.

Natilla, A., Hammond, R. W., & Nemchinov, L. G. (2006). Epitope presentation system

based on Cucumber mosaic virus coat protein expressed from a Potato virus X-based vector. *Archives of Virology*, *151*(7), 1373–1386.

Natilla, A., Piazzolla, G., Nuzzaci, M., Saldarelli, P., Tortorella, C., Antonaci, S., & Piazzolla, P. (2004). Cucumber mosaic virus as carrier of a Hepatitis C virus-derived epitope. *Archives of Virology*, *149*(1), 137–154.

Natilla, A., & Nemchinov, L. G. (2008). Improvement of PVX/CMV CP expression tool for display of short foreign antigens. *Protein Expression and Purification*, *59*(1), 117–121.

Nemchinov, L. G., Liang, T. J., Rifaat, M. M., Mazyad, H. M., Hadidi, A., & Keith, J. M. (2000). Development of a plant-derived subunit vaccine candidate against Hepatitis C virus. *Archives of virology*, *145*(12), 2557-2573.

Nguyen, H. D., & Iii, C. L. B. (2008). Generalized structural polymorphism in self-assembled viral particles. *Nano Letters*, *8*(12), 4574–4581.

Nguyen, H. D., Reddy, V. S., Iii, C. L. B., Uni, N., V, V. A., Uni, V., & Arbor, A. (2009). Invariant polymorphism in virus capsid assembly. *Journal of American Chemical Society*, *131*, 2606–2614.

Nicholas, B. L., Brennan, F. R., Martinez-Torrecuadrada, J. L., Casal, J. I., Hamilton, W. D., & Wakelin, D. (2002). Characterization of the immune response to Canine parvovirus induced by vaccination with chimaeric plant viruses. *Vaccine*, *20*(21–22), 2727–2734.

Nichols, M. E. K., Stanislaus, T., Keshavarz-moore, E., & Young, H. A. (2002). Disruption of leaves and initial extraction of wildtype CPMV virus as a basis for producing vaccines from plants. *Journal of Biotechnology*, *92*, 229–235.

Niehl, A., Appaix, F., Boscá, S., van der Sanden, B., Nicoud, J.-F., Bolze, F., & Heinlein, M. (2016a). Fluorescent Tobacco mosaic virus-derived bio-nanoparticles for intravital two-photon imaging. *Frontiers in Plant Science*, *6*, 1244.

Niehl, A., Wyrsch, I., Boller, T., & Heinlein, M. (2016b). Double-stranded RNA s induce a pattern-triggered immune signaling pathway in plants. *New Phytologist*, *211*(3), 1008–1019.

Nieto, C., Rodríguez-Moreno, L., Rodríguez-Hernández, A. M., Aranda, M. A., & Truniger, V. (2011). Nicotiana benthamiana resistance to non-adapted Melon necrotic spot virus results from an incompatible interaction between virus RNA and translation initiation factor 4E. *The Plant Journal*, *66*(3), 492–501.

Nikitin, N. A., Trifonova, E. A., Karpova, O. V, & Atabekov, J. G. (2016). Biosafety of plant viruses for human and animals. *Moscow University Biological Sciences Bulletin*, *71*(3), 128–134.

Nikitin, N. A., Zenin, V. A., Trifonova, E. A., Ryabchevskaya, E. M., Kondakova, O. A., Fedorov, A. N., … Karpova, O. V. (2018). Assessment of structurally modified plant virus as a novel adjuvant in toxicity studies. *Regulatory Toxicology and Pharmacology*, *97*, 127–133.

Nikitin, N.A., Ksenofontov, A., Trifonova, E., Arkhipenko, M., Petrova, E., Kondakova, O., … Karpova, O. (2016). Thermal conversion of filamentous Potato virus X into spherical particles with different properties from virions. *FEBS Letters*, *590*(10), 1543–1551.

Nkanga, C. I., & Steinmetz, N. F. (2021). The pharmacology of plant virus nanoparticles. *Virology*, *556*, 39-61.

Noda, T. (2012). Native morphology of influenza virions. *Frontiers in Microbiology*, *2*, Article#269.

Noda, T., Sagara, H., Yen, A., Takada, A., Kida, H., & Cheng, R. H. (2006). Architecture of ribonucleoprotein complexes in Influenza A virus particles. *Nature*, *439*, 490–492.

Nuñez-Rivera, A., Fournier, P. G. J., Arellano, D. L., Rodriguez-Hernandez, A. G., Vazquez-Duhalt, R., & Cadena-Nava, R. D. (2020). Brome mosaic virus-like particles as siRNA nanocarriers for biomedical purposes. *Beilstein Journal of Nanotechnology*, *11*(1), 372–382.

O'Hanlon, R., & Shaw, M. L. (2019). Baloxavir marboxil: The new influenza drug on the market. *Current Opinion in Virology*, *35*, 14–18.

Ocampo-García, B. E., Ramírez, F. de M., Ferro-Flores, G., De León-Rodríguez, L. M., Santos-Cuevas, C. L., Morales-Avila, E., … Camacho-López, M. A. (2011). 99mTc-labelled gold nanoparticles capped with HYNIC-peptide/mannose for sentinel lymph node detection. *Nuclear Medicine and Biology*, *38*(1), 1–11.

Oda, Y., Saeki, K., Takahashi, Y., Maeda, T., Naitow, H., Tsukihara, T., & Fukuyama, K. (2000). Crystal Structure of Tobacco necrosis virus at 2.25A resolution. *Journal of Molecular Biology*, *300*, 153–169.

Ohno, T., Inoue, H., & Okada, Y. (1972). Assembly of rod-shaped virus in vitro: reconstitution with cucumber green mottle mosaic virus protein and tobacco mosaic virus RNA. *Proceedings of the National Academy of Sciences*, *69*(12), 3680-3683.

Okada, Y. (1986). Cucumber green mottle mosaic virus. In *The plant viruses* (pp. 267-281). Springer, Boston, MA.

Ole Kemnade, J., Seethammagari, M., Collinson-pautz, M., Kaur, H., Spencer, D. M., & Mccormick, A. A. (2014). Tobacco mosaic virus efficiently targets DC uptake , activation and antigen-specific T cell responses in vivo. *Vaccine*, *32*(33), 4228–4233.

Oliveira, L. T., Garcia, G. M., Kano, E. K., Tedesco, A. C., & Mosqueira, V. C. F. (2011). HPLC-FLD methods to quantify chloroaluminum phthalocyanine in nanoparticles, plasma and tissue: Application in pharmacokinetic and biodistribution studies. *Journal of Pharmaceutical and Biomedical Analysis*, *56*(1), 70–77.

Omidi, S., & Kakanejadifard, A. (2019). Modification of chitosan and chitosan nanoparticle by long chain pyridinium compounds: Synthesis, characterization, antibacterial, and antioxidant activities. *Carbohydrate Polymers*, *208*, 477–485.

Ooi, A., Tan, S., Mohamed, R., Rahman, N. A., & Othman, R. Y. (2006). The full-length clone of Cucumber green mottle mosaic virus and its application as an expression system for Hepatitis B surface antigen. *Journal of Biotechnology*, *121*(4), 471–481.

Oran, A. E., & Robinson, H. L. (2003). DNA vaccines, combining form of antigen and method of delivery to raise a spectrum of IFN- γ and IL-4-producing CD4 + and CD8 + T cells. *The Journal of Immunology*, *171*, 1999–2005.

Ortiz, J. R., & Neuzil, K. M. (2017). Influenza immunization of pregnant women in resource-constrained countries: An update for funding and implementation

decisions. *Current Opinion in Infectious Diseases*, *30*, 455–462.

Osterholm, M. T., & Ph, D. (2005). Preparing for the next pandemic. *New England Journal of Medicine*, *352*, 1839–1842.

Ostrowsky, J., Arpey, M., Moore, K., Osterholm, M., Friede, M., Gordon, J., … Bresee, J. (2020). Tracking progress in universal influenza vaccine development. *Current Opinion in Virology*, *40*, 28–36.

Othman, R. Y., Teoh, P. G., Ooi, A. S., & Abubakar, S. (2009). Virus-specific read-through codon preference affects infectivity of chimeric Cucumber green mottle mosaic viruses displaying a dengue virus epitope. *Journal of Biomedicine and Biotechnology*, *2009*.

Oyarzun, P, & Kobe, B. (2015). Computer-aided design of T-cell epitope-based vaccines: Addressing population coverage. *International Journal of Immunogenetics*, *42*, 313–321.

Oyarzun, Patricio, & Kobe, B. (2016). Recombinant and epitope-based vaccines on the road to the market and implications for vaccine design and production. *Human Vaccines & Immunotherapeutics*, *12*(3), 763–767.

Palazzo, M., Gariboldi, S., Zanobbio, L., Dusio, G. F., Selleri, S., Bedoni, M., … Rumio, C. (2008). Cross-talk among Toll-like receptors and their ligands. *International Immunology*, *20*(5), 709–718.

Palese, P, & Shaw, M. L. (2007). Orthomyxoviridae: The Viruses and Their Replication, 404 p. *Fields Virology, Fifth Edition Ed*, *2*, 405.

Palese, Peter, & Young, J. F. (1981). Variation of Influenza A , B , and C viruses. *Science*, *215*(19), 1468–1474.

Park, C. H., Ju, H. K., Han, J. Y., Park, J. S., Kim, I. H., Seo, E. Y., … Lim, H. S. (2017). Complete nucleotide sequences and construction of full-length infectious cDNA clones of Cucumber green mottle mosaic virus (CGMMV) in a versatile newly developed binary vector including both 35S and T7 promoters. *Virus Genes*, *53*(2), 286–299.

Park, E., Choi, J., Park, Y., & Park, K. (2008). Oxidative stress induced by cerium oxide nanoparticles in cultured BEAS-2B cells. *Toxicology*, *245*, 90–100.

Park, J., Wen, A. M., Gao, H., Shin, M. D., Simon, D. I., Wang, Y., & Steinmetz, N. F. (2021). Designing S100A9-targeted plant virus nanoparticles to target deep vein thrombosis. *Biomacromolecules*, *22*(6), 2582-2594.

Pasquale, A. Di, Preiss, S., Silva, F. T. Da, & Garçon, N. (2015). Vaccine adjuvants: From 1920 to 2015 and beyond. *Vaccines*, *3*(2), 320–343.

Paterson, D., & Fodor, E. (2012). Emerging roles for the Influenza A virus nuclear export protein (NEP). *PLoS Pathogens*, *8*(12), Article#e1003019.

Peabody, D. S. (2003). A viral platform for chemical modification and multivalent display. *Journal of Nanobiotechnology*, *1*, 1–8.

Pérez Filgueira, D. M., Brayfield, B. P., Phiri, S., Borca, M. V., Wood, C., & Morris, T. J. (2004a). Preserved antigenicity of HIV-1 p24 produced and purified in high yields from plants inoculated with a Tobacco mosaic virus (TMV)-derived vector. *Journal of Virological Methods*, *121*(2), 201–208.

Pérez Filgueira, D. M., Mozgovoj, M., Wigdorovitz, A., Dus Santos, M. J., Parreño, V., Trono, K., … Borca, M. V. (2004b). Passive protection to Bovine rotavirus (BRV) infection induced by a BRV VP8 produced in plants using a TMV-based vector. *Archives of Virology*, *149*(12), 2337–2348.

Pérez Filgueira, D. M., Zamorano, P. I., Domínguez, M. G., Taboga, O., Del Médico Zajac, M. P., Puntel, M., … Sadir, A. M. (2003). Bovine herpes virus gD protein produced in plants using a recombinant Tobacco mosaic virus (TMV) vector possesses authentic antigenicity. *Vaccine*, *21*(27–30), 4201–4209.

Peyret, H., & Lomonossoff, G. P. (2015). When plant virology met Agrobacterium: The rise of the deconstructed clones. *Plant Biotechnology Journal*, *13*(8), 1121–1135.

Pham, N. L. L., Pewe, L. L., Fleenor, C. J., Langlois, R. A., Legge, K. L., Badovinac, V. P., & Harty, J. T. (2010). Exploiting cross-priming to generate protective CD8 T-cell immunity rapidly. *Proceedings of the National Academy of Sciences*, *107*(27), 12198–12203.

Phelps, J. P., Dang, N., & Rasochova, L. (2007). Inactivation and purification of Cowpea mosaic virus-like particles displaying peptide antigens from Bacillus anthracis. *Journal of Virological Methods*, *141*(2), 146–153.

Piazzolla, G., Nuzzaci, M., Tortorella, C., Panella, E., Natilla, A., Boscia, D., … Antonaci, S. (2005). Immunogenic properties of a chimeric plant virus expressing a Hepatitis C virus (HCV)-derived epitope: New prospects for an HCV vaccine. *Journal of Clinical Immunology*, *25*(2), 142–152.

Pitek, A. S., Wen, A. M., Shukla, S., & Steinmetz, N. F. (2016). The protein corona of plant virus nanoparticles influences their dispersion properties, cellular interactions, and in vivo fates. *Small*, *12*(13), 1758–1769.

Plummer, E. M., & Manchester, M. (2011). Viral nanoparticles and virus-like particles: platforms for contemporary vaccine design. *Nanomedicine and Nanobiotechnology*, *3*, 174–196.

Plummer, E. M., & Manchester, M. (2013). Endocytic uptake pathways utilized by CPMV nanoparticles. *Molecular Pharmaceutics*, *10*(1), 26–32.

Pokorski, J. K., & Steinmetz, N. F. (2011). The art of engineering viral nanoparticles. *Molecular Pharmaceutics*, *8*(1), 29–43.

Pomwised, R., Intamaso, U., Teintze, M., Young, M., & Pincus, S. H. (2016). Coupling peptide antigens to virus-like particles or to protein carriers influences the Th1/Th2 polarity of the resulting immune response. *Vaccines*, *4*(2), Article#15.

Porta, C., Spall, V. E., Findlay, K. C., Gergerich, R. C., Farrance, C. E., & Lomonossoff, G. P. (2003). Cowpea mosaic virus-based chimaeras: Effects of inserted peptides on the phenotype, host range, and transmissibility of the modified viruses. *Virology*, *310*(1), 50–63.

Portela, A., & Digard, P. (2002). The influenza virus nucleoprotein : A multifunctional RNA-binding protein pivotal to virus replication. *Journal of General Virology*, *83*, 723–734.

Portney, N. G., & Ozkan, M. (2006). Nano-oncology: Drug delivery, imaging, and sensing. *Analytical and Bioanalytical Chemistry*, *384*, 620–630.

Prechl, J., Tchorbanov, A., Horváth, A., Baiu, D. C., Hazenbos, W., Rajnavölgyi, É., …

Erdei, A. (1999). Targeting of influenza epitopes to murine CR1/CR2 using single-chain antibodies. *Immunopharmacology*, *42*(1–3), 159–165.

Protein calculator v3.3 (2012). Retrieved on 15th, May, 2013, from http://www.scripps.edu/~cdputnam/protcalc.html.

Pumplin, N., & Voinnet, O. (2013). RNA silencing suppression by plant pathogens: Defence, counter-defence and counter-counter-defence. *Nature Reviews Microbiology*, *11*(11), 745–760.

Rae, C. S., Khor, W., Wang, Q., Destito, G., Gonzalez, M. J., Singh, P., … Finn, M. G. (2005). Systemic trafficking of plant virus nanoparticles in mice via the oral route. *Virology*, *343*(2), 224–235.

Rahman, M. ., Wong, K. ., Hanafiah, A., & Isahak, I. (2014). Influenza and respiratory syncytial viral infections in Malaysia: Demographic and clinical perspective. *Pakistan Journal of Medical Sciences*, *30*(1), 161–165.

Rajendran, L., Knölker, H. J., & Simons, K. (2010). Subcellular targeting strategies for drug design and delivery. *Nature Reviews Drug Discovery*, *9*(1), 29–42.

Rajoka, M. S. R., Mehwish, H. M., Zhang, H., Ashraf, M., Fang, H., Zeng, X., … He, Z. (2020). Antibacterial and antioxidant activity of exopolysaccharide mediated silver nanoparticle synthesized by Lactobacillus brevis isolated from Chinese koumiss. *Colloids and Surfaces B: Biointerfaces*, *186*, Article#110734.

Rana, A., Yadav, K., & Jagadevan, S. (2020). A comprehensive review on green synthesis of nature-inspired metal nanoparticles: Mechanism, application and toxicity. *Journal of Cleaner Production*, *272*, Article#122880.

Reed, S. G., Bertholet, S., Coler, R. N., & Friede, M. (2009). New horizons in adjuvants for vaccine development. *Trends in Immunology*, *30*(1), 23–32.

Reid, A. H., Fanning, T. G., Hultin, J. V, & Taubenberger, J. K. (1999). Origin and evolution of the 1918 "" Spanish "" influenza virus hemagglutinin gene. *Proceedings of the National Academy of Sciences*, *96*(4), 1651-1656.

Ren, Y., Wong, S. M., & Lim, L. Y. (2006). In vitro-reassembled plant virus-like particles for loading of polyacids. *Journal of General Virology*, *87*(9), 2749–2754.

Richardson, J. C., Sciences, B., & Collins, F. (1991). NS2 protein of influenza virus is found in purified virus and phosphorylated in infected cells. *Archives of Virology*, *116*, 69–80.

Rioux, G., Babin, C., Majeau, N., & Leclerc, D. (2012). Engineering of Papaya mosaic virus (PapMV) nanoparticles through fusion of the HA11 peptide to several putative surface-exposed sites. *PLoS One*, *7*(2), Article#e31925.

Riwilaijaroen, B. N. S., & Uzuki, Y. S. (2012). Molecular basis of the structure and function of H1 hemagglutinin of influenza virus. *Proceedings of the Japan Academy, Series B*, *88*, 226–249.

Roeder, J., Fischer, R., & Commandeur, U. (2017). Engineering Potato virus X particles for a covalent protein based attachment of enzymes. *Small*, *13*(48), Article#1702151.

Rojas, S., Gispert, J. D., Martín, R., Abad, S., Menc C., Pareto, D., … Herance, J. R. (2011). Biodistribution of amino-functionalized diamond nanoparticles. In vivo studies based on 18F radionuclide emission. *ACS Nano*, *5*(7), 5552–5559.

Rolfes, M. A., Goswami, D., Tahia, A., Yeasmin, S., Parvin, N., Nahar, K., … Brooks, W. A. (2017). Efficacy of trivalent influenza vaccine against laboratory-confirmed influenza among young children in a randomized trial in Bangladesh. *Vaccine*, *35*(50), 6967-6976.

Rossman, J. S., Jing, X., Leser, G. P., Balannik, V., Pinto, L. H., & Lamb, R. A. (2010a). Influenza virus M2 ion channel protein is necessary for filamentous virion formation. *Journal of Viirology*, *84*(10), 5078–5088.

Rossman, J. S., Jing, X., Leser, G. P., & Lamb, R. A. (2010b). Influenza virus M2 protein mediates ESCRT-independent membrane scission. *Cell*, *142*(6), 902–913.

Roy, I., Ohulchanskyy, T. Y., Pudavar, H. E., Bergey, E. J., Oseroff, A. R., Morgan, J., … Prasad, P. N. (2003). Ceramic-based nanoparticles entrapping water-insoluble photosensitizing anticancer drugs: A novel drug-carrier system for photodynamic therapy. *Journal of American Chemical Society*, *125*, 7860–7865.

Saeed, M., Gao, J., Shi, Y., Lammers, T., & Yu, H. (2019). Engineering nanoparticles to reprogram the tumor immune microenvironment for improved cancer immunotherapy. *Theranostics*, *9*(26), Article#7981.

Saejung, W., Fujiyama, K., Takasaki, T., Ito, M., Hori, K., Malasit, P., … Seki, T. (2007). Production of dengue 2 envelope domain III in plant using TMV-based vector system. *Vaccine*, *25*(36), 6646–6654.

Sahrawat, T. R., & Kaur, A. (2016). In-silico design of an Epitope-based peptide vaccine: A computational biology approach. *International Journal for Computational Biology*, *5*(2), 1–5.

Sainsbury, F., & Lomonossoff, G. P. (2014). Transient expressions of synthetic biology in plants. *Current Opinion in Plant Biology*, *19*, 1–7.

Salleh, A., Naomi, R., Utami, N. D., Mohammad, A. W., Mahmoudi, E., Mustafa, N., & Fauzi, M. B. (2020). The potential of silver nanoparticles for antiviral and antibacterial applications: a mechanism of action. *Nanomaterials*, *10*(8), Article#1566.

Sam, I., Shaw, R., Chan, Y., Hooi, P., Hurt, A. C., & Barr, I. G. (2013). Seroprevalence of seasonal and pandemic Influenza A in Kuala Lumpur , Malaysia in 2008 – 2010. *Journal of Medical Virology*, *1425*, 1420–1425.

Sam, J. I. (2015). The burden of human influenza in Malaysia. *Medical Journal Malaysia*, *70*(3), 127–130.

Sanchez-Trincado, J. L., Gomez-Perosanz, M., & Reche, P. A. (2017). Fundamentals and methods for T- and B-cell epitope prediction. *Journal of Immunology Research*, *2017*.

Sanfaçon, H. (2015). Plant translation factors and virus resistance. *Viruses*, *7*(7), 3392–3419.

Santi, L., Giritch, A., Roy, C. J., Marillonnet, S., Klimyuk, V., Gleba, Y., … Mason, H. S. (2006). Protection conferred by recombinant Yersinia pestis antigens produced by a rapid and highly scalable plant expression system. *Proceedings of the National Academy of Sciences*, *103*(4), 861–866.

Santoni, M., Zampieri, R., & Avesani, L. (2020). Plant virus nanoparticles for vaccine applications. *Current Protein and Peptide Science*, *21*(4), 344–356.

Saylan, Y., Erdem, Ö., Ünal, S., & Denizli, A. (2019). An alternative medical diagnosis method: Biosensors for virus detection. *Biosensors*, *9*(2), Article#65.

Schnell, J. R., & Chou, J. J. (2008). Structure and mechanism of the M2 proton channel of influenza A virus. *Nature*, *451*, 591–596.

Schubert, D., Dargusch, R., Raitano, J., & Chan, S. (2006). Cerium and yttrium oxide nanoparticles are neuroprotective. *Biochemical and Biophysical Research Communications*, *342*, 86–91.

Shahgolzari, M., & Pazhouhandeh, M. (2020). Plant viral nanoparticles for packaging and in vivo delivery of bioactive cargos. *Wiley Interdisciplinary Reviews: Nanomedicine and Nanobiotechnology*, *12*(5), Article#e1629.

Shang, Y., Hasan, M., Ahammed, G. J., Li, M., Yin, H., & Zhou, J. (2019). Applications of nanotechnology in plant growth and crop protection: a review. *Molecules*, *24*(14), Article#2558.

Shao, F. (2014). Toxicity of silver nanoparticles on virus. *Journal of Materials and Environmental Science*, *5*(2), 587–590.

Shaw, M. L., & Palese, P. (2013). Orthomyxoviridae. *Fields Virology*, *1*, 1151–1185.

Sheikh, Q. M., Gatherer, D., Reche, P. A., & Flower, D. R. (2016). Towards the knowledge-based design of universal influenza epitope ensemble vaccines. *Bioinformatics*, *32*(21), 3233–3239.

Shi, J., Zhang, J., Li, S., Sun, J., Teng, Y., & Wu, M. (2015). Epitope-based vaccine target screening against highly pathogenic MERS-CoV :An in silico approach applied to emerging infectious diseases. *PLoS ONE*, *10*(12), Article#e0144475.

Shoeb, E., & Hefferon, K. (2019). Future of cancer immunotherapy using plant virus-based nanoparticles. *Future Science*, *5*(7), 1–8.

Shtyrya, Y. A., Mochalova, L. V, & Bovin, N. V. (2009). Influenza virus neuraminidase : Structure and function. *Acta Naturae*, *1*(2), 26–32.

Shuai, C., Yang, W., He, C., Peng, S., Gao, C., Yang, Y., Qi, F., & Feng, P. (2020). A magnetic micro-environment in scaffolds for stimulating bone regeneration. *Materials & Design*, *185*, Article#108275.

Shukla, S., Ablack, A. L., Wen, A. M., Lee, K. L., Lewis, J. D., & Steinmetz, N. F. (2013). Increased tumor homing and tissue penetration of the filamentous plant viral nanoparticle Potato virus X. *Molecular Pharmaceutics*, *10*(1), 33–42.

Shukla, S., Dickmeis, C., Fischer, R., Commandeur, U., & Steinmetz, N. F. (2018). In planta production of fluorescent filamentous plant virus-based nanoparticles. In *Virus-Derived Nanoparticles for Advanced Technologies* (pp. 61-84). Humana Press, New York, NY.

Shukla, S., Myers, J. T., Woods, S. E., Gong, X., Czapar, A. E., Commandeur, U., … Steinmetz, N. F. (2017). Plant viral nanoparticles-based HER2 vaccine: Immune response influenced by differential transport, localization and cellular interactions of particulate carriers. *Biomaterials*, *121*, 15–27.

Shukla, S., Wen, A. M., Ayat, N. R., Commandeur, U., Gopalkrishnan, R., Broome, A. M., … Steinmetz, N. F. (2014a). Biodistribution and clearance of a filamentous plant virus in healthy and tumor-bearing mice. *Nanomedicine*, *9*(2), 221–235.

Shukla, S., Wen, A. M., Commandeur, U., & Steinmetz, N. F. (2014b). Presentation of HER2 epitopes using a filamentous plant virus-based vaccination platform. *Journal of Materials Chemistry B*, *2*(37), 6249–6258.

Si, Y., Wen, Y., Kelly, S. H., Chong, A. S., & Collier, J. H. (2018). Intranasal delivery of adjuvant-free peptide nanofibers elicits resident CD8+ T cell responses. *Journal of Controlled Release*, *282*, 120–130.

Sikkema, F. D., Comellas-aragon, M., Fokkink, R. G., & Verduin, B. J. M. (2007). Monodisperse polymer–virus hybrid nanoparticles. *Organic and Biomolecular Chemistry*, *5*, 54–57.

Simeckova-Rosenberg, J., Yun, Z., Wyde, P. R., & Atassi, M. Z. (1995). Protection of mice against lethal viral infection by synthetic peptides corresponding to B- and T-cell recognition sites of Influenza A hemagglutinin. *Vaccine*, *13*(10), 927–932.

Singh, P., Destito, G., Schneemann, A., & Manchester, M. (2006). Canine parvovirus-like particles, a novel nanomaterial for tumor targeting targeting. *Journal of Nanobiotechnology*, *4*(2), 1–11.

Singh, P., Prasuhn, D., Yeh, R. M., Destito, G., Rae, C. S., Osborn, K., … Manchester, M. (2007). Bio-distribution, toxicity and pathology of Cowpea mosaic virus nanoparticles in vivo. *J Control Release*, *100120*(1–2), 41–50.

Skwarcynski, M., & Toth, I. (2016). Peptide-based synthetic vaccines. *Chemical Science*, *7*, 842–854.

Sokullu, E., Abyaneh, H. S., & Gauthier, M. A. (2019). Plant/bacterial virus-based drug discovery, drug delivery, and therapeutics. *Pharmaceutics*, *11*(5), Article#221.

Soussan, E., Cassel, S., Blanzat, M., & Rico-lattes, I. (2009). Drug Delivery by soft matter: Matrix and vesicular carriers angewandte. *Drug Vectors*, *48*, 274–288.

Speshock, J. L., Murdock, R. C., Braydich-Stolle, L. K., Schrand, A. M., & Hussain, S. M. (2010). Interaction of silver nanoparticles with Tacaribe virus. *Journal of Nanobiotechnology*, *8*, Article#19.

Spicer, C. D., Jumeaux, C., Gupta, B., & Stevens, M. M. (2018). Peptide and protein nanoparticle conjugates: Versatile platforms for biomedical applications. *Chemical Society Reviews*, *47*(10), 3574–3620.

Staczek, J., Bendahmane, M., Gilleland, L. B., Beachy, R. N., & Gilleland, H. E. (2000). Immunization with a chimeric *Tobacco mosaic virus* containing an epitope of outer membrane protein F of *Pseudomonas aeruginosa* provides protection against challenge with *P. aeruginosa*. *Vaccine*, *18*(21), 2266–2274.

Steinmetz, N. F. (2010). Viral nanoparticles as platforms for next-generation therapeutics and imaging devices. *Nanomedicine: Nanotechnology, Biology, and Medicine*, *6*(5), 634–641.

Steinmetz, N. F. (2011). Viral nanoparticles as platforms for next-generation therapeutics and imaging devices. *Nanomedicine*, *6*(5), 634–641.

Steinmetz, N. F., & Evans, D. J. (2007). Utilisation of plant viruses in bionanotechnology. *Organic and Biomolecular Chemistry*, *5*, 2891–2902.

Strauss, J.H., & Strauss, E.G. (1988). Evolution of RNA viruses. *Annual review of microbiology*, *42*, 657-683.

Sugawara, K., Nishimura, H., Hongo, S., Kitame, F., & Nakamura, K. (1991). Antigenic characterization of the nucleoprotein and matrix protein of Influenza C virus with monoclonal antibodies. *Journal of General Virology*, *72*, 103–109.

Sun, Y., Niu, X., & Fan, M. (2017). Genome-wide identification of cucumber green mottle mosaic virus-responsive microRNAs in watermelon. *Archives of Virology*, *162*(9), 2591–2602.

Tan, S.H., Nishiguchi, M., Murata, M., & Motoyoshi, F. (2000). The genome structure of kyuri green mottle mosaic tobamovirus and its comparison with that of cucumber green mottle mosaic tobamovirus. *Archives of Virology*, *145*(6), 1067-1079.

Tang, Z., Zhang, X., Shu, Y., Guo, M., Zhang, H., & Tao, W. (2021). Insights from nanotechnology in COVID-19 treatment. *Nano Today*, *36*, Article#101019.

Taniguchi, N. (1974). On the basic concept of nanotechnology. *Proceeding of the ICPE*.

Tanji, H., Ohto, U., Shibata, T., Taoka, M., Yamauchi, Y., Isobe, T., … Shimizu, T. (2015). Toll-like receptor 8 senses degradation products of single-stranded RNA. *Nature Structural & Molecular Biology*, *22*(2), Article#109.

Tao, Y. Y., Li, J. X., Hu, Y. M., Hu, Y. S., Zeng, G., & Zhu, F. C. (2021). Quadrivalent Influenza Vaccine (Sinovac Biotech) for seasonal influenza prophylaxis. *Expert Review of Vaccines*, *20*(1), 1-11.

Taubenberger, J. K., Reid, A. H., Janczewski, T. A., & Fanning, T. G. (2001). Integrating historical, clinical and molecular genetic data in order to explain the origin and virulence of the 1918 Spanish infuenza virus. *Philosophical Transactions of the Royal Society of London. Series B*, *356*, 1829–1839.

Taubenberger, J. K., Reid, M. H., Krafft, A. E., Bijwaard, K. E., & Fanning, T. G. (1997). Initial Genetic Characterization of the 1918 "Spanish" Influenza Virus. *Science*, *275*(5307), 1793–1796.

Taylor, K. M., Lin, T., Porta, C., Mosser, G., Giesing, H., Lomonossoff, G. P., & Johnson, J. E. (2000). Influence of three-dimensional structure on the immunogenicity of a peptide expressed on the surface of a plant virus. *Journal of Molecular Recognition : JMR*, *13*(2), 71–82.

Tenbusch, M., Grunwald, T., Niezold, T., genannt Bonsmann, M. S., Hannaman, D., Norley, S., & Überla, K. (2010). Codon-optimization of the hemagglutinin gene from the novel swine origin H1N1 influenza virus has differential effects on CD4+ T-cell responses and immune effector mechanisms following DNA electroporation in mice. *Vaccine*, *28*(19), 3273–3277.

Teoh, P., Ooi, A., Abubakar, S., & Othman, R. Y. (2009). Virus-specific read-through codon preference affects infectivity of chimeric Cucumber green mottle mosaic viruses displaying a dengue virus epitope. *Journal of Biomedicine and Biotechnology*, *2009*.

Testa, J. S., & Philip, R. (2012). Role of T-cell epitope-based vaccine in prophylactic and therapeutic applicationstherapeutic applications. *Future Virology*, *7*(11), 1077–1088.

Thérien, A., Bédard, M., Carignan, D., Rioux, G., Landry, L. G., Ève, M., … Leclerc, D. (2017). A versatile papaya mosaic virus (PapMV) vaccine platform based on sortase-mediated antigen coupling. *Journal of nanobiotechnology*, *15*(1), 1-13.

Thurber, G. M., Schmidt, M. M., & Wittrup, K. D. (2010). Antibody tumor penetration: Transport opposed by systemic and antigen-mediated clearance. *Advanced Drug Delivery Reviews*, *60*(12), Article#1421.

Tian, Y., Gao, S., Wu, M., Liu, X., Qiao, J., Zhou, Q., … Niu, Z. (2016). Tobacco mosaic virus-based 1D nanorod-drug carrier via the integrin-mediated endocytosis pathway. *ACS Applied Materials & Interfaces*, *8*(17), 10800–10807.

Tian, Y., Zhou, M., Shi, H., Gao, S., Xie, G., Zhu, M., … Niu, Z. (2018). Integration of cell-penetrating peptides with rod-like bionanoparticles: Virus-inspired gene-silencing technology. *Nano Letters*, *18*(9), 5453–5460.

Tizard, I. R. (2021). Adjuvants and adjuvanticity. *Vaccines for Veterinarians*, 75.

Tong, S., Zhu, X., Li, Y., Shi, M., Zhang, J., Bourgeois, M., … Donis, R. O. (2013). New world bats harbor diverse Influenza A viruses. *PLoS Pathogens*, *9*(10), Article#e1003657.

Torchilin, V P. (2007). Micellar nanocarriers :Pharmaceutical perspectives. *Pharmaceutical Research*, *24*(1).

Torchilin, Vladimir P. (2005). Recent advances with liposomes as pharmaceutical carriers. *Drug Discovery*, *4*, 145–160.

Tran, H. H., Chen, B., Chen, H., Menassa, R., Hao, X., Bernards, M., … Wang, A. (2019). Development of a Cucumber green mottle mosaic virus-based expression vector for the production in cucumber of neutralizing epitopes against a devastating animal virus. *Journal of Virological Methods*, *269*, 18–25.

Truniger, V., & Aranda, M. A. (2009). Recessive resistance to plant viruses. *Advances in Virus Research*, *75*, 119–231.

Turrell, L., Lyall, J. W., Tiley, L. S., Fodor, E., & Vreede, F. T. (2013). The role and assembly mechanism of nucleoprotein in Influenza A virus ribonucleoprotein complexes. *Nature Communications*, *4*, Article#1591.

Uehara, T., Hayden, F. G., Kawaguchi, K., Omoto, S., Hurt, A. C., De Jong, M. D., … Baba, K. (2020). Treatment-emergent influenza variant viruses with reduced baloxavir susceptibility: Impact on clinical and virologic outcomes in uncomplicated influenza. *The Journal of Infectious Diseases*, *221*(3), 346–355.

Ugaki, M., Tomiyama, M., Kakutani, T., Hidaka, S., Kiguchi, T., Nagata, R., … Nishiguchi, M. (1991). The complete nucleotide sequence of Cucumber green mottle mosaic virus (SH strain) genomic RNA. *Journal of General Virology*, *72*(7), 1487–1495.

Uhde-Holzem, K., Fischer, R., & Commandeur, U. (2007). Genetic stability of recombinant Potato virus X virus vectors presenting foreign epitopes. *Archives of Virology*, *152*(4), 805–811.

Uhde-holzem, K., Schlösser, V., Viazov, S., Fischer, R., & Commandeur, U. (2010). Immunogenic properties of chimeric Potato virus X particles displaying the Hepatitis C virus hypervariable region I peptide R9. *Journal of Virological Methods*, *166*, 12–20.

Usha, R., Rohll, J. B., Spall, V. E., Shanks, M., Maule, A. J., Johnson, J. E., & Lomonossoff, G. P. (1993). Expression of an animal virus antigenic site on the surface of a plant virus particle. *Virology*, *197*(1), 366-374.

Uyeki, T. M. (2018). A step forward in the treatment of influenza. *The New England Journal of Medicine*, *379*(10), Article#975.

van Rijn, P., & Böker, A. (2011). Bionanoparticles and hybrid materials: tailored structural properties, self-assembly, materials and developments in the field. *Journal of Materials Chemistry*, *21*, Article#16735.

Vankayala, R., Bahena, E., Guerrero, Y., Singh, S. P., Ravoori, M. K., Kundra, V., & Anvari, B. (2020). Virus-mimicking nanoparticles for atrgeted near infrared fluorescence imaging of intraperitoneal ovarian tumors in mice. *Annals of Biomedical Engineering*, *49*(2), 548-559.

Vardhan, G. P. V., Sushmitha, M. H. C., Usha, H. S. S., & Murthy, N. M. R. N. (2018). Development of Sesbania mosaic virus nanoparticles for imaging. *Archives of virology*, *164*(2), 497-507.

Vasquez, K. O., Casavant, C., & Peterson, J. D. (2011). Quantitative whole body biodistribution of fluorescent-labeled agents by non-invasive tomographic imaging. *PLoS ONE*, *6*(6), Article#e20594.

Villagrana-Escareño, M. V, Reynaga-Hernández, E., Galicia-Cruz, O. G., Durán-Meza, A. L., la Cruz-González, D., Hernández-Carballo, C. Y., & Ruíz-García, J. (2019). VLPs derived from the CCMV plant virus can directly transfect and deliver heterologous genes for translation into mammalian cells. *BioMed Research International*, *2019*.

Virus World (2017). Retrieved on 22nd, July, 2017, from http://www.virology.wisc.edu/virusworld/viruslist.php 2017.

Vita, R., Mahajan, S., Overton, J. A., Dhanda, S. K., Martini, S., Cantrell, J. R., … Peters, B. (2019). The immune epitope database (IEDB): 2018 update. *Nucleic Acids Research*, *47*(D1), D339–D343.

Vita, R., Overton, J. A., Greenbaum, J. A., Ponomarenko, J., Clark, D., Cantrell, J. R., … Peters, B. (2015). The immune epitope database (IEDB) 3 . 0. *Nucleic Acids Research*, *43*, D405–D412.

Vita, R., Zarebski, L., Greenbaum, J. A., Emami, H., Hoof, I., Salimi, N., … Peters, B. (2010). The immune epitope database 2.0. *Nucleic Acids Research*, *38*(suppl_1), D854–D862.

Vitiello, A., Yuan, L., Chesnut, R. ., Sidney, J., Southwood, S., Farness, P., … Sette, A. (2020). Immunodominance analysis of CTL responses to Influenza PR8 virus reveals two new dominant and subdominant Kb-restricted epitopes. *The Journal of Immunology*, *157*, 5555–5562.

Wagner, B., Hufnagl, K., Radauer, C., Wagner, S., Baier, K., Scheiner, O., … Breiteneder, H. (2004). Expression of the B subunit of the heat-labile enterotoxin of Escherichia coli in Tobacco mosaic virus-infected Nicotiana benthamiana plants and its characterization as mucosal immunogen and adjuvant. *Journal of Immunological Methods*, *287*(1–2), 203–215.

Wagner, R., Wolff, T., Herwig, A., Pleschka, S., & Liebig-universita, J. (2000). Interdependence of hemagglutinin glycosylation and neuraminidase as regulators of influenza virus growth: A study by reverse genetics. *Jorrnal of Virology*, *74*(14), 6316–6323.

Wang, C., Beiss, V., & Steinmetz, N. F. (2019a). Cowpea mosaic virus nanoparticles and

empty virus-like particles show distinct but overlapping immunostimulatory properties. *Journal of Virology*, *93*(21), Article#e00129-19.

Wang, C., Fiering, S. N., & Steinmetz, N. F. (2019b). Cowpea mosaic virus promotes anti-tumor activity and immune memory in a mouse ovarian tumor model. *Advanced Therapeutics*, *12*, 1–11.

Wang, H., & Stubbs, G. (1994). Structure determination of Cucumber green mottle mosaic virus by X-ray fiber diffraction: Significance for the evolution of Tobamoviruses. *Journal of Molecular Biology*, *239*, 371–384.

Wang, J., Qiu, J. X., Soto, C., & De Grado, W. F. (2011). Structural and dynamic mechanisms for the function and inhibition of the M2 proton channel from Influenza A virus. *Current Opinion in Structural Biology*, *21*(1), 68–80.

Wang, Q., Lin, T., Johnson, J. E., Finn, M. G., & Jolla, L. (2002). Natural supramolecular building blocks: Cysteine-added mutants of Cowpea mosaic virus. *Chemistry & Biology*, *9*, 813–819.

Wang, Y., Deng, L., Gonzalez, G. X., Luthra, L., Dong, C., Ma, Y., … Wang, B. (2020). Double-layered M2e-NA protein nanoparticleo immunization induces broad cross-protection against different influenza viruses in mice. *Advance Healthcare Materials*, *9*, 1–14.

Wang, Y., Deng, L., Kang, S. M., & Wang, B. Z. (2018). Universal influenza vaccines: From viruses to nanoparticles. *Expert Review of Vaccines*, *17*(11), 967–976.

Ward, B. J., Gobeil, P., Séguin, A., Atkins, J., Boulay, I., Charbonneau, P. Y., … Finkle, C. (2021). Phase 1 randomized trial of a plant-derived virus-like particle vaccine for COVID-19. *Nature Medicine*, *27*(6), 1071–1078.

Watanabe, T., Honda, A., Iwata, A., Ueda, S., Hibi, T., & Ishihama, A. (1999). Isolation from Tobacco Mosaic Virus-Infected Tobacco of a Solubilized Template-Specific RNA-Dependent RNA Polymerase Containing a 126K / 183K Protein Heterodimer. *Journal of virology*, *73*(4), 2633-2640.

Wege, C., & Geiger, F. (2018). Dual functionalization of rod-shaped viruses on single coat protein subunits. In *Virus-derived nanoparticles for advanced technologies* (pp. 405-424). Humana Press, New York, NY.

Weiss, C., Carriere, M., Fusco, L., Capua, I., Regla-Nava, J. A., Pasquali, M., … Mattevi, C. (2020). Toward nanotechnology-enabled approaches against the COVID-19 pandemic. *ACS Nano*, *14*(6), 6383–6406.

Wellink, J. (1998). Comovirus isolation and RNA extraction. *Methods in Molecular Biology*, *81*, 205–209.

Wen, A. M., Infusino, M., De Luca, A., Kernan, D. L., Czapar, A. E., Strangi, G., & Steinmetz, N. F. (2015). Interface of physics and biology: Engineering virus-based nanoparticles for biophotonics. *Bioconjugate Chemistry*, *26*(1), 51–62.

Wen, A. M., & Steinmetz, N. F. (2016). Design of virus-based nanomaterials for medicine, biotechnology, and energy. *Chemical Society Reviews*, *45*(15), 4074–4126.

Werner, S., Marillonnet, S., Hause, G., Klimyuk, V., & Gleba, Y. (2006). Immunoabsorbent nanoparticles based on a tobamovirus displaying protein A. *Proceedings of the National Academy of Sciences*, *103*(47), 17678–17683.

Wong, S. M., & Ren, Y. (2018). In vitro-reassembled plant virus-like particles of Hibiscus chlorotic ringspot virus (HCRSV) as nano-protein cages for drugs. In *Virus-derived nanoparticles for advanced technologies* (pp. 229-236). Humana Press, New York, NY.

Wu, J., Zheng, K., Huang, X., Liu, J., Liu, H., Boccaccini, A. R., … Shao, Z. (2019). Thermally triggered injectable chitosan/silk fibroin/bioactive glass nanoparticle hydrogels for in-situ bone formation in rat calvarial bone defects. *Acta Biomaterialia*, *91*, 60–71.

Wu, L., Jiang, L., Zhou, Z., Fan, J., Zhang, Q., Zhu, H., … Xu, Z. (2003). Expression of Foot-and-mouth disease virus epitopes in tobacco by a Tobacco mosaic virus-based vector. *Vaccine*, *21*(27–30), 4390–4398.

Wu, M., Shi, J., Fan, D., Zhou, Q., Wang, F., Niu, Z., & Huang, Y. (2013). Biobehavior in normal and tumor-bearing mice of Tobacco mosaic virus. *Biomacromolecules*, *14*(11), 4032–4037.

Wu, T., Guan, J., Handel, A., Tscharke, D. C., Sidney, J., Sette, A., … Gruta, N. L. La. (2019). Quantification of epitope abundance reveals the effect of direct and cross-presentation on influenza CTL responses. *Nature Communications*, *10*(1), 1–14.

Xia, T., Kovochich, M., Liong, M., Ma, L., Gilbert, B., Shi, Ḱ. H., … Nel, A. E. (2008). Comparison of the mechanism of toxicity of zinc oxide and cerium oxide nanoparticles based on dissolution and oxidative stress properties. *ACS Nano*, *2*(10), 2121–2134.

Xie, Y., Lu, W., & Jiang, X. (2006). Improvement of cationic albumin conjugated pegylated nanoparticles holding NC-1900, a vasopressin fragment analog, in memory deficits induced by scopolamine in mice. *Behavioural Brain Research*, *173*, 76–84.

Xing, Y., & Rao, J. (2008). Quantum dot bioconjugates for in vitro diagnostics & in vivo imaging. *Cancer Biomarkers*, *4*, 307–319.

Xue, Y., Wang, N., Zeng, Z., Huang, J., Xiang, Z., & Guan, Y. Q. (2020). Neuroprotective effect of chitosan nanoparticle gene delivery system grafted with acteoside (ACT) in Parkinson's disease models. *Journal of Materials Science & Technology*, *43*, 197–207.

Yamashita, M., Krystal, M., & Palese, P. (1988). Evidence that the matrix protein of Influenza C virus is coded for by a spliced mRNA. *Journal of Virological Methods*, *62*(9), 3348–3355.

Yan, Y., Yao, D., & Li, X. (2021). Immunological mechanism and clinical application of PAMP adjuvants. *Recent Patents on Anti-Cancer Drug Discovery*, *16*(1), 30–43.

Yang, C. D., Liao, J. T., Lai, C. Y., Jong, M. H., Liang, C. M., Lin, Y. L., … Liang, S. M. (2007). Induction of protective immunity in swine by recombinant Bamboo mosaic virus expressing Foot-and-mouth disease virus epitopes. *BMC Biotechnology*, *7*, Article#62.

Yang, J., Yan, R., Roy, A., Xu, D., Poisson, J., & Zhang, Y. (2015). The I-TASSER suite: Protein structure and function prediction. *Nature Methods*, *12*(1), 7–8.

Yao, Y., Zhou, Y., Liu, L., Xu, Y., Chen, Q., Wang, Y., … Shao, A. (2020). Nanoparticle-based drug delivery in cancer therapy and its role in overcoming drug resistance. *Frontiers in Molecular Biosciences*, *7*.

Yasawardene, S. G., Lomonossoff, G. P., & Ramasamy, R. (2003). Expression & immunogenicity of malaria merozoite peptides displayed on the small coat protein of chimaeric Cowpea mosaic virus. *Indian Journal of Medical Research*, *118*, Article#115.

Yasuda, J., Nakada, S., Kato, A., Toyoda, T., & Ishihma, A. (1993). Molecular assembly of influenza virus association of the NS2 protein with virion matrix. *Virology*, *196*, 249–255.

Yildiz, I., Lee, K. L., Chen, K., Shukla, S., & Steinmetz, N. F. (2013). Infusion of imaging and therapeutic molecules into the plant virus-based carrier Cowpea mosaic virus: Cargo-loading and delivery. *Journal of controlled release*, *172*(2), 568-578.

Yildiz, I., Tsvetkova, I., Wen, A. M., Shukla, S., Masarapu, M. H., Dragnea, B., & Steinmetz, N. F. (2012). Engineering of Brome mosaic virus for biomedical applications. *RSC Advances*, *2*(9), 3670–3677.

Young, M., Willits, D., Uchida, M., & Douglas, T. (2008). Plant viruses as biotemplates for materials and their use in nanotechnology. *Annual Review of Phytopathology*, *46*, 361–384.

Yuan, L., Tang, Q., Yang, D., Zhang, J. Z., Zhang, F., & Hu, J. (2011). Preparation of pH-responsive mesoporous silica nanoparticles and their application in controlled drug delivery. *The Journal of Physical Chemistry C*, *115*, 9926–9932.

Yusibov, V., Hooper, D. C., Spitsin, S. V., Fleysh, N., Kean, R. B., Mikheeva, T., … Koprowski, H. (2002). Expression in plants and immunogenicity of plant virus-based experimental rabies vaccine. *Vaccine*, *20*(25–26), 3155–3164.

Yusibov, V., Modelska, A., Steplewski, K., Agadjanyan, M., Weiner, D., Hooper, D. C., & Koprowski, H. (1997). Antigens produced in plants by infection with chimeric plant viruses immunize against rabies virus and HIV-1. *Proceedings of the National Academy of Sciences*, *94*(11), 5784–5788.

Yusibov, V., Mett, V., Mett, V., Davidson, C., Musiychuk, K., Gilliam, S., … Mann, D. (2005). Peptide-based candidate vaccine against Respiratory syncytial virus. *Vaccine*, *23*(17–18), 2261–2265.

Zamberi, S., Zulkifli, I., & Ilina, I. (2003). Respiratory viruses detected in hospitalised paediatric patients with respiratory infections. *Medical Journal Malaysia*, *58*(5), 681–687.

Zanker, D., Quinn, K., Waithman, J., Lata, R., Murphy, R., La Gruta, N. L., & Chen, W. (2015). T cells recognizing a 11mer influenza peptide complexed to H-2Db show promiscuity for peptide length. *Immunology and Cell Biology*, *93*(5), 500–507

Zelepukin, I. V., Yaremenko, A. V., Shipunova, V. O., Babenyshev, A. V., Balalaeva, I. V., Nikitin, P. I., … Nikitin, M. P. (2019). Nanoparticle-based drug delivery via RBC-hitchhiking for the inhibition of lung metastases growth. *Nanoscale*, *11*(4), 1636–1646.

Zhang, G., Leung, C., Murdin, L., Rovinski, B., & White, K. a. (2000). In planta expression of HIV-1 p24 protein using an RNA plant virus-based expression vector. *Molecular Biotechnology*, *14*(2), 99–107.

Zhang, J., & Landick, R. (2016). A two-way street: regulatory interplay between RNA polymerase and nascent RNA structure. *Trends in Biochemical Sciences*, *41*(4),

293–310.

Zhang, L., Gu, F. X., Chan, J. M., Wang, A. Z., Langer, R. S., & Farokhzad, O. C. (2008). Nanoparticles in medicine: Therapeutic applications and developments. *Clinical Pharmacology and Therapeutics*, *83*(5), 761–769.

Zhang, Y. (2008). I-TASSER server for protein 3D structure prediction. *BMC bioinformatics*, *9*(1), 1-8.

Zheng, H., Xiao, C., Han, K., Peng, J., Lin, L., Lu, Y., … Li, G. (2015). Development of an agroinoculation system for full-length and GFP-tagged cDNA clones of Cucumber green mottle mosaic virus. *Archives of Virology*, *160*(11), 2867–2872.

Zhong, W., Reche, P. A., Lai, C. C., Reinhold, B., & Reinherz, E. L. (2003). Genome-wide characterization of a viral cytotoxic T lymphocyte epitope repertoire. *Journal of Biological Chemistry*, *278*(46), 45135–45144.

Zhu, Y., Li, J., Li, W., Zhang, Y., Yang, X., Chen, N., … Zhao, Y. (2012). The biocompatibility of nanodiamonds and their application in drug delivery systems. *Theranostics*, *2*(3), 302–312.

Zhuang, J., Holay, M., Park, J. H., Fang, R. H., Zhang, J., & Zhang, L. (2019). Nanoparticle delivery of immunostimulatory agents for cancer immunotherapy. *Theranostics*, *9*(25), Article#7826.

Zimmerman, R. K. (2007). Rationing of influenza vaccine during a pandemic: Ethical analyses. *Vaccine*, *25*, 2019–2026.